Intervertebral Disc Height Loss and Restoration:

Outcomes and Implications

by

Christian Balkovec

A thesis

presented to the University of Waterloo

in fulfillment of the

thesis requirement for the degree of

Doctor of Philosophy

In

Kinesiology

Waterloo, Ontario, Canada, 2016

Author's Declaration

I hereby declare that I am the sole author of this thesis. This is a true copy of the thesis, including any final revisions, as accepted by my examiners. I understand that my thesis may be made electronically available to the public.

Christian Balkovec

Abstract

This thesis is unified around the theme of disc height loss. Current knowledge in the area of spine research identifies mechanical overload as the culprit for the initiation of injury to the spine. While genetic predispositions may play a factor in the severity of spine degeneration or in the resiliency to applied load, ultimately, injury occurs when a load exceeds a tissue's tolerance.

Disc height loss has the potential to be a primary factor in the progression of spinal degeneration. For example, disc height has been touted as a major component for the initiation of pathological and degenerative changes to the spine. Pathologic, non-recoverable disc height loss can occur through herniation or endplate fracture and could result in a degenerative cascade of injury that eventually involves the facet joints, narrows nerve root space, and increases stress at adjacent segments. What is not known is the degree to which disc height affects the degenerative cascade; that is, there is no quantitative data outlining the progression of mechanical consequences at adjacent segments or at the injured segment itself during disc height loss. Further, the degree to which restoring disc height, if even possible, will reverse the process of degeneration is not entirely clear. There is data which suggests that nucleus replacement can restore stress distributions within an injured disc, but the extent of repair material survivability is unknown. Finally, clinical categories of measuring spinal degeneration are based on visual cues and features from medical imaging. Understanding the links between joint visual cues and aberrant movement may help to guide clinical practice; researchers will gain greater insight into the mechanical consequences of anatomical features associated with degeneration.

This thesis was comprised of three studies. Study 1 examined the effect of disc height loss and subsequent restoration using an injectable hydrogel on the relative kinematics of a segment with height loss and an adjacent segment. It was found that disc height loss produced

an immediate effect, where relative angular displacement was reduced in the segment with height loss and increased in the adjacent segment. Restoring disc height with an injectable hydrogel brought the relative angular displacement of both segments back to their initial values. This study is the first of its kind to examine the immediate effects of disc height loss via loss of nucleus pulposus and restoration. Whether these effects are as clear *in-vivo* remains to be seen.

Study 2 evaluated the efficacy of a novel repair strategy to restore the mechanical profile of a spine segment with disc height loss initiated via compressive fracture. The strategy employed the use of PMMA injected into the vertebral body to attempt to seal a fracture from above the disc, and an injectable hydrogel to restore disc height. The use of PMMA was found to restore the compressive stiffness of the injured segment to within approximately 20% of its initial value, while the use of the injectable hydrogel restored the sagittal plane rotational stiffness to within approximately 50-80% of its initial value. After further repetitive compression had been applied to the spine segment however, the restorative influence of both interventions was lost in terms of rotational and compressive stiffness. It was found that large cracks in the endplate prevented the hydrogel from being contained and quickly returned the segment back to its injured profile. Future efforts at restoring the disc while maintaining its anatomical structures need better methods of creating a sufficient seal inside the disc to allow it to re-pressurize and sustain the stresses encountered on a daily basis.

Study 3 employed the use of a novel spine tracking algorithm developed as part of this thesis to evaluate sagittal plane cervical spine motion of a series of patient image sequences who had experienced trauma and had a chief complaint related to their neck, head, or shoulders. Some patients had evidence of disc height loss while others did not. Clinical subgroups were created that classified disc height loss as either moderate/severe (3 cases), mild (8 cases), or non-existent (9 cases). When normalized angular displacement of the C5/C6 segment in a group with moderate to severe height loss was compared to the same level in a

group with no height loss, there was a statistically significant difference in angular displacement between the two groups ($p = 0.004$). Angular displacement at C5/C6 was 20.2% ± 2.3% of total measured neck angular displacement in the moderate/severe height loss group compared to 30.6% ± 4.0% of total measured neck angular displacement in the group without height loss. Based on the limited sample size of this study it would appear that disc height loss creates a loss in range of motion. This work has further revealed the heterogeneous nature of individual segmental movement patterns. However, in the group without height loss, there was a systematic trend seen of an increasing angular displacement with descending segmental level. This was not observed in those with moderate to severe disc height loss.

The broad implications of this work are that disc height loss influences spine kinematics, which has implications with respect to further injury propagation through the spinal linkage. Angular displacement of a spine segment appears to be governed by its local stiffness. Restoration of disc height under real injury scenarios is a difficult proposition and any attempts at repair need to sufficiently seal the disc space and prevent extrusion of nucleus pulposus or hydrogel-based implants. We now appreciate the difficulty in this objective. Further, repeating the mechanism of injury will reduce the mechanical effects of the restorative intervention, preventing this is highly important.

Acknowledgements

I wish to thank my supervisor Dr. Stuart McGill for his advice, encouragement, mentorship, support, and most importantly, his friendship. I would also like to thank my committee members Dr. Jack Callaghan, Dr. Richard Wells, Dr. Wayne Brodland for their advice and support. Thank you to my external committee member Dr. Jim Dickey for the time and input you have dedicated.

I would like to express thanks to my host advisors in Bristol, Dr. Michael Adams, and Dr. Trish Dolan who were kind enough to allow me to visit and perform research in their lab during my PhD. Your insights and support have helped to shape me into who I am as a scientist.

Thank you to my collaborators, Dr. Jennifer Vernengo for supplying hydrogel and providing valuable expertise in its use, Dr. John W. Baird for providing use of your clinic space, equipment, time, and expertise, and Dr. Peter Stevenson for helping to obtain equipment for vertebroplasty. Without your help this work would have been impossible to complete.

Thank you to Jim Veldhuis, your programming expertise and key role in developing the tracking algorithm was invaluable, and its creation would not have been possible without you. Your dedication of time, and infinite patience in helping me with analysis techniques will not be forgotten.

Thank you to Jeff Rice, your support and assistance with equipment and instrumentation have made this work possible. Thank you to Marg Burnett and Denise Hay, your support and the work you do for all grad students is beyond measure.

Thank you to my parents, your love and support have helped me to persevere, your patience and values have shaped me into who I am today.

Special thanks to Ed Cambridge, Jordan Cannon, and Natalie Sidorkewicz. I am proud to call you friends.

Special thanks to Jaimie Kazienko, your unquestioning love and support has given me a brighter outlook on everything.

Table of Contents

List of Figures

List of Tables

Chapter 1: Description of Thesis

This document first provides an introduction to the issues (Chapter 2) where the role of disc height loss is placed into context with respect to changes in spine kinematics and subsequent impact on injury mechanisms. Further, the specific projects and global objectives of this thesis are also presented. A review of the literature is presented in Chapter 3, while Chapter 4 outlines Study 1, which examined the effect of disc height loss on the kinematics of an adjacent segment using an *in-vitro* porcine model. Study 2 is presented in Chapter 5 which examined the efficacy of a novel surgical approach in restoring the mechanics of a compressively injured porcine spine segment. Chapter 6 contains Study 3 which involved characterizing the effect of disc height loss on the segmental kinematics of the cervical spine *in-vivo*. Chapter 7 discusses and integrates the results of the four studies and summarizes their scientific contribution.

Eight appendices are contained in this thesis work. Appendix A outlines the development of the novel tracking method used to track segmental spine motion *in-vivo*. Appendix B outlines the specific methodology utilized to obtain relative joint angles. Appendix C outlines the calculations for obtaining relative joint angles for Study 3. Appendix D contains the consent forms signed by patients whose data was used for Study 3, additional information on the patients used in Study 3, and a detailed outline of the calculation of disc height index. Appendix E highlights the work I performed at the University of Bristol under Dr. Michael Adams and Dr. Patricia Dolan, and contains a brief comparison of human lumbar spines and porcine cervical spines. Appendix F discusses the mechanical implications of using multi-segmented porcine cervical spine specimens in the servohydraulic tissue testing system. Appendix G contains a comprehensive set of time-history graphs used for the patient validation tracking

stage of Appendix A. Appendix H contains a comprehensive set of neutral posture radiographs and relative spine joint motion time-histories for the patient cases examined in Study 3.

Chapter 2: General Introduction of Issues Linked to Disc Height Loss

The intervertebral disc is a complex mechanical structure with hydraulic and deformable solid properties. All components contribute to the overall structural integrity necessary for proper function. When mechanical overload occurs in a disc, such as an endplate fracture or herniation for example, structural integrity of one component can be compromised, thereby affecting the functioning of all other components. Loss of disc height is the variable of interest in this work that has potential consequences with respect to altering the mechanics of other segments. Through this mechanism, the annulus bulges (Brinckmann and Horst, 1985) and other structures such as the facets assume an increased role in weight-bearing (Arbit and Pannullo, 2001, Gotfried et al., 1986). This cascade of events influences mechanical behaviour at adjacent levels, given that they react as members of a linkage. Mechanical damage as been posited as the primary factor that results in degeneration and dysfunction of a disc (Adams et al., 2015). Regardless of the primary driver of degeneration (endplate-driven or annulus-driven) (Adams et al., 2015), the common factor is disc height loss. This could be a cause or consequence in terms of both mechanism and clinical implications.

Further biological consequences may result through loss of disc height. There is a delicate cellular environment within the intervertebral disc that prevents dysfunctional growth of neural (Johnson et al., 2002) and vascular (Johnson et al., 2005) structures. Loss in intervertebral disc pressure (which occurs during height loss) has been shown to result in the infiltration of blood vessels and nerves (Stefanakis et al., 2012), a potential pathway to pain and sensitization. This may be due to nerves and blood vessels not being able to survive in the extreme pressure of the intact disc, but when pressure is lost in some regions, they are able to infiltrate.

While there are observed diurnal variations in disc height (Healey et al., 2011), this thesis addresses pathological disc height, or disc height that is unrecoverable. Height lost through structural failure at some point in the disc is what leads to degenerative change (Adams and Roughley, 2006), and the work here attempts to describe the biomechanical consequences of this.

There are many ways in which the disc can become injured, but the most succinct explanation is that injury to the spine occurs when a load exceeds a tissue's tolerance (McGill, 2007). Injury to the endplate, annulus, or nucleus itself can result in dysfunction of the spine and place further risk in the progression of injury. The spine functions as a linkage, and so aberrant loading or a change in how load is distributed at one segment through disc height loss may affect how it is distributed at another segment. Prevention of disc height loss, or restoration of disc height would then reduce the risk to adjacent segments and possibly interrupt the cascade that eventually causes disruption to other structures.

Invasive approaches to disc restoration involve disc replacement, nucleus augmentation, annular repair, and vertebroplasty. When surgery has been deemed to be the most appropriate route to repairing the defects caused by disc injury, total disc replacement has become a mainstream option. A developing technique is the use of injectable hydrogels which are designed to mimic the nucleus pulposus and maintain the majority of the disc's original anatomy as opposed to total disc replacement. Evaluation of the mechanical outcomes to disc height restoration through novel injectable hydrogels has been rare, but preliminary research does support its benefits (Dahl et al., 2010, Balkovec et al., 2013).

Further work is needed to fully quantify the processes that occur due to disc height loss. Observation of the timeline and an attempt to characterize a 'typical' process of degenerative change with disc height loss has not been done. An observation of how the spine functions under both normal and perturbed situations could begin to parse out exactly what role disc height has in the kinematics of the spine. Part of this task would then be to observe how disc

height restoration affects the mechanics of an injured disc and the degree to which such an intervention could prevent further cascade of injury. Finally, this all must be distilled in a manner that frontline healthcare practitioners can put into use to deliver better levels of care to their patients.

This thesis is comprised of three data collections:

1. Characterizing the kinematic outcomes on injured and adjacent segments during disc height loss.

2. Investigating the efficacy of a combined surgical approach to restoring disc height and joint mechanics of the intervertebral disc.

3. Quantifying the impact *in-vivo* of pathologic disc height loss through examination of the kinematic response in those with flattened cervical spine discs.

This document is organized to review the literature relevant to the mechanical consequences of disc height damage. Then, the literature is summarized to create a statement of what is known and what is not. Finally, the experiments are described.

The following flow chart is intended as a general overview of how all three studies integrate to form the overall theme of the thesis:

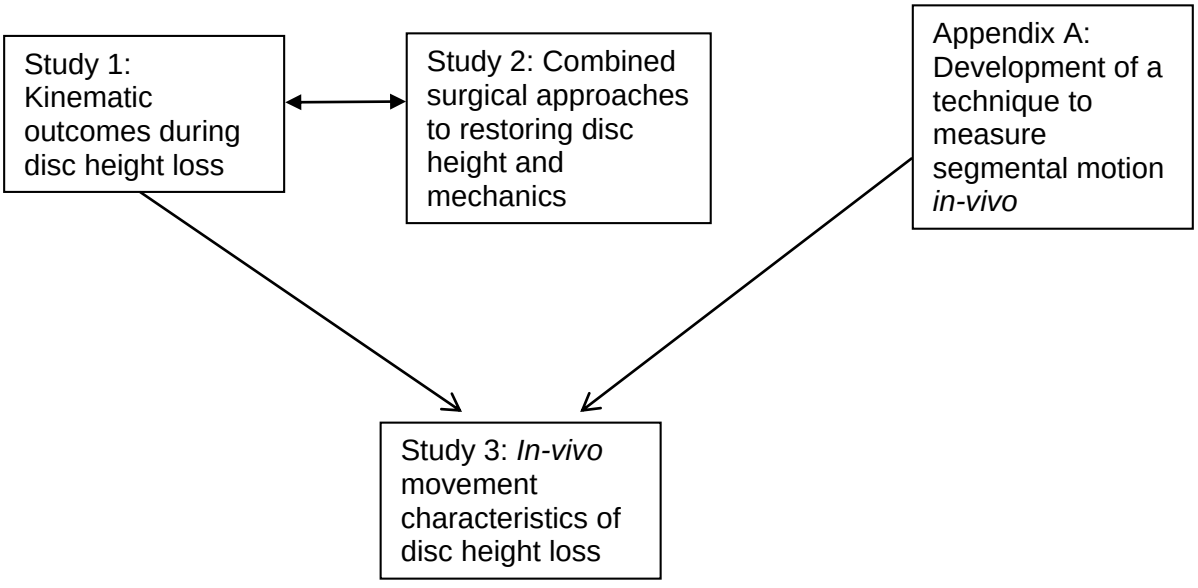

2.1 Rationale and Justification for This Thesis:

The influence of disc height loss and restoration of this loss on normal function remains unknown. What is known is that it appears to be an important element in exacerbating further progression of injury, and therefore warrants further investigation. Disc height is a simple and easily identifiable feature to examine on medical imaging for clinicians with expertise in treating the spine. Identifying the link between disc height loss and mechanical function will begin to further understanding in methods of repair and help to influence clinical practice. Thus, the following three studies were performed:

1. Characterizing the kinematic outcomes on injured and adjacent segments during disc height loss.
2. Investigating the efficacy of a combined surgical approach to restoring disc height and joint mechanics of the intervertebral disc.
3. Measuring the effect of disc height loss on injured spines *in-vivo*.

Study 1 identified the effect of disc height loss at one segment on an adjacent segment. It quantified adjacent segment perturbation through kinematic measurements. This study tested the following hypotheses:

1. Disc height loss will result in a lower relative angular displacement by the injured disc.
2. Disc height restoration via hydrogel injection will return injured discs to their initial relative levels of angular displacement.
3. Disc height loss in the upper and lower discs will produce the same kinematic effect.

Study 2 identified how disc height restoration restored the stiffness characteristics of a compressively damaged spinal segment. It determined the efficacy of combining two surgical

modalities (nucleus restoration via hydrogel injection and vertebroplasty) on restoring mechanical integrity to an injured spine. Study 2 addressed the following hypotheses:

1. Hydrogel injection will alter rotational stiffness levels from the compressively fatigued state.

2. PMMA injection will alter compressive stiffness levels from the compressively fatigued state.

Study 3 examined cervical spine motion *in-vivo* under fluoroscopic imaging in cases with and without disc height loss. This study identified the variety of movement strategies that can occur with disc height loss and discerned a common response that occurs with disc height loss *in-vivo*. This study tested the following hypotheses:

1. Disc height loss will cause diminished segmental mobility at the affected segment.

2. Some individuals without disc height loss will also exhibit diminished mobility at one segment as well as segments that exhibit enhanced mobility.

Chapter 3: Literature Review

3.1 Functional Anatomy of the Intervertebral Disc

The elements of the intervertebral disc function together to provide mobility to the spine, load transferring properties that span the spinal column, and cellular nutrition. For convenience, the disc can be thought of as three separate elements; a nucleus pulposus which is located in the center of the disc, an annulus fibrosus surrounding the nucleus pulposus, and two vertebral endplates consisting of cartilage located superiorly and inferiorly to the nucleus pulposus and the annulus fibrosus (Bogduk, 2005). A human lumbar intervertebral disc is approximately 9-17mm in height, thoracic discs are approximately 5mm, and cervical discs approximately 3mm (Shapiro and Risbud, 2014) which gradually decreases with daily activity as water migrates outwards due to elevated hydrostatic pressure from joint loading (Adams et al., 2006a).

Together, all the components of the intervertebral disc comprise a structure that is able to facilitate bending in any direction, gliding and twisting movements, and allow weight-bearing (Bogduk, 2005).

3.1.1 Nucleus Pulposus

The nucleus pulposus (nucleus) is a gelatinous structure that is located in the center of the disc and surrounded by the annulus fibrosus (Coventry et al., 1945). It is composed primarily of water, proteoglycans, and type II collagen (Adams et al., 2006a). Proteoglycans, which comprise 50% of the dry weight of the nucleus pulposus have the ability to hold large amounts of water, allowing it to maintain mechanical integrity while transferring compressive load between vertebral bodies and acting to brace the annulus (Adams et al., 2006a).

A proteoglycan is a unit that consists of a protein core with glycosaminoglycan (polysaccharide) side chains (Esko et al., 2009); due to their high polarity, these side chains are very hydrophilic and readily attract water. Aggrecan, the primary constituent proteoglycan of the nucleus (Roughley, 2004) has side chains of chondroitin sulfate and keratin sulfate (Kiani et al., 2002). It forms large aggregates with hyaluronan (Watanabe et al., 1997), where many molecules of aggrecan are covalently bound and stabilized via link protein (Neame and Barry, 1993). With age, the levels of these aggregate molecules decrease (Johnstone and Bayliss, 1995), thereby increasing proportions of non-aggregate proteoglycans (Oegema et al., 1979). The consequences of this degradation are not entirely clear given that the non-aggregated proteoglycans can still contribute to the water retaining properties of the nucleus, as they cannot escape from the central disc space under non-injured conditions (Roughley, 2004). The nucleus also contains small amounts of lumican, fibromodulin (Sztrolovics et al., 1999), versican (Sztrolovics et al., 2002), perlecan (Smith et al., 2009), lubricin (Shine et al., 2009), chondroadherin (Haglund et al., 2009), decorin, and biglycan (Singh et al., 2009). Water content is highest in the nucleus and decreases in the annulus (Antoniou et al., 1996) with regions of lower proteoglycan content (and by extension-water content) within the nucleus itself being associated with aging (Urban and McMullin, 1988) and higher levels of degeneration (Iatridis et al., 2007, Antoniou et al., 1996).

The nucleus, despite being viscous during the juvenile stages of development is not without significant structural composition. Its behavior is unique in that its material properties are load-rate dependent, behaving more like a viscoelastic solid under dynamic conditions, and more like a fluid under transient stress (Iatridis et al., 1996). Type II collagen in the nucleus is arranged in a random fashion (Inoue, 1981) along with the short-chain highly branched collagen VI (Roberts et al., 1991a), fibrillar collagen V, and fibril-associated collagen IX (Nerlich et al., 1998, Nerlich et al., 1997). Type IX collagen is found cross-linked in articular cartilage perpendicularly to the long-chain fibrillar type II collagen (van der Rest and Mayne, 1988).

Conflicting evidence exists however, with respect to how common type IX collagen is in the human disc (Roberts et al., 1991b). Both studies find agreement in that it seems to be associated with sites of damage. A network of elastin within the extracellular matrix has also been demonstrated in a bovine tail model, suggesting a possible role in structural connections and cellular function (Yu et al., 2007). In light of the evidence for its profound structural elements, the nucleus is clearly unique and exhibits properties beyond that of a simple fluid.

The nucleus is a remnant of the notochord in human infants (Walmsley, 1953) and as development occurs, notochord cells are lost and the nucleus becomes much more viscous and firm, still producing proteoglycans, but also higher levels of collagen (Urban et al., 2000). As aging continues, water, proteoglycans, and type II collagen levels all continue to decrease (Murakami et al., 2010). While some research maintains that the nucleus is simply an isolated entity (Inoue, 1981, Inoue and Takeda, 1975), other studies suggest a disorganized attachment between nucleus fibers and the endplate (Roberts et al., 1989), with more recent research describing this interface as being much more highly organized, at least in sheep (Wade et al., 2011). Additionally, integration of the nucleus with the annulus fibrosus has also been identified with this same animal model (Wade et al., 2012).

The hydrophilic nature of the nucleus via its proteoglycan constituents dictates that it has an inherent osmotic pressure (Urban et al., 1979). The negatively charged glycosaminoglycan side chains create a fixed charge density within the nucleus that causes the disc to swell as a result of fluid absorption (Urban and Maroudas, 1981). Positively charged sodium ions are initially drawn into the negatively charged disc matrix via simple diffusion, with a preference for entry into regions of the disc with a higher concentration of glycosaminoglycan side chains (Urban et al., 2000). With a higher concentration of these positive cations inside of the disc compared to outside, water is drawn in via osmosis (Cortes and Elliott, 2014). As a disc swells it induces tensile stress and stiffness in the disc (Cortes and Elliott, 2014). Swelling will stop when the stress created by the osmotic pressure is in balance with the external stresses

resisting its expansion (Broom and Marra, 1985), which in the case of the disc would be the stress created by tension in the annulus. Stress causes fluid to be expelled from the disc and increases the effective concentration of proteoglycans, enabling the disc to re-imbibe fluid when unloaded (Urban and McMullin, 1988). This osmotic pressure is dependent on the concentration of disc proteoglycans, and a loss decreases the ability of the disc to remain hydrated (Urban and McMullin, 1988).

Movement of the spine tends to cause the nucleus to migrate; with flexion being associated with posterior movement and extension causing anterior movement (Fennell et al., 1996). Mobility of the nucleus has been described as tethered, with organized nodes and streaming fibers of the nucleus into the cartilaginous endplate providing some element of support (Wade et al., 2011). Similar sites of attachment are also evident at the innermost fibers of the annulus fibrosus (Wade et al., 2012). The pressure generated by the nucleus allows it to withstand compressive loading (Hukins and Meakin, 2000), with different body orientations being associated with different levels of compressive load (Nachemson, 1981, Wilke et al., 1999).

3.1.2 Annulus Fibrosus

Surrounding the nucleus is the annulus fibrosus (annulus). It is made up of individual collagenous lamellae that layer concentrically around the disc (Adams et al., 2006a) with outer lamellae having the greatest thickness and subsequent layers decreasing inwards (Inoue and Takeda, 1975, Inoue, 1981). The number of lamellar layers varies throughout regions of the disc with a general range of 15-25 distinct layers and a higher number in the anterior region compared to the posterior (Marchand and Ahmed, 1990). Further, the posterior layers have a tendency to be thinner than the anterior layers (Inoue and Takeda, 1975). Each additional lamella orients itself in an oblique fashion compared to the last layer (Bogduk, 2005), with a trend for the angle of insertion of each lamella to decrease moving towards the center of the

disc with respect to the vertical axis (Cassidy et al., 1989). The annulus is made up of type I and type II collagen (Eyre and Muir, 1977), with the periphery of the annulus consisting exclusively of type I collagen, and the levels of type II collagen increasing closer to the center of the disc (Schollmeier et al., 2000). This distribution is not uniform, but rather, there is a higher level of type I collagen at the anterior of the disc and a thinning towards the posterior (Schollmeier et al., 2000). Additional types of collagen in the annulus include types III, V, VI (Nerlich et al., 1998, Roberts et al., 1991b), IX (Nerlich et al., 1998, Nerlich et al., 1997), and X (Nerlich et al., 1997). With age, type I collagen infiltrates further into the inner lamellar layers (Schollmeier et al., 2000). The annulus also contains a network of elastic fibers thought to aid in controlling deformation and re-orientation of the collagen fibers, preventing excessive damage (Smith and Fazzalari, 2009). The nature of the annulus allows it to facilitate motion of the disc in any direction while at the same time resisting excessive sliding and twisting movements based on the tensile properties of the individual fibers (Adams et al., 2006a). Lamellae of the outer annulus fibrosus attach themselves to the bony endplate and vertebral epiphysis via strong Sharpey's fibers (Johnson et al., 1982, Green et al., 1993). More centrally, collagen fibers of the inner annulus and nucleus coalesce to insert obliquely into the cartilaginous endplate (Bogduk, 2005). Research using an animal model has also identified structural bridging elements that assist with cohesive attachments between lamellae (Pezowicz et al., 2006).

In addition to its collagenous components, the annulus also has proteoglycan constituents which like the nucleus, consists mainly of aggrecan (Johnstone and Bayliss, 1995). Additionally, versican and perlecan are present in the annulus of the fetal spine (Smith et al., 2009). Lubricin has also been shown to be part of the annulus with concentrations diminishing moving outwards towards the periphery (Shine et al., 2009). Aosporin has been identified primarily in the outer annulus, with higher levels being associated with greater levels of degeneration (Gruber et al., 2009). Decorin, lumican, fibromodulin, and biglycan are also small

proteoglycans present in the annulus, with their relative concentrations dependent on age (Singh et al., 2009).

Both the annulus and nucleus exist in a symbiosis of sorts; with the pressurized nucleus bracing the annulus and preventing it from buckling under compressive load, and the annulus containing the nucleus and preventing it from extruding out of the disc (Adams et al., 2006a). In an ideal scenario, the nucleus is fully contained by the annulus, but repetitive stress such as flexion under a compressive load (Balkovec and McGill, 2012, Scannell and McGill, 2009), or repeated flexion and extension under compressive load (Callaghan and McGill, 2001, Balkovec and McGill, 2012) have all been shown to cause herniation of nuclear material. Under these conditions nuclear material passes through breaches in delaminated annulus collagen which appear to develop as a consequence of repeated stress-strain reversals (Tampier et al., 2007). The annulus derives much of its strength from connections between collagen and the surrounding matrix of proteoglycans instead of connections from endplate to endplate (Adams and Green, 1993). Detailed research on the micro-anatomy of collagen fibers in the disc has revealed that they form crosslinks with each other that decrease in number with aging (Pokharna and Phillips, 1998). The annulus behaves more like a chopped fiber composite (Hukins et al., 1984) and remains strong provided the individual reinforcing fibers are of sufficient length.

Studies on the material properties of the annulus under uniaxial tensile stress-strain loading have shown that initially it exhibits a distinct toe region, followed by a heel region and linear region (Guerin and Elliott, 2007). Upon closer examination of the microstructure of individual lamellae, this relationship is very clearly explained. Un-stretched collagen fibers of the annulus exhibit a characteristic crimp - with the angle of crimp increasing moving from the disc periphery inwards (Cassidy et al., 1989) - and there is very little resistance to their initial straightening. As more fibers straighten, the overall annular stiffness increases as it resists tensile load (Cortes and Elliott, 2014). Annulus fibers also have a tendency to re-orient to the

direction of the loading axis when subject to tension in a single axis (Guerin and Elliott, 2006). Whether uniaxial material tests accurately mimic loading of the annulus *in-vivo* is debatable however; biaxial tensile testing may more closely relate to what is naturally seen (Gregory and Callaghan, 2011).

The annulus has been shown to have anisotropic properties, with permeability in the radial direction being greatest in non-degenerate discs (Gu et al., 1999). Further, the anisotropic nature of the annulus extends to its mechanical properties, withstanding far greater stresses when loaded circumferentially in tension as opposed to axially (Guerin and Elliott, 2007).

3.1.3 Endplate

The endplate is a cartilaginous structure present at the upper and lower portions of the disc, encapsulating it at these ends (Bogduk, 2005). The endplates are attached to the subchondral bone of the vertebral bodies (Adams et al., 2006a) and surrounded by the ring apophysis (Bogduk, 2005). The cartilaginous endplate contains type II (Nosikova et al., 2012) and type X collagen (Aigner et al., 1998), with the latter being associated with cartilage calcification (Kirsch and von der Mark, 1991). The endplate is also rich in proteoglycans with the central region having higher levels of proteoglycans and lower levels of collagen and the opposite being the case near the outer annulus (Roberts et al., 1989). These proteoglycans appear to have a critical role in the containment of other proteoglycans in the nucleus and in nutrient transport (Roberts et al., 1996).

From the disc side, the hyaline cartilage of the endplate in an animal model has been shown to integrate with the annulus and nucleus (Wade et al., 2011). The outer lamellae of the annulus insert into the bony endplate and vertebral epiphysis via strong Sharpey's fibers (Johnson et al., 1982, Green et al., 1993). Centrally, collagen fibers of the inner annulus and nucleus blend with the cartilaginous endplate via oblique insertions (Bogduk, 2005).

Microscopic perforations in the endplate (Benneker et al., 2005, Rodriguez et al., 2011) provide a pathway for nutrients to flow into the disc and waste products to flow outwards (Urban et al., 1977). Only 0.6-1mm thick (Roberts et al., 1989), the endplate is a delicate structure that experiences tensile strain (Fields et al., 2010) and is easily damaged (Adams et al., 2006a). It is often the first structure to be injured under high compressive load (Brinckmann et al., 1989), although these characteristics can change under varying loading rates (Yingling et al., 1997). Endplates show a characteristic deflection behavior under compression with these sites of deflection being associated with structural weakness and likely regions for failure (Jackman et al., 2014). Unsurprisingly, the endplate becomes weaker with age and degeneration (Hansson et al., 1987), further augmented by changes to the underlying trabecular bone from a more closed structure with horizontal struts to one with more open rod-like struts that lack horizontal connectivity (Ferguson and Steffen, 2003).

Interestingly, accounts of double endplates in some discs have been noted, where there is a second layer of bone present (Rodriguez et al., 2012, Zhao et al., 2009). This distinct type of endplate has been associated with a thinner superficial layer, higher glycosaminoglycan content, higher permeability, and it has been suggested that they promote significant benefits in preventing degenerative changes of the disc (Fields et al., 2012).

3.1.4 Nerve and Vascular Supply

The vascular components of the intervertebral disc are unlike other structures in the body; with the disc itself being completely free of arteries, veins, or capillaries (Hassler, 1969). Under non-pathologic conditions, aggrecan in the nucleus prevents growth of nerves (Johnson et al., 2002) and endothelial cells (Johnson et al., 2005). Rather, there is a dense capillary network surrounding the disc (Hassler, 1969), allowing any nutrients to reach the disc through passive diffusion at the endplate (Rudert and Tillmann, 1993). Changes to the structure or

properties of the endplate, subchondral bone, or blood supply can affect the nutrition of the disc and produce further degenerative changes (Urban et al., 2004).

Nerves are found on the outer-third of the annulus; The disc is innervated anteriorly, posteriorly, and laterally, with its nerve supply derived from nerve roots off the spinal cord (Adams et al., 2006a, Bogduk, 2005). Anterior and lateral innervation to the disc is via a plexus of nerves derived from the sympathetic trunks and branches of the grey rami communicantes, while posteriorly the annulus receives its innervation from a plexus originating from the sinuvertebral nerves (Bogduk, 2005, Adams et al., 2006a). The disc is also innervated above the endplate with entry through the basivertebral foramen (Bailey et al., 2011). The origin of these nerves is most likely via the sinuvertebral nerve, where they are clustered primarily above the nucleus region (Fagan et al., 2003) in the center of the vertebral body and are thought to play a nociceptive role (Bailey et al., 2011). Damage such as annular fissures provide an environment for the ingrowth of nerves and blood vessels (Stefanakis et al., 2012). This may be due to nerves and vascular vessels not being able to survive in the extreme pressure of a healthy nucleus. Loss of this pressure may allow the in-growth of these vessels (private communication with Professor Mike Adams, 2015). Degenerated nucleus pulposus cells also have been shown to release neurotrophic growth factor and brain-derived neurotrophic factor, thought to further enhance neural growth within the disc (Richardson et al., 2012).

3.1.5 Cellular Environment of the Intervertebral Disc

Cells of the intervertebral disc have yet to be fully characterized, rather, they are described as chondrocyte-like in the nucleus (Trout et al., 1982) and fibroblast-like in the annulus (Walmsley, 1953). During the first few years of life there are notochord cells in the nucleus which are rapidly lost and replaced by mature cells (Peacock, 1952). In numerous animal species, notochord cells are maintained throughout life, with the exception of cows (Alini et al., 2008), sheep, and chondrodystrophoid dogs (Hunter et al., 2004). Cells of the

intervertebral disc produce the constituents required for its functioning. Dysfunction of the cells can result in a loss of this production or changes that shift the balance of the disc environment to one that favors a net catabolic breakdown of tissues (Risbud and Shapiro, 2014). A considerable effort has therefore been put into identifying ways to restore or replace dysfunctional cells and rebuild the non-pathologic environment of the intervertebral disc (Benneker et al., 2014).

The environment that the cells are required to exist in is harsh, with high pressure (Nachemson, 1981) and low levels of oxygen (Bartels et al., 1998). As a result, the cells have developed adaptive capabilities to survive under these conditions. Use of hypoxic inducible factors, which are transcription factors, helps cells of the nucleus to withstand and thrive within their natural environment (Chen et al., 2014); loss of these has been shown to result in a complete lack of development of the nucleus (Merceron et al., 2014), which would have profound mechanical consequences to spine function. Cells in the disc utilize glycolytic pathways to produce energy (Holm et al., 1981), and efficiently reuse unnecessary constituents within their cytosol to produce critical proteins (Xu et al., 2014). One drawback is that the environmental balance required for cellular survival is extremely delicate, with any factor that blocks the passively diffusing nutrients required being able to severely alter their viability (Urban et al., 2004). Mechanically-induced structural damage to the intervertebral discs has the potential to alter the microenvironment and produce damage on a scale that the intervertebral disc cells simply cannot keep pace with (Adams and Dolan, 1997). This augments any mechanically induced damage and could potentially lead to a spiral of latent dysfunction with further structural and neural consequences.

3.2 Architectural and Functional Differences between the Cervical and Lumbar Spine

Since some experimentation in this thesis involved both the cervical spine and the lumbar spine, they are contrasted here. While part of the same structure, the cervical and lumbar spines possess anatomical and functional differences. Vertebral bodies of the cervical spine are smaller and have long spinous processes with respect to the size of the vertebra itself (Adams et al., 2006a). Compared to the lumbar spine, the nucleus of the cervical spine also contains a fibrocartilaginous core (Mercer and Bogduk, 1999), and the discs overall are relatively large in terms of height compared to the surrounding bony elements (Adams et al., 2006a). The cervical spine has a high range of motion (Lansade et al., 2009), which is desirable for the neck and is reflective of the large variety of head postures that can be adopted. A more fibrous nucleus could potentially reduce the propensity for herniation, although cervical disc herniations do occur (Wong et al., 2014). Further, the posterior annulus is limited to only a few layers (Mercer and Bogduk, 1999), making a more fluid-like nucleus undesirable, given the presumably higher propensity for rupture through the posterior annular layers with a nucleus that is less tethered within the disc space. The annulus also does not layer in a criss-cross fashion, but rather, orients mostly towards the anterior portion of the superior vertebra (Mercer and Bogduk, 1999).

Facet joints of the cervical spine also have an orientation approximately 40° to the vertical (Nowitzke et al., 1994) (biological average), whereas in the lumbar spine they are nearly parallel with the vertical axis (Bogduk, 2005). While limiting rotation movements in the lumbar spine (Bogduk, 2005), the facets in the cervical spine facilitate rotation and gliding of one vertebra over another (Nowitzke et al., 1994). In addition to the facets, the cervical spine also has Luschka joints, which are formed by uncinate processes on the vertebra above and the

uncus on the vertebra below (Bogduk and Mercer, 2000). These joints modify axial rotation of one cervical vertebra over another and help to guide sagittal plane movements (Bogduk and Mercer, 2000).

Despite these differences, the discs of the cervical spine still act as a mechanical fulcrum for relative rotations of vertebral bodies, just as they do in the lumbar spine. In this fashion, the cervical and lumbar spines are relatable in terms of overall trends and functional changes during disc height loss. While the details of their functional differences do not allow for direct comparison, relating gross changes in disc height between the cervical and lumbar spine is appropriate when caution is used to not directly relate specific values, but rather overall approximate trends.

3.3 Perturbed Mechanics and Injury to the Intervertebral Disc

There are numerous factors that can contribute to a disc failing to function in its intended manner. Physical damage (Adams et al., 1993), alterations in fluid content (Andersson and Schultz, 1979), abnormal growths (Al-Rawahi et al., 2011), and repetitive loading (Callaghan and McGill, 2001) can all change the mechanical function of the intervertebral disc.

3.3.1 Perturbations and Injury to the Nucleus Pulposus

Primary constituents of the nucleus are proteoglycans and water (Iatridis et al., 2007). Given the role of the nucleus in reducing radial bulge of the annulus (Brinckmann and Grootenboer, 1991, Meakin et al., 2001), an injury to the nucleus pulposus could be classified as an event which does not permit it to perform this role. Increased compressive loading has been shown to induce apoptosis within the nucleus cells (Lotz et al., 1998, Lotz and Chin, 2000), preventing the production of proteoglycans, and therefore reducing the ability of the disc to retain water (Adams et al., 2006a). Cells of the intervertebral disc, which produce its

constituents that dictate its mechanical properties respond to mechanical loading (Korecki et al., 2008). There exists an optimal loading region to the disc that could aptly be described as a U-shaped function, too much or too little load and catabolic processes could take over (Walsh and Lotz, 2004). Disc cells respond to sub-optimal conditions through the release of proteinases and cytokines. Common proteinases include metalloproteinases (MMPs) and a disintegrin and metalloproteinase with thrombospondin motifs (ADAMTS) (Sztrolovics et al., 1997) while the inflammatory cytokine response is dominated by TNFα and interleukin-1β (Wang et al., 2011). Proteinases cleave proteoglycan aggregates which increases the chances for them to escape from the disc space (Melrose and Roughley, 2014). Presumably, the presence of a mechanically induced injury such as an annular fissure or endplate fracture would facilitate this process. Loss of proteoglycans results in a decreased fixed charge density in the nucleus, which reduces its osmotic swelling potential and affects its ability to retain water and transmit load evenly across the adjacent endplates (Melrose and Roughley, 2014).

Removal of nucleus material such as during a discectomy procedure results in a loss of disc height and pressure, and an increase in the radial bulge of the disc (Brinckmann and Grootenboer, 1991). This has the potential to affect other tissues as well, such as increasing the load on the posterior elements of the spine (Dunlop et al., 1984) or an increased disc bulge impinging posterior nerves (Brinckmann and Grootenboer, 1991). Without a sufficient amount of nucleus located in the disc, compressive loads cause portions of the annulus to bulge inwards (Meakin et al., 2001). This is presumably because there is not enough pressure generated by the nucleus to act as a sufficient brace; intrinsic disc pressure has been shown to act as a barometer for degeneration grade (Panjabi et al., 1988). Internal disc pressure drops when the nucleus is disrupted but the gradient of pressure across the disc increases which presumably increases the shear load sustained by lamellae of the annulus and contributes to their delamination (Stefanakis et al., 2014). Under normal conditions, the pressure and proteoglycan content in the nucleus inhibits the growth of nerves (Johnson et al., 2002) and

blood vessels (Johnson et al., 2005). When that proteoglycan content is lost and regions of altered pressure exist in the nucleus region, the potential for nociceptive nerve growth is enhanced (Stefanakis et al., 2012). The nucleus is also seen as foreign to the body's own immune system; as a result, breaching of the nucleus outside of the disc space has the potential to result in a response that can result in inflammation and neo-innervation (Repanti et al., 1998).

Under normal circumstances the nucleus braces the annulus and prevents it from buckling while its expansion in the radial direction is consequently resisted by the annulus (Adams et al., 2006a). Together, this creates a structure with inherent stability, and when nuclear material is lost, so is that stability (Cannella et al., 2008).

3.3.2 Perturbations and Injury to the Annulus Fibrosus

The annulus is anisotropic, and its permeability is higher in the radial direction (Gu et al., 1999), making herniation of nuclear material a likely injury under the correct conditions. Repetitive flexion coupled with extension (Callaghan and McGill, 2001, Balkovec and McGill, 2012) in addition to pure repetitive flexion (Scannell and McGill, 2009) and fixed flexion with repeated compression (Adams and Hutton, 1985) has been shown to produce intervertebral disc herniations. The site of herniation has been shown to be determined by the bending axis (Aultman et al., 2005), and the total area/pathway which nuclear material diffuses through has been shown to be dependent on disc shape (Yates et al., 2010). As stress is repeatedly applied to the annular fibres, and the nuclear material is hydraulically pumped towards the posterior of the disc during flexion (Fennell et al., 1996), nucleus infiltrates the individual lamellar layers in addition to travelling through delaminated collagen fibers (Tampier et al., 2007). Interestingly, there is some evidence to suggest that there is far more prolific diffusion of nucleus through the annulus when a cycle of flexion is coupled with extension (Balkovec and McGill, 2012). Presumably, the potential for increased stress on the posterior fibers of the annulus during

extension (Adams et al., 2000b) can induce higher levels of deterioration and therefore ease the tracking of nuclear material through the annulus.

Twisting or the generation of axial torque on its own has not been shown to produce any evidence of disc herniation, however, when coupled with flexion/extension motions, axial twisting as well as static torque (Drake et al., 2005) caused higher levels of radial delamination (Marshall and McGill, 2010, Drake et al., 2005). Clinically, there are various classifications to describe annular disruption via the migration of nuclear material. It is important to use appropriate terms to ensure that results and observations are communicated accurately and understandably. A bulging disc is not considered a herniation and is classified as the presence of disc tissue beyond the periphery of the ring apophysis and covering more than 50% of the circumference (Morgan, 2013). Herniations are classified as local displacements of disc material beyond the normal disc space; they are further sub-categorized as protrusions, extrusions, sequestrations, contained, and uncontained (Fardon et al., 2014). Specific to the annulus, gross injuries to it are in the form of fissures, which are described as either concentric, radial, or transverse (Fardon et al., 2014).

Perturbation of the annulus has also been shown to affect the mechanics of the intervertebral disc. Fissures created in the annulus reduce the stiffness characteristics of the disc (Latham et al., 1994), and similarly, incisions made in the annulus during discectomy increase the motion of a disc under a given moment (Natarajan et al., 2002) and reduce its ability to resist motion (Thompson et al., 2004). Increased motion or translation of a vertebral body or increased bulging of a disc could potentially lead to nerve root impingement (Reuber et al., 1982). Failure of the annulus to contain the nucleus is evident during disc herniation as nucleus works its way through delaminated collagen fibers (Tampier et al., 2007). The implication of this is also a loss in disc pressure and therefore greater annular bulging.

3.3.3 Perturbations and Injury to the Endplate

High levels of compressive load are the primary culprit for endplate injuries (Brinckmann et al., 1989, Yingling et al., 1997). Repeated flexion motions under compressive load have a higher likelihood of resulting in an endplate fracture if the compressive load exceeds 30% of the predicted tolerance (Parkinson and Callaghan, 2009). Anterior-posterior shear loading also has the potential to produce endplate avulsions (Yingling and McGill, 1999). Schmorl's nodes, which is the infiltration of nucleus through small pits the endplate and into the vertebral body (McGill, 2007) are present in a large distribution of age groups and appear to be associated with high levels of repetitive or acute stress (Burke, 2012).

As the weak-point of the intervertebral disc (Adams et al., 2006a), injury to the endplate and the subsequent alterations in mechanical function is a concern. Fracture to the endplate can decrease nucleus pressure by 37% (Przybyla et al., 2006) and unfortunately, is often the first component of the intervertebral disc injured under compression (Brinckmann et al., 1989) with the cranial endplate usually injured before the caudal (Zhao et al., 2009). By comparison, damage to the outer layers of the annulus have only been shown to decrease intradiscal pressure by 1% (Przybyla et al., 2006). Evidence shows that the endplate experiences high tensile strain during compression, given that bone is most susceptible to tensile failure, the endplate is pointed out as the most likely site for failure to first occur (Fields et al., 2010). As with dysfunction of the annulus or nucleus, loss in disc pressure, which accompanies endplate fracture can result in the characteristic bulging of the annulus, loss in the disc's stiffness characteristics, and resistance to motion.

The interface between the hyaline cartilage and the subchondral bone of the endplate has also been implicated as the weak point of the disc in tension (Lama et al., 2014, Balkovec et al., 2015). This is most likely the origin of bone (Rajasekaran et al., 2013) and cartilage (Willburger et al., 2004) fragments found in herniated material in some instances. Exposure of the disc to the external environment via a transverse fissure (or rim lesion) as described has

important implications first to the mechanical integrity of the disc, but also with respect to bacterial infection (Lama et al., 2014).

3.4 The Degenerative Cascade

The degenerative process of spinal injury was first described by Kirkaldy-Willis and Farfan in 1982 where the spine goes through three distinct phases of temporary dysfunction, instability, and then stabilization (Kirkaldy-Willis and Farfan, 1982). Prior to that, Kirkaldy-Willis and colleagues described how injury at one level in the spine led to degenerative changes at subsequent levels over time (Kirkaldy-Willis et al., 1978).

3.4.1 Disc Degeneration

Since the pioneering work of Kirkaldy-Willis and colleagues, the term degeneration as it applies to intervertebral discs has been refined; a proposed definition of disc degeneration is that it is "an aberrant, cell-mediated response to progressive structural failure", and that "a degenerate disc is one with structural failure combined with accelerated or advanced signs of ageing" (Adams and Roughley, 2006).

By altering the structural integrity at one portion of the disc, the load borne by adjacent tissues is increased (Adams et al., 2006a). Disc degeneration has been initiated through mechanical means (Adams et al., 2000a) and it is thought that mechanical factors, more specifically tissue overload, are the primary culprit to disc degeneration (Stokes and Iatridis, 2004). While some epidemiological research points the primary cause of disc degeneration squarely in the favour of genetic predisposition (Battie et al., 2009), this could be a flawed manner of examining the issue. While genetic inheritance may predispose an individual to have certain characteristics related to their spinal tissues, there still needs to be a mechanical event to initiate the injury process. This also adds an element of defeatism towards prevention and

treatment of spine injury, potentially prompting individuals and health care practitioners to passively blame the issue on genetics with no recourse for improving an individual's situation. It also has dangerous implications for the medico-legal sector, neglecting a massive body of literature that shows how mechanical factors dictate injury and could prevent legitimately injured individuals from receiving appropriate compensation.

While it may be genetics that determine the tolerance of an individual to given stresses, it is most likely their environment and loading history that determine future degenerative changes. This research also makes certain assumptions with respect to the relative disparity in the amount of physical loading between occupations. It would be short-sighted to draw comparisons between an office worker and a truck driver and say that one involves fundamentally different physical loads and exposures. Disparity with respect to load exposure with typical manual labour occupations versus occupations with prolonged seating such as office work may not be as great as they are made out to be. With seated posture there is considerable flexion of the lumbar spine (De Carvalho et al., 2010). Given that flexion has been shown to create mechanically-induced injury to the spine (Callaghan and McGill, 2001, Walter et al., 2011), it comes as no surprise that two occupations involving prolonged sitting would develop similar degenerative changes. Genetics in this case would play a role through setting the relative threshold where injury would happen, but rather than spontaneously developing a degenerated disc, mechanical events would have initiated the process.

There are a series of methods which attempt to classify degrees of degeneration within the disc (Adams et al., 1986, Pfirrmann et al., 2001, Thompson et al., 1990) which have all been classified as reliable and reproducible in a clinical setting. Some classification schemes have been based on discograms obtained from cadaveric specimens to classify the degree of a disc's degeneration into one of four grades (Adams et al., 1986), others have used MRI (Pfirrmann et al., 2001), while others have taken a purely observational approach (Thompson et al., 1990). Of particular note is the reproducibility in a clinical setting (Agorastides et al., 2002), allowing

reliable classifications of degeneration grade to take place between different observers. This is an important objective to not only have clinicians agreeing on a given degeneration grade, but also to appropriately prescribe the correct intervention if it is determined to be necessary. What seems to be lacking though, is a functional classification of degeneration grade. While a disc may have a certain appearance, this may not necessarily correlate with its functional abilities and inherent stability characteristics. By targeting degenerative classifications towards function, clinicians could have more success in targeting treatments towards patients and help return them to performing daily activities without perturbation of adjacent tissues through compensatory mechanisms. Targeting a classification scheme towards function could help clinicians answer what a patient can do, what they can't do, and what impairs their progress.

There is a level of ambiguity with respect to disc degeneration, as it is based off of visually observable features (Thompson et al., 1990, Pfirrmann et al., 2001) that would encompass the natural aging process as well as the consequences of injury and not necessarily have any bearing on function or pain. This could help to explain why there exists a host of controversy within the literature on the association of disc degeneration with back pain, and emerging evidence of specific degenerative phenotypes (Adams and Dolan, 2012). Further, disc degeneration or degenerative changes do not necessarily guarantee that an individual will develop painful symptoms or continue to have painful symptoms, so while the level of degeneration may worsen with time, the painful response may diminish. Some research has attempted to debunk that a darkened disc under MRI presents with higher incidences of lower back pain (Bendix et al., 2008). Ultimately however, this work does not show whether the black disc is the cause of pain, the pathology may have manifested in adjacent discs. Recently, attempts have been made to create classification systems with more emphasis on disc height and structural changes that may impact mechanics (Riesenburger et al., 2015). The impact of these structural changes on mechanics remains to be determined.

3.4.2 Sequence of Events in Disc Degeneration

Features evident in disc degeneration can all be induced through mechanical loading (Adams et al., 2010), and mechanical damage has been found *in-vivo* to be associated with degenerative changes (Sharma et al., 2014). Any mechanical alteration to a spinal structure can cause a change in mechanics, but a common occurrence is a loss in nucleus pressure within the disc (Adams et al., 1996). Damage to a vertebral body (Adams et al., 1993) or intervertebral disc herniation (Tampier et al., 2007, Callaghan and McGill, 2001) can result in a loss of nucleus from the center of the disc and alter the load bearing characteristics of the segment as a result of nucleus depressurization (Adams et al., 2000a).

Through alteration in the load bearing characteristics of the disc, the annulus begins to bulge (Brinckmann and Grootenboer, 1991, Meakin et al., 2001) and spinal segment stability is reduced (Zhao et al., 2005). With the loss in disc height associated with this, there is the potential for increased load bearing by the neural arch (Pollintine et al., 2004b); this can potentially decrease bone mass in the anterior portion of the spine and place an individual at greater risk for developing an anterior fracture of the vertebral body (Pollintine et al., 2004a, Adams et al., 2006b).

What remains unknown is to what degree the initial disc height loss associated with an endplate fracture or herniation affects passive tissues at the pathologic segment and at adjacent segments. There is no established “timeline” which outlines the degree of specific mechanical deterioration and loss in function of damaged or overloaded tissues. By being able to determine a concrete mechanical characteristic in response to a visual degenerative characteristic, better understanding between degeneration and function can be established. Quantifying the mechanical changes associated with a given degree of disc height loss will help to determine the given range or margin of safety a person has with respect to their daily mobility and continued exacerbation of spinal tissues through perturbed mechanical loading.

3.4.3 Degeneration versus Aging

It can be easy to confuse the effects of aging with degeneration, as aging is one of the primary risk factors for disc degeneration (Bogduk, 2012). Rather, degeneration can be thought of as involving a structural failure (Adams et al., 2006a) while aging in the spine involves more minute changes to a cellular sub-structure that can manifest themselves as changes to the gross structure over time.

Some research suggests that the blood supply at the endplate decreases during the twenties which therefore reduces the nutrition of the intervertebral disc and directly affects the nucleus (Boos et al., 2002). Nutrient supply to the intervertebral disc is one of the key components to maintaining viability of the disc cells which produce the disc matrix constituents and contribute to its mechanical integrity (Urban et al., 2004). It has been suggested that changes to the endplate such as sclerosis prevents nutrients from diffusing through the endplate and reaching the cells (Benneker et al., 2005). This view has been challenged, with the potential for cellular dysfunction or loss of vascularity within the vertebral body itself being implicated in the loss of nutrient supply (Rodriguez et al., 2011). Interestingly, more mature cells of the intervertebral disc have been shown to produce fewer matrix constituents compared to their younger counterparts, further supporting the notion of cellular dysfunction (Korecki et al., 2009). With higher grades of degeneration, pores in the endplate reduce in overall number, but those that are left increase in overall size (Benneker et al., 2005); there could potentially be localized concentrations of nutrients to some cells, but none left for others. Within the disc nucleus, there is also proteoglycan fragmentation that begins to occur with age (Buckwalter, 1995); this affects the fluid content of the nucleus and its ability to hold water (Adams and Hutton, 1983). The nucleus dries out (Adams et al., 1986) and loses its ability to maintain intradiscal pressure (Adams et al., 2006a). The annulus also exhibits a small effect on its tensile properties with age (Acaroglu et al., 1995).

Because both aging and mechanical overload occur in tandem, it is difficult to parse out what is aging and what is the result of degeneration due to mechanical overload. What is unique between aging and degeneration is that with aging there is generally no evidence of disc height loss (Koeller et al., 1986); disc height therefore, would be a hallmark characteristic of degeneration. Indeed, disc height is used as one of the metrics for determining degeneration grade (Pfirrmann et al., 2001), and it has been shown via finite element modelling that in the higher grades of degeneration (where higher levels of disc height loss are included) the mechanics of the segment change significantly (Park et al., 2013).

3.4.4 Adjacent Segment Degeneration Following Disc Height Loss

Loss of disc height has implications with respect to altering the mechanics of the injured disc which can initiate degeneration at adjacent levels (Bao et al., 1996). As adjacent levels begin to face an increased demand to compensate for movement and load distribution, the pressure inside the nucleus increases (Holm et al., 2007). Alteration of the load distribution or surgical intervention at one segment has consequences at adjacent segments with respect to further injury risk (Tzermiadianos et al., 2008), motion profile (Tang and Rebholz, 2012), and stress distribution (Tchako and Sadegh, 2009). There has been no attempt however, to characterize any sort of timeline of adjacent segment perturbation and follow the progression of degenerative changes with disc height loss of varying degrees. Current research has examined the global effects of degeneration on spine mechanics (Fujiwara et al., 2000), that is, how specific grade categories function. This is important work as it enables observable features to be categorized into functional deficits. Knowledge of how each visual feature independently impacts mechanics however, would allow for even more specific insight into the aberrant movement expected by the injured segment and consequences along the spinal linkage.

3.5 Modalities of Disc Height Restoration

Restoration of disc height through surgical means can be performed using two main methods; total disc replacement, and injection/implantation with a hydrogel. Both methods seek to restore function to an injured segment and ultimately reduce pain in patients.

3.5.1 Total Disc Replacement

Total disc replacement is achieved through use of a pre-fabricated implant such as the Prodisc™, Charité®, or Maverick™ devices. While studies suggest that the outcomes of using such devices are generally good (Park et al., 2012, Shim et al., 2007), these terms are loosely defined, and not constant between studies. There is also evidence of facet degeneration at adjacent levels with total disc replacement (Shim et al., 2007) and it has been shown that a successful total disc replacement device must mimic the non-linear behaviour of the disc in its normal range of motion (van den Broek et al., 2012). Given this criteria, it would behoove future surgical alternatives to maintain as much of a patient's original anatomy as possible. It would therefore be beneficial for clinicians to be able to view a medical image of a patient's spine and ascertain the functionality of the components (annulus, nucleus, endplate) in order to determine the most appropriate pathway for surgery.

Normal functioning of a disc as it moves through its range of motion is for the center of rotation to constantly be changing within the region of the nucleus as vertebral bodies glide anteriorly and posteriorly relative to each other (Adams et al., 2006a). During degeneration the center of rotation changes drastically compared to a healthy disc (Gertzbein et al., 1985) and has been shown to even shift to the facet joints when the disc is in extension (Zhao et al., 2005). This has implications for wearing out of the facet joints and producing higher levels of damage due to potentially higher stress concentrations in this area. It would be beneficial therefore, for disc replacement surgeries to be able to mimic the natural center of rotation changes in a

healthy disc. As the implants have fixed points of rotation though, this is not possible and therefore other options to restore disc height and normal disc function may prove to be more beneficial to patients in the long term.

3.5.2 Nucleus Replacement via Hydrogel

Nucleus replacement involves maintaining the annular components of the disc and using either a self-contained implant that goes into the center of the disc where the nucleus would be (Bertagnoli and Schonmayr, 2002), or through injection of a free gel that conforms to the unique shape of the disc (Vernengo et al., 2008). This method maintains the bulk of the anatomy of the disc instead of removing it altogether. The nature of the procedure is also less invasive overall compared to total disc replacement; involving only a needle puncture to the disc in the case of using a freely injectable gel.

Some data suggests that the use of a hydrogel that conforms to the shape of the disc is optimal in re-establishing and maintaining a normal stress distribution within the disc (Dahl et al., 2010). One issue though, is in containing the implanted gel and preventing implant migration (Klara and Ray, 2002). While this may be an issue for when a pre-formed pillow implant is inserted through an incision, it may be less of a factor when a hydrogel liquid is inserted through a needle puncture and then changes state from a liquid to a gel (Vernengo et al., 2008).

There are many different formulations for hydrogels acting as artificial nucleus replacements. From collagen-hyaluronan (Calderon et al., 2010) to gellan-gum (Silva-Correia et al., 2011) to poly(N-isopropylacrylamide) (PNIPAAm)/ poly(ethylene glycol) (PEG) (Vernengo et al., 2008), the essential goal of all these formulations is to restore disc height and mimic the natural mechanical properties of the nucleus.

3.5.3 Vertebroplasty

Vertebroplasty involves the injection of poly(methyl methacrylate) (PMMA) bone cement into a fractured vertebral body in the attempt to provide stabilization and structural support (Luo et al., 2010). It has been shown to have a positive effect in restoring normal spine mechanics (Luo et al., 2010, Luo et al., 2007). The effect of combining vertebroplasty along with nucleus replacement via hydrogel injection remains unknown. In the case of severely damaged spinal segments disc height restoration may only restore segment kinematics and kinetics to a certain degree. It would therefore be beneficial to assess the effect of restoring both disc height and vertebral body stress distributions to evaluate the worthiness and cost-benefit of attempting both these surgical procedures rather than only a single one.

Use of vertebroplasty, as with any surgical procedure should be approached with caution as there is evidence of it initiating degenerative changes to the disc (Kang et al., 2014, Zhao et al., 2014). Once this procedure has been performed therefore, there is a bleak outlook with respect to ever restoring cellular function, creating a dependency on the efficacy of artificial means of restoration.

3.6 Distinguishing Between Normal and Pathologic Disc Height Loss

Over the course of a day, intervertebral discs exhibit creep, and slowly lose height compared to where they started at the beginning of the day just prior to getting out of bed (McGill, 2007). This is due to the fixed charge density of the disc which gives it an osmotic pressure; weight bearing activities, muscle activation, and anything that applies compressive load to the disc can overcome this pressure and cause water to diffuse outwards (Urban et al., 2000). This is normally not an issue, as the disc is able to re-imbibe water during sleep, restore height, and begin the cycle again the following morning (Boos et al., 1993). Obviously, this is a component of normal spine function and any disc height loss through this mechanism should

not be considered pathologic. With proteoglycan fragmentation and escape from the disc via various mechanisms, the disc loses some of its fixed charge density and some of its osmotic pressure (Urban et al., 2000). This would hinder its ability to take in water and regain height, it would also alter the material properties of the nucleus and change the load distribution pattern in the disc (Adams et al., 1990). Whether the slow change in nucleus properties over the course of decades is clinically significant in terms of producing severe pain and dysfunction is questionable. Sudden change however, over the course of months or even several years via mechanical mechanisms such as compressive fracture or herniation could produce more insidious injuries that result in clinical pathology (Adams et al., 2015).

It is important then, to distinguish between pathologic and normal disc height loss. In the case of pathologic disc height loss, there is most likely significant height loss only at a single segment rather than at multiple segments. Pathologic disc height loss would be unrecoverable through unloading of the disc, contrary to what is seen with diurnal variations in disc height. Pathologic disc height loss may also accompany other degenerative features such as radial tears of the annulus (Adams et al., 2000a) or the presence of osteophytes (Al-Rawahi et al., 2011). In the case of aT2-weighted MRI, a pathologic disc may appear dark, signifying that it has lost most of its hydration, appearing different from other discs at different levels (Haughton, 2011). Essentially, the pathologic disc typically appears in the spine as an anomaly from other discs. Often, clues on whether the disc is pathologic can be derived from the loading history of a patient or any complaints regarding pain. Using these cues along with information gleaned through studies regarding functional consequences of degenerative features, an accurate profile of how a pathologic segment will function can be gained. This information can be used to assess what impact on spinal function a pathologic level will have and whether surgery or conservative treatment should be utilized.

3.7 Fluoroscopy

Fluoroscopy involves using x-rays against a fluorescent screen with an object placed in between. Modern fluoroscopy involves the use of an image intensifier and video camera to record the images digitally and play them on a monitor (Pallan et al., 2011). Fluoroscopy is essentially a moving x-ray allowing internal observation of an individual during dynamic tasks. Fluoroscopy has been used in the past to observe lumbar spine segmental motion (Cholewicki and McGill, 1992), with this particular modality estimated to present a radiation exposure equivalent to a single traditional x-ray over an 18 second trial. Fluoroscopy therefore provides a readily available technique to observing intervertebral disc motion with a low radiation exposure to individuals.

There are several groups worldwide involved actively in research using quantitative fluoroscopy techniques, that is, techniques that use advanced tracking algorithms to obtain vertebral body rotations through time via fluoroscopy (Breen et al., 2012). Various approaches have been taken in order to achieve further accuracy with tracking measurements, but there is difficulty in truly validating an algorithm across all possible contingencies that it may be used for. It would be counterproductive to the field of quantitative fluoroscopy to cease attempting to identify ways in which accuracy can be improved. One method may be better in some circumstances of tracking vertebral body motion than others and vice-versa. It is important therefore, to continue to explore novel avenues and approaches in quantitative fluoroscopy techniques.

Typical x-ray approaches involve examining the spine in a single static pose, or neutral to full flexion and extension. With fluoroscopy, a sequence of images can be obtained that show the spine as it moves through the midranges. It can be an important diagnostic tool that identifies aberrant spine motion that conventional static x-rays do not have the capability to

identify. Continued use of fluoroscopy along with techniques that quantify motion of vertebrae will help to elucidate aberrant movement strategies and propagation of injury.

3.8 Use of Multi-Segment Specimens

A potential limiting factor for testing of multi-segment spine specimens is the possibility for the unsupported vertebral body to experience buckling, instability, and non-physiologic movement and loading. This would obviously be undesirable when attempting to mimic movement of the spine *in-vivo*.

Entire lumbar spines have been shown to buckle under 88N of load when a specimen is restrained from moving in an anterior-posterior direction (Crisco et al., 1992). In contrast to this, Lysack and colleagues (Lysack et al., 2000) developed a device used for testing multiple segment lumbar spine specimens and determined that while potential for what they characterized as “off-axis moments” can occur to multiple segment specimens, this instability is greatly reduced as long as the specimen is provided with a low-friction interface with which to float on (Lysack et al., 2000). Multi-segment testing of the entire lumbar spine has also been successfully performed provided the specimens were again, given an interface on which to translate (Ilharreborde et al., 2010). In cases where both ends of the vertebral segments are fixed and not able to translate properly, the use of a follower load, where the compressive axis travels with the specimen through flexion and extension motions has facilitated the ability to provide physiological levels of load to a multi-level spine specimen (Patwardhan et al., 2000, DiAngelo and Foley, 2004).

In the case of study 1 proposed for this thesis work, any evidence of segmental buckling in the non-fixed vertebral body due to deficits in the testing apparatus will be evident in the initial tests. Instability resulting from acute disc height loss in the experimental group could be

evidence of the “unstable phase” characterized by Kirkaldy-Willis and Farfan (Kirkaldy-Willis and Farfan, 1982) and thus not a confounding factor.

3.9 Summary: What is known and what is not

Mechanical overload produces injury and structural defects within the intervertebral disc (Adams et al., 2000a, Callaghan and McGill, 2001, Tampier et al., 2007, Yingling et al., 1997). Loss of disc height has the potential to set off a cascade of degenerative changes affecting the structure and mechanical function of a segment and segments adjacent to it (Arbit and Pannullo, 2001). Ultimately it is unknown to what degree disc height affects the kinetics and kinematics of adjacent tissues and the time-history of degeneration and perturbed mechanics that accompanies disc height loss. It is also unknown how novel surgical repair modalities fare with regard to restoring disc height and restoring mechanical function to a disc and its neighbours. Further, in the case of severely damaged segments, the degree to which disc height restoration is enough to return function or if further repair to the vertebral body should take place is unknown. It remains to be seen what role pathologic disc height loss plays in the normal rhythm of spine movement and how it affects the response of adjacent segments. Finally, there is a need to bring current thinking of disc degeneration to functional impairment. Ultimately, medical images of spinal segments with height loss should be able to yield an immediate determination of the functional capabilities of an individual’s spine. Disc height loss is an important factor in the mechanical and biological consequences of disc degeneration (Jarman et al., 2015). It is thus important to examine disc height loss outside of other degenerative factors across a variety of pathologies to determine the mechanical consequences.

Chapter 4: Study 1

A Characterization of the Kinematic Outcomes on Spinal Tissues at an Injured and Adjacent Segment during Disc Height Loss

4.1 Background

Identifying the mechanical consequences of disc height loss on adjacent tissues is an important first step in examining the impact of disc height loss on the degenerative cascade. This work will help to identify the role disc height plays in modulating the kinematics of the spine and whether disc height restoration can return spine kinematics to their original conditions. When disc height is lost, there is a change in the manner in which it functions; facet joints become involved, nerve roots are impinged, and the annulus bulges (Arbit and Pannullo, 2001). This can have an impact on how other tissues are loaded and influence a pathway for cascading injury to adjacent segments. It is unknown how the course of mechanical perturbation transpires within a spine when disc height has been lost at one segment. The consequences of losing disc height may transfer higher stress concentrations to adjacent discs and passive tissues (Adams et al., 2000a). The fact that perturbation can occur at segments other than the one that is injured elicits concern over what exactly those consequences are and how the tolerance of tissues is altered. To date, there is no research that has examined the result of disc height loss directly on the mechanics of the intervertebral disc and an adjacent segment. Previous work has examined degenerative changes on mechanics of the spine (Tanaka et al., 2001, Lee et al., 2015, Lao et al., 2015a), but degenerative changes include confounding factors other than disc height loss. Examining disc height loss in the absence of other pathological changes will help to establish its influence on aberrant movement.

Disc height loss can be initiated through injury such as herniation or endplate fracture. Under these injuries, nucleus volume would be at least partially lost, and thus mechanical tests involving a decrease in nuclear volume to produce disc height loss would be most applicable. Degenerative grading also includes disc height loss (Pfirrmann et al., 2001), suggesting that it has a progressive component. Degeneration is difficult to reconcile with mechanical injury especially since lower grades include components of disc "degeneration" that are seen with normal aging (Adams et al., 2015). Adams and Roughley (2006) describe a degenerate disc as having structural failure combined with accelerated or advanced signs of aging (Adams and Roughley, 2006). Elements of structural failure include annular tears, disc prolapse, and endplate damage (Adams and Roughley, 2006); all of these drivers of degeneration would include loss of nucleus volume and progressive disc height loss over time.

The use of hydrogels to alter disc mechanics under injury conditions has been evaluated in previous work where its efficacy in reversing the mechanical consequences of injury was examined and identified that sagittal plane rotational stiffness could be returned to pre-injury values (Balkovec et al., 2013). With all the various formulations of hydrogels for this purpose (Calderon et al., 2010, Silva-Correia et al., 2011, Vernengo et al., 2008), the ability to restore the mechanical properties of an injured disc under minimally invasive conditions would prove very valuable indeed.

Motion of a spine specimen *in-vitro* is driven by applied moments, loads, and the stiffness of the passive tissues being tested. Ultimately, stiffness controls motion in this scenario. Under fatigue, single functional spinal units have been shown to stiffen, requiring a higher applied moment to reach the same target angle, or undergoing a smaller angular displacement under the same applied moment (Callaghan and McGill, 2001). With disc height loss, the stiffness of the affected level is anticipated to increase. The presence of an additional segment that does not have a change in disc height may affect the kinematics at several joints – this is not well understood. With increased stiffness at one level and a loss in height, the forces

and moments applied through the specimen will change, and alter the degree to which segments rotate.

4.2 Significance

Understanding the mechanical consequences of disc height loss and identifying trends in the pathomechanics of the spine allows for greater understanding with respect to viewing an anatomical feature and understanding its functional implications. The purpose of this investigation is to determine the kinematic outcomes of disc height loss on both the injured and adjacent disc in an *in-vitro* spine model. This study will also determine the viability of an injectable hydrogel in restoring disc height and segmental mechanics. The challenges were several. First, given that the hydrogel was designed to be a free liquid for injection at cool temperatures, but formed a gel at *in-vivo* body temperatures, this environment had to be created. A chamber was designed and custom-fabricated to control humidity and temperature.

4.3 Hypotheses

1. Disc height loss will result in a lower relative angular displacement by the injured disc.
2. Disc height restoration via hydrogel injection will return injured discs to their initial relative levels of angular displacement.
3. Disc height loss in the upper and lower discs will produce the same kinematic effect.

4.4 Methods

4.4.1 Specimens & Preparation

Twenty porcine cervical spines (age: 6 months, weight: 80kg) were used for this study. Specimens were dissected into a multi-segmented unit consisting of the C3/C4 and C4/C5 discs and the C3, C4, and C5 vertebral bodies; consisting therefore, of two functional spinal units. During dissection, as much muscle tissue was removed as possible while leaving the disc and ligamentous structures intact. Specimens were mounted in stainless steel cups using two screws drilled through the exposed endplates on the superior and inferior ends of the specimen, non-exothermic dental stone (Denstone®, Miles, South Bend, IN, USA), and wire looped bilaterally around the lamina and anterior processes. Wood screws were also partially drilled into the superior and inferior vertebral bodies (the ends placed into the mounting cups) in order to further secure specimens and prevent movement anywhere but the two vertebral joints.

4.4.2 Equipment & Testing

All specimens were tested in a servohydraulic dynamic testing machine (Instron, model: 8511, Instron Canada, Burlington, Ontario, Canada). Free translation of the bottom cup was facilitated by a platform of ball bearings while flexion-extension motions were applied by an electric brushless servo-motor (model BNR3018D, Cleveland Machine Controls, Billerica, MA, USA) and planetary gear head (model 34PL040, Applied Motion Products, Watsonville, CA, USA) controlled using a customized software interface. Specimens were required to be heated to body temperature during the testing protocol, and as a result, a customized temperature chamber was built surrounding the testing apparatus (Figure 4.1). The apparatus allowed for steam to be delivered from a heated water bath through a PVC pipe and injected into the chamber. The flow of steam was directed upwards in the chamber away from the specimen, preventing overheating. Temperature was monitored using a digital thermistor in the

chamber mounted at the bearing tray where the specimen was placed which provided instantaneous feedback to any changes. A vent was placed at the rear, and could be made larger or smaller, facilitating adjustments in temperature. At the front of the chamber was an access door, allowing for the specimen to be taken in and out, and to facilitate recording of data trials.

Figure 4.1 Temperature chamber and experimental setup. A specimen was able to be inserted into the chamber while steam was brought in through a PVC pipe, heating the enclosure. A digital thermistor monitored the temperature of the chamber, and venting in the rear of the enclosure allowed for internal temperature adjustments. A door at the front of the chamber was able to be lifted in order for an orthogonally placed digital camera to capture video of sagittal flexion-extension movements.

Sagittal movement of each vertebral joint was recorded using a digital video camera (GoPro, model: Hero3, GoPro, San Mateo, CA, USA) placed orthogonally to the specimen. Video was captured using the narrow field of view, at 60 frames per second, and a resolution of 1920 by 1080 pixels. Three small rigid bodies with four circular reflective markers on each were

placed on the specimens: two were placed on the superior and inferior mounting cups, and one was rigidly fixed using screws onto the C4 vertebra (Figure 4.2). These three placements captured movement of the three vertebral bodies, their relative orientation could then be determined to calculate relative vertebral joint angles. A non-moving rigid body was fixed to the Instron itself and used to calibrate the initial position of all three rigid bodies, and base any relative motion off of this initial starting position.

Disc height was restored using a thermally responsive hydrogel. This hydrogel could be injected into the disc through a small needle puncture at room temperature, and then once at a temperature above 33°C, formed into a gel which would not flow back through the needle puncture, effectively creating a customized nucleus implant.

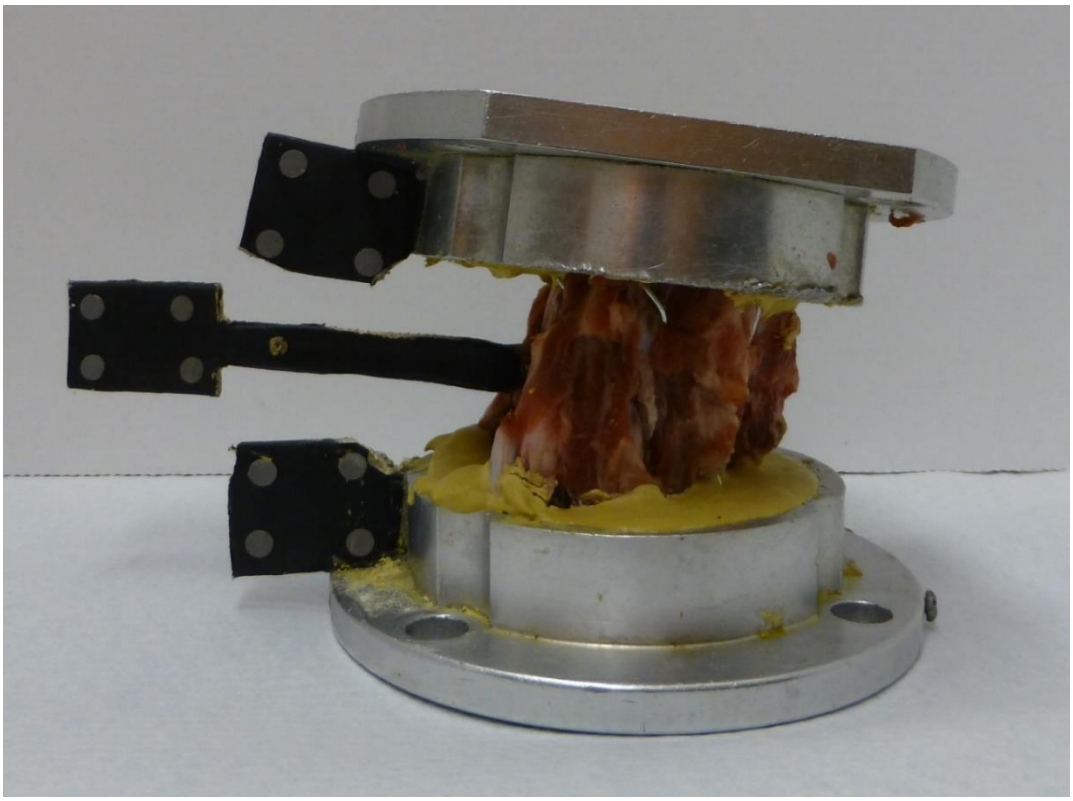

Figure 4.2 Rigid body marker setup on spine specimens. Two rigid bodies were fixed to the superior and inferior mounting cups (these did not move relative to the superior and inferior vertebral bodies) while another rigid body was fixed via small wood screws to the middle vertebral body.

A flow chart outlining the experimental procedure is located in Figure 4.3. Specimens were placed in the servohydraulic testing apparatus and brought to body temperature prior to any testing taking place. Pilot testing revealed that the temperature at the disc periphery, taken with a digital probe thermometer, was a suitable surrogate for the temperature inside of the disc. Additionally, this temperature measurement technique has been used previously with success (Balkovec et al., 2013). After heating, specimens were preloaded under 300N of compressive load for 15 minutes in order to reduce any post-mortem swelling (Callaghan and McGill, 2001, Adams et al., 1996). This test also established the designated neutral posture for the specimen which was the position of the motor arm that corresponded to zero torque for the whole specimen overall. Following the preload process, a passive flexion/extension test was performed under 1000N of compressive load. Due to the specimens having multiple segments, and given the limitations of the testing apparatus for testing multi-segmented specimens, there were two distinct linear regions of torque vs. angular displacement. Angular movement was initiated at the upper segment first, and then after the moment applied to the lower segment was high enough to overcome the resistance of the passive tissues, movement of the lower segment commenced. The flexion/extension angular displacement limits were based on where the beginning and end of both linear regions were for each specimen (Figure 4.4). Since the specimens tested were composed of two motion segments, the loading profile of each specimen was different from the traditional functional spinal unit that the apparatus was originally designed to test. Initially, a pure moment was applied to the superior vertebra; a bending moment was also created about the segments from the applied compressive load and varied in magnitude and direction depending on the posture the specimen was in and the segmental level being considered. Thus, the cumulative moment was the result of the pure moment applied to the superior vertebra and the bending moment applied by the compressive force. Passive tissues in the specimen (facet joint capsule, annulus, ligaments, etc.) resisted bending and created a counter-moment opposing the applied force and moment. The lower segment was not

observed to rotate initially, as stiffness of the upper segment was presumed to be lower. As the specimen rotated further, the stiffness in the upper segment increased, and the bending moment at the lower segment increased, causing rotation to occur about the lower segment (Figure 4.5, Figure 4.6). Rotation about the lower segment was the point where translation in the specimen occurred (Figure 4.7). The posterior translation of the floating bottom cup increased the bending moment. Schematic and free-body diagrams of the testing apparatus with multi-segmented specimens are located in Appendix F. Testing was performed with the hydraulic ram of the Instron under load control, while the motor arm which applied flexion/extension moments was operated in position control, bringing specimens to the same target angle for each trial. Angular displacement cycles were performed at a rate of 1Hz.

Prior to any angular displacement tests, a video calibration trial was taken with the specimen in its starting position. Calculated vertebral joint motion was based off of this zero-displacement position. Specimens were first tested under 1000N of compression and angular displacement range determined by an operator from the passive test. Each specimen underwent 10 cycles of repeated full flexion to extension motions while the positions of the rigid bodies were recorded. Following this initial angular displacement test, the upper or lower disc (randomly selected) was punctured anteriorly using a 12-gauge needle (Figure 4.8). This was the smallest gauge needle that would still allow for the flow of nucleus from the disc, immediately, it initiated disc height loss in the punctured disc without any other damage occurring.

After puncturing, each specimen underwent 50 cycles of repeated flexion to extension motions to ensure that no more nucleus pulposus could be forcibly extruded from the disc. After nuclear extrusion, a second angular displacement trial was performed. The specimen underwent 10 cycles of repeated flexion to extension; each segment's angular displacement was measured with one segment's disc height reduced. Disc height was then restored through use of the hydrogel injected into the damaged disc. The disc was injected until it would not

passively contain any more hydrogel and the plunger on the syringe would no longer depress. The specimen was then left unloaded for 15 minutes in order to fully ensure that the hydrogel changed state from a liquid to a gel form. The needle was left in the disc during this 15-minute period and acted as a stopper to prevent any outflow of fluid hydrogel. Once testing recommenced, the needle was removed.

Following disc height restoration, a final angular displacement trial was taken, with the specimen taken through a further 10 cycles of repeated flexion to extension. This trial measured the segmental kinematics of the specimen with disc height restored.

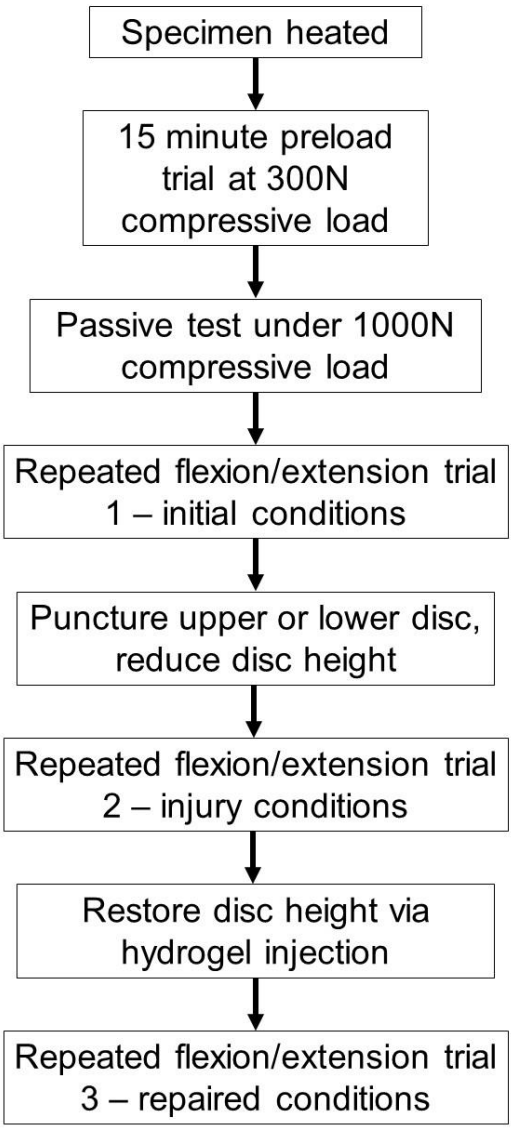

Figure 4.3 Flow chart of experimental protocol for Study 1.

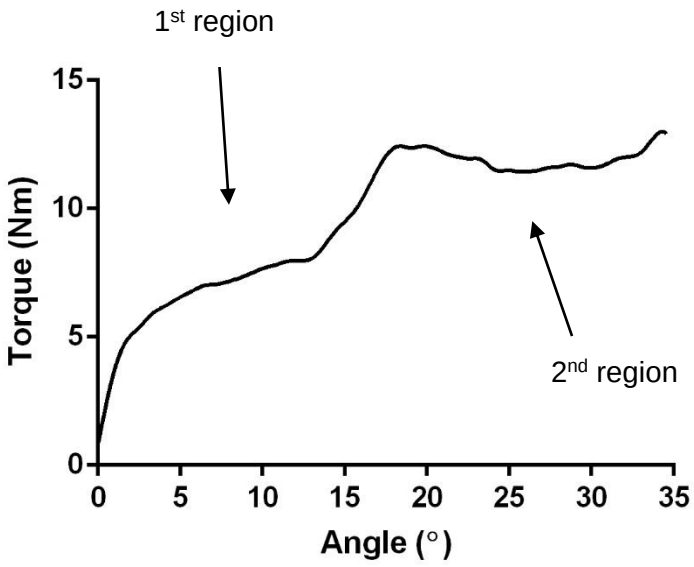

Figure 4.4 Typical passive test angle-torque relationship for an uninjured, intact multi-segment specimen. Two distinct linear regions were observed. The observed behaviour is discussed in detail in Appendix F.

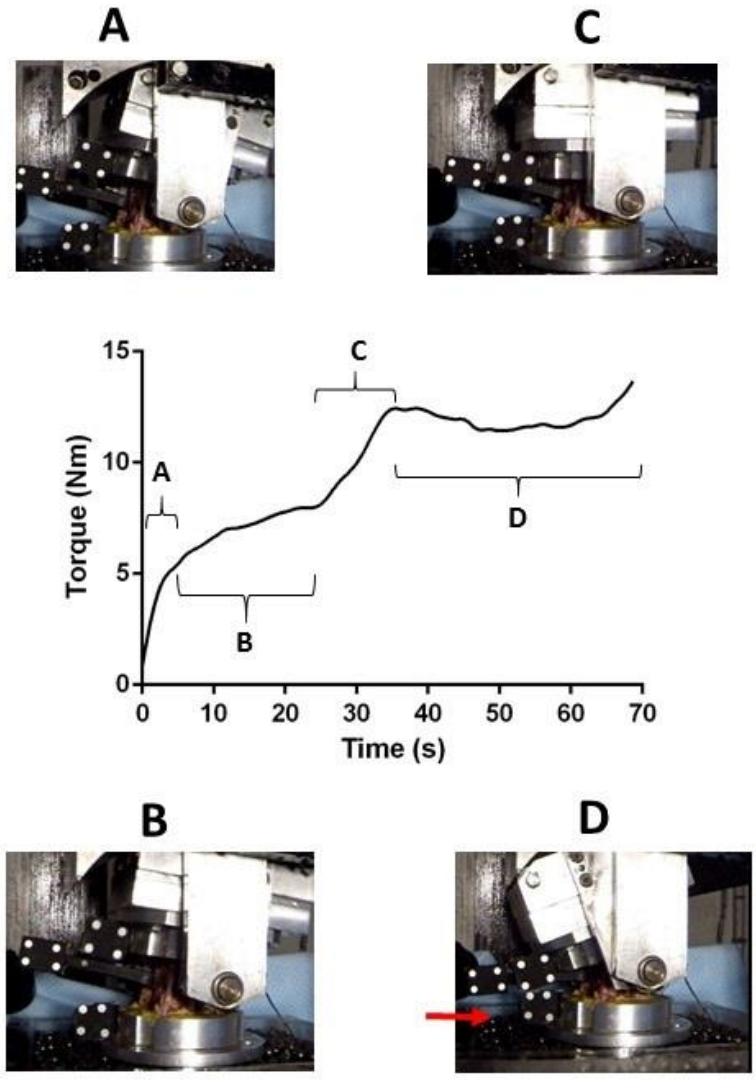

Figure 4.5 Sequence of events during moment application to the multi-segmented specimen, rigid bodies are fixed to each of the three vertebrae. A. A moment is applied to the superior vertebra, the specimen is stiff and resists rotation due to the applied compressive load, which is the reason for the high rate of torque application initially. B. Torque is applied by the motor arm, but the specimen has a lower resistance than in (A). This is presumably due to the compressive force from the hydraulic ram being positioned directly above the center of rotation of the upper disc and thus not creating a bending moment that counters the direction of rotation as in (A). C. A coupling occurs about the superior segment and no more rotation occurs about it. Motion continues about the inferior segment. The same stiffness and resistance to rotation (as in A) is evident as the applied compressive load creates a bending moment counter to the direction of rotation. D. Translation of the specimen occurs (shown with arrow) and the bending moment increases as translation continues, increasing the moment arm and reducing the rate of moment application by the motor arm.

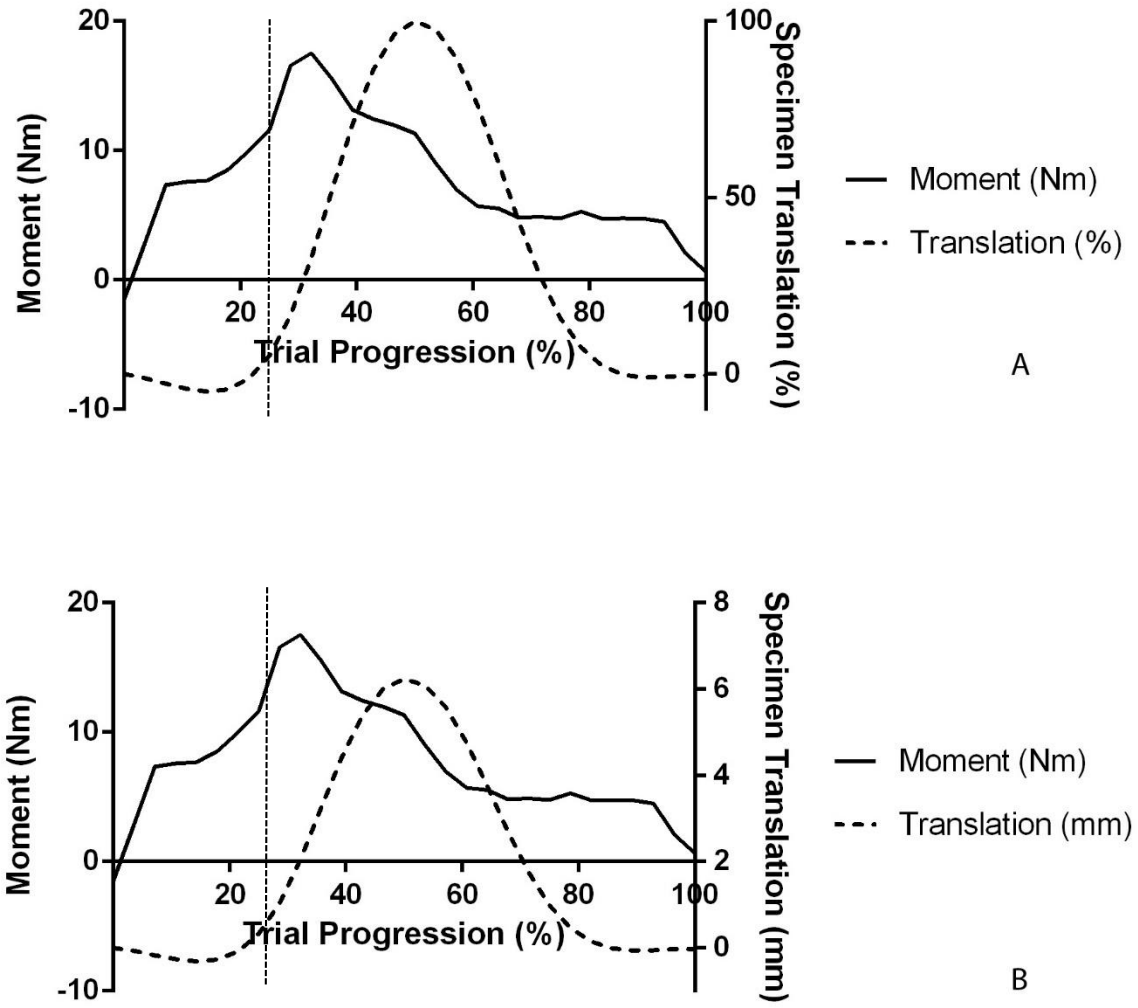

Figure 4.6 Relationship between the moment resisted by the specimen and horizontal translation of the base. Moment is scaled to the left y-axis while translation is scaled to the right y-axis. Translation begins to occur at the 'C' region defined in Figure 4.5 (shown with vertical dashed line) when rotation about the upper segment is nearly exhausted. A. Translation is normalized to the maximum reached by the specimen. B. Translation is expressed in units of millimeters.

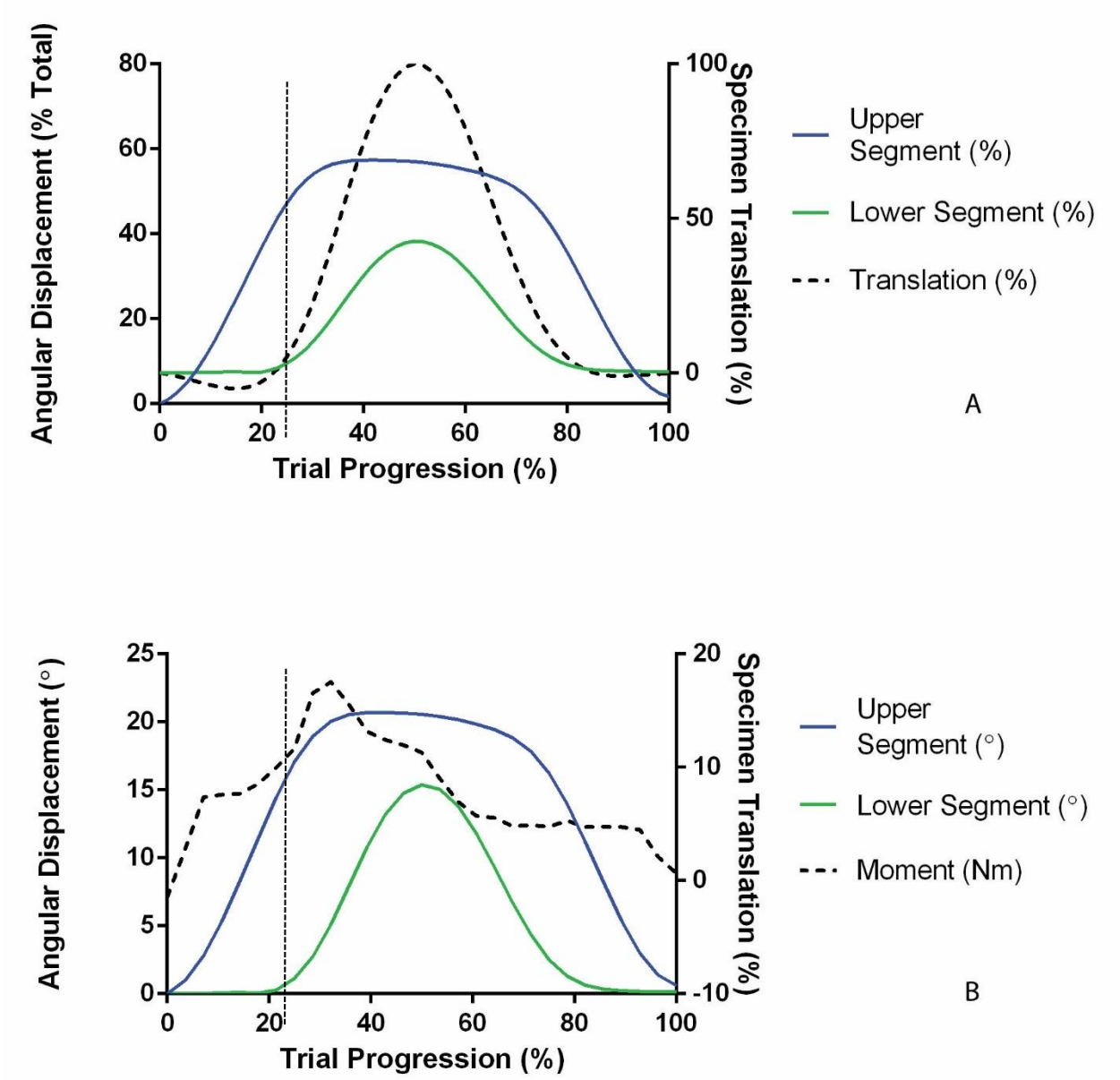

Figure 4.7 A. Relationship between rotation of the upper and lower segments and the translation of the bottom cup on the platform of ball bearings. Rotations are scaled to the left y-axis while translation is scaled to the right y-axis. Translation of the bottom cup begins to occur when rotation about the upper segment has nearly ceased (shown with vertical dashed line). B. Relationship between rotation of the upper and lower segments and the moment resisted by the specimen. Rotations are scaled to the left y-axis while moment is scaled to the right y-axis. Rotation about the lower segment begins to occur in the 'C' region defined in Figure 4.5.

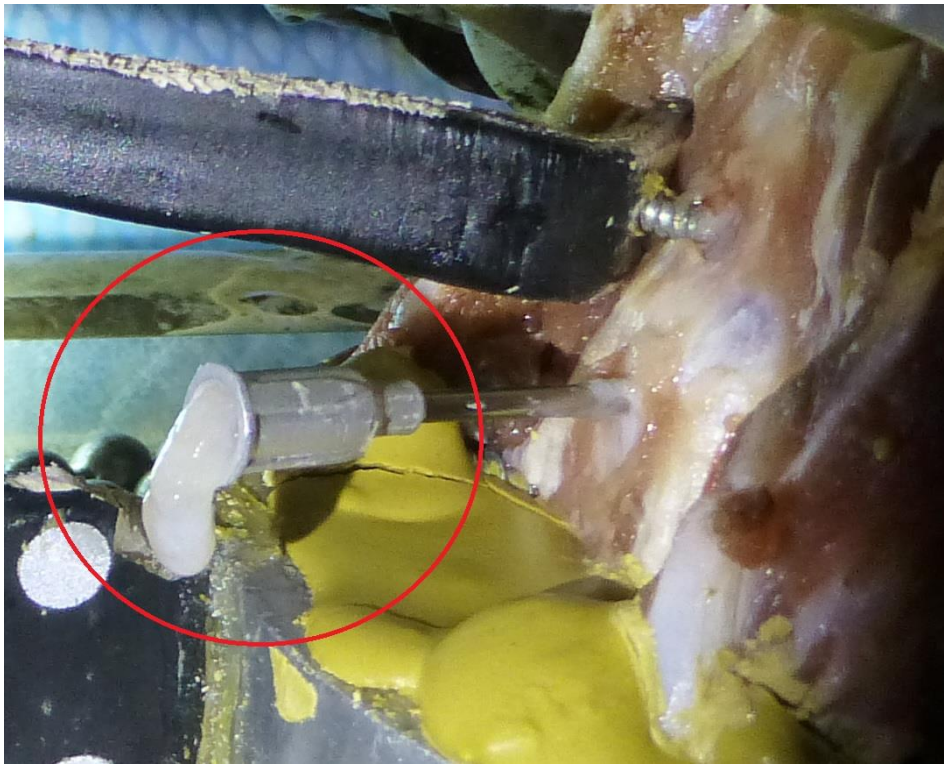

Figure 4.8 Needle puncture at the anterior of the disc caused nucleus to extrude and disc height to be lost.

4.4.3 Data Analysis

Disc height was measured using the relative position of the hydraulic ram on the Instron. This method was found to be superior to measurement using plain-film x-rays, since the loss of nucleus did not prevent passive recovery of disc height after the specimen was unloaded in the x-ray chamber. Under prolonged loading, Gooyers and Callaghan (2015) found that total specimen height is not an accurate measure of disc height (Gooyers and Callaghan, 2015). These conclusions however, were found in cyclic loading of 5000 repetitions. Under repeated cyclic loading, height is progressively lost in both the vertebrae and the disc. Specimens in the present study underwent 80 cycles of loading total, and were loaded at 1000N, a small load relative to the compressive tolerance of functional spinal units (Yingling et al., 1997). In this study, specimen height was measured, the disc punctured, and then measured again, with 50 cycles transpiring between these two measures. For this reason, it was assumed that height

loss in the vertebral bodies was very minor compared to the disc. Thus, given the sub-failure loads the specimens were placed under, the relatively low amount of cyclic loading they went through, and the inaccuracy of x-ray measurements, it was assumed that changes in the Instron hydraulic ram position were due primarily to disc height loss. Total torque applied by the motor arm during repetitive sagittal plane motion trials was also recorded and normalized to the first repetitive trial to facilitate comparison between specimens. Reflective markers were digitized semi-automatically using commercially available digitizing software (Maxtraq: Innovision Systems, Columbiaville, MI, USA). Following digitization, the relative angular displacements of each vertebral joint in the sagittal plane were computed using customized Matlab software (Mathworks, Natick, MA, USA). Magnitudes of angular displacement for each joint (C3/C4 and C5/C6) were taken from the 10th repetition of flexion/extension in each of the data trials (Bisschop et al., 2013). Joint angular displacement magnitudes were normalized to the total magnitudes (sum of both joints) for each trial to facilitate comparisons across specimens and trials. Detailed outlines of the procedure for computing relative angular displacement for each segment as well as an error analysis for the video measurement system used are in Appendix B.

4.4.4 Statistical Analysis

Independent variables for this investigation are intervention (pre-disc height loss, disc height loss, repaired condition) and level of disc height loss (superior or inferior level). The dependent variable for this investigation is the normalized magnitude of segmental angular displacement within each specimen (Table 4.1).

Hypotheses 1 and 2 were tested by a mixed ANOVA, which was used to test for differences within specimens in normalized segmental angular displacement data across the three trials (pre-disc height loss, disc height loss, repaired condition), and across the two groups. Pairwise comparisons between the initial angular displacement of the disc and the

injured angular displacement of the disc were made to test hypothesis 1, while pairwise comparisons between the initial angular displacement of the disc and the height restored angular displacement of the disc were made to test hypothesis 2. A Bonferroni post-hoc was used to correct for multiple comparisons. Significance was defined at a level of $p<0.05$. Hypothesis 3 was tested via the test for within-subjects effects for the independent variable of "intervention". The Greenhouse-Geisser correction factor was used to ensure that sphericity of data was not violated. All statistical tests were performed using SPSS software (IBM, Somers, NY, USA).

Table 4.1. Independent and Dependent Variables for Study 1

Independent Variables	Dependent Variables
• Disc Height Loss • Segmental Level Damaged (group)	• Normalized Segmental Angular Displacement

4.5 Results

A systematic effect was seen across specimens for the relative contribution to total angular displacement for the three movement trials. When disc height loss was induced, less angular displacement occurred about the level with height loss while more angular displacement occurred about the adjacent level compared to the initial trial pre-disc height loss (Figure 4.9, Figure 4.10). Average relative angular displacement for the upper disc damage group decreased 13.8% ± 5.3% at the level with height loss, while the lower disc group decreased 4.5% ± 2.1% at the level with height loss, relative to the initial motion measured in the pre-disc height loss trial. This was found to be statistically significant across groups for pairwise comparisons of the intervention variable ($p = 2.6x10^{-8}$). Following disc height restoration,

relative angular displacement about upper and lower segments was found to return to pre disc height loss levels (Figure 4.9, Figure 4.10). A sample set of time-history graphs showing a single specimen going through each of the three trials is located in Figure 4.11. This figure shows normalized angular displacement for the upper and lower levels initially (pre-disc height loss), after disc height is lost at the upper level, and after disc height is restored. On average, the upper disc group increased angular displacement by 12.7% ± 5.5% at the level with height loss compared to the motion of the same level in the height loss trial while the lower disc group increased angular displacement 6.4% ± 4.2% at the level with height loss. This was found to be statistically non-significant when compared with pre-disc height loss angular magnitude across groups for pairwise comparisons of the intervention variable ($p = 1.00$). The test of within-subjects effects across groups for the intervention variable was found to be statistically significant ($p = 1.5x10^{-11}$). A significant interaction was also found between the group and intervention variables ($p = 0.00015$), this is not surprising, as the magnitude of relative angular displacement change between upper and lower disc groups was visibly different (Figure 4.9, Figure 4.10).

Average specimen height lost was 0.97mm ± 0.41mm while after hydrogel injection specimen height increased an average of 0.09mm ± 0.44mm relative to the initial height (height was increased beyond pre-disc height loss levels). There was a systematic effect observed across specimens where height was increased after hydrogel injection relative to the disc height loss condition. Some specimens did not fully regain height to pre-disc height loss levels, this is suspected to be due to hydrogel extrusion in some of the cases occurring before height was measured. Normalized torque values resisted by specimens after disc height loss were found to increase by 20.9% ± 14.6% relative to the pre-disc height loss trials. After hydrogel injection, normalized torque values decreased by 7.8% ± 9.5% relative to the pre-disc height loss trials.

Following disc height restoration and injection of the hydrogel into the disc space, partial ejection of hydrogel material was seen in some cases once the specimen was put under load.

This was due to the relatively large diameter needle used to initiate the extrusion of nucleus from the disc, creating a large cavity that material could flow out of with ease. Previous work found no issues with hydrogel containment when a smaller gauge needle was used (Balkovec et al., 2013). Translations of the bottom cup were measured and averaged 7.3mm ± 1.2mm, 7.6mm ± 1.7mm, and 7.6mm ± 1.4mm for the pre-disc height loss trials, disc height loss trials, and disc height restored trials respectively.

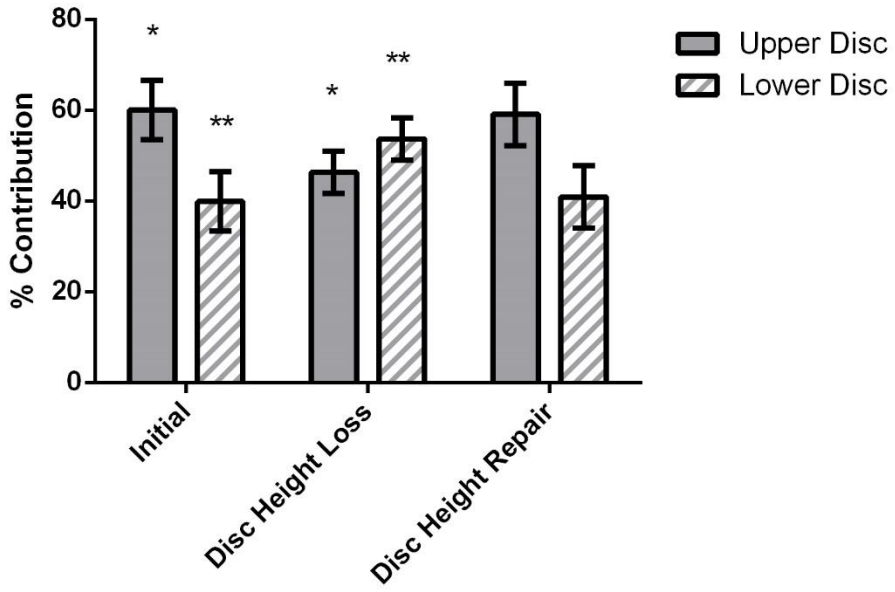

Figure 4.9 Summary angular displacement data for the upper disc damage group. Disc height loss of the upper disc resulted in a lower contribution of angular displacement from the upper disc and a higher contribution from the lower disc relative to the initial trial. After disc height restoration via hydrogel injection, both segments returned to pre-injury levels of angular displacement. Asterisks denote significance between respective time-points.

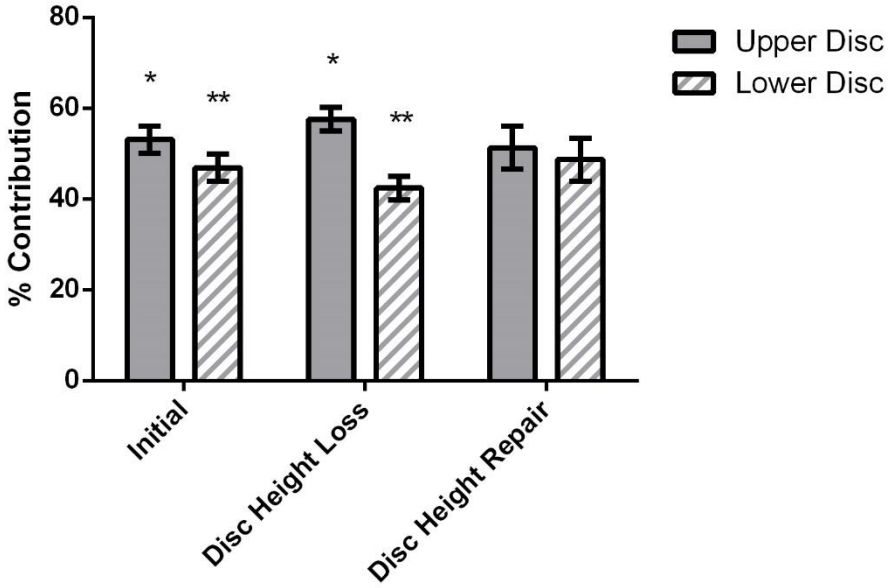

Figure 4.10 Summary angular displacement data for the lower disc damage group. Disc height loss of the lower disc resulted in a lower contribution of angular displacement from the lower disc and a higher contribution from the upper disc relative to the initial trial. After disc height restoration via hydrogel injection, both segments returned to pre-injury levels of angular displacement. Asterisks denote significance between respective time-points.

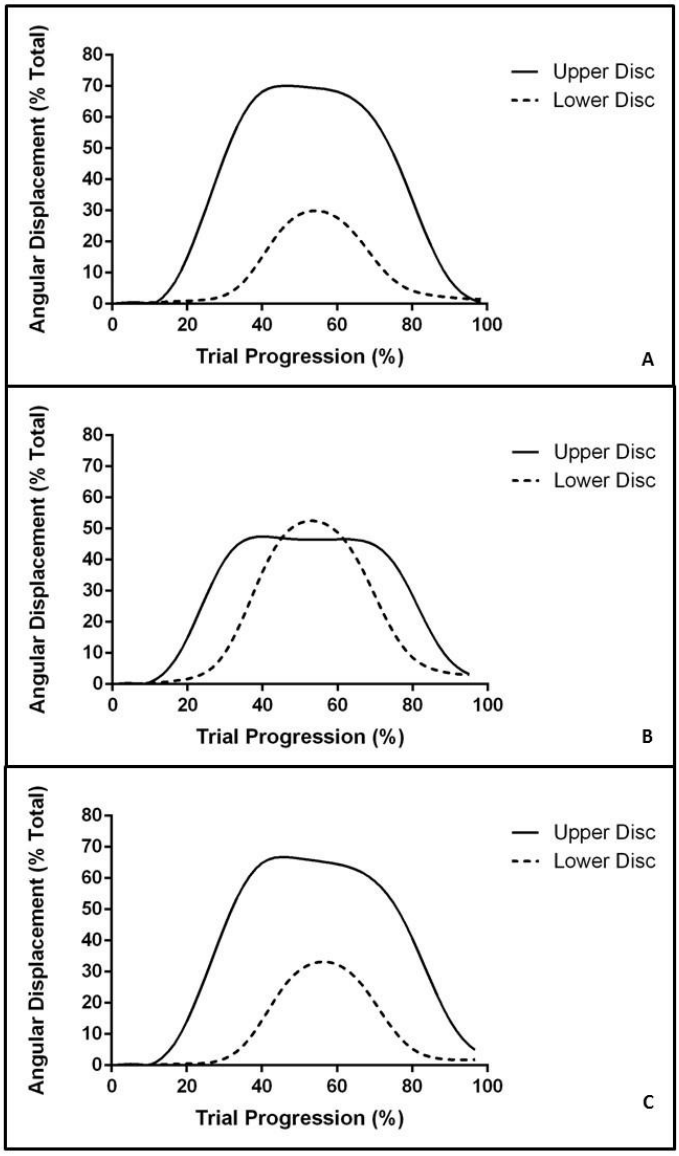

Figure 4.11 Sample time-history data for an upper disc damage specimen. (A) Displacement about the upper and lower segments occur at a fixed distribution between the two. (B) The upper disc is punctured and disc height is lost, causing less angular displacement to occur about that level while more angular displacement occurs about the adjacent level. (C) Hydrogel is injected into the upper disc and disc height is restored, Angular displacement about both upper and lower segments returns to the same distribution as in (A).

4.6 Discussion

The hypothesis (hypothesis 1) that disc height loss would result in a lower level of angular displacement by the injured disc was supported. This indicates that disc height has a significant effect on the mechanics of a segment and an adjacent level, as rotation increased about the non-injured segment. The hypothesis (hypothesis 2) that disc height restoration via hydrogel injection would return injured discs to their initial relative levels of angular displacement was also supported. The tests for within-subjects effect across the two groups indicated that there was a significant difference between the three intervention conditions ($p = 1.5x10^{-11}$), confirming hypothesis 3.

This study has shown that loss of disc height via loss of nucleus pulposus can affect the kinematics of both the injured and the adjacent segment. When disc height is lost, there is lower angular displacement about the injured segment and compensation, via increased angular displacement, is seen about the adjacent segment. One explanation for why this occurs could be due to local rotational stiffness at each disc. Previous work has shown that when a disc undergoes cyclic flexion to extension motions in order to produce a herniation, stiffness of the segment increases (Callaghan and McGill, 2001, Balkovec et al., 2013). Disc height during this process has also been shown to decrease (Scannell and McGill, 2009, Balkovec et al., 2013). In the present study, the torque resisted by specimens was observed to increase by 20.9% ± 14.6% when disc height loss was induced, indicating an increase in the specimen stiffness presumably at the level that was damaged. When being taken to a target flexion-extension angle and there are two possible segments in the current experimental setup that motion can be elicited from, motion occurs about the segment that is most compliant. When disc height loss is induced however, the stiffness in the affected segment will be greater and thus, the moment required to initiate rotation will need to be greater. Given that there is a more compliant segment for rotation to occur about however, the observed quantity of rotation that occurs about

the segment with disc height loss will decrease. This investigation used position control to bring specimens to the same target angle as opposed to torque control which would use the same applied moment. Under torque control, less motion would have occurred given the increased overall stiffness of the specimens. Thus, the results from this investigation apply to scenarios where movement is position controlled.

Previous research on cadaveric specimens (Tanaka et al., 2001) and finite element models (Kim et al., 1991, Ruberte et al., 2009), has mostly focused on grouping based on degenerative grade, which makes direct comparison with the present research difficult. Interestingly however, higher grades of degeneration include disc height loss or disc thinning (amongst other visual features) in their criteria (Pfirrmann et al., 2001, Thompson et al., 1990, Adams et al., 1986). In work that examines cadaveric tissue at higher grades of degeneration, there is an associated decrease in range of motion, presumably due to the fibrotic nature of the tissue that leads to a higher disc stiffness (Tanaka et al., 2001, Lao et al., 2015a). In vivo work has found similar results, with higher grades of degeneration (and thus disc height loss) being associated with less angular displacement at that particular level and a compensation by other segments (Lee et al., 2015). Recent work has also examined the effects of Schmorl's nodes on spine kinematics in vivo, resulting in observations that movement is reduced at the level of damage (Hayashi et al., 2014, Yin et al., 2015). A Schmorl's node would result in disc height loss due to the migration of nucleus into the vertebral body space. Certainly there are other factors that may have affected segmental mechanics in those studies, however, the results from this research indicate that disc height loss is a large contributing factor.

While the results of this work may seem to disagree with the findings of Kirkaldy-Willis and Farfan (Kirkaldy-Willis and Farfan, 1982), the findings are not necessarily incompatible. Disc height loss is proposed here to increase the rotational stiffness of a disc and will result in a lower angular displacement about that segment. The general findings of Kirkaldy-Willis and Farfan where they characterize degenerative changes to the spine as undergoing temporary

dysfunction, an unstable phase, and stabilization do not explicitly look at disc height loss, but rather spinal injury in general (Kirkaldy-Willis and Farfan, 1982). Further, their findings were related to joint micro-movements and not the larger rotations that were described here. To reconcile their findings with mechanics of a spine specimen, the initial stage would involve the point of structural failure, the second stage would involve a decrease in segment stiffness, and the third would involve an increase in segment stiffness. It is also plausible that specimens in this study were unstable with respect to joint micro-movements of one vertebra over another when disc height loss was induced. Disc height loss was observed during the testing protocol to cause a qualitative bulging of the annulus. This bulging would presumably create slack in the ligamentous structure of a segment and make the occurrence of micro-movements more common. These results therefore, stand alongside Kirkaldy-Willis and Farfan and serve to guide more specific conclusions with respect to the mechanical capabilities of a segment with disc height loss.

The results from this study highlight that disc height loss results in increased angular displacement about an adjacent segment under sagittal-plane motions. While in a full spinal column, the roughly 15% loss in angular displacement could be distributed throughout multiple segments, the data presented in this study are merely the acute results. The consequences could become even more drastic as further degeneration and stabilization of the injured joint take place. Further, the cumulative effects of even a relatively small amount of extra range of motion applied to an adjacent segment could potentially result in a faster rate of tissue failure. This is all dependent on the individual and their tendencies to replicate the mechanism of injury. For example, an individual who herniates a disc through repeated bending will lose disc height at the herniated level, stiffening the segment. Continuing to bend (replicating the mechanism of their injury) will cause compensation along the intervertebral joint linkage and potentially increase the bending, stress, and risk of tissue failure at adjacent segments.

Disc height loss represents a very drastic change to the environment of the disc; acute disc height loss could be seen as “the beginning of the end” or the start of increased pathological changes (Jarman et al., 2015). With height loss, the annulus is placed under a higher magnitude of axial compressive stress and could more readily increase the rate at which concentric rings of collagen are delaminated (Tampier et al., 2007), promoting further degradation of tissue. Disc height loss also has the potential to alter the stress distribution within the disc (Adams et al., 1996), which has implications for transferring load to the neural arch and posterior elements in the spine (Adams and Hutton, 1980, Pollintine et al., 2004b). Pressure between facet joints during disc height loss has also been found to increase (Dunlop et al., 1984), potentially creating arthritic problems in the future and a potential avenue for causing pain from the facet joint capsule (Crosby et al., 2014). Further consequences of altered disc height include the cellular environment, which has implications for the longer term degenerative consequences of the disc. With disc height loss inducing a lower nucleus volume, the fixed charge density of the disc would change due to the lower proteoglycan content (Urban and Maroudas, 1981). This would have implications with respect to the swelling pressure of the disc and the microenvironment that sustains the chondrocyte-like cells of the nucleus (Trout et al., 1982, Xu et al., 2014). They are uniquely suited to surviving in high-pressure hypoxic environments (Jiang et al., 2014, Chen et al., 2014), and a loss of these conditions could result in their dysfunction. Further, altered stress distributions in the disc along with loss of proteoglycans, promotes the ingrowth of blood vessels and nerves (Stefanakis et al., 2012).

The use of the hydrogel in this study provides mechanical evidence that disc height restoration could potentially restore the kinematics of a disc with height loss. It is important to note that the discs tested in this investigation were acutely injured and then repaired, it is unclear how kinematics would be restored in a spine that is further degenerated. For example, the presence of osteophytes would increase the stiffness of the segment alongside disc height loss, potentially inhibiting a return of pre-injury kinematics. Regardless, it provides a viable

alternative to more invasive surgical procedures when warranted; future work should begin to look at its viability in live-animal models.

Limitations of this study include its use of a juvenile porcine spine model. Disc height loss was induced in specimens with uninjured tissues, it is unclear how other confounding factors such as osteophytes or endplate defects would influence the mechanics of a segment. Nevertheless, this is the first study that has examined the effects of disc height loss via loss of nucleus pulposus on a disc and its adjacent segment. This research provides an important starting point to begin to examine the effects of other factors in altering the mechanics of the spine. Further the porcine cervical spine has been shown to be a suitable analog for the human lumbar spine with respect to anatomy, geometry (Yingling et al., 1999), and function (Tampier et al., 2007) for the purpose of discerning injury mechanisms.

Further considerations for the experimental setup used and its influence on the observed spine kinematics need to be taken into account. A limitation of the apparatus used was that each segment was subject to different applied moments. This caused the observed effect of the upper segment rotating almost fully to its observed end-range reached in the protocol before rotation was initiated in the lower segment. Despite this limitation, rotation of each segment was limited by the resistance of its passive tissues and its inherent stiffness. When disc height was lost, stiffness increased and motion occurred to a greater extent about the non-affected (and more compliant) segment. It is presumed that the local stiffness at that segment was lower than the local stiffness at the segment with height loss. Thus, more motion occurred about the joint with lower stiffness. This local stiffness of the segment would be the same property driving motion *in-vivo*. The translations of the specimen are similar to the translations that occur *in-vivo*, and are designed to mimic a person bending forward. Translation of the whole spine would occur about the pelvis, and thus, the bending moment generated at lower levels as the result of the gravitational loading of the torso would vary depending on the segmental level, the same as was observed in this study. From this, the findings of this study are limited and

comparable to only specific loading scenarios *in-vivo*, and do not necessarily reflect the influence of disc height loss under other loading paradigms.

This study has shown that disc height loss through loss of nucleus pulposus induces kinematic changes which have consequences beyond the injured disc under the tested loading conditions. When disc height is lost, the sagittal plane range of motion of the injured disc is reduced and the angular displacement from an adjacent segment is increased. This research provides novel data on how disc height loss via loss of nucleus pulposus influences spinal mechanics. Future work will be able to use this data as a starting point to determine the effect of further features of injury and damage in inducing kinematic changes to the spine.

Chapter 5: Study 2

The Efficacy of a Combination of PMMA and Injectable Hydrogels on Mitigating Bony Damage and Restoring Joint Mechanics to a Vertebral Body Motion Segment

5.1 Background

Compressive fracture of a vertebral body can produce profound changes in a spinal motion segment. Axial injury to the spine has been shown to produce a variety of fracture patterns (Yingling et al., 1997) with the potential to damage the vertebral body, intervertebral disc, or both structures. Damage to the disc via fracturing of the underlying cartilaginous endplate could result in migration of nucleus into the vertebral body itself, causing depressurization of the disc space (Adams et al., 1993) and height loss. Fracturing of the vertebral body results in a loss of compressive stiffness which could affect additional segments and their mechanical properties. Clinically, vertebral body fractures can result in a kyphotic deformity in the case of anterior wedge fractures (Landham et al., 2015b, Liu et al., 2015). The vertebral body also has a rich vascular and nerve supply (Bailey et al., 2011), and damage could result in sensitization and nociception (Bailey et al., 2011, Fields et al., 2014). Attempts to surgically repair a compressive fracture need to address both the loss in disc height and nuclear material, as well as the damage to the underlying trabecular bone in the vertebral body. Restoring the mechanical profile of a compressively injured spine segment could help to mitigate further degenerative changes and restore function. Two techniques which present the potential ability to restore the mechanical profile of a compressively damaged spine motion segment are hydrogel injection and vertebroplasty. While both have been tested individually (Balkovec et al., 2013, Luo et al., 2009), they have never been combined before. They provide

a plausible solution to restoring both the compressive and rotational mechanical properties of axial compressive injuries.

The use of injectable hydrogels is an emerging technique to restoring height and function to a pathologic disc. It preserves the original anatomy of the disc rather than replacing it entirely. In addition, vertebroplasty has been used to repair fractured vertebral bodies and restore stiffness characteristics to vertebrae. Vertebroplasty has been shown to restore stress distributions and stiffness to the vertebral body (Luo et al., 2009) and hydrogel implants have also been shown to do this for the disc (Bertagnoli et al., 2005). The impact of both these repair modalities together has never been tested before but could offer a viable alternative to some instances of spinal fusion surgery, maintaining function in the patient as well as restoring the structural integrity of the injured segment.

The purpose of the following investigation was to determine if the combined use of hydrogel injection and vertebroplasty could restore the mechanical profile of an axially injured spinal motion segment.

5.2 Significance

Findings from this study will improve understanding in how disc height restoration plays a role in restoring mechanics to severely damaged spines. It will also begin to parse out the different roles of the components of a spinal segment in the normal mechanical functioning of the disc. This research will help to unify two separate clinical procedures and lay the groundwork for producing a novel surgical technique that provides both repair and restoration of function in injured spinal segments.

5.3 Hypotheses

1. Hydrogel injection will alter rotational stiffness levels from the compressively fatigued state.
2. PMMA injection will alter compressive stiffness levels from the compressively fatigued state.

5.4 Methods

5.4.1 Specimens and Preparation

Two groups of seven porcine cervical spines (age: 6 months, weight: 80kg) were used for this investigation. For each cervical spine, two functional spinal units were obtained, consisting of the C3/C4 vertebral bodies and C5/C6 vertebral bodies along with the intervening disc. Each specimen therefore, consisted of two vertebral bodies and their intervening disc. Specimens were randomly divided into two groups that dictated the order in which they would receive each intervention. Group 1 used three C3/C4 motion segments and four C5/C6 motion segments and received hydrogel injection first. Group 2 used four C3/C4 motion segments and three C5/C6 motion segments and received PMMA injection first. The porcine cervical spine has been shown to be a suitable analog for the human lumbar spine with respect to anatomy, geometry (Yingling et al., 1999), and function (Tampier et al., 2007) for the purpose of discerning injury mechanisms.

Specimens were dissected by removing as much muscular tissue as possible while leaving ligamentous structures intact. Following dissection, specimens were mounted in customized stainless steel cups and secured using screws drilled through the superior and inferior endplates and wire looped bilaterally through the lamina and anterior processes. Non-exothermic dental stone (Denstone®, Miles, South Bend, IN, USA), further secured the specimens in their mounting cups.

5.4.2 Equipment

All specimens were tested in a servohydraulic dynamic testing machine (Instron, model: 8511, Instron Canada, Burlington, Ontario, Canada) as described in Section 4.4.2. Due to the nature of the hydrogel being used in this investigation, specimens also had to be heated to body temperature for testing. This was performed using the same temperature chamber described in Section 4.4.2, which brought the specimens up to body temperature and maintained it throughout the testing protocol. Omnipaque was injected into the disc space using a 21-gauge needle; this served to monitor the location of the nucleus under x-ray and assist in determining whether the administered endplate fracture was created in the superior or inferior endplate.

5.4.3 Vertebroplasty

The technique used to inject the PMMA cement was similar to that used by Landham and colleagues (Landham et al., 2015a). PMMA cement (Spineplex, Stryker Instruments, Howmedica International, Limerick, Ireland) was prepared by mixing 20g of powder with the provided ampoule of liquid. Two 10-gauge needles were inserted through the pedicles of the fractured vertebra (Figure 5.1). Sagittal and frontal plane x-rays were used to ensure that the needles were placed near the fracture site. 2 cm^3 of cement was injected through each needle, and the stylet of each cannula was re-inserted to ensure that there was no backflow of cement. After 10 minutes, the needles were removed, and the cement was allowed to set over a one-hour period. X-rays were taken to confirm that the cement had been placed properly. After this, specimens were loaded under 300N of axial compression for 30 minutes to allow the cement to consolidate (Landham et al., 2015a).

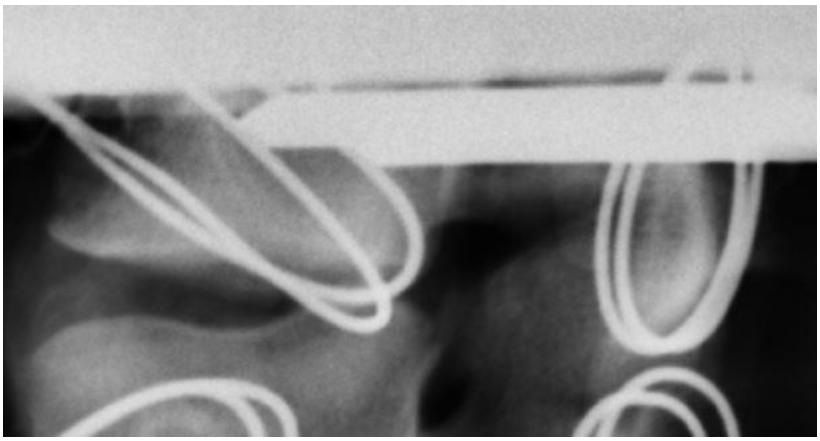

Figure 5.1 Insertion of 10 gauge needles through the pedicles of the vertebral body, sagittal view.

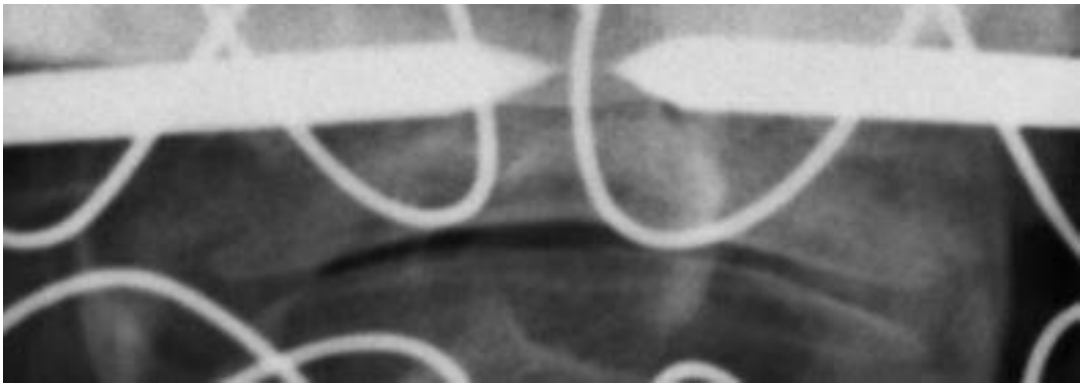

Figure 5.2 Insertion of 10 gauge needles into the vertebral body, frontal view.

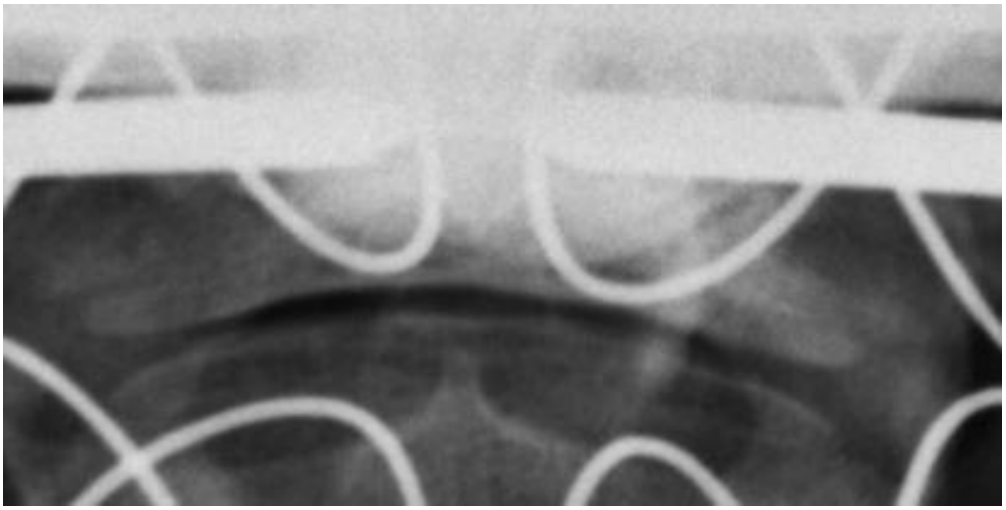

Figure 5.3 Needles present in vertebral body following injection of bone cement.

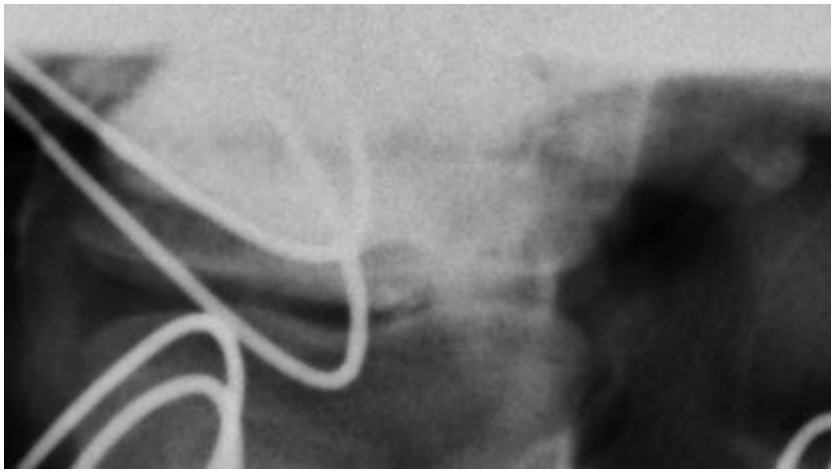

Figure 5.4 Sagittal view of bone cement injected into superior vertebra.

5.4.4 Hydrogel

The hydrogel used was a composition of thermally-responsive branched copolymers of poly(N-isopropylacrylamide) (PNIPAAm) and poly(ethylene glycol) (PEG) (Vernengo et al., 2008). The copolymer was prepared by free radical polymerization of PNIPAAm monomer in the presence of PEG (4600 g/mol) dimethylacrylate in a molar ratio of 700 to 1. The advantage of this hydrogel is that the solidification process occurs inside the disc without the use of any toxic monomers or crosslinkers. This property allowed it to be injected and conform to the unique shape of the disc, something that has been found with model data to be ideal in restoring normal stress distribution to the disc (Dahl et al., 2010).

Hydrogel was injected into the specimens using an 18-gauge needle and syringe. Following injection, specimens were left unloaded for 15 minutes to ensure that it had fully changed to its gel state.

5.4.5 Specimen Testing Protocol

Specimens were preloaded for 15 minutes at 300N in order to counter any post-mortem swelling which may have occurred. Specimens were then loaded to 1000N of axial compression and brought through a passive range of flexion and extension to establish the range of motion where there is a linear relationship between angular displacement and torque (Panjabi et al., 1989). A flow chart of the experimental procedure is located in Figure 5.5.

Following the passive test, specimens were brought to a reference load of 300N in the neutral position, defined as the point where there was zero moment applied to the specimen by the motor arm. This load was used for the measurement of specimen height via the hydraulic ram position of the Instron. After the reference load trial, specimens were subject to a compressive stiffness test and a repeated rotational stiffness test. Values used for compressive stiffness and cyclic compression were based off of the predictive equation for estimating compressive strength by Parkinson and colleagues (Parkinson et al., 2005). Dimensions of the intact disc were estimated using the average of the medial-lateral width and anterior-posterior length of the two exposed endplates on a specimen. Those two values were then used to estimate the cross sectional area of the disc by using the equation for the surface area of an ellipse ($\pi/4$ * Anterior-Posterior Length * Medial-Lateral Width) in the same manner as Callaghan and McGill (Callaghan and McGill, 1995).

The order in which the two tests were performed was randomized. During the compressive stiffness test, specimens were loaded in axial compression to 50% of their estimated compressive strength at a loading rate of 1000N/s, this was performed twice to ensure that there was no aberrant stiffness value produced by unloading the specimen. The rotational stiffness test brought specimens through 10 cycles of flexion and extension angles pre-defined in the passive test under 1000N of axial compressive load. These tests established the baseline compressive and rotational stiffness of a specimen under non-injury conditions. All

angular displacement tests were performed with the motor arm of the Instron in position control, bringing specimens to a target angular displacement for each cycle at a rate of 1Hz.

After initial stiffness measurements were made, specimens were loaded in axial compression to failure. Failure was defined as a deflection in the force-displacement curve of 3.125% over a period of 25ms (Figure 5.6). Specimens were then subject to cyclic compressive loading to 30% of their estimated compressive strength for 1000 cycles at a loading rate of 0.5Hz (Hansson et al., 1987, Holmes and Hukins, 1994, Parkinson and Callaghan, 2007).

After failure loading, the reference load, compressive stiffness test, and rotational stiffness test were repeated to establish the change in the specimen's mechanical properties after injury. Following this, specimen group 1 was injected with hydrogel while group 2 was treated using PMMA. The reference load, compressive, and rotational stiffness tests were repeated followed by group 1 receiving PMMA injection, and group 2 receiving a hydrogel injection. The second intervention for each group was followed by another round of reference loading, compressive stiffness, and rotational stiffness tests.

After both groups had received both interventions of hydrogel and PMMA injection, specimens were subject to a final 1000 cycles of repeated compressive loading at 30% of their estimated compressive strength. Radiographs of testing stages are shown in (Figure 5.7, Figure 5.8, Figure 5.9, Figure 5.10, Figure 5.11, Figure 5.12, and Figure 5.13).

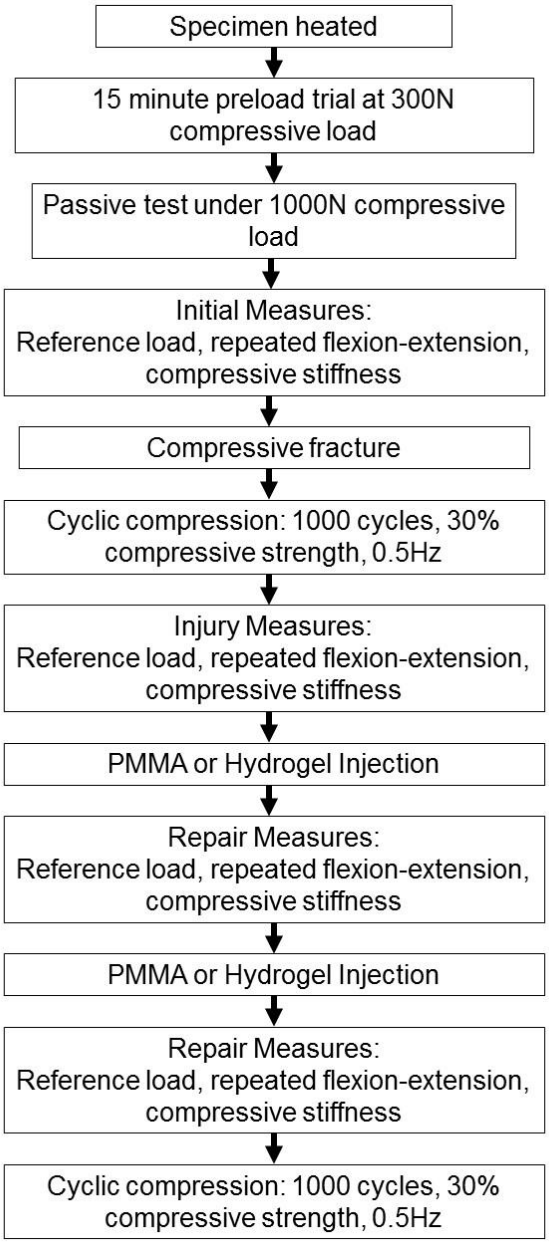

Figure 5.5 Flow chart of experimental protocol for Study 2.

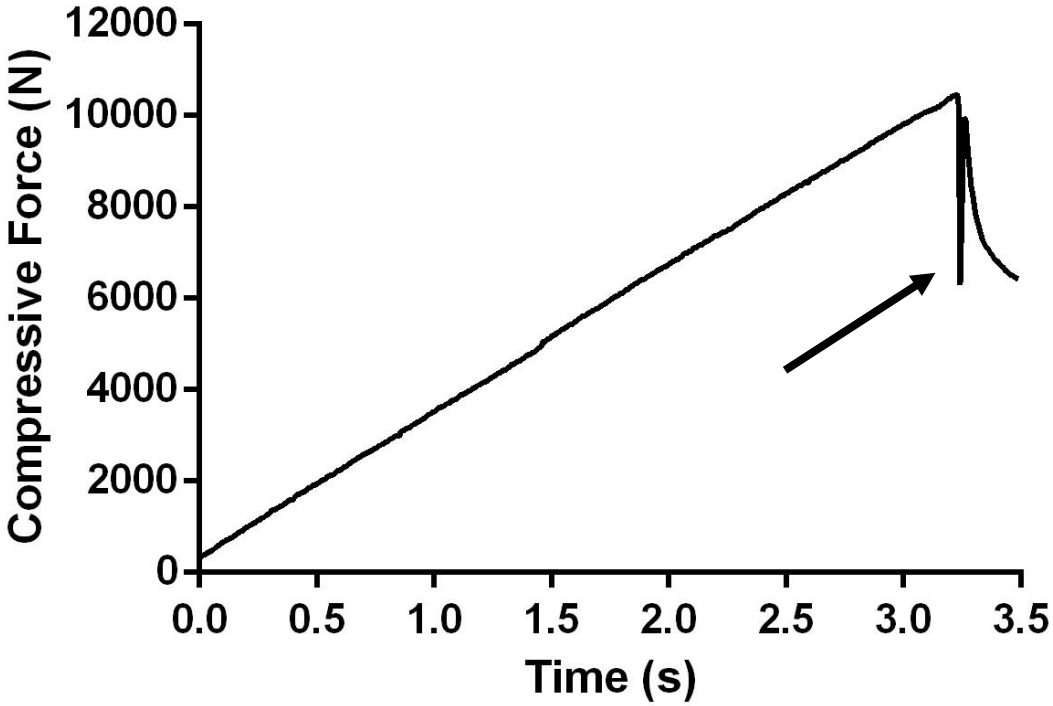

Figure 5.6 Sample specimen failure point showing the deflection in the load applied by the hydraulic ram.

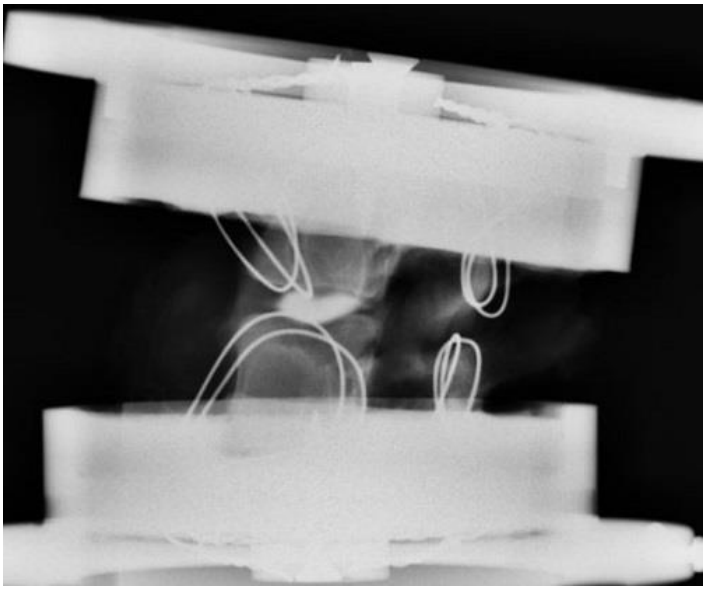

Figure 5.7 Initial specimen condition. A radio-opaque dye was injected into the nucleus.

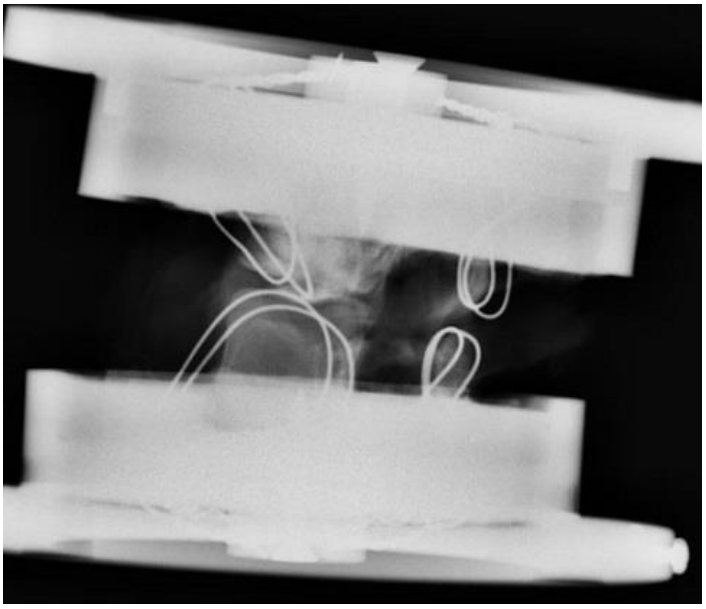

Figure 5.8 Specimen post-fracture, the dye can be seen in the superior vertebral body indicating a superior endplate fracture.

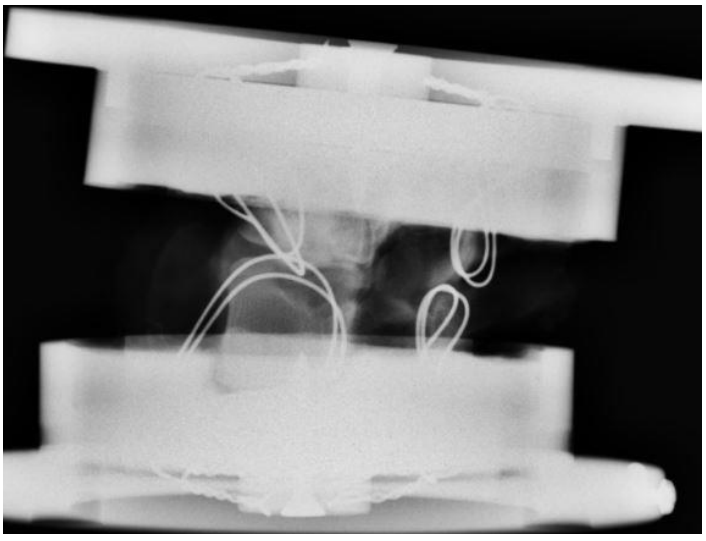

Figure 5.9 Specimen post cyclic compressive cycles.

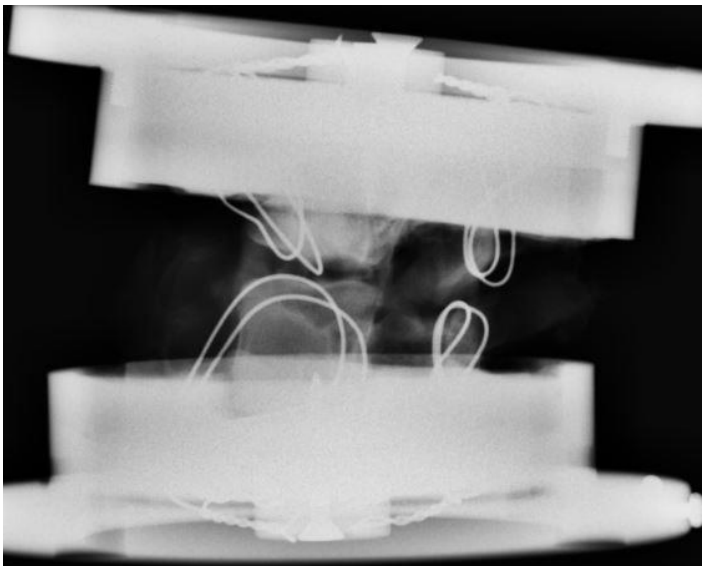

Figure 5.10 Specimen post-hydrogel injection, increased disc height as a result of injection can be seen.

Figure 5.11 Specimen post PMMA injection. The cement was radio-opaque and its injection site can be visualized.

Figure 5.12 Specimen post cement consolidation.

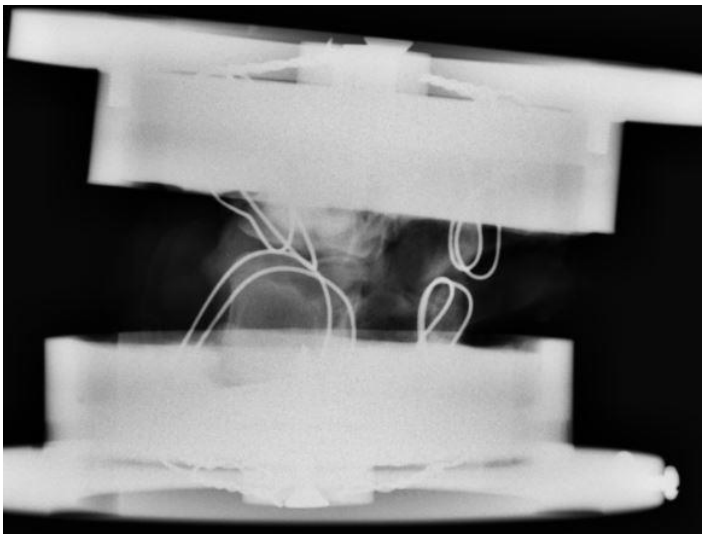

Figure 5.13 Specimen following another round of cyclic compressive loading. The disc height can be visually seen as diminished compared to the hydrogel injection stage.

5.4.6 Data Analysis

Rotational stiffness was calculated by taking the average rotational stiffness value for each time point over the course of a trial of 10 cycles of repeated flexion to extension. Rotational stiffness values were expressed in units of Nm/°. Compressive stiffness was calculated by dividing the peak compressive load that specimens were exposed to by the relative vertical displacement of the hydraulic ram on the Instron to yield compressive stiffness expressed in units of kN/mm. After calculation, and to facilitate comparison between specimens, values were normalized as a percentage of the initial values for rotational and compressive stiffness. Each of the values obtained: compressive stiffness, and rotational stiffness were compared within subjects for the initial values, values post-injury, and values after each intervention (hydrogel and PMMA injection). Specimen height was also tracked through the testing protocol as a function of the position of the hydraulic ram. Values obtained after fatigue testing once both interventions had been administered were used to characterize the degradation of the mechanical profile of each of these interventions and examine when specimens could be expected to return to their post-injury state.

5.4.7 Statistical Analysis

This experiment incorporated a crossover design where both groups were treated to the same conditions but at different time points. Currently, both of these interventions could be performed independent of each other in an *in-vivo* surgical scenario. Vertebroplasty is a common procedure performed on its own already, and there are some instances of nucleus replacement *in-vivo* (Bertagnoli and Schonmayr, 2002, Ahrens et al., 2009). Thus, the study design allows for the role of each intervention to be examined independently and combined with another intervention. For the purposes of statistical analysis, a 2x5 repeated measures ANOVA was performed with independent variables consisting of order of treatment (between subjects) and time (within subjects). Dependent variables were the response of specimens after the initial

fatigue trial, after hydrogel injection, after PMMA injection, and after the fatigue trial once both interventions had been performed, all compared to the initial value. These variables are listed in Table 5.1. A test was performed for both rotational stiffness values and for compressive stiffness values. A Bonferroni post-hoc adjusted for multiple comparisons. All statistical tests were performed using SPSS software (IBM, Somers, NY, USA).

Table 5.1. Independent and Dependent Variables for Study 2

Independent Variables	Dependent Variables
• Order of intervention (hydrogel first vs. PMMA first) • Time	• Response after initial fatigue trial • Response after hydrogel injection • Response after PMMA injection • Response after final fatigue trial

5.5 Results

Rotational stiffness values were significantly influenced within subjects over time ($p = 0.00004$) while there was no interaction between group and time ($p = 0.36$). Pairwise comparisons revealed that while the hydrogel was able to restore the rotational stiffness values and change them compared to the fatigue conditions ($p = 0.003$, $p = 0.005$), it could not maintain this effect after repeated cyclic compression as rotational stiffness returned back to initial fatigue values following the second compressive fatigue protocol ($p = 0.96$). Overall, rotational stiffness was found to be influenced over time (Figure 5.14). Normalized rotational stiffness values for all specimens throughout the testing stages are presented in Table 5.3 and Table 5.4.

As with rotational stiffness, there was a significant influence of time for compressive stiffness values within subjects ($p = 0.001$) while there was no interaction between group and

time ($p = 0.63$). Pairwise comparisons revealed that PMMA injection could significantly alter the compressive stiffness value of a specimen compared to the fatigue conditions ($p = 0.02$, $p = 0.0003$). As with rotational stiffness values however, this effect could not be maintained with repeated cyclic compression as compressive stiffness returned back to initial fatigue values ($p = 0.344$). Overall, the compressive stiffness was found to be influenced over time (Figure 5.15). Normalized compressive stiffness values for all specimens throughout the testing stages are presented in Table 5.5 and Table 5.6.

Over testing, there was no observed containment issue between the hydrogel and the initial injection site at the anterior of the disc. Endplate fractures featuring a more open crack however, were not able to facilitate hydrogel containment (Figure 5.16). Given that no hydrogel extruded through the injection site, it was presumed to be ejected from the disc through cracks in the endplate. Upon dissection, no evidence of hydrogel was present in these discs with open cracks while those without breaches in the endplate contained evidence of hydrogel (Figure 5.17). Specimen height values were tracked throughout testing and expressed relative to their initial height, these values are contained in Table 5.7 and Table 5.8.

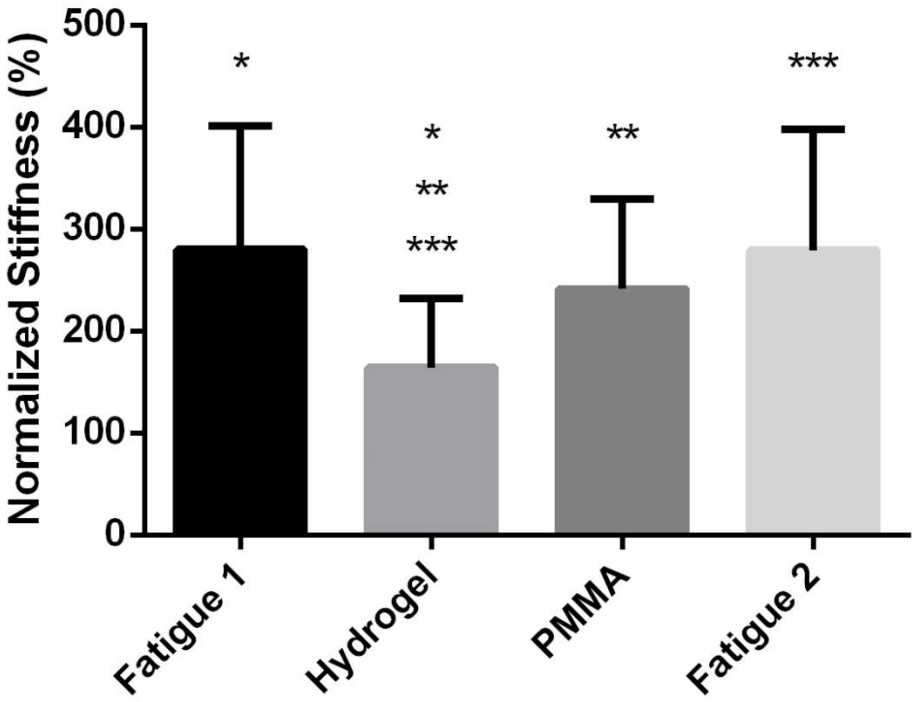

Figure 5.14 Normalized rotational stiffness values for both specimen groups. Asterisks denote significance between matching pairs. The hydrogel injection significantly restored rotational stiffness values to near initial values (100%).

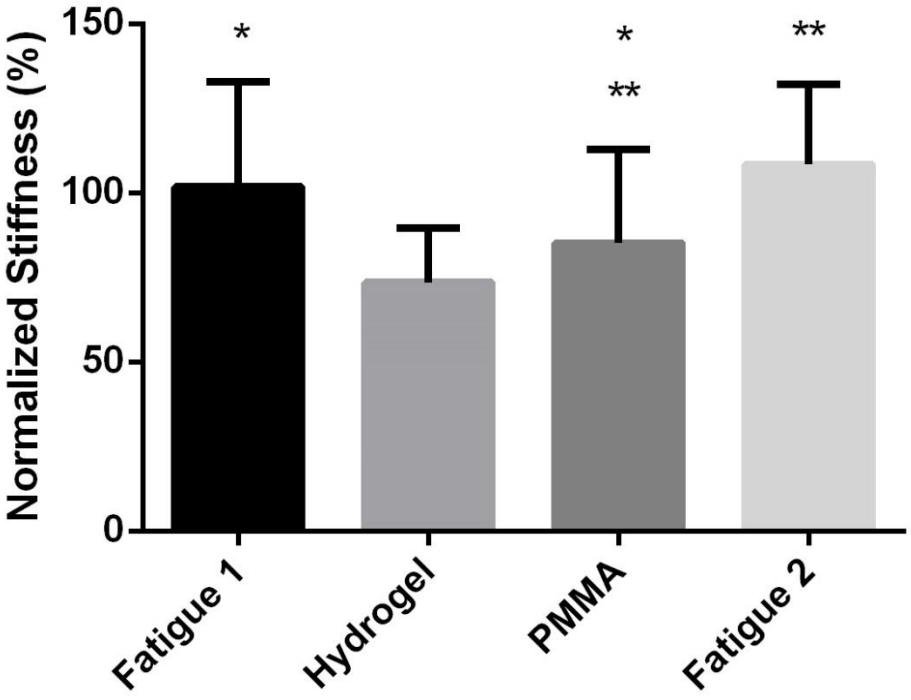

Figure 5.15 Normalized compressive stiffness values for both specimen groups. Asterisks denote significance between matching pairs. PMMA injection significantly reduced compressive stiffness values compared to fatigue trials.

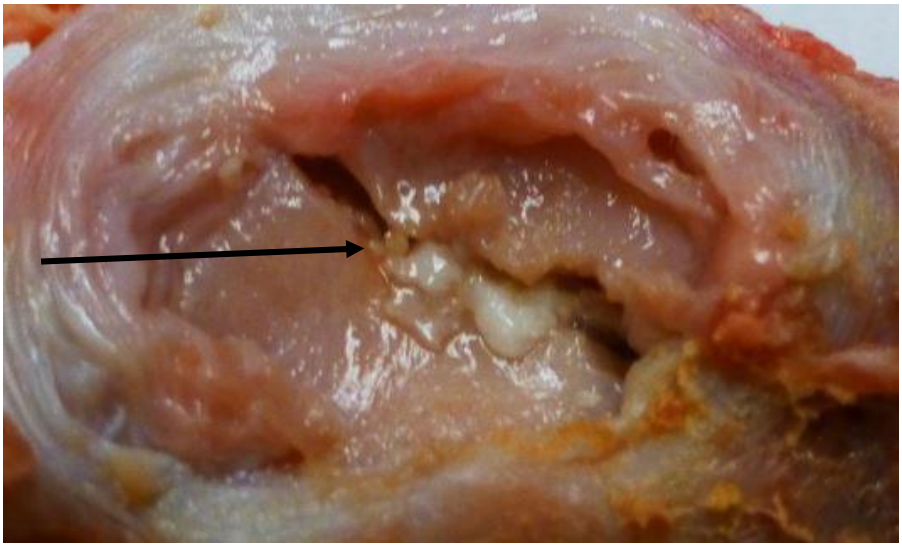

Figure 5.16 A large breach in the endplate is evident here, exposing the internal disc space to the vertebral body.

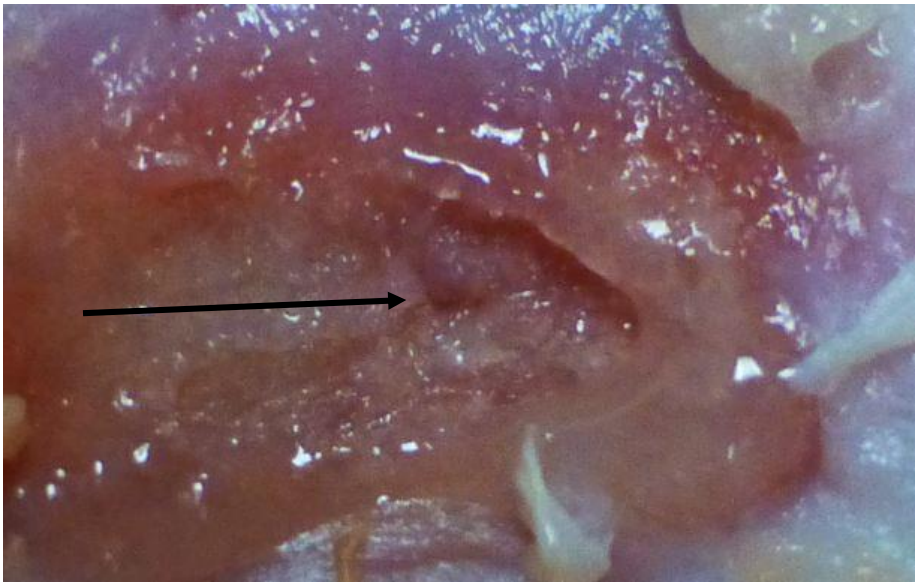

Figure 5.17 A fracture that did not breach the cancellous bone of the endplate, there was still evidence of hydrogel within the discs of these specimens.

Table 5.2. Specimen Failure and Fracture Data

	Failure Load (kN)	Fracture Type (Endplate Breach vs. No Breach)	Endplate Cross-Sectional Area (mm^2)
Specimen 1	7.5	No Breach	526
Specimen 2	11.3	No Breach	495
Specimen 3	10.0	No Breach	618
Specimen 4	9.9	No Breach	646
Specimen 5	9.4	Breach	499
Specimen 6	10.5	Breach	594
Specimen 7	12.1	No Breach	592
Specimen 8	10.5	Breach	614
Specimen 9	12.2	No Breach	609
Specimen 10	11.8	Breach	614
Specimen 11	10.3	Breach	668
Specimen 12	9.7	Breach	614
Specimen 13	14.2	Breach	605
Specimen 14	12.5	Breach	479
Average (SD)	**10.8 (1.6)**		**584 (60)**

Table 5.3. Specimen group 1 normalized rotational stiffness values throughout testing trials.

	Initial (%)	Fracture (%)	Fatigue loading (%)	Hydrogel injection (%)	PMMA injection (%)	Fatigue loading (%)
Specimen 1	100	205.8	289.2	107.6	231.3	270.1
Specimen 2	100	102.8	212.8	67.4	201.2	262.3
Specimen 3	100	501.5	555.5	118.2	373.4	583.4
Specimen 4	100	456.6	485.7	266.8	427.6	487.6
Specimen 5	100	172.5	271.2	252.1	312.4	282.6
Specimen 6	100	81.4	103.8	77.5	98.3	132.4
Specimen 7	100	161.2	190.1	170.8	154.5	166.3
Average (SD)	**100**	**240.3 (168.9)**	**301.2 (162.7)**	**151.5 (81.0)**	**257.0 (119.1)**	**312.1 (164.9)**

Table 5.4. Specimen group 2 normalized rotational stiffness values throughout testing trials.

	Initial (%)	Fracture (%)	Fatigue loading (%)	PMMA injection (%)	Hydrogel injection (%)	Fatigue loading (%)
Specimen 8	100	166.7	277.2	246.7	100.4	294.5
Specimen 9	100	170.9	244.3	231.1	189.6	236.5
Specimen 10	100	227.4	216.9	210.6	216.3	230.6
Specimen 11	100	156.9	193.3	160.4	133.3	248.6
Specimen 12	100	233.3	368.7	279.6	261.1	227.1
Specimen 13	100	244.0	318.2	277.7	143.3	274.9
Specimen 14	100	176.0	194.2	177.3	196.6	214.4
Average (SD)	**100**	**196.5 (36.8)**	**259.0 (66.3)**	**226.2 (46.4)**	**177.2 (54.9)**	**246.7 (28.5)**

Table 5.5. Specimen group 1 normalized compressive stiffness values throughout testing trials.

	Initial (%)	Fracture (%)	Fatigue loading (%)	Hydrogel injection (%)	PMMA injection (%)	Fatigue loading (%)
Specimen 1	100	124.0	113.6	83.8	124.0	134.5
Specimen 2	100	110.1	143.9	71.3	112.4	144.6
Specimen 3	100	80.0	103.6	89.8	109.3	139.5
Specimen 4	100	74.8	113.9	94.5	99.7	118.3
Specimen 5	100	58.3	81.9	69.4	57.3	81.5
Specimen 6	100	68.4	76.1	75.0	49.3	75.2
Specimen 7	100	42.7	74.2	85.1	73.1	80.3
Average (SD)	**100**	**79.8 (25.2)**	**101.0 (25.4)**	**81.3 (9.6)**	**89.3 (29.3)**	**110.6 (30.7)**

Table 5.6. Specimen group 2 normalized compressive stiffness values throughout testing trials.

	Initial (%)	Fracture (%)	Fatigue loading (%)	PMMA injection (%)	Hydrogel injection (%)	Fatigue loading (%)
Specimen 8	100	88.5	132.7	96.4	70.3	116.4
Specimen 9	100	84.1	150.8	127.4	46.8	112.1
Specimen 10	100	43.6	61.1	40.5	47.9	84.4
Specimen 11	100	39.8	67.4	63.4	47.8	121.0
Specimen 12	100	102.3	136.7	93.3	84.4	125.3
Specimen 13	100	53.9	65.4	77.5	89.6	95.9
Specimen 14	100	47.9	104.1	68.4	74.0	89.1
Average (SD)	**100**	**65.7 (25.2)**	**102.6 (38.2)**	**81.0 (27.9)**	**89.3 (29.3)**	**106.3 (16.3)**

Table 5.7. Specimen group 1 height values throughout testing as given by the position of the hydraulic ram (negative indicates height loss). All values were relative the initial height.

	Initial (mm)	Fracture (mm)	Fatigue loading (mm)	Hydrogel Injection (mm)	PMMA Injection (mm)	Fatigue loading (mm)
Specimen 1	0.0	-2.1	-3.2	-0.6	-2.4	-3.2
Specimen 2	0.0	-1.8	-3.0	-0.3	-2.7	-3.9
Specimen 3	0.0	-3.2	-4.0	-2.0	-3.3	-4.7
Specimen 4	0.0	-4.2	-6.0	-3.6	-5.3	-6.2
Specimen 5	0.0	-5.0	-7.5	-5.1	-6.9	-8.3
Specimen 6	0.0	-5.2	-8.1	-5.3	-3.7	-7.9
Specimen 7	0.0	-10.1	-12.7	-11.6	-11.1	-12.9
Average (SD)	**0.0**	**-4.5 (2.8)**	**-6.4 (3.4)**	**-4.1 (3.9)**	**-5.1 (3.1)**	**-6.8 (3.4)**

Table 5.8. Specimen group 2 height values throughout testing as given by the position of the hydraulic ram (negative indicates height loss). All values were relative the initial height.

	Initial (mm)	Fracture (mm)	Fatigue loading (mm)	PMMA Injection (mm)	Hydrogel Injection (mm)	Fatigue loading (mm)
Specimen 8	0.0	-1.2	-2.3	-1.9	0.5	-2.5
Specimen 9	0.0	-3.1	-4.4	-4.4	-1.9	-4.5
Specimen 10	0.0	-3.5	-5.2	-3.7	-2.8	-5.8
Specimen 11	0.0	-4.7	-6.3	-6.3	-4.0	-7.6
Specimen 12	0.0	-4.2	-6.2	-5.6	-3.2	-6.2
Specimen 13	0.0	-3.3	-4.0	-4.7	-2.3	-6.0
Specimen 14	0.0	-5.5	-7.4	-5.1	-4.8	-7.3
Average (SD)	**0.0**	**-3.6 (1.4)**	**-5.1 (1.7)**	**-4.5 (1.4)**	**-2.7 (1.7)**	**-5.7 (1.7)**

5.6 Discussion

The hypothesis (hypothesis 1) that hydrogel injection would alter rotational stiffness from the compressively fatigued state was supported. Hydrogel injection lowered the normalized rotational stiffness levels relative to the fatigue state in group 1 and group 2 to 151.5% ± 81% and 177.2% ± 54.9% of initial values (100%) respectively. This indicates that disc height has a significant effect on the rotational stiffness of a motion segment, but the integrity of the vertebral body also plays a role. The hypothesis (hypothesis 2) that PMMA injection would alter compressive stiffness levels from the compressively fatigued state was also supported. In some specimens, compressive fatigue increased the normalized stiffness relative to the initial value while in other specimens it was decreased. In general, PMMA injection reduced the compressive stiffness which meant that some specimens became more compliant compared to their initial values while others returned closer to baseline. This could be caused by the PMMA restoring some spacing to crushed trabecular bone, or simply through unloaded recovery of the specimens. Further, injection of PMMA would displace blood and bone marrow contained within the vertebral body. The redistribution of these constituents, similar to increasing the plunger

height on a hydraulic ram, could have created a damping effect via the viscous drag of the fluids, reducing stiffness.

While the influences on the rotational stiffness measurements were clear in all cases, the hydrogel caused some confounding effects for the compressive stiffness measurements. With hydrogel injection, disc height was restored and compressive stiffness decreased for all specimens in addition to the expected decrease in rotational stiffness. This indicates that while disc height could be restored, the disc could not regain the same hydrostatic pressure and resulted in greater deformation of the specimen under a compressive load. It was also thought that PMMA would help to contain the hydrogel within the disc, however, this was not the case; containment of the hydrogel in some instances of endplate fracture appears to be more challenging. Further, a trade-off must be made in terms of PMMA injection in order to prevent cement leakage into the disc. PMMA was injected above the fracture site at a level that would prevent cement leakage into the disc through the large cracks present in some specimens. If this had not been a concern, the cement could have been injected much closer to the fracture and containment of the hydrogel may have been enhanced. Further, the presence of blood and bone marrow within the vertebral body itself could have contributed to the difficulty of sealing the endplate, as the displacement of these substances occurs unpredictably and could have left regions where the cement did not penetrate.

There were more instances of endplate breach in group 2 (PMMA injection first) compared to group 1 (hydrogel injection first). It is not entirely clear why this is the case given that the breaches occurred before any of the interventions had been performed. Small differences between the specimens could have been a factor in terms of why some breached while others did not. More brittle endplates in some specimens could have led to the breaching observed in addition to differences within the microarchitecture of the trabecular bone directly underlying the endplate. With less trabecular volume or less trabecular connectivity, there

would have been less support behind the endplates of these specimens, potentially resulting in the observed endplate breaches.

The results of this study agree with findings by Landham and colleagues (Landham et al., 2015a) who found that vertebroplasty made a compressively injured spine specimen more compliant. They also found increased specimen compliance after repetitive loading injury which is in contrast to the results from this study. There were differences however, in the nature of the injuries produced between the two studies which could explain the apparent difference. In terms of compressive stiffness, this study also agrees with work by Luo and colleagues (Luo et al., 2007, Luo et al., 2009) with regard to the pattern of compressive stiffness changes seen. One potential explanation for these results is the phenomenon of unloaded recovery on the part of the specimens. During PMMA injection, specimens are unloaded while undergoing needle placement and allowing the cement to properly set. While they are re-loaded during cement consolidation, it is possible that specimens are able to recover during this unloaded phase. What the cement provides, is protection from further creep deformity (Luo et al., 2015).

Vertebroplasty has been put forward as a preferred procedure to kyphoplasty, which involves the use of an inflatable balloon to restore wedge and compressive deformities in the affected vertebrae. Greater wedge deformity correction is associated with higher adjacent level fracture risk in patients (Liu et al., 2015). Vertebroplasty is also lower cost, and has similar long-term patient outcomes (Liu et al., 2015).

Previous work on herniated discs has shown that the hydrogel is able to restore rotational stiffness characteristics and last through further cyclic flexion-extension motions (Balkovec et al., 2013). This work reveals that endplate fractures make the situation much more complicated, with containment issues and the variety of injuries that can occur. The hydrogel was able to restore the rotational stiffness characteristics of the injured segment to a degree, however, with the added complexity of a fractured vertebral body, full restoration was prevented.

Disc repair is a difficult endeavour, and there are currently many strategies in practice and research that attempt to accomplish it. Options include trying to promote cellular repair through stem cell injection (Benneker et al., 2014), total disc replacement (van den Broek et al., 2012), use of hydrogels (Silva-Correia et al., 2012), and preformed nuclear implants (Ray, 2002). Ideally, disc repair would fully maintain the anatomical structures and restore their mechanical characteristics and cellular microenvironments. Current strategies seem to only accomplish some of these criteria, but continued work will bring full disc repair closer to reality. The strategy employed in this study attempted to maintain the disc's anatomical structures and restore the mechanical environment of the disc. Hydrogel injection and vertebroplasty could potentially inhibit some cellular functioning by blocking the endplate and inhibiting the pathway for nutrition to the disc. There is work which suggests that vertebroplasty can initiate further degenerative changes in younger subjects (Kang et al., 2014, Zhao et al., 2014), so caution should be exercised. Further work is also required to develop a more robust containment strategy for the hydrogel regardless of the injury. This study is the first to attempt such a repair of a motion segment by using an injectable hydrogel combined with vertebroplasty and offers valuable information for future attempts at mechanical repair of the injured disc.

Further cyclic compressive loading returned specimens to their injured mechanical profile via increased relative compressive and rotational stiffness. No repair strategy can sustain continued repetition of the conditions which caused the injury as every material is prone to failure at some point. It is therefore imperative that the mechanism of injury is not repeated in order to prevent injury re-occurrence.

The present study has found that PMMA and hydrogel injection can improve the mechanical profile of a compressively injured spine segment. This is the first study to evaluate a combination of these procedures and assess the mechanical outcomes. The data from this work reveals that compressive injury produces a variety of fracture types that are not always simple to repair using a single strategy. In discs with large cracks in the endplate, containment

for the hydrogel becomes an issue that needs to be addressed. Future work needs to develop more robust containment strategies for the hydrogel in the disc to facilitate its re-pressurization and enhance outcomes.

Chapter 6: Study 3

The Effects of Disc Height Loss on Cervical Spine Motion *In-Vivo*

6.1 Background

Pain has the ability to influence movement behavior (de Vries et al., 2015). While tissue studies offer high control in isolating a single factor and its influence on how a tissue functions, the response *in-vivo* may not be the same. Research that quantifies movement of the cervical spine in individuals presenting with pathology is lacking. Fluoroscopic imaging allows for the observation of a spine under motion and provides insight into midrange movements in addition to end-range movements. Being able to observe how a spine moves as opposed to static postures at end ranges of motion could provide more information with respect to subtle changes in movement patterns or strategies that could be potentially seen as aberrant. Being able to track and quantify segmental spine motion could help to reveal patterns and trends that assist in explaining why individuals move the way they do. This could help to provide a backbone for further investigation that identifies key anatomical features and how they contribute to aberrant movement, along with any mechanical consequences.

While generalized movement of the cervical spine has been described in previous work (Bogduk and Mercer, 2000, van Mameren, 1988), there has been no numerical quantification or analysis on individuals with pain/pathology. Having the tools to quantify segmental spine motion *in-vivo* could help to identify movement differences and commonalities in individuals with pain. Being able to link certain painful pathologies with the aberrant movement patterns that accompany them could be a powerful means to understand why individuals move the way they do and identify some strategies that remove mechanisms of injury.

Disc height loss has been identified as one of the key contributors to dysfunction in the spine (Jarman et al., 2015). In the lumbar spine, loss in height at a segment introduces changes to facet joint interactions (Dunlop et al., 1984, Gotfried et al., 1986), and shifts the areas of the disc that bear load (Adams et al., 1996). There is also the potential to affect nutrient transport and the long-term degenerative response (Lotz and Chin, 2000). Understanding the kinematic response of disc height loss across individuals with pain could be a helpful tool in identifying injury mechanisms and characterizing aberrant movement.

Previous research has also examined the possibility of adjacent segment degeneration that occurs as a result of degenerative changes to a spinal segment that propagate further from the site of injury. Fusion (Dekutoski et al., 1994), herniation (Lao et al., 2015b), and degenerative grade (Lee et al., 2015) have all been examined, but no study has explicitly examined disc height. So while there may be a weak association with some of the factors mentioned above, disc height could present a clearer relationship between pathology and aberrant motion of adjacent segments.

6.2 Significance

Quantifying cervical spine movement *in-vivo* on pained individuals with and without disc height loss will help to identify if there is a common behavior across individuals for an easily observable feature on medical imaging. Pain could potentially introduce many heterogeneous kinematic responses in individuals that are dependent on individual intrinsic factors as well as the injury itself. Identifying a common kinematic response to disc height loss in the cervical spine could help to identify an important subgroup of patients with respect to kinematic function. Future work could then investigate whether there are deleterious consequences as a result of a given movement pattern. Typically, judgements on medical imaging are based on what is seen by the eye. This study sought to evaluate and compare clearly visible disc height loss cases to

non-disc height loss cases and determine whether disc height loss produced a unique mechanical characteristic in the quantified angular displacement.

6.3 Hypotheses

1. Disc height loss will cause diminished segmental mobility at the affected segment.
2. Some individuals without disc height loss will also exhibit diminished mobility at one segment as well as segments that exhibit enhanced mobility.

6.4 Methods

6.4.1 Data Collection

Sagittal-plane image sequences of cervical spine flexion-extension motions were obtained from a local specialist. Fluoroscopic exams were taken with a Digital Motion X-Ray that provided continuous x-ray at 70-90 kVp at 2-3.5 mA at a 40-inch flange focal distance. A 9-inch image intensifier (Precise Optics, Bay Shore, NY, USA) transferred the signal to a digital CCD camera outputting a 150dpi stream to a DICOM recorder (NAI Tech Products, Auburn, CA, USA).

Each sequence was from a patient who had experienced trauma and had a chief complaint related to their neck, head, or shoulders. All image sequences were made anonymous and patients filled out an informed consent form which released their image sequences for research purposes (Appendix D). Further information related to the patients including age, gender, complaint, and traumatic event is also contained in Appendix D. A total of 20 image sequences were used, these were assessed by a third-party clinician qualified to perform radiological assessments; they had no prior experience with the patients and had not assessed the images previously. The clinician was highly trained in diagnostic imaging

interpretation, with formal training spanning four years, from foundational studies to advanced clinical topics. They continue to read radiographs for their practice in addition to radiographs for two other full-time clinicians in active practice. They also write all clinical imaging reports when referrals based on imaging findings are required. Disc height loss was classified as either mild, moderate, or severe. Grading of disc height loss was based on clinical impression given that there were no pre-post image sequences of the patient cases. Disc height loss is a subtle feature to quantify without pre-post images, and there are no formal clinical evaluation criteria for quantifying disc height loss. In order to provide the most clinical relevance to the subgroup classifications, the impression of a clinician with a special practice in treating and evaluating the spine was deemed the most appropriate measure. Of the 20 cases, eight had mild disc height loss in at least one level, three had moderate or severe height loss in at least one level, and nine had no height loss at any of the levels visible in the radiographs.

In addition to the clinical appraisal of disc height loss, disc height index was also calculated similar to the method of Frobin and colleagues (Frobin et al., 2002). Detailed discussion of the calculation of this value is contained in Appendix D. Disc height at each level was also normalized to and expressed as a percentage of total disc height across all levels measured for each case. For this, the average height was taken between the anterior and posterior margins of each vertebral level. The sum of these averages was taken and then each measured height was normalized to the sum of the averages and expressed as a percentage. Disc height loss cases considered moderate or severe were included in the “disc height loss” group of cases while those with only mild height loss were examined separately. Including those who did not have disc height loss allowed for the observation of whether other factors (such as pain and different movement patterns) could produce similar results to those seen in disc height loss patients. Analysis of these data required a separate assay for each case, as the data for all patients was viewed separately and analyzed on an individual basis.

6.4.2 Tracking Procedure

From each image sequence, a full repetition of cervical spine neutral to full flexion and then to full extension was chosen. From this, the images were imported into a customized software interface that utilized the vertebral body tracking algorithm described in Appendix A. An operator selected 4 corners of each vertebral body that exhibited high contrast and a defined edge relative to surrounding structures. This would ensure that the coordinate would track accurately. From this, the vertebral body motion was tracked through the entire image sequence to obtain raw coordinates of all four corners of each vertebral body.

Due to patient anatomical and movement differences, a variable number of vertebral bodies were tracked for each individual image sequence. In some cases, vertebral bodies disappeared from the field of view as the patient moved, and in others they had more mass surrounding the shoulders that obscured the underlying vertebrae from view under fluoroscopy.

Following tracking, each set of image sequences was visually assessed to determine if the tracking points sufficiently tracked the corner of each vertebral body. This ensured that the angular displacement outputs were accurate to the segmental motion actually occurring.

6.4.3 Data Analysis

Relative joint angles and relative joint shear was obtained for each set of image sequences using the techniques described in Appendix B and Appendix C. Kinematic data was filtered using a dual pass 2^{nd} order butterworth filter with a cut-off frequency at 1Hz as determined by residual analysis. Given the heterogeneous nature of the patient data and the small sample size of disc height loss cases, image sequences were assessed on a case by case basis to determine if a common pattern could be obtained from disc height loss cases compared to the non-disc height loss cases. Patient time-histories were examined to evaluate the stepwise onset of relative segmental motion and any visual disparities in flexion or extension in a particular segment. Total angular displacement was also examined and compared to data

collected by van Mameren (1988) on healthy individuals. Their general findings were an increase in relative angular displacement moving from C2/C3 to C5/C6 (van Mameren, 1988).

In order to provide some comparison between groups, angular displacement was normalized as a percentage of total range of motion for each joint in every patient case. Average angular displacement was calculated for each group. Cases that did not have angular displacement values for four joints were excluded from the calculations given the difference in relative proportion that arose with fewer joints quantified. In the moderate/severe height loss group, there was evidence of height loss at the C5/C6 level in all cases. Due to this, the proportional angular displacement of the C5/C6 level was compared via an independent samples t-test between the moderate/severe height loss group and the group with no height loss. Statistical significance was accepted at the $p < 0.05$ level, with statistical testing performed using SPSS software (IBM, Somers, NY, USA).

6.5 Results

Select patient images and time-histories have been included in this chapter. Radiographs and angular displacement time-histories for all patient image sequences have been included in Appendix H. In the disc height loss group (moderate or severe height loss), there was evidence of diminished mobility at levels with height loss when compared to the trend of increasing angular contribution found by van Mameren (1988) (Table 6.1, Table 6.2, Table 6.3). In the mild disc height loss set of cases the relationship was not as clear, with some cases presenting in the same manner as those in the disc height loss group and others exhibiting angular displacement profiles that matched the findings of van Mameren (1988). In the non-disc height loss case group, all cases exhibited a trend towards increasing segmental angular displacement moving down from the level of C2/C3.

Group averages (Table 6.4) revealed that in the moderate/severe height loss group, there was a lower average proportional angular displacement at lower levels (20.2% ± 2.3%) where height loss was present compared to the group with no height loss (30.6% ± 4.0%). The independent samples t-test revealed a statistically significant difference between these two groups (p=0.004). Averages from the mild height loss group were not as clear given that the levels with height loss were distributed throughout the segments. There was similarity to the averages from Van Mameren (1988) and the group with no disc height loss (Table 6.4).

Disc height index values revealed a slightly lower index (0.30 ± 0.09) for C5/C6 in the moderate/severe group compared to the non height loss group (0.34 ± 0.02). Disc height index values for each case are located in Table 6.5 while average values for each group are located in Table 6.6. Average proportional disc height values revealed a lower proportion of C5/C6 disc height (21% ± 5.6%) in the moderate/severe height loss group compared to the same level in the no height loss group (26% ± 1.4%). Proportional disc height values for all patient cases are located in Table 6.7 while average values for the clinical subgroups are located in Table 6.8.

In all of the cases of disc height loss, there was a non-stepwise initiation of segmental angular motion (Figure 6.2, Figure 6.4, Figure 6.8), meaning that rotation occurred about lower levels before upper levels. In the mild disc height loss group, there was again a disparity, with some cases exhibiting the same non-stepwise trend as the disc height loss group and others exhibiting stepwise angular motion.

Table 6.1.Total range of motion of each segmental level for each case. Listed in order of moderate/severe disc height (DH) cases, mild height loss (MH) cases, and no height loss (NH) cases. Levels exhibiting disc height loss are shaded, with light shading indicating mild height loss, medium shading indicating moderate height loss, and dark shading indicating severe height loss. Values from healthy individuals found by van Mameren (1988) are also listed at the bottom and show the general trend of increasing angular displacement with descending segmental level. Disc height loss cases exhibited the opposite of this.

Case	C2/C3 Total Displacement (°)	C3/C4 Total Displacement (°)	C4/C5 Total Displacement (°)	C5/C6 Total Displacement (°)
DH 1	11.8	10.6	13.1	8.1
DH 2	15.1	12.5	12.9	9.6
DH 3	2.0	13.6	10.1	7.6
MH 1	12.0	16.9	16.2	14.3
MH 2	14.9	10.9	13.9	14.5
MH 3	7.5	13.7	16.2	7.3
MH 4	10.0	14.0	23.2	12.4
MH 5	13.1	11.9	14.2	
MH 6	17.1	16.9	12.1	15.5
MH 7	7.8	12.6	10.4	9.1
MH 8	10.1	15.1	22.4	18.7
NH 1	13.9	15.3	17.2	
NH 2	10.0	13.1	17.5	19.4
NH 3	9.5	14.9	14.0	14.4
NH 4	9.5	16.8	16.3	16.2
NH 5	16.5	18.1	22.9	23.0
NH 6	8.2	6.3	9.4	
NH 7	10.3	13.9	18.4	25.8
NH 8	5.3	8.7		
NH 9	10.0	13.0	18.3	18.0
van Mameren (1988) (Averages)	**13.4**	**17.6**	**20.4**	**22.6**

Table 6.2. Range of motion of each segmental level for each case in flexion and extension. Listed in order of moderate/severe disc height (DH) cases, mild height loss (MH) cases, and no height loss (NH) cases. Levels exhibiting disc height loss are shaded, with light shading indicating mild height loss, medium shading indicating moderate height loss, and dark shading indicating severe height loss. Cells that are shaded fully black indicate levels that could not be quantified due to not being within the fluoroscope field of view.

Case	C2/C3 Flexion (°)	C2/C3 Extension (°)	C3/C4 Flexion (°)	C3/C4 Extension (°)	C4/C5 Flexion (°)	C4/C5 Extension (°)	C5/C6 Flexion (°)	C5/C6 Extension (°)
DH 1	3.2	-8.6	3.2	-7.5	2.8	-10.3	2.0	-6.1
DH 2	12.5	-2.5	7.8	-4.7	7.2	-5.7	7.2	-2.4
DH 3	1.2	-0.8	5.1	-8.4	0	-10.1	4.6	-3.0
MH 1	9.0	-3.0	11.4	-5.5	9.6	-6.6	8.9	-5.4
MH 2	8.7	-6.2	8.4	-2.5	8.0	-6.0	11.7	-2.9
MH 3	2.2	-5.3	1.1	-12.6	3.3	-12.9	2.0	-5.3
MH 4	5.3	-4.7	10.4	-3.6	13.8	-9.4	12.4	0
MH 5	5.9	-7.2	11.4	-0.5	11.9	-2.3		
MH 6	8.5	-8.6	5.1	-11.8	6.9	-5.2	10.5	-5.0
MH 7	5.9	-1.9	12.6	0	9.7	-0.7	8.7	-0.4
MH 8	6.0	-4.0	6.3	-8.8	5.8	-16.6	7.1	-11.6
NH 1	5.4	-8.5	8.6	-6.7	10.5	-6.7		
NH 2	8.1	-1.9	10.3	-2.8	6.6	-10.9	8.9	-10.5
NH 3	2.9	-6.7	3.6	-11.4	5.0	-9.0	10.7	-3.6
NH 4	2.4	-7.0	4.6	-12.1	5.1	-11.1	10.8	-5.4
NH 5	9.5	-7.0	12.8	-5.3	15.5	-7.5	13.8	-9.3
NH 6	3.1	-5.2	2.9	-3.3	3.7	-5.7		
NH 7	6.4	-3.9	8.2	-5.7	8.7	-9.7	14.5	-11.3
NH 8	1.5	-3.8	6.4	-2.3				
NH 9	9.0	-0.9	9.1	-3.9	10.4	-7.8	10.9	-7.0

Table 6.3. Proportional range of motion (%) of each segmental level for each case. Listed in order of disc height (DH) cases, mild height loss (MH) cases, and no height loss (NH) cases. Levels exhibiting disc height loss are shaded, with light shading indicating mild height loss, medium shading indicating moderate height loss, and dark shading indicating severe height loss. Cells that are shaded fully black indicate levels that could not be quantified due to not being within the fluoroscope field of view.

Case	C2/C3 Relative Displacement (%)	C3/C4 Relative Displacement (%)	C4/C5 Relative Displacement (%)	C5/C6 Relative Displacement (%)
DH 1	27.1	24.4	30.0	18.6
DH 2	30.1	25.0	25.7	19.2
DH 3	5.9	40.8	30.5	22.8
MH 1	20.2	28.4	27.3	24.1
MH 2	27.4	20.1	25.7	26.8
MH 3	16.7	30.7	36.3	16.3
MH 4	16.8	23.4	38.9	20.9
MH 5	33.4	30.4	36.4	
MH 6	27.8	27.4	19.6	25.2
MH 7	19.5	31.6	26.1	22.7
MH 8	15.2	22.8	33.8	28.2
NH 1	29.9	33.0	37.1	
NH 2	16.7	21.9	29.1	32.3
NH 3	18.1	28.2	26.5	27.2
NH 4	16.1	28.6	27.7	27.6
NH 5	20.4	22.5	28.4	28.6
NH 6	34.5	26.3	39.2	
NH 7	15.0	20.3	27.0	37.7
NH 8	37.9	62.1		
NH 9	16.8	21.9	30.9	30.4
van Mameren (1988) (Averages)	**18.1**	**23.8**	**27.6**	**30.5**

Table 6.4. Proportional range of motion (%) averages and standard deviations for each group. Cases without angular displacement values for all four levels were excluded from calculations given the altered proportional displacement with fewer levels accounted for.

Group	C2/C3 Proportional Displacement Average (%) (SD)	C4/C4 Proportional Displacement Average (%) (SD)	C4/C5 Proportional Displacement Average (%) (SD)	C5/C6 Proportional Displacement Average (%) (SD)
Moderate/Severe Height Loss	21.0 (13.2)	30.1 (9.3)	28.7 (2.6)	20.2 (2.3)
Mild Height Loss	20.5 (5.1)	26.4 (4.3)	29.7 (6.9)	23.4 (4.0)
No Height Loss	17.2 (1.9)	23.9 (3.6)	28.3 (1.6)	30.6 (4.0)
Van Mameren (1988) (Averages)	18.1	23.8	27.6	30.5

Table 6.5. Disc height index values for all patient cases. Expressed as a ratio of disc height to vertebra height. A principle issue with this technique is that disc height loss is hidden if a vertebra is fractured and has also lost height. Cells that are shaded fully black indicate levels that could not be quantified due to not being within the fluoroscope field of view.

Case	C2/C3 Disc Height Index	C3/C4 Disc Height Index	C4/C5 Disc Height Index	C5/C6 Disc Height Index
DH 1	0.29	0.39	0.38	0.34
DH 2	0.18	0.34	0.41	0.36
DH 3	0.32	0.38	0.31	0.20
MH 1	0.28	0.30	0.28	0.21
MH 2	0.28	0.31	0.30	0.34
MH 3	0.24	0.38	0.36	0.28
MH 4	0.29	0.32	0.38	0.35
MH 5	0.22	0.41	0.39	
MH 6	0.24	0.33	0.32	0.32
MH 7	0.22	0.25	0.33	0.53
MH 8	0.30	0.24	0.31	0.29
NH 1	0.23	0.28	0.35	
NH 2	0.31	0.37	0.31	0.36
NH 3	0.24	0.36	0.30	0.33
NH 4	0.25	0.33	0.33	0.32
NH 5	0.31	0.29	0.33	0.35
NH 6	0.33	0.33	0.35	
NH 7	0.27	0.31	0.28	0.37
NH 8	0.24	0.31		
NH 9	0.30	0.29	0.30	0.32

Table 6.6. Average disc height index values for the three groups of patient cases.

Group	C2/C3 Disc Height Index Average (SD)	C4/C4 Disc Height Index Average (SD)	C4/C5 Disc Height Index Average (SD)	C5/C6 Disc Height Index Average (SD)
Moderate/Severe Height Loss	0.26 (0.07)	0.37 (0.03)	0.37 (0.05)	0.30 (0.09)
Mild Height Loss	0.26 (0.03)	0.32 (0.06)	0.33 (0.04)	0.33 (0.10)
No Height Loss	0.27 (0.04)	0.32 (0.03)	0.32 (0.03)	0.34 (0.02)

Table 6.7. Proportional disc height values for all cases. Values are expressed as a percentage of the total disc height across all levels measured. Cells that are shaded fully black indicate levels that could not be quantified due to not being within the fluoroscope field of view.

Case	C2/C3 Proportional Disc Height (%)	C3/C4 Proportional Disc Height (%)	C4/C5 Proportional Disc Height (%)	C5/C6 Proportional Disc Height (%)
DH 1	25.3	27.2	25.4	22.1
DH 2	18.6	25.3	30.2	25.9
DH 3	31.4	29.4	24.3	14.9
MH 1	30.0	27.2	24.8	18.0
MH 2	27.1	24.6	23.2	25.1
MH 3	22.5	28.9	26.6	22.0
MH 4	25.5	22.8	26.3	25.4
MH 5	26.1	39.4	34.5	
MH 6	24.3	27.4	24.7	23.7
MH 7	21.3	20.0	24.1	34.6
MH 8	30.2	20.2	25.6	24.0
NH 1	30.8	30.9	38.3	
NH 2	25.8	27.2	21.7	25.2
NH 3	22.9	27.9	22.9	26.3
NH 4	24.1	25.5	25.2	25.1
NH 5	28.3	21.4	24.6	25.7
NH 6	36.7	31.4	31.9	
NH 7	23.8	24.7	22.9	28.6
NH 8	48.9	51.1		
NH 9	27.6	23.2	24.2	25.1

Table 6.8. Average proportional disc height values for clinical subgroups. Cases without disc height values for all four levels were excluded from calculations given the altered proportional disc height with fewer levels accounted for.

Group	C2/C3 Proportional Disc Height Average (%) (SD)	C4/C4 Proportional Disc Height Average (%) (SD)	C4/C5 Proportional Disc Height Average (%) (SD)	C5/C6 Proportional Disc Height Average (%) (SD)
Moderate/Severe Height Loss	25.1 (6.4)	27.3 (2.0)	26.6 (3.1)	21.0 (5.6)
Mild Height Loss	25.8 (3.5)	24.4 (3.6)	25.0 (1.2)	24.7 (5.0)
No Height Loss	25.4 (2.2)	25.0 (2.4)	23.6 (1.3)	26.0 (1.4)

6.5.1 Disc Height Loss (DH1)

DH1 presented with moderate disc height loss at the level of C5/C6 and severe height loss at C6/C7 (angular displacement could not be quantified), along with moderate anterior osteophytes at C5/C6 and severe at C6/C7 (Figure 6.1). Upon analysis of the joint angle time-history graph it could be seen that in extension, while the C5/C6 joint did not continue extending, the extension continued about the adjacent joint (Figure 6.2). Even in flexion, very little of the total angular displacement of the neck was about this level, and only began to displace after displacement commenced about other joints. These data suggest that while the joint motion does occur about this level with height loss, it is inherently stiff. Total angular displacement for the C2/C3, C3/C4, C4/C5 and C5/C6 joints were 11.8°, 10.6°, 13.1°, and 8.1° respectively; this goes against the general trend of angular displacement increasing with descending segmental level.

Motion onset occurred about the C2/C3 joint and to some extent the C4/C5 joint, angular displacement occurred about the C3/C4 and C5/C6 joints at a later point in an apparently synchronized manner (Figure 6.2).

6.5.2 Disc Height Loss (DH2)

DH2 presented with moderate disc height loss at the level of C4/C5 and C6/C7 and severe height loss at C5/C6 (Figure 6.3). Osteophytes were evident anteriorly and classified as mild at C4/C5, moderate at C6/C7 and severe at C5/C6. Due to C7 moving out of frame during sagittal plane motions, the angular displacement at C6/C7 could not be quantified. There was a non-stepwise initiation of movement with rotation occurring first about C3/C4, followed by C4/C5 (Figure 6.4). As with Case 1, total angular displacement decreased with descending segmental level. The disc with severe height loss rotated the least while the level with moderate height loss had a similar total displacement with its superior adjacent level. Total angular displacement for the C2/C3, C3/C4, C4/C5, and C5/C6 joints were 15.1°, 12.5°, 12.9°, and 9.6° respectively.

6.5.3 Disc Height Loss (DH3)

DH3 presented with moderate height loss at C4/C5 and severe height loss at C5/C6. There was also severe height loss at C6/C7 but due to the positioning of C7, it could not be tracked as the vertebral body did not stay within the field of view. Osteophytic lipping was evident as well, with moderate levels at C4/C5 and severe levels at C5/C6 and C6/C7. There was also a kyphotic deformity of the neck in the individual's neutral posture (Figure 6.5). The overall range of motion of the neck was severely limited, with most of the motion being qualitatively observed at the craniocervical junction. During flexion, there was observed gliding of the facets at C5/C6 as a small amount of flexion was observed to occur about that level (Figure 6.6), osteophytes at the anterior margins of both vertebral bodies appeared to make contact and prevented further motion. As the spine extended, the facets of the C5/C6 joint appeared to limit extension range of motion of the segment (Figure 6.7). Total angular displacement magnitude at C5/C6 was 7.6°. Nearly all displacement in extension occurred about the adjacent joint (C4/C5) with less severe height loss, as well as the C3/C4 joint without height loss (Figure 6.8). Interestingly, the majority of angular displacement occurred about the joint without height loss (C3/C4) with a total angular displacement magnitude of 13.6°.

What is also interesting in this case is the near complete lack of motion at the C2/C3 joint, a joint with no observable height loss. It is clear that there are other factors such as pain, individual motor patterns, and possibly muscle guarding that have the potential to dictate the motion at a spinal joint.

Also of note in DH3 are the relative joint translations or shear measurements. The C2/C3 joint, with the least angular displacement, had the highest shear displacement (0.44mm in flexion and 0.27mm in extension). Joints C3/C4 and C4/C5 were seen to go into a slight amount of anterior shear displacement (0.21mm) and then posterior shear displacement

(0.35mm) as the neck went into flexion and then extension, but there was almost no shear displacement at the C5/C6 joint which had the most severe height loss (Figure 6.9).

6.5.4 General Height Loss Case Observations

Two general observations were found from all three disc height loss cases: a tendency for the disc with the most severe height loss to contribute the least to total angular displacement, and a non-stepwise onset of joint angular displacement. It is unclear however, if this non-stepwise onset of joint angular displacement was a result of the disc height loss.

6.5.5 Mild Height Loss Cases

The mild height loss cases did not appear to exhibit the same systematic effect as the disc height loss cases. There were instances where there was a high level of angular displacement at segments with mild height loss and in general, most cases followed a pattern where the angular displacement increased at the lower segments.

Cases MH3 and MH4 exhibited a lower segmental angular displacement about the C5/C6 joints compared to the C4/C5 joints of 8.9° and 10.8° respectively. These two cases appeared to be the exceptions, with other cases exhibiting smaller differences (<4°) in angular displacement between C4/C5 and C5/C6 segments. In the case of MH3, the C6 vertebral body appeared to have a posterior lip that when viewed under fluoroscopy limited movement of the C5/C6 joint in extension (Figure 6.10, Figure 6.13). The lack of mobility for MH4 appeared to also be in extension (Figure 6.11, Figure 6.15).

6.5.6 Cases without Height Loss

In all of the non-height loss cases, there was a general trend for relative segmental angular displacement to increase with a descending segmental level. This followed the overall trend found by van Mameren (1988) despite these cases still presenting with pathology. Some

of these cases did not have a stepwise initiation of movement, and the presence of this non-stepwise initiation of segmental motion appeared to be present in all of the case sub-categories, with the disc height loss cases all exhibiting this pattern. At this point it is unclear what physical factors (if any) cause this and whether it is an important finding clinically.

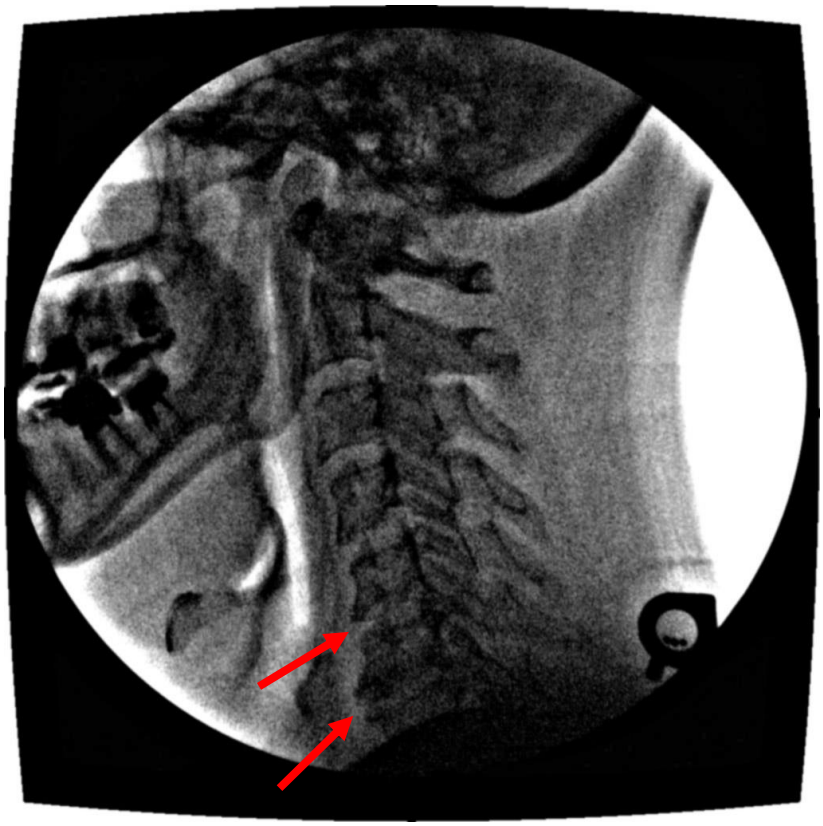

Figure 6.1 DH1 disc height loss. Height loss was found at the C5/C6 level and the C6/C7 level (indicated by arrows). Given that the C7 vertebral body was not in the field of view, only the C5/C6 joint and those above could be tracked. Osteophytes can be seen anteriorly at C5/C6 and C6/C7.

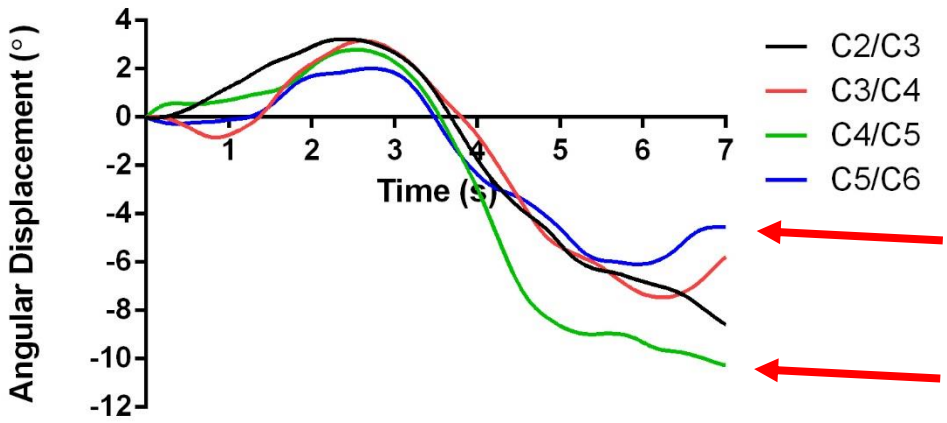

Figure 6.2 Time history angular displacement graph for DH1. There is a large disparity in the extension angular displacement for the C5/C6 joint (with height loss) relative to the C4/C5 joint (without height loss). There is also a non-stepwise behaviour in terms of movement initiation about joints, with movement initiating about C4/C5 followed by C2/C3 and then C3/C4 and C5/C6.

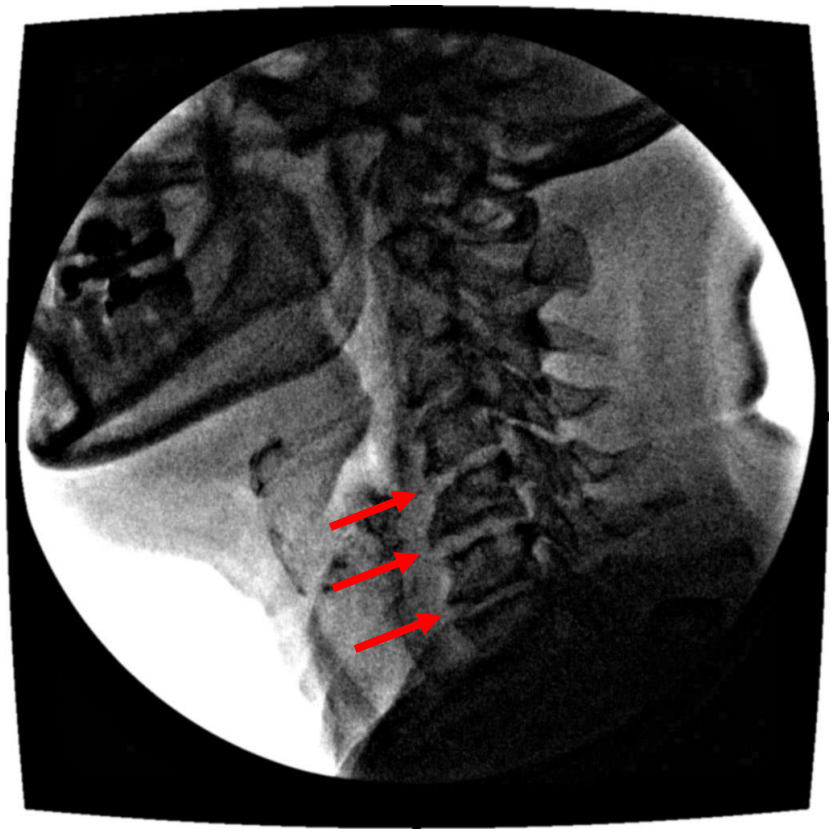

Figure 6.3 DH2 disc height loss. Height loss was found at the C4/C5, C5/C6, and C6/C7 levels (indicated by arrows). Anterior osteophyte growth is evident at C4/C5, C5/C6, and C6/C7. C6/C7 was not able to be quantified due to the C7 vertebra moving out of frame.

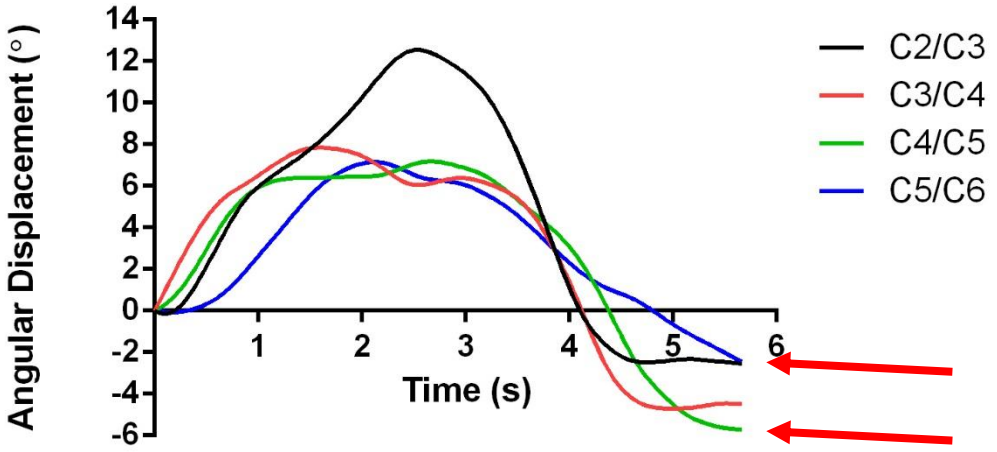

Figure 6.4 Time history graph of the relative joint angular displacement for DH2. There was a large disparity in relative angular displacement in extension between C5/C6 and C4/C5 (indicated by arrows), with the majority of extension displacement occurring about C4/C5 and C3/C4. There is also an observable non-stepwise behaviour in onset of motion between joints with motion initiating about C2/C3 and C4/C5.

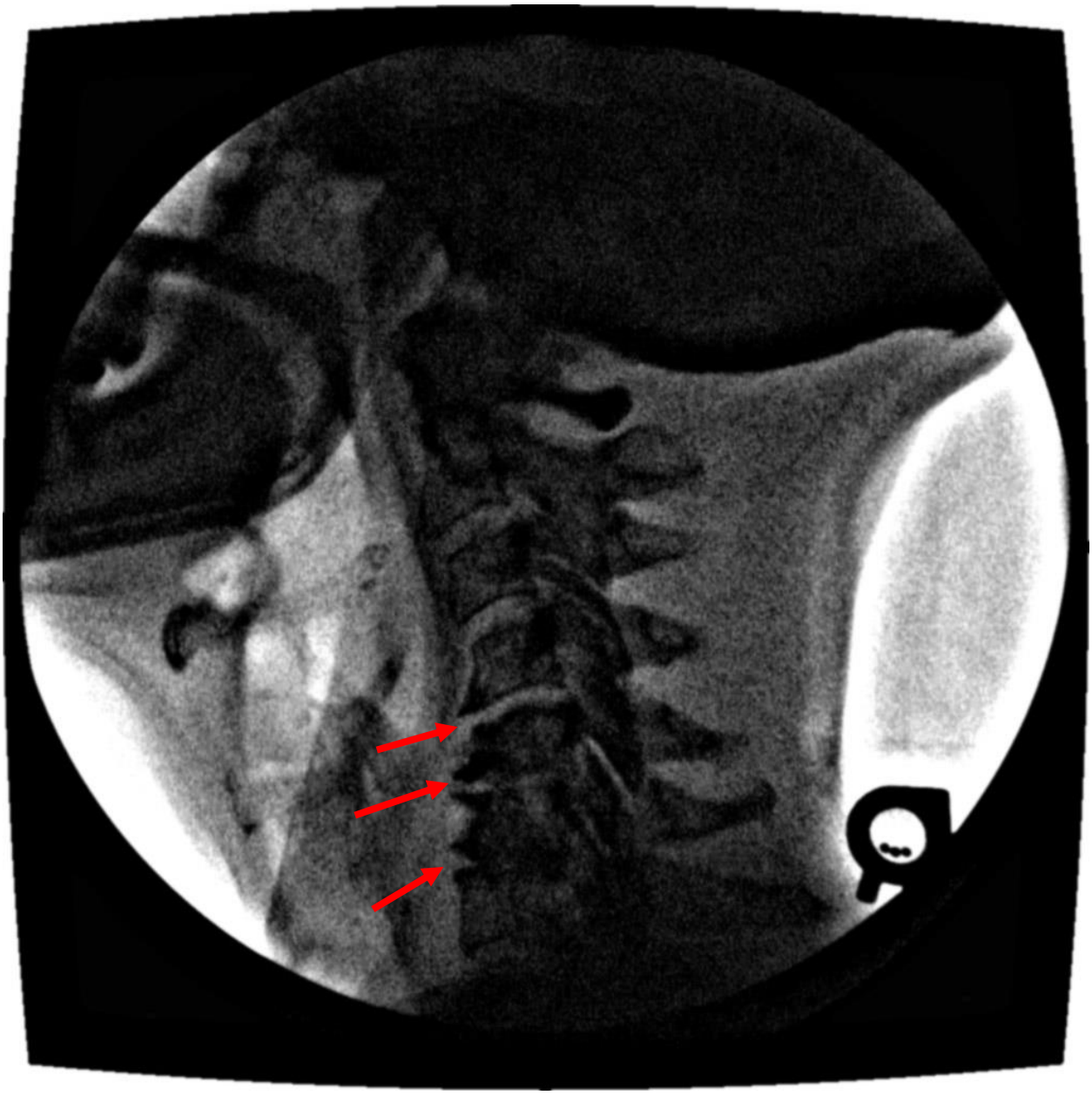

Figure 6.5 DH3 disc height loss. There was height loss at multiple levels from C4/C5 to C6/C7 (indicated by arrows). C6/C7 was not able to be tracked as some features of the vertebral body moved out of the field of view. Also note the kyphotic posture of the entire neck in its neutral position.

Figure 6.6 DH3 disc height loss in flexion. Note the increased facet spacing (circle) as the C5/C6 joint moves into a slight amount of flexion but is restricted by the osteophytes present at the anterior margins of both vertebrae.

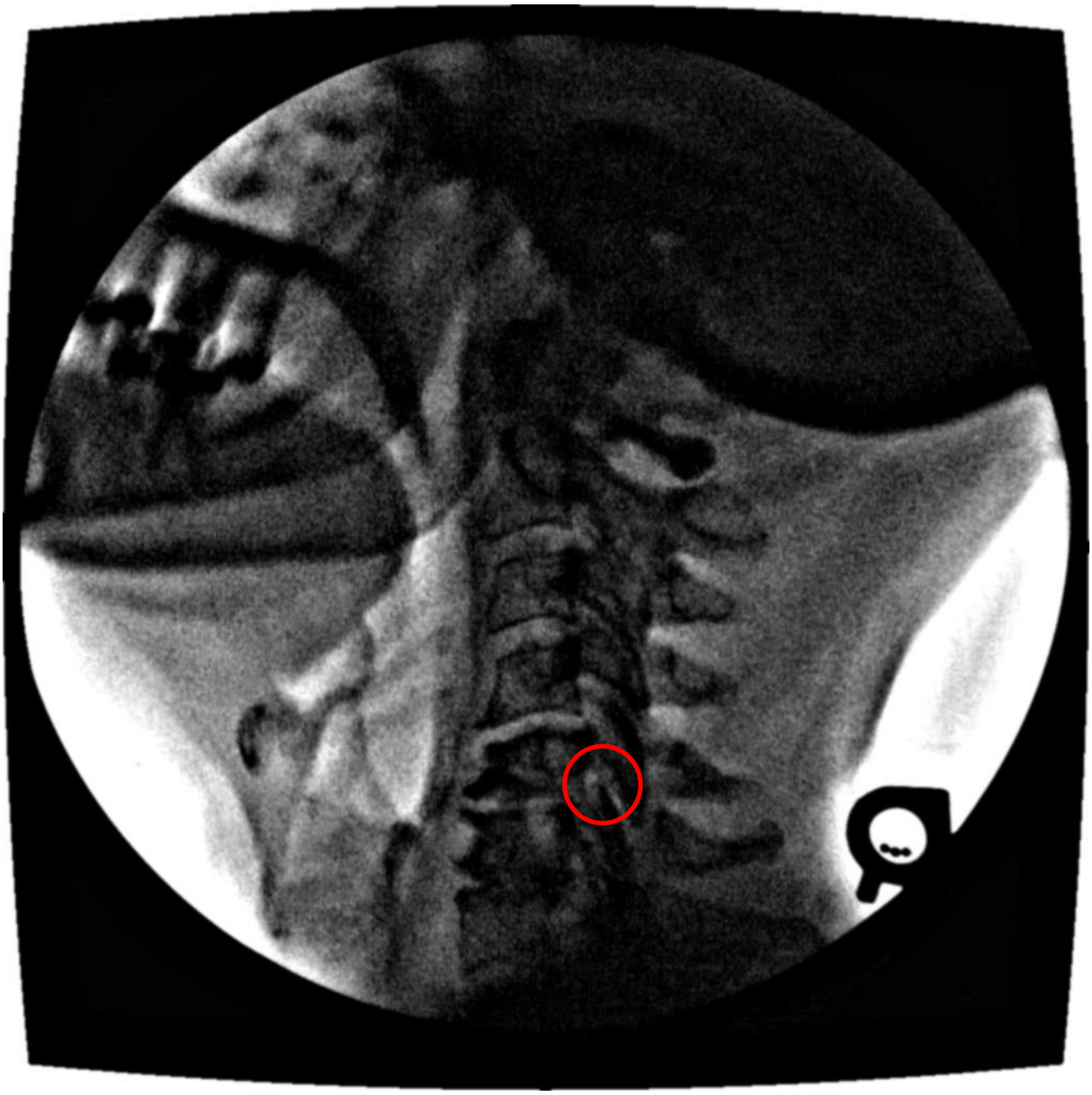

Figure 6.7 DH3 disc height loss in extension. There is very little extension of the entire neck overall. The C5/C6 joint also appeared to be restricted in its movement into extension as the facets would not allow any further angular displacement (circle).

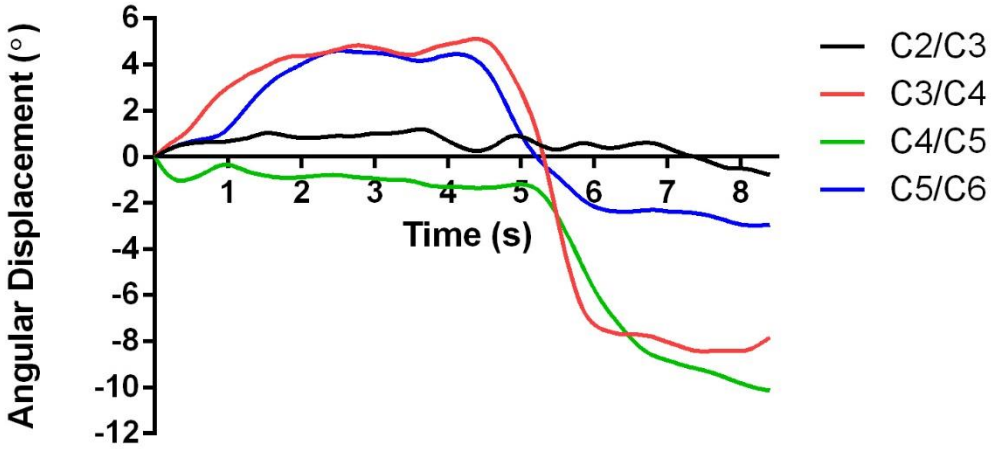

Figure 6.8 DH3 relative joint angular displacement time history graph. As with the other cases there is a non-stepwise behaviour in terms of the onset of joints into flexion. Flexion occurs about C5/C6 before it isrestricted in extension. The C3/C4 joint which did not exhibit any height loss is able to move in both flexion and extension.

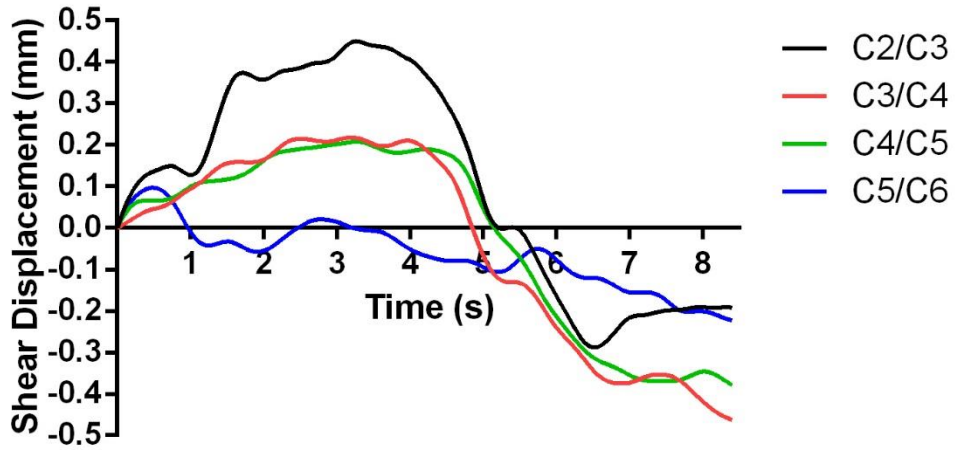

Figure 6.9 DH3 shear displacement time history graph. The C2/C3 joint displaced the most in shear without rotating. The C5/C6 joint is seen here to barely translate at all indicating a stiff joint that can be predicted from the osteophytes evident on the radiograph.

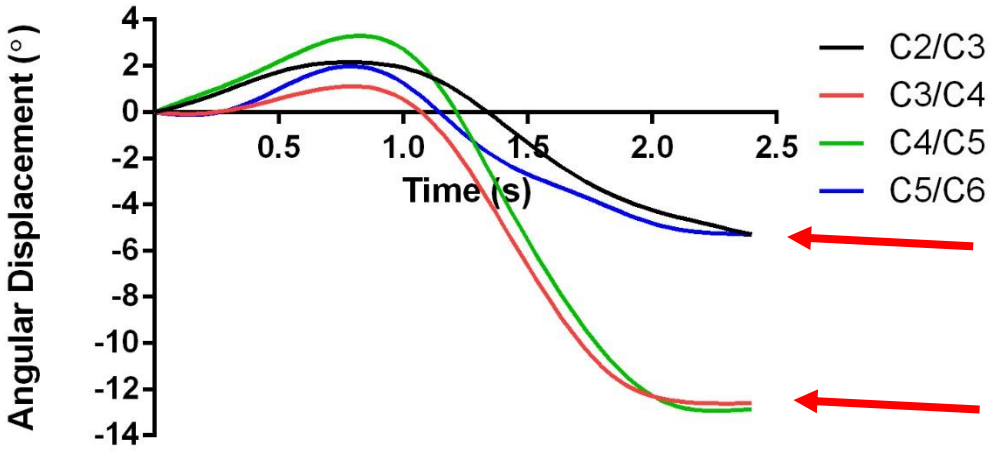

Figure 6.10 Time history of angular displacement for case MH3. There was mild height loss at C4/C5 and C5/C6 with an associated with a loss in cervical lordosis. A posterior lip at the C6 vertebra appeared to limit movement of the C5/C6 joint in extension.

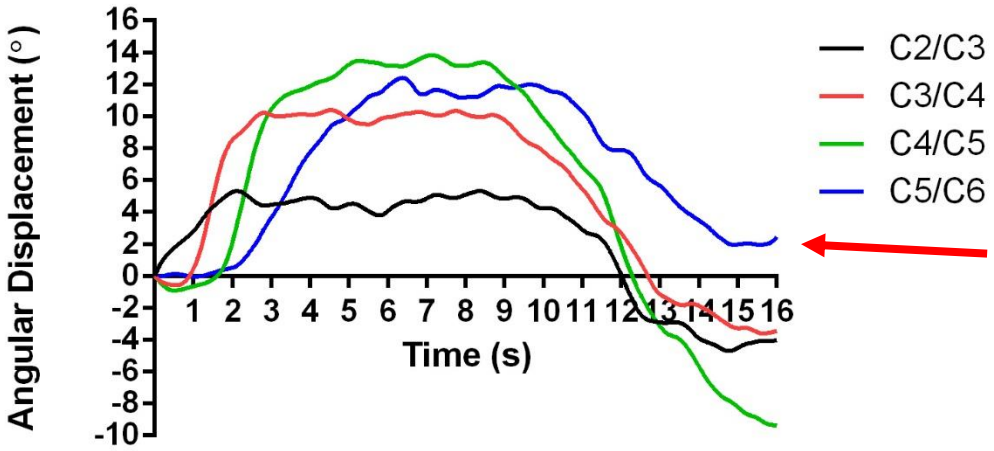

Figure 6.11 Time history of angular displacement for case MH4. There was mild disc height loss at C4/C5 and C5/C6. Lack of mobility at C5/C6 appeared to be in extension (indicated by arrow). This could be due to facet joint stiffness.

Figure 6.12 Neutral posture for case MH3. Mild height loss was evident at C4/C5 and C5/C6. Note the posterior lip that was evident on the C6 vertebra along with associated loss of cervical lordosis.

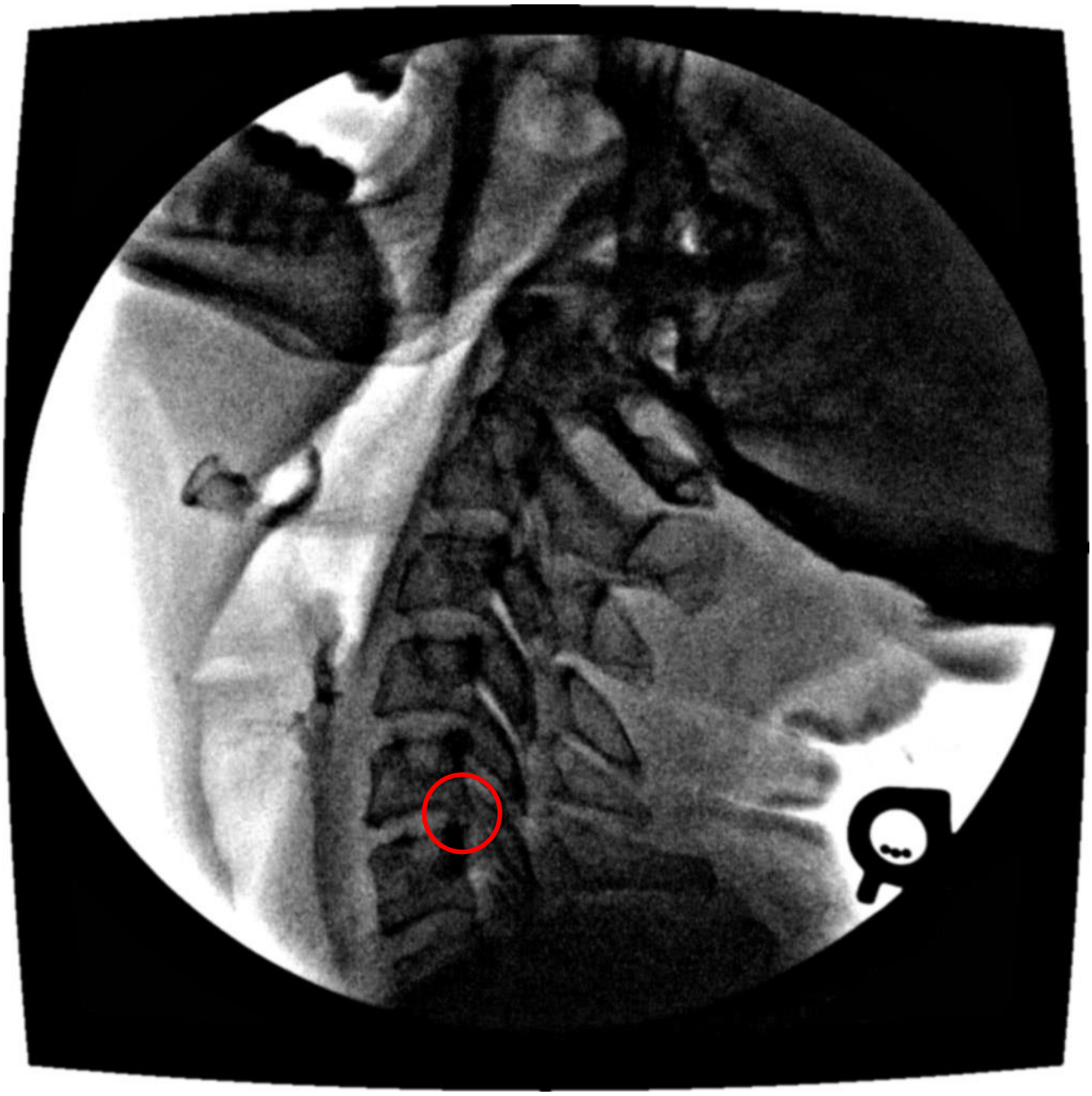

Figure 6.13 Case MH3 in the extended posture. Note that the posterior lip on the C6 vertebral body appears to be limiting movement of the C5/C6 joint in extension.

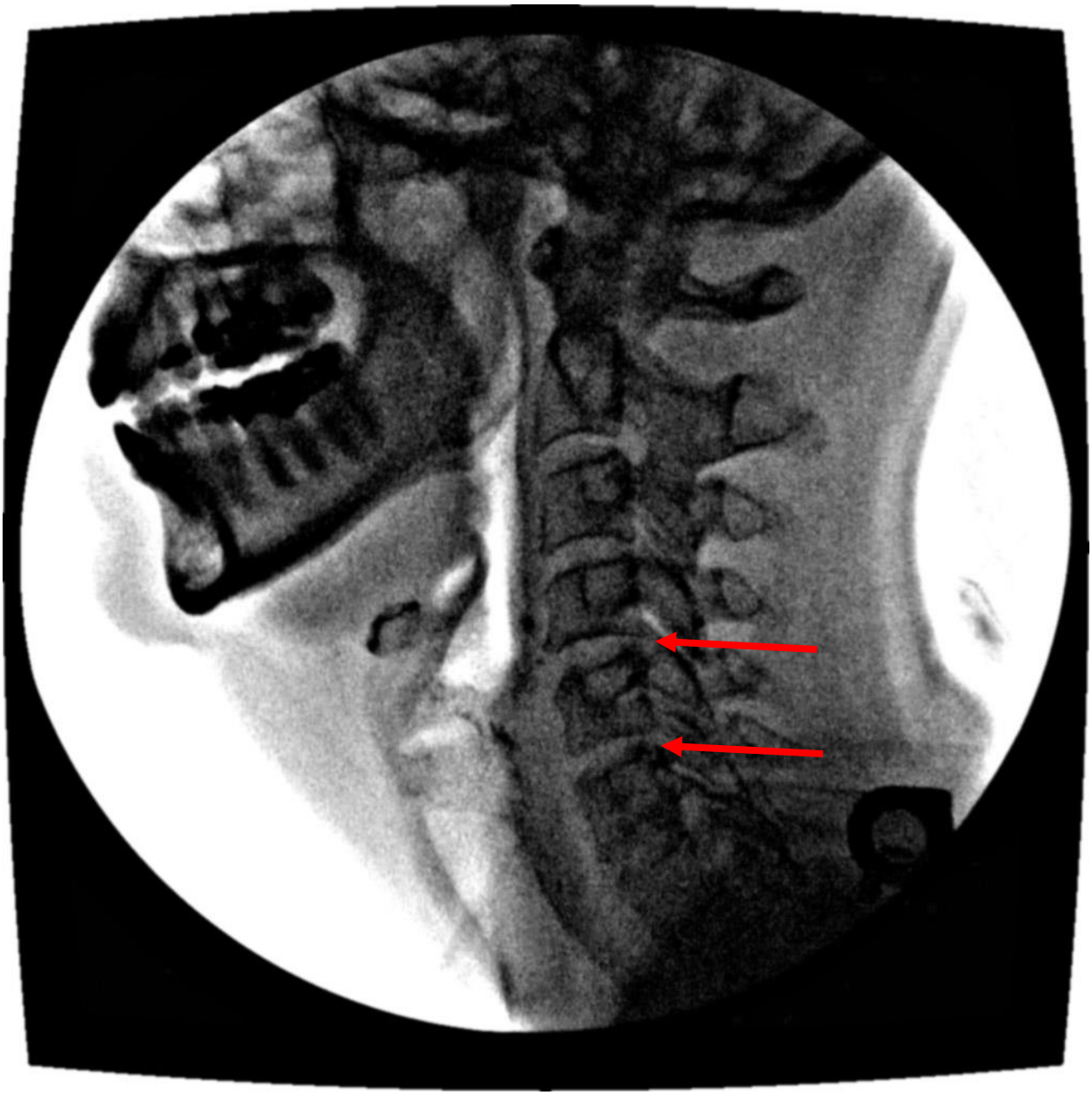

Figure 6.14 Neutral posture for case MH4. Mild height loss was evident at C4/C5 and C5/C6 (indicated by arrows).

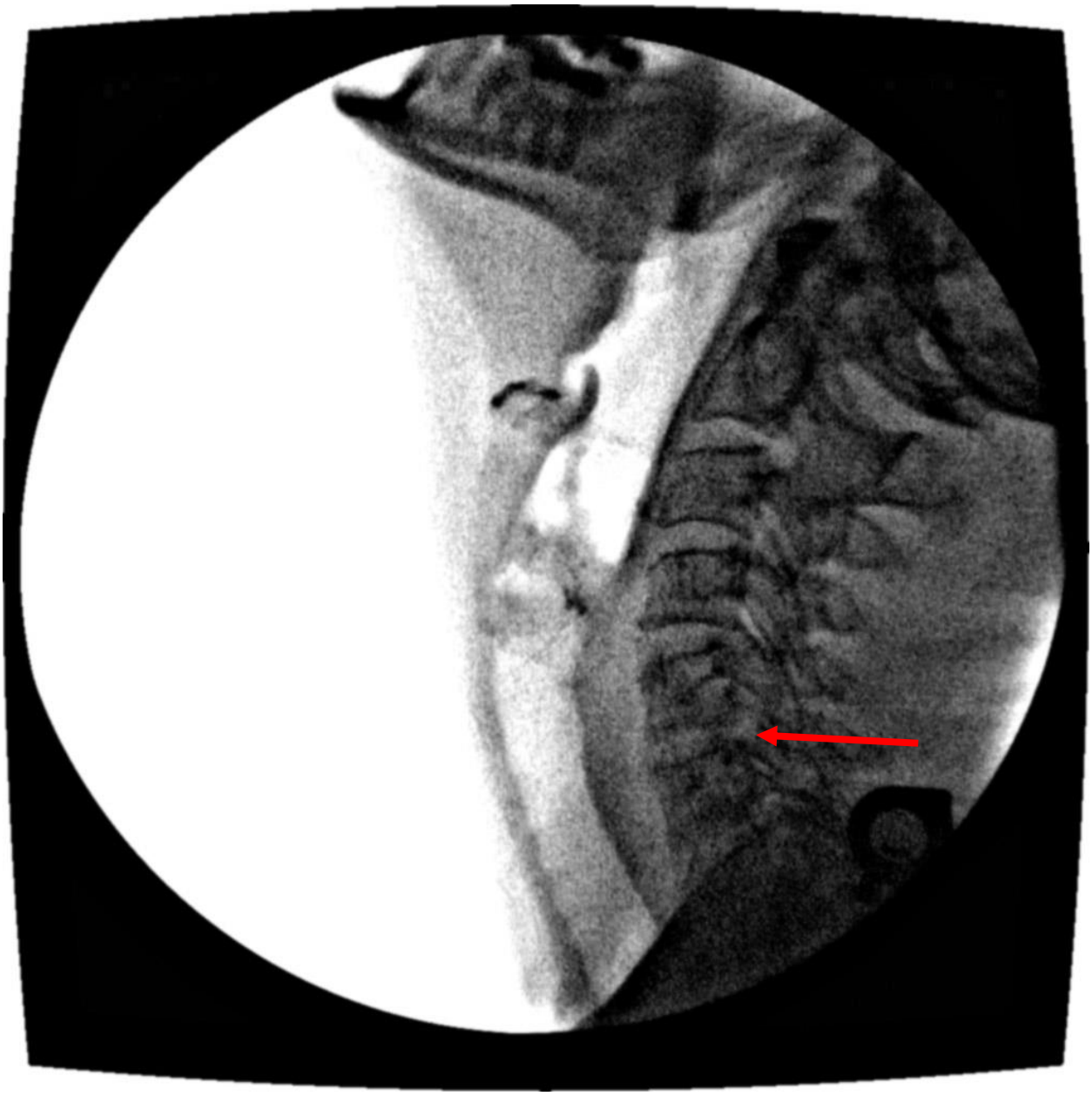

Figure 6.15 Case MH4 in the extended posture. Note how the C5/C6 joint is still in a neutral configuration relative to the other joint levels that all appear to be in extension (indicated with arrow).

6.6 Discussion

Lower relative angular displacement occurred about C5/C6 in patient cases with height loss compared to those without height loss (p=0.004). This finding is supportive of hypothesis 1. In the group without height loss, there was a very uniform trend for increasing angular displacement with descending segmental level along with very small standard deviations for each level. This finding does not support hypothesis 2.

The cases outlined here highlight a common theme in terms of disc height loss. Moderate to severe height loss cases did not follow the trend observed with non-height loss cases for increasing angular displacement with descending segmental level. The cause for the loss in relative angular displacement at the affected joint is most likely an anatomical one. Osteophytes and closer proximity between facet joints present physical barriers that would prevent motion and increase local stiffness of the segment. What the data also reveals however, is that this can occur, but is not as common in cases with mild disc height loss. In some of the mild height loss cases presented, there was evidence for a disparity in relative joint motion between adjacent segments. This is not surprising as the other cases still presented with pain and dysfunction. The cervical facet joints are one of the most common areas in the neck to be the origin of pain (Cavanaugh et al., 2006, Chen et al., 2006). It would therefore be plausible that a painful facet joint would limit voluntary movement into extension, preventing coupled stepwise motion with other joints through the linkage. Further, the anatomical features that were evident in one of the cases (MH3) showed a physical barrier to motion with displacement in extension at the C5/C6 joint.

In addition to the disc height loss, osteophytes would also cause a vertebral joint to become highly stiffened. This appears to be nature's way of stabilizing a joint with micro-movements from height loss. In the present study osteophytes were present in all of the

individuals with severe height loss, there is no doubt that these features contributed to the observed diminished mobility. Under height loss, the annulus begins to bulge radially (Brinckmann and Grootenboer, 1991) and loading is transferred to the neural arch and margins of the vertebrae (Pollintine et al., 2004b). It is therefore no surprise that disc height loss is associated with osteophytes and arthritic facets (Videman et al., 1995). While a causal relationship cannot be established based on this work, the cascade appears to follow the course of a structural failure that initiates the progression of height loss, altered loading as a result of height loss and its continued progression, and then growth of osteophytes in response to the altered loading along with potential development of facet joint arthritis causing a further stiffening of the affected joint.

One challenge with the disc height index metric is that the height of the disc is expressed as a ratio of the height of the superior and inferior vertebrae. If there are fractured vertebrae accompanying the disc height loss (highly likely in instances of severe disc height loss), the measure may not be entirely reflective of disc height loss. Without pre-post measures of disc height for each patient at each level, it is difficult to capture a metric for disc height that is truly representative. Disc height loss is a subtle measure when attempting to represent it numerically. Since disc height is a small value to begin with, changes tend to be small as well. While the disc height averages reveal slight differences between groups, it is difficult to capture differences in tenths of millimeters in some cases with percentage measures.

This work highlights the necessity of the case study. Injury, pain, and anatomy is a highly individual phenomenon that is difficult to generalize. In the cases presented here, while all had disc height loss, there were numerous differences in anatomy alone. Without a detailed individualized analysis, many factors that could help to explain the phenomena seen, could be washed out. The small details are what help to influence movement and presumably guide treatment. This is an important message clinically; one single approach to treatment cannot

encompass the plethora of mitigating factors that could be present. Not considering the individual could lead to poor outcomes in treatment.

In the mild height loss group, there was no clear effect of disc height loss reducing mobility at one segment, and in-fact, some cases (MH3 and MH4) had very high mobility at segments exhibiting mild height loss. The results from this study agree with the work of Kirkaldy-Willis and Farfan (1982) when disc height loss is considered to be progressive. In the mild height loss group there were fewer instances of osteophyte growth at the anterior and posterior margins of the vertebral bodies, indicating that there had not been enough time for osteophyte growth, if there was structural injury present, it could be presumed to be relatively new. In contrast, the disc height loss cases all presented with osteophytes indicating an older injury, or response to the increased loading that occurs at the margins of the disc with height loss. In the case of the mild height loss group, aside from cases where anatomical anomalies reduced mobility at a segment, rotation still occurred about the segment and could very likely be classified in the unstable phase (Kirkaldy-Willis and Farfan, 1982). In contrast, the stiffer discs of the disc height loss group could be considered to be in the stable phase (Kirkaldy-Willis and Farfan, 1982). While the work of Kirkaldy-Willis and Farfan (1982) was referring to micro-movements with the designated classifications, the observations from this study are simply the by-product of that classification, with injury influencing joint stiffness, and micro-movements promoting the growth of osteophytes.

In healthy individuals, the work of van Mameren found that the C4/C5 and C5/C6 joints had the greatest range of motion in the cervical spine (Van Mameren et al., 1990). Interestingly, from the grouped averages in cervical joint range of motion, they did not find a greater than 3° difference from C0-C6 in relative joint displacement between adjacent joints (Van Mameren et al., 1990). Examination of the individual patient cases however, finds that there were cases with differences in range of motion between adjacent segments greater than 3° and that non-stepwise motion of the cervical spine joints is common within a normal population (van

Mameren, 1988). In the non-disc height loss cases, there was no evidence of one single joint lacking motion, all cases followed the general trend of increasing range of motion as segmental level descended. One question that arises from this work is whether patients who exhibit large differences in relative segmental joint displacement are more likely to develop pain in the future. Further, intra-individual motion was found to be highly variable (van Mameren, 1988), while the present work cannot speak to the presence of this in the patient population, perhaps individuals with lower movement variability are more prone to injury. Regardless, motion of the cervical spine is highly complex (Bogduk and Mercer, 2000) and as evidenced by this work, highly variable. Further work characterizing spine motion in individuals with and without disc height loss is required before any concrete conclusions can be made. What is important to consider is the difference in range of motion between adjacent segments found in disc height loss cases compared to what is seen in a pain-free population.

The majority of relative angular motion occurring about a single segment could potentially initiate damage in the facet joints of the more mobile segments. This could presumably produce pain and dysfunction (Dunlop et al., 1984, Jaumard et al., 2014) under consistent repetitive use. Alternatively, assuming that the joint with height loss has a reduced mobility, the individual may simply alter their movement patterns to compensate for this (Malakoutian et al., 2015). Non-stepwise initiation of movement in the joint segments, while observed in pain-free populations (van Mameren, 1988), could also increase strain placed on the bending disc. A stepwise movement pattern could reduce the moment on adjacent segments through reduction of the moment arm during flexion (Figure 6.16, Figure 6.17). When the mass of the head moves forward into flexion, articulated stepwise motion would presumably create the smallest moment arm possible. While the effect may not be large, repeated motion in this fashion could produce fatigue in the extensor muscles countering the moment produced by the head. Higher extensor fatigue could result in load bearing duties being applied to the passive tissues and potentially develop injury over time.

With reduced overall mobility at one segment, there are two possible outcomes: either an individual simply reduces their overall mobility, or adjacent segments are forced to compensate for the lack of mobility at one (or more) of the segments. Both outcomes are likely to occur in the daily movement behaviours of individuals with disc height loss. An individual could compensate for a reduced segmental mobility by simply moving less, but this is considerably more difficult to do when the task is target-based. Looking down at a mobile device or looking up at a highly placed monitor for example, forces an individual to adopt a posture that caters to the position of an object, in these cases there must be compensation at some point in the linkage.

This study is not without its limitations. A highly heterogeneous group of cases has been presented here with only three moderate to severe disc height loss cases. Further analysis with more cases of disc height loss is required before more concrete conclusions can be made in terms of common functional deficits. This work however, provides a starting point for further investigation and the first set of data to quantitatively examine the effects of disc height loss on spine kinematics. The general population is not homogeneous, and thus common trends that can be taken from a heterogeneous group can help to enhance our knowledge in terms of spine function, detecting aberrant movement, and guiding treatment. This study also does not present data on individuals without pathology, and most of the cases in this study presented with neck pain. Pain-free individuals may also present with some of the aberrant movement patterns seen in this investigation. The detection of these patterns in a pain-free population however, does not necessarily discount the results seen here, as the question would become whether these individuals will develop pain in the future as a result of their movement patterns and loading history. More research and prospective studies are required to help clarify and answer these questions. Lack of pain is also a confounding factor with respect to comparison to disc height loss. It was necessary in this case to use individuals in pain without disc height loss to serve as comparison since those with disc height loss are also in pain and have pathology. To compare

disc height loss cases to those cases without pain or pathology would be to neglect a confounding factor that has been shown in this investigation to impact movement patterns. Regardless, despite the heterogeneous phenomenon of pain in all the cases, disc height loss was a sufficient predictor of segmental angular displacement patterns.

This study has identified three cases of moderate to severe disc height loss that showed lower angular displacement compared to adjacent segments. These patterns were also visible in other cases that presented with pain but not disc height loss. Further, height loss at C5/C6 was shown to decrease relative angular displacement compared to those without height loss. This work has identified that factors influencing movement are complex, and a case-study approach is beneficial for identifying those influencing details. Prospective studies that identify if aberrant movement patterns result in pain or disc height loss will also help to further determine the impact of disc height loss within subjects. Further, assessment of the intra-individual variability of movement is an important avenue to explore and identify if it has a role in dysfunction.

This study presents a starting point for further research in examining the effects of disc height loss. It remains to be seen whether disc height loss across a larger group of individuals, or within subjects as disc height loss progresses in the same individual shows the same patterns observed here.

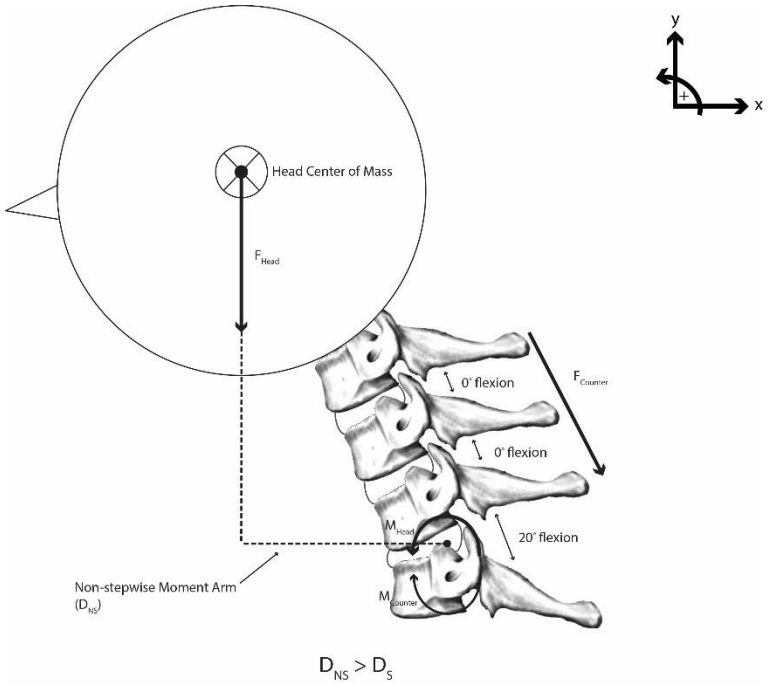

Figure 6.16 Non-stepwise motion generates a larger moment arm from the lowermost bending disc. The extensor muscles would be required to create a higher force to counter the resultant moment which could produce fatigue and pass the bearing of load onto the passive tissues. The farther the motion is from the head mass during neck flexion, the greater the compressive load. More compressive load results from the extensor tissues needed to balance this moment.

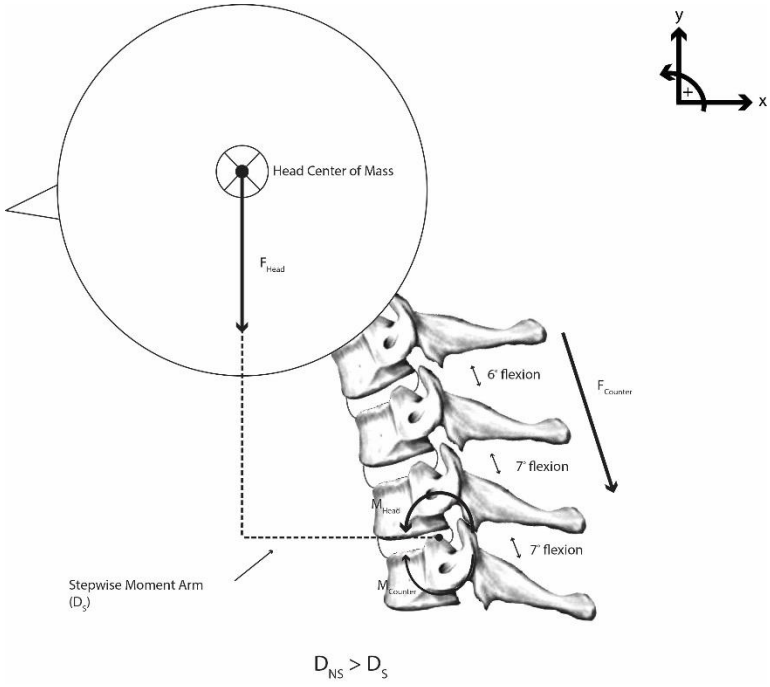

Figure 6.17 Stepwise motion creates a smaller moment arm about the lowermost disc that is bending. This would lower the force output required by the extensors to counter the resultant moment compared to the non-stepwise movement scenario. Presumably, this would result in a higher margin of safety when considering fatigue of extensor muscles and load bearing by the passive tissues.

Chapter 7: General Discussion

Non-recoverable, pathologic disc height loss is one of the most important indicators for further severe degenerative changes to manifest (Jarman et al., 2015). Height loss can cause the annulus to bulge (Brinckmann and Horst, 1985) and the facets assume an increased role in weight-bearing (Arbit and Pannullo, 2001, Gotfried et al., 1986) and develop increased levels of pressure (Dunlop et al., 1984). Disc height loss represents the threshold between more mild and higher levels of degeneration under current grading schemes (Pfirrmann et al., 2001). Clearly, further study specifically evaluating disc height loss and its mechanical effects on the spine is warranted.

In this thesis work, three studies were performed that focused on the kinematic effects of disc height loss or the mechanical outcomes of its restoration. Study 1 examined the effects of disc height loss and subsequent restoration on a single adjacent segment *in-vitro*. Study 2 examined the efficacy of a novel procedure aimed at restoring disc height while maintaining the anatomical structures of the affected segment. Study 3 quantified sagittal-plane cervical spine motion on a series of fluoroscopy image sequences of patients with pathology; some of these patients had disc height loss while others did not.

Study 1 identified that disc height loss causes an immediate change in the kinematics of a porcine cervical spine with a single adjacent segment. Losing disc height caused less angular displacement to occur about the level with height loss and more displacement to occur about the adjacent segment. Following disc height restoration using an injectable hydrogel, the kinematics of both segments returned to the initial state.

This study showed the immediate effects of disc height loss in isolation from other confounding factors such as degeneration. Losing disc height causes a spine segment to become stiffer when tested *in-vitro*. As a result, a larger applied moment is required to bring it

to a given target angle. If an adjacent segment is present, it will rotate more, compared to the stiffer segment. The results from this study also outlined the effectiveness of a hydrogel in restoring the initial stiffness characteristics to an affected segment.

Some criticisms of this study include the use of only two segments. In an *in-vivo* scenario there are many segments present for angular displacement to occur about. Lee and colleagues showed that in the lumbar spine, upper levels will compensate for motion loss at lower levels (Lee et al., 2014). The most likely reconciliation of this would be to examine exposure on a case by case basis. Even small changes in angular displacement spread across multiple segments could result in pathological change if repeated enough, some individuals may become injured while others who limit their exposure to this will not.

A further issue from this study was the lack of hydrogel containment in some specimens. The size of needle used for nucleus extrusion created a bore hole in the annulus that caused hydrogel containment to be an issue. Unfortunately, a large gauge needle had to be used in order to facilitate ejection of the nucleus pulposus to create disc height loss. Doing so resulted in a large hole in the anterior annulus that could not entirely contain the hydrogel in some circumstances. Containment of this hydrogel with the use of a smaller gauge needle in porcine cervical spine segments has been achieved in the past however, under repeated cyclic loading (Balkovec et al., 2013).

Study 1 showed that disc height loss via loss of nucleus pulposus produced immediate kinematic changes in the affected and adjacent segments. It also showed that restoration of disc height caused an immediate restoration to the kinematic profile of an injured spine specimen.

Study 2 evaluated the efficacy of a novel surgical protocol at restoring the mechanical profile of a spine segment after disc height loss induced by compressive fracture and repeated compressive loading. Results agreed with previous work (Landham et al., 2015a, Luo et al., 2007) examining the effects of PMMA on reducing the compressive stiffness of an injured spine

segment. Additionally, the data agreed with previous work examining the effects of hydrogel injection on the rotational stiffness of an injured spine segment (Balkovec et al., 2013). Ultimately however, the difficulties associated with containment of hydrogel in the disc space with some complex fractures proved difficult and the restored mechanical profile of the spine in terms of compressive and rotational stiffness could not be maintained after continued repetitive loading.

This study brought important issues to the forefront with respect to disc height restoration. There are many ways in which a disc can become injured and many factors that can affect whether a particular intervention is successful or not. In the case of this work, large cracks in the endplate, despite the use of PMMA in the vertebral body to attempt to create a seal from above, proved unsuccessful in terms of the containment of the hydrogel. Further progress in disc restoration cannot be made however, without these issues being addressed. It would therefore be a worthy task to develop a strategy to fill in large cracks in the endplate from the disc-side as well as from the vertebral body. Creating an environment that contains nucleus pulposus/hydrogel and can withstand the stresses that the disc encounters on a daily basis is an absolutely necessary next step in the development of a conservative disc restoration procedure.

Not to detract from current efforts aimed at cellular restoration of the intervertebral disc (Benneker et al., 2014), a procedure like the one described in Study 2 would be employed on spine segments where structural healing requires intervention beyond what the cells are capable of. Mechanical function would be restored by completely artificial means and potentially reduce cell viability in the hopes that it would be maintained at other non-injured segments in the spine. This procedure could also be an important stop-gap in the process of disc height restoration, where complete healing through cellular means is most likely reserved for use further in the future.

Study 2 identified two processes that can be used to restore the mechanical profile of a compressively injured spine segment while maintaining the majority of its anatomical structures. There is difficulty however, in using this procedure on more severely injured segments and its long-term viability is brought into question if the mechanism of injury is repeated. It is important to state that regardless of the efficacy of a restoration procedure, if the mechanism of injury is repeated, re-injury will occur.

In Studies 1 and 2, disc height was instantaneously lost, which provided direct insight into its role on mechanics. *In-vivo*, the relationship may be confounded with other factors that could alter movement. Disc height loss could occur over a prolonged period of time, or it could be accompanied by osteophyte growth. Pain could also act as a behavioural modulator and result in aberrant movement. In cases where disc height loss occurs over a long period of time, tissues could potentially have more time to adapt, allowing for their tolerance to acclimate to their new mechanical conditions. Despite the limitations of studies 1 and 2, they provide important insight into the direct role of disc height and its importance in segmental spine mechanics. Future work should involve and incorporate human data that adds further validity.

Using the novel algorithm created in Appendix A, Study 3 quantified the kinematics of a series of patient cervical spine image sequences. In each case, patients had a history of pathology, with the majority experiencing neck pain. Some of the patients presented with disc height loss while others did not. In the disc height loss cases less proportional angular displacement occurred about the C5/C6 level (20.2% ± 2.3%) compared to those without height loss (30.6% ± 4.0%). Despite pain and various injury histories, disc height loss was enough to identify aberrant movement with respect to segmental angular displacement. Previous work on pain-free individuals indicates that initiation of motion is not necessarily step-wise, and in some cases there is a large difference between ranges of motion in adjacent segments (van Mameren, 1988). When taken together however, the data on pain-free individuals showed that there was never a greater than 3° difference in the range of motion between adjacent segments

(Van Mameren et al., 1990) indicating that this could be used as an indicator of dysfunction. There is also the question of whether a pain-free individual who presents with such a disparity in adjacent segment ranges of motion will be more likely to develop pain.

Appendix A involved the development of a novel tracking algorithm for the purposes of tracking vertebral body motion under fluoroscopy. The algorithm uses an established normalized cross-correlation function (Velduis and Brodland, 1999) and incorporates unique template features, iterative refinement passes, and image processing. Evaluation of the algorithm was twofold and involved the use of a porcine cervical spine rotating within a fluoroscope field of view to compare the algorithm to ground-truth measurements in addition to evaluating the repeatability of measurements made on three patient spine image sequences. Overall measures of error were less than half a degree in angular displacement and a tenth of a millimeter in shear in terms of the RMS error over a trial. This represents a highly accurate method of systematically measuring vertebral body motion from a source that contains a high level of noise and distortion. The prospect of measuring segmental motion *in-vivo* with high accuracy is attractive in terms of future work that attempts to examine motion patterns in various groups of individuals. Creating this algorithm provides another tool to track segmental spine motion with and will help to enhance the research output of studies that attempt to use fluoroscopy to analyze spine motion *in-vivo*.

From the data analyzed in Study 3, disc height loss resulted in significantly lower angular displacement about C5/C6 compared to cases without height loss ($p = 0.004$). These findings would agree with those from Study 1 in terms of diminished segmental mobility at the level with height loss, however, caution must be emphasized in generalizing these conclusions.

Study 3 presents a series of findings that warrant further research. Further analysis of more disc height loss cases should be performed before any generalized conclusions can be made. Additionally, prospective studies that examine disc height loss within individuals over

time could facilitate a more concrete understanding of how disc height loss influences kinematics and more importantly, progression of injury.

The work performed in this thesis has found that disc height loss influences kinematics of an affected and adjacent segment (Study 1), presents a challenge to repair when induced through compressive failure (Study 2), and creates a decreased range of motion *in-vivo* (Study 3). The tools developed in this work (Appendix A) will assist in the continued measurement of spine motion *in-vivo* to follow-up on the work presented here. Further research into the mechanisms of disc height loss will help to solidify the findings of this work and enhance knowledge of the influence of disc height loss to the course of injury in the spine.

Disc height loss *in-vivo* is a complex phenomenon to describe. Kinematic changes to segmental movement can be attributed to a number of behavioural and anatomical factors. In short, when trying to determine the consequences of disc height loss on kinematic outcomes, the answer is, “it depends”. Disc height loss needs to be taken into account with various anatomical features and the tendencies of the individual themselves. The complexity of this is explored in the flow diagram in Figure 7.1 where injury and disc height loss is placed in context with behavioural, structural, and chemical responses. Structural failure of a tissue could result in disc height loss; from here structural remodelling via cellular activity can take place, but there will be immediate changes in the loading and stresses placed on surrounding tissues. These changes could result in altered movement strategies in order to compensate. If the altered movement strategies begin to load additional tissues and exceed their tolerance, further injury will occur.

Rotations observed *in-vitro* in Study 1 had differences with respect to the rotations observed *in-vivo* in Study 3. To broadly characterize this, the rotations in Study 1 were consistent between specimens while there was higher variability observed between patient cases *in-vivo*. In Study 1, specimens were loaded externally in an identical manner, with a pure moment/compressive load paradigm. In Study 3, there was variability in the anatomy and

structural injury between patients. Features such as osteophytes add increased stiffness to a segment, and would alter the movement characteristics at that level (and were shown to). Figure 7.2 outlines a sample time-history sequence of a patient performing sagittal plane motion of the neck. Movement is quickly initiated about all segments, but there is a stepwise pattern evident from the C3/C4 level downwards. C2/C3 is the only segment that does not exhibit this behaviour. All segments contribute to angular displacement, but at different time-points, and the disc height loss at C4/C5 and C5/C6 along with osteophytes at those levels seem to stiffen the joint and prevent any displacement greater than the displacement of the C2/C3 or C3/C4 levels.

Figure 7.3 outlines angular displacement in a porcine spine specimen with two functional segments. Height loss has been induced via nucleus extrusion in the superior disc. Similar to what is shown in Figure 7.2, motion is initiated in a stepwise fashion, but due to the apparatus, peak angular displacement measured during the trial is nearly achieved in the superior disc before motion occurs about the inferior disc. Despite the difference in rotation sequence between the *in-vitro* and some *in-vivo* scenarios, the rotations are driven by the applied moments and localized stiffness of the segments. When disc height is lost, localized stiffness is presumed to increase at that segment. Under the higher applied moment, the segment without height loss displaces further given the lower localized stiffness. From this, to reconcile the results seen between *in-vitro* and *in-vivo* motion, angular motion about a segment is governed by its local stiffness. Disc height loss increases the localized stiffness of a segment and reduces its displacement under a given applied moment. In the *in-vivo* cases, the presence of osteophytes further adds to the local stiffness of a segment. To summarize, Studies 1 and 2 represented an acute height loss condition, which is closest to a fresh injury. The *in-vivo* study represents height loss with a healing process or a response that has resulted in a cascade involving facet changes and osteophyte growth.

This work puts into context how disc height can influence movement behaviour (Study 1), but must ultimately be put into the broader scope of the individual and their personal

tendencies and anatomy. Future work needs to further identify how movement is influenced under the complex network of anatomical, physiological, and behavioural factors. Specifically, further studies should examine if aberrant movement patterns are repeatable and how additional factors such as facet size and osteophytes influence movement and injury progression alongside disc height loss. Ultimately, future work must follow individuals over time and identify how aberrant movement influences disc height loss and vice-versa, along with identifying how disc height loss influences injury progression. With the groundwork in this thesis and the tools developed to perform precision measurement of *in-vivo* segmental spine motion, future research will be able to identify further specific influences to spine function and pathology and potentially help guide clinical practice.

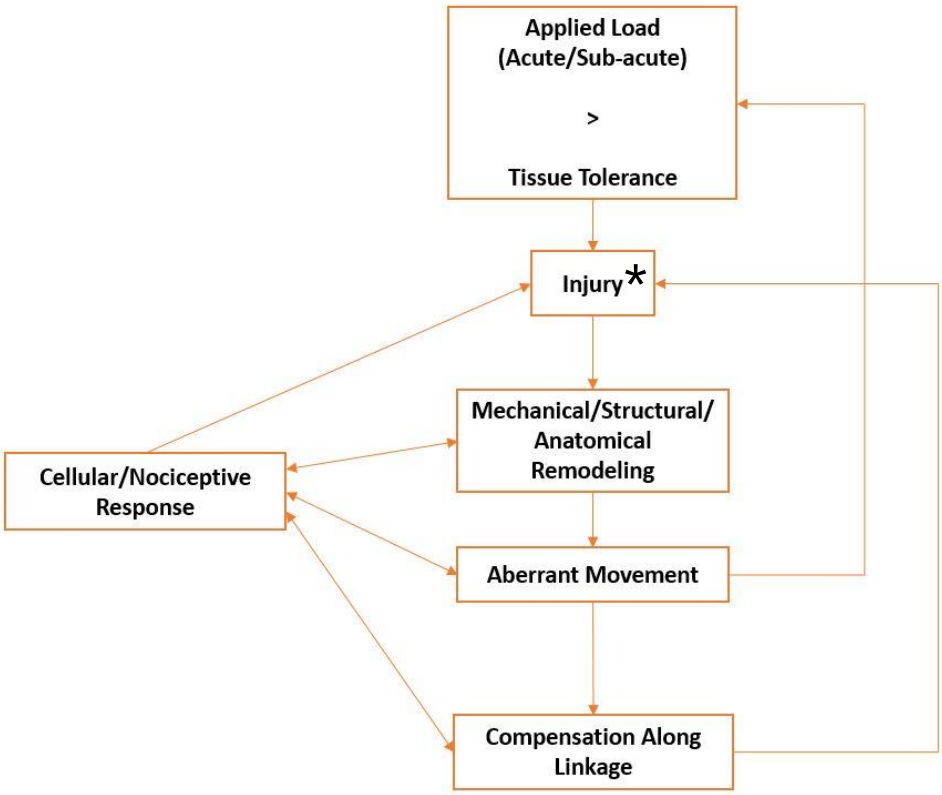

Figure 7.1Flow diagram of mechanical injury to the intervertebral disc and resultant effect. Applied loading exceeds a tissue's tolerance and the tissue fails resulting in injury. Disc height loss has the potential to occur at this step (denoted by asterisk). From here, there is the potential for the alteration of the cellular environment within the disc depending on the type and scale of tissue failure that occurred. Nociception can also occur depending on the type and scale of injury. These influences are outside the scope of the curent discussion of mechanical compensation as a result of disc height loss, but are included for completeness and to illustrate that pain could alter behaviour and movement strategies. With tissue injury, there is an alteration in the structural environment and therefore a change in how tissues are loaded. This altered loading could result in exceeding the tolerance of additional tissues/structures and result in further injury. Disc height loss would result in changes to the mechanical environment in terms of increasing the local stiffness of the disc. This would result in a lower range of motion (as seen in Studies 1 and 3) at that segment, and potentially result in compensation at adjacent segments (as seen in Study 1). Loading adjacent segments beyond the tolerance (acute or chronic) of their structures could result in further injury.

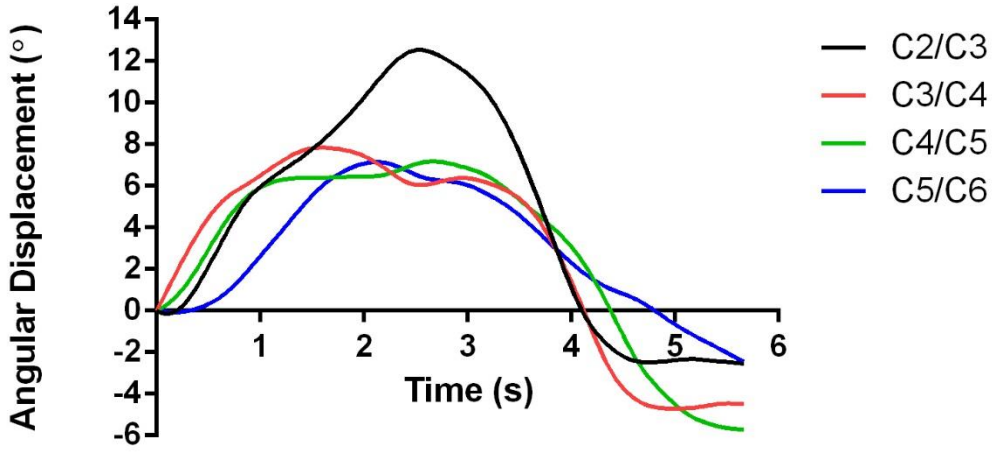

Figure 7.2 Angular displacement of neck flexion for a patient case with disc height loss. Motion is initiated in a stepwise fashion (except for the C2/C3 segment), and while angular displacement occurs at all segments, the displacement at C4/C5 and C5/C6 with height loss would be expected to be higher. Localized stiffness of those segments created by disc height loss and osteophytes prevents further rotation.

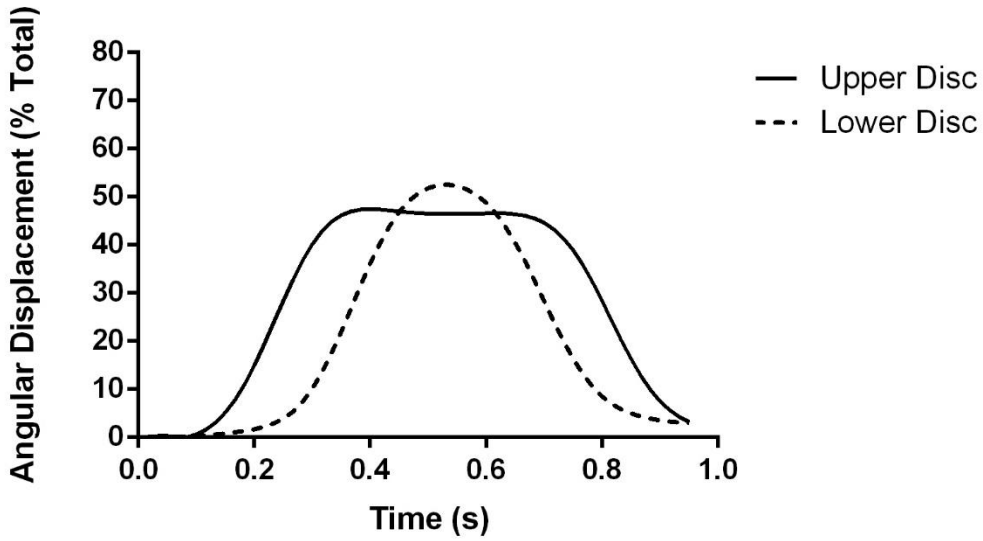

Figure 7.3 Angular displacement time-history for a multi-segmented spine specimen, height loss has been induced via nucleus extraction in the superior disc. Motion is initiated in a stepwise fashion, but due to the testing apparatus, is a more drastic case compared to *in-vivo*. Peak angular displacement is nearly achieved in the superior segment before motion occurs about the inferior segment. Regardless, the motion is driven by the localized stiffness in the segment. With a greater applied moment, the inferior segment (without height loss) displaces more since the local stiffness in that segment is lower.

References

ACAROGLU, E. R., IATRIDIS, J. C., SETTON, L. A., FOSTER, R. J., MOW, V. C. & WEIDENBAUM, M. 1995. Degeneration and aging affect the tensile behavior of human lumbar anulus fibrosus. *Spine (Phila Pa 1976),* 20**,** 2690-701.

ADAMS, M. A., BURTON, K., BOGDUK, N. & DOLAN, P. 2006a. *The Biomechanics of Back Pain,* Edinburgh, UK, Elsevier Health Sciences.

ADAMS, M. A. & DOLAN, P. 1997. Could sudden increases in physical activity cause degeneration of intervertebral discs? *Lancet,* 350**,** 734-5.

ADAMS, M. A. & DOLAN, P. 2012. Intervertebral disc degeneration: evidence for two distinct phenotypes. *J Anat,* 221**,** 497-506.

ADAMS, M. A., DOLAN, P. & HUTTON, W. C. 1986. The stages of disc degeneration as revealed by discograms. *J Bone Joint Surg Br,* 68**,** 36-41.

ADAMS, M. A., DOLAN, P., HUTTON, W. C. & PORTER, R. W. 1990. Diurnal changes in spinal mechanics and their clinical significance. *J Bone Joint Surg Br,* 72**,** 266-70.

ADAMS, M. A., FREEMAN, B. J., MORRISON, H. P., NELSON, I. W. & DOLAN, P. 2000a. Mechanical initiation of intervertebral disc degeneration. *Spine (Phila Pa 1976),* 25**,** 1625-36.

ADAMS, M. A. & GREEN, T. P. 1993. Tensile properties of the annulus fibrosus. I. The contribution of fibre-matrix interactions to tensile stiffness and strength. *Eur Spine J,* 2**,** 203-8.

ADAMS, M. A. & HUTTON, W. C. 1980. The effect of posture on the role of the apophysial joints in resisting intervertebral compressive forces. *J Bone Joint Surg Br,* 62**,** 358-62.

ADAMS, M. A. & HUTTON, W. C. 1983. The effect of posture on the fluid content of lumbar intervertebral discs. *Spine (Phila Pa 1976),* 8**,** 665-71.

ADAMS, M. A. & HUTTON, W. C. 1985. Gradual disc prolapse. *Spine (Phila Pa 1976),* 10**,** 524-31.

ADAMS, M. A., LAMA, P., ZEHRA, U. & DOLAN, P. 2015. Why do some intervertebral discs degenerate, when others (in the same spine) do not? *Clin Anat,* 28**,** 195-204.

ADAMS, M. A., MAY, S., FREEMAN, B. J., MORRISON, H. P. & DOLAN, P. 2000b. Effects of backward bending on lumbar intervertebral discs. Relevance to physical therapy treatments for low back pain. *Spine (Phila Pa 1976),* 25**,** 431-7; discussion 438.

ADAMS, M. A., MCNALLY, D. S. & DOLAN, P. 1996. 'Stress' distributions inside intervertebral discs. The effects of age and degeneration. *J Bone Joint Surg Br,* 78**,** 965-72.

ADAMS, M. A., MCNALLY, D. S., WAGSTAFF, J. & GOODSHIP, A. E. 1993. Abnormal stress concentrations in lumbar intervertebral discs following damage to the vertebral bodies: a cause of disc failure? *Eur Spine J,* 1**,** 214-21.

ADAMS, M. A., POLLINTINE, P., TOBIAS, J. H., WAKLEY, G. K. & DOLAN, P. 2006b. Intervertebral disc degeneration can predispose to anterior vertebral fractures in the thoracolumbar spine. *J Bone Miner Res,* 21**,** 1409-16.

ADAMS, M. A. & ROUGHLEY, P. J. 2006. What is intervertebral disc degeneration, and what causes it? *Spine (Phila Pa 1976),* 31**,** 2151-61.

ADAMS, M. A., STEFANAKIS, M. & DOLAN, P. 2010. Healing of a painful intervertebral disc should not be confused with reversing disc degeneration: implications for physical therapies for discogenic back pain. *Clin Biomech (Bristol, Avon),* 25**,** 961-71.

AGORASTIDES, I. D., LAM, K. S., FREEMAN, B. J. & MULHOLLAND, R. C. 2002. The Adams classification for cadaveric discograms: inter- and intra-observer error in the clinical setting. *Eur Spine J,* 11**,** 76-9.

AHMADI, A., MAROUFI, N., BEHTASH, H., ZEKAVAT, H. & PARNIANPOUR, M. 2009. Kinematic analysis of dynamic lumbar motion in patients with lumbar segmental instability using digital videofluoroscopy. *Eur Spine J,* 18**,** 1677-85.

AHRENS, M., TSANTRIZOS, A., DONKERSLOOT, P., MARTENS, F., LAUWERYNS, P., LE HUEC, J. C., MOSZKO, S., FEKETE, Z., SHERMAN, J., YUAN, H. A. & HALM, H. 2009. Nucleus replacement with the DASCOR disc arthroplasty device: interim two-year efficacy and safety results from two prospective, non-randomized multicenter European studies. *Spine (Phila Pa 1976),* 34**,** 1376-84.

AIGNER, T., GRESK-OTTER, K. R., FAIRBANK, J. C., VON DER MARK, K. & URBAN, J. P. 1998. Variation with age in the pattern of type X collagen expression in normal and scoliotic human intervertebral discs. *Calcif Tissue Int,* 63**,** 263-8.

AL-RAWAHI, M., LUO, J., POLLINTINE, P., DOLAN, P. & ADAMS, M. A. 2011. Mechanical function of vertebral body osteophytes, as revealed by experiments on cadaveric spines. *Spine (Phila Pa 1976),* 36**,** 770-7.

ALINI, M., EISENSTEIN, S. M., ITO, K., LITTLE, C., KETTLER, A. A., MASUDA, K., MELROSE, J., RALPHS, J., STOKES, I. & WILKE, H. J. 2008. Are animal models useful for studying human disc disorders/degeneration? *Eur Spine J,* 17**,** 2-19.

ANDERSSON, G. B. & SCHULTZ, A. B. 1979. Effects of fluid injection on mechanical properties of intervertebral discs. *J Biomech,* 12**,** 453-8.

ANTONIOU, J., STEFFEN, T., NELSON, F., WINTERBOTTOM, N., HOLLANDER, A. P., POOLE, R. A., AEBI, M. & ALINI, M. 1996. The human lumbar intervertebral disc: evidence for changes in the biosynthesis and denaturation of the extracellular matrix with growth, maturation, ageing, and degeneration. *J Clin Invest,* 98**,** 996-1003.

ARBIT, E. & PANNULLO, S. 2001. Lumbar stenosis: a clinical review. *Clin Orthop Relat Res,* Mar**,** 137-43.

AULTMAN, C. D., SCANNELL, J. & MCGILL, S. M. 2005. The direction of progressive herniation in porcine spine motion segments is influenced by the orientation of the bending axis. *Clin Biomech (Bristol, Avon),* 20**,** 126-9.

BAILEY, J. F., LIEBENBERG, E., DEGMETICH, S. & LOTZ, J. C. 2011. Innervation patterns of PGP 9.5-positive nerve fibers within the human lumbar vertebra. *J Anat,* 218**,** 263-70.

BALKOVEC, C., ADAMS, M. A., DOLAN, P. & MCGILL, S. M. 2015. Annulus Fibrosus Can Strip Hyaline Cartilage End Plate from Subchondral Bone: A Study of the Intervertebral Disk in Tension. *Global Spine J,* 5**,** 360-5.

BALKOVEC, C. & MCGILL, S. 2012. Extent of nucleus pulposus migration in the annulus of porcine intervertebral discs exposed to cyclic flexion only versus cyclic flexion and extension. *Clin Biomech (Bristol, Avon),* 27**,** 766-70.

BALKOVEC, C., VERNENGO, J. & MCGILL, S. M. 2013. The use of a novel injectable hydrogel nucleus pulposus replacement in restoring the mechanical properties of cyclically fatigued porcine intervertebral discs. *J Biomech Eng,* 135**,** 61004-5.

BAO, Q. B., MCCULLEN, G. M., HIGHAM, P. A., DUMBLETON, J. H. & YUAN, H. A. 1996. The artificial disc: theory, design and materials. *Biomaterials,* 17**,** 1157-67.

BARTELS, E. M., FAIRBANK, J. C., WINLOVE, C. P. & URBAN, J. P. 1998. Oxygen and lactate concentrations measured in vivo in the intervertebral discs of patients with scoliosis and back pain. *Spine (Phila Pa 1976),* 23**,** 1-7; discussion 8.

BATTIE, M. C., VIDEMAN, T., KAPRIO, J., GIBBONS, L. E., GILL, K., MANNINEN, H., SAARELA, J. & PELTONEN, L. 2009. The Twin Spine Study: contributions to a changing view of disc degeneration. *Spine J,* 9**,** 47-59.

BENDIX, T., KJAER, P. & KORSHOLM, L. 2008. Burned-out discs stop hurting: fact or fiction? *Spine (Phila Pa 1976),* 33**,** E962-7.

BENNEKER, L. M., ANDERSSON, G., IATRIDIS, J. C., SAKAI, D., HARTL, R., ITO, K. & GRAD, S. 2014. Cell therapy for intervertebral disc repair: advancing cell therapy from bench to clinics. *Eur Cell Mater,* 27**,** 5-11.

BENNEKER, L. M., HEINI, P. F., ALINI, M., ANDERSON, S. E. & ITO, K. 2005. 2004 Young Investigator Award Winner: vertebral endplate marrow contact channel occlusions and intervertebral disc degeneration. *Spine (Phila Pa 1976),* 30**,** 167-73.

BERTAGNOLI, R., SABATINO, C. T., EDWARDS, J. T., GONTARZ, G. A., PREWETT, A. & PARSONS, J. R. 2005. Mechanical testing of a novel hydrogel nucleus replacement implant. *Spine J,* 5**,** 672-81.

BERTAGNOLI, R. & SCHONMAYR, R. 2002. Surgical and clinical results with the PDN prosthetic disc-nucleus device. *Eur Spine J,* 11 Suppl 2**,** S143-8.

BIFULCO, P., CESARELLI, M., ALLEN, R., SANSONE, M. & BRACALE, M. 2001. Automatic recognition of vertebral landmarks in fluoroscopic sequences for analysis of intervertebral kinematics. *Med Biol Eng Comput,* 39**,** 65-75.

BISSCHOP, A., KINGMA, I., BLEYS, R. L., PAUL, C. P., VAN DER VEEN, A. J., VAN ROYEN, B. J. & VAN DIEEN, J. H. 2013. Effects of repetitive movement on range of motion and stiffness around the neutral orientation of the human lumbar spine. *J Biomech,* 46**,** 187-91.

BOGDUK, N. 2005. *Clinical Anatomy of the Lumbar Spine and Sacrum,* Edinburgh, UK, Elsevier Churchill Livingstone.

BOGDUK, N. 2012. Degenerative joint disease of the spine. *Radiol Clin North Am,* 50**,** 613-28.

BOGDUK, N. & MERCER, S. 2000. Biomechanics of the cervical spine. I: Normal kinematics. *Clin Biomech (Bristol, Avon),* 15**,** 633-48.

BOOS, N., WALLIN, A., GBEDEGBEGNON, T., AEBI, M. & BOESCH, C. 1993. Quantitative MR imaging of lumbar intervertebral disks and vertebral bodies: influence of diurnal water content variations. *Radiology,* 188**,** 351-4.

BOOS, N., WEISSBACH, S., ROHRBACH, H., WEILER, C., SPRATT, K. F. & NERLICH, A. G. 2002. Classification of age-related changes in lumbar intervertebral discs: 2002 Volvo Award in basic science. *Spine (Phila Pa 1976),* 27**,** 2631-44.

BOOTSMA, G. J. & BRODLAND, G. W. 2005. Automated 3-D reconstruction of the surface of live early-stage amphibian embryos. *IEEE Trans Biomed Eng,* 52**,** 1407-14.

BREEN, A., ALLEN, R. & MORRIS, A. 1989. A digital videofluoroscopic technique for spine kinematics. *J Med Eng Technol,* 13**,** 109-13.

BREEN, A. C., TEYHEN, D. S., MELLOR, F. E., BREEN, A. C., WONG, K. W. & DEITZ, A. 2012. Measurement of intervertebral motion using quantitative fluoroscopy: report of an international forum and proposal for use in the assessment of degenerative disc disease in the lumbar spine. *Adv Orthop,* 2012**,** 802350.

BRINCKMANN, P., BIGGEMANN, M. & HILWEG, D. 1989. Prediction of the compressive strength of human lumbar vertebrae. *Spine (Phila Pa 1976),* 14**,** 606-10.

BRINCKMANN, P. & GROOTENBOER, H. 1991. Change of disc height, radial disc bulge, and intradiscal pressure from discectomy. An in vitro investigation on human lumbar discs. *Spine (Phila Pa 1976),* 16**,** 641-6.

BRINCKMANN, P. & HORST, M. 1985. The influence of vertebral body fracture, intradiscal injection, and partial discectomy on the radial bulge and height of human lumbar discs. *Spine (Phila Pa 1976),* 10**,** 138-45.

BROOM, N. D. & MARRA, D. L. 1985. New structural concepts of articular cartilage demonstrated with a physical model. *Connect Tissue Res,* 14**,** 1-8.

BUCKWALTER, J. A. 1995. Aging and degeneration of the human intervertebral disc. *Spine (Phila Pa 1976),* 20**,** 1307-14.

BURKE, K. L. 2012. Schmorl's nodes in an American military population: frequency, formation, and etiology. *J Forensic Sci,* 57**,** 571-7.

CALDERON, L., COLLIN, E., VELASCO-BAYON, D., MURPHY, M., O'HALLORAN, D. & PANDIT, A. 2010. Type II collagen-hyaluronan hydrogel--a step towards a scaffold for intervertebral disc tissue engineering. *Eur Cell Mater,* 20**,** 134-48.

CALLAGHAN, J. P. & MCGILL, S. M. 1995. Frozen storage increases the ultimate compressive load of porcine vertebrae. *J Orthop Res,* 13**,** 809-12.

CALLAGHAN, J. P. & MCGILL, S. M. 2001. Intervertebral disc herniation: studies on a porcine model exposed to highly repetitive flexion/extension motion with compressive force. *Clin Biomech (Bristol, Avon),* 16**,** 28-37.

CANNELLA, M., ARTHUR, A., ALLEN, S., KEANE, M., JOSHI, A., VRESILOVIC, E. & MARCOLONGO, M. 2008. The role of the nucleus pulposus in neutral zone human lumbar intervertebral disc mechanics. *J Biomech,* 41**,** 2104-11.

CASSIDY, J. J., HILTNER, A. & BAER, E. 1989. Hierarchical structure of the intervertebral disc. *Connect Tissue Res,* 23**,** 75-88.

CAVANAUGH, J. M., LU, Y., CHEN, C. & KALLAKURI, S. 2006. Pain generation in lumbar and cervical facet joints. *J Bone Joint Surg Am,* 88 Suppl 2**,** 63-7.

CHEN, C., LU, Y., KALLAKURI, S., PATWARDHAN, A. & CAVANAUGH, J. M. 2006. Distribution of A-delta and C-fiber receptors in the cervical facet joint capsule and their response to stretch. *J Bone Joint Surg Am,* 88**,** 1807-16.

CHEN, J. W., LI, B., YANG, Y. H., JIANG, S. D. & JIANG, L. S. 2014. Significance of hypoxia in the physiological function of intervertebral disc cells. *Crit Rev Eukaryot Gene Expr,* 24**,** 193-204.

CHOLEWICKI, J. & MCGILL, S. M. 1992. Lumbar posterior ligament involvement during extremely heavy lifts estimated from fluoroscopic measurements. *J Biomech,* 25**,** 17-28.

CHOLEWICKI, J., MCGILL, S. M., WELLS, R. P. & VERNON, H. 1991. Method for measuring vertebral kinematics from videofluoroscopy. *Clin Biomech (Bristol, Avon),* 6**,** 73-8.

CORTES, D. H. & ELLIOTT, D. M. 2014. The Intervertebral Disc: Overview of Disc Mechanics. *In:* SHAPIRO, I. M. & RISBUD, M. V. (eds.) *The Intervertebral Disc.* Wien, Austria: Springer.

COVENTRY, M. B., GHORMLEY, R. K. & KERNOHAN, J. W. 1945. The intervertebral disc: its microscopic anatomy and pathology: part I: anatomy, development, and physiology. *The Journal of Bone & Joint Surgery,* 27**,** 105-112.

CRISCO, J. J., PANJABI, M. M., YAMAMOTO, I. & OXLAND, T. R. 1992. Euler stability of the human ligamentous lumbar spine. Part II: Experiment. *Clin Biomech (Bristol, Avon),* 7**,** 27-32.

CROSBY, N. D., GILLILAND, T. M. & WINKELSTEIN, B. A. 2014. Early afferent activity from the facet joint after painful trauma to its capsule potentiates neuronal excitability and glutamate signaling in the spinal cord. *Pain,* 155**,** 1878-87.

DAHL, M. C., AHRENS, M., SHERMAN, J. E. & MARTZ, E. O. 2010. The restoration of lumbar intervertebral disc load distribution: a comparison of three nucleus replacement technologies. *Spine (Phila Pa 1976),* 35**,** 1445-53.

DE CARVALHO, D. E., SOAVE, D., ROSS, K. & CALLAGHAN, J. P. 2010. Lumbar spine and pelvic posture between standing and sitting: a radiologic investigation including reliability and repeatability of the lumbar lordosis measure. *J Manipulative Physiol Ther,* 33**,** 48-55.

DE VRIES, J., ISCHEBECK, B. K., VOOGT, L. P., VAN DER GEEST, J. N., JANSSEN, M., FRENS, M. A. & KLEINRENSINK, G. J. 2015. Joint position sense error in people with neck pain: A systematic review. *Man Ther,* in press.

DEKUTOSKI, M. B., SCHENDEL, M. J., OGILVIE, J. W., OLSEWSKI, J. M., WALLACE, L. J. & LEWIS, J. L. 1994. Comparison of in vivo and in vitro adjacent segment motion after lumbar fusion. *Spine (Phila Pa 1976),* 19**,** 1745-51.

DIANGELO, D. J. & FOLEY, K. T. 2004. An improved biomechanical testing protocol for evaluating spinal arthroplasty and motion preservation devices in a multilevel human cadaveric cervical model. *Neurosurg Focus,* 17**,** E4.

DRAKE, J. D., AULTMAN, C. D., MCGILL, S. M. & CALLAGHAN, J. P. 2005. The influence of static axial torque in combined loading on intervertebral joint failure mechanics using a porcine model. *Clin Biomech (Bristol, Avon),* 20**,** 1038-45.

DUNLOP, R. B., ADAMS, M. A. & HUTTON, W. C. 1984. Disc space narrowing and the lumbar facet joints. *J Bone Joint Surg Br,* 66**,** 706-10.

EILAGHI, A., FLANAGAN, J. G., BRODLAND, G. W. & ETHIER, C. R. 2009. Strain uniformity in biaxial specimens is highly sensitive to attachment details. *J Biomech Eng,* 131**,** 091003.

ESKO, J. D., KIMATA, K. & LINDAHL, U. 2009. *Proteoglycans and Sulfated Glycosaminoglycans. In: Varki A, Cummings RD, Esko JD, et al., editors. Essentials of Glycobiology. 2nd edition.,* Cold Spring Harbor (NY), Cold Spring Harbor Laboratory Press.

EYRE, D. R. & MUIR, H. 1977. Quantitative analysis of types I and II collagens in human intervertebral discs at various ages. *Biochim Biophys Acta,* 492**,** 29-42.

FAGAN, A., MOORE, R., VERNON ROBERTS, B., BLUMBERGS, P. & FRASER, R. 2003. ISSLS prize winner: The innervation of the intervertebral disc: a quantitative analysis. *Spine (Phila Pa 1976),* 28**,** 2570-6.

FARDON, D. F., WILLIAMS, A. L., DOHRING, E. J., MURTAGH, F. R., GABRIEL ROTHMAN, S. L. & SZE, G. K. 2014. Lumbar disc nomenclature: version 2.0: Recommendations of the combined task forces of the North American Spine Society, the American Society of Spine Radiology and the American Society of Neuroradiology. *Spine J,* 14**,** 2525-45.

FENNELL, A. J., JONES, A. P. & HUKINS, D. W. 1996. Migration of the nucleus pulposus within the intervertebral disc during flexion and extension of the spine. *Spine (Phila Pa 1976),* 21**,** 2753-7.

FERGUSON, S. J. & STEFFEN, T. 2003. Biomechanics of the aging spine. *Eur Spine J,* 12 Suppl 2**,** S97-S103.

FIELDS, A. J., LEE, G. L. & KEAVENY, T. M. 2010. Mechanisms of initial endplate failure in the human vertebral body. *J Biomech,* 43**,** 3126-31.

FIELDS, A. J., LIEBENBERG, E. C. & LOTZ, J. C. 2014. Innervation of pathologies in the lumbar vertebral end plate and intervertebral disc. *Spine J,* 14**,** 513-21.

FIELDS, A. J., SAHLI, F., RODRIGUEZ, A. G. & LOTZ, J. C. 2012. Seeing double: a comparison of microstructure, biomechanical function, and adjacent disc health between double- and single-layer vertebral endplates. *Spine (Phila Pa 1976),* 37**,** E1310-7.

FROBIN, W., BRINCKMANN, P., LEIVSETH, G., BIGGEMANN, M. & REIKERAS, O. 1996. Precision measurement of segmental motion from flexion-extension radiographs of the lumbar spine. *Clin Biomech (Bristol, Avon),* 11**,** 457-465.

FROBIN, W., LEIVSETH, G., BIGGEMANN, M. & BRINCKMANN, P. 2002. Vertebral height, disc height, posteroanterior displacement and dens-atlas gap in the cervical spine:

precision measurement protocol and normal data. *Clin Biomech (Bristol, Avon),* 17**,** 423-31.

FUJIWARA, A., LIM, T. H., AN, H. S., TANAKA, N., JEON, C. H., ANDERSSON, G. B. & HAUGHTON, V. M. 2000. The effect of disc degeneration and facet joint osteoarthritis on the segmental flexibility of the lumbar spine. *Spine (Phila Pa 1976),* 25**,** 3036-44.

GERTZBEIN, S. D., SELIGMAN, J., HOLTBY, R., CHAN, K. H., KAPASOURI, A., TILE, M. & CRUICKSHANK, B. 1985. Centrode patterns and segmental instability in degenerative disc disease. *Spine (Phila Pa 1976),* 10**,** 257-61.

GOOYERS, C. E. & CALLAGHAN, J. P. 2015. Exploring interactions between force, repetition and posture on intervertebral disc height loss and bulging in isolated porcine cervical functional spinal units from sub-acute-failure magnitudes of cyclic compressive loading. *J Biomech,* 48**,** 3710-7.

GOTFRIED, Y., BRADFORD, D. S. & OEGEMA, T. R., JR. 1986. Facet joint changes after chemonucleolysis-induced disc space narrowing. *Spine (Phila Pa 1976),* 11**,** 944-50.

GREEN, T. P., ADAMS, M. A. & DOLAN, P. 1993. Tensile properties of the annulus fibrosus II. Ultimate tensile strength and fatigue life. *Eur Spine J,* 2**,** 209-14.

GREGORY, D. E. & CALLAGHAN, J. P. 2011. A comparison of uniaxial and biaxial mechanical properties of the annulus fibrosus: a porcine model. *J Biomech Eng,* 133**,** 024503.

GRUBER, H. E., INGRAM, J. A., HOELSCHER, G. L., ZINCHENKO, N., HANLEY, E. N., JR. & SUN, Y. 2009. Asporin, a susceptibility gene in osteoarthritis, is expressed at higher levels in the more degenerate human intervertebral disc. *Arthritis Res Ther,* 11**,** R47.

GU, W. Y., MAO, X. G., FOSTER, R. J., WEIDENBAUM, M., MOW, V. C. & RAWLINS, B. A. 1999. The anisotropic hydraulic permeability of human lumbar anulus fibrosus. Influence of age, degeneration, direction, and water content. *Spine (Phila Pa 1976),* 24**,** 2449-55.

GUERIN, H. A. & ELLIOTT, D. M. 2006. Degeneration affects the fiber reorientation of human annulus fibrosus under tensile load. *J Biomech,* 39**,** 1410-8.

GUERIN, H. L. & ELLIOTT, D. M. 2007. Quantifying the contributions of structure to annulus fibrosus mechanical function using a nonlinear, anisotropic, hyperelastic model. *J Orthop Res,* 25**,** 508-16.

HAGLUND, L., OUELLET, J. & ROUGHLEY, P. 2009. Variation in chondroadherin abundance and fragmentation in the human scoliotic disc. *Spine (Phila Pa 1976),* 34**,** 1513-8.

HANSSON, T. H., KELLER, T. S. & SPENGLER, D. M. 1987. Mechanical behavior of the human lumbar spine. II. Fatigue strength during dynamic compressive loading. *J Orthop Res,* 5**,** 479-87.

HASSLER, O. 1969. The human intervertebral disc. A micro-angiographical study on its vascular supply at various ages. *Acta Orthop Scand,* 40**,** 765-72.

HAUGHTON, V. 2011. The "dehydrated" lumbar intervertebral disk on MR, its anatomy, biochemistry and biomechanics. *Neuroradiology,* 53 Suppl 1**,** S191-4.

HAYASHI, T., DAUBS, M. D., SUZUKI, A., PHAN, K., SHIBA, K. & WANG, J. C. 2014. Effect of Modic changes on spinal canal stenosis and segmental motion in cervical spine. *Eur Spine J,* 23**,** 1737-42.

HEALEY, E. L., BURDEN, A. M., MCEWAN, I. M. & FOWLER, N. E. 2011. Diurnal variation in stature: do those with chronic low-back pain differ from asymptomatic controls? *Clin Biomech (Bristol, Avon),* 26**,** 331-6.

HOLM, S., EKSTROM, L., KAIGLE HOLM, A. & HANSSON, T. 2007. Intradiscal pressure in the degenerated porcine intervertebral disc. *Vet Comp Orthop Traumatol,* 20**,** 29-33.

HOLM, S., MAROUDAS, A., URBAN, J. P., SELSTAM, G. & NACHEMSON, A. 1981. Nutrition of the intervertebral disc: solute transport and metabolism. *Connect Tissue Res,* 8**,** 101-19.

HOLMES, A. D. & HUKINS, D. W. 1994. Fatigue failure at the disc-vertebra interface during cyclic axial compression of cadaveric specimens. *Clin Biomech (Bristol, Avon),* 9**,** 133-4.

HUKINS, D. W., ASPDEN, R. M. & YARKER, Y. E. 1984. Fibre reinforcement and mechanical stability in articular cartilage. *Eng Med,* 13**,** 153-6.

HUKINS, D. W. L. & MEAKIN, J. R. 2000. Relationship Between Structure and Mechanical Function of the Tissues of the Intervertebral Joint1. *American Zoologist,* 40**,** 42-52.

HUNTER, C. J., MATYAS, J. R. & DUNCAN, N. A. 2004. Cytomorphology of notochordal and chondrocytic cells from the nucleus pulposus: a species comparison. *J Anat,* 205**,** 357-62.

IATRIDIS, J. C., MACLEAN, J. J., O'BRIEN, M. & STOKES, I. A. 2007. Measurements of proteoglycan and water content distribution in human lumbar intervertebral discs. *Spine (Phila Pa 1976),* 32**,** 1493-7.

IATRIDIS, J. C., WEIDENBAUM, M., SETTON, L. A. & MOW, V. C. 1996. Is the nucleus pulposus a solid or a fluid? Mechanical behaviors of the nucleus pulposus of the human intervertebral disc. *Spine (Phila Pa 1976),* 21**,** 1174-84.

ILHARREBORDE, B., ZHAO, K., BOUMEDIENE, E., GAY, R., BERGLUND, L. & AN, K. N. 2010. A dynamic method for in vitro multisegment spine testing. *Orthop Traumatol Surg Res,* 96**,** 456-61.

INOUE, H. 1981. Three-dimensional architecture of lumbar intervertebral discs. *Spine (Phila Pa 1976),* 6**,** 139-46.

INOUE, H. & TAKEDA, T. 1975. Three-dimensional observation of collagen framework of lumbar intervertebral discs. *Acta Orthop Scand,* 46**,** 949-56.

JACKMAN, T. M., HUSSEIN, A. I., ADAMS, A. M., MAKHNEJIA, K. K. & MORGAN, E. F. 2014. Endplate deflection is a defining feature of vertebral fracture and is associated with properties of the underlying trabecular bone. *J Orthop Res,* 32**,** 880-6.

JARMAN, J. P., ARPINAR, V. E., BARUAH, D., KLEIN, A. P., MAIMAN, D. J. & TUGAN MUFTULER, L. 2015. Intervertebral disc height loss demonstrates the threshold of major pathological changes during degeneration. *Eur Spine J,* 24**,** 1944-50.

JAUMARD, N. V., UDUPA, J. K., WELCH, W. C. & WINKELSTEIN, B. A. 2014. Kinematic magnetic resonance imaging to define the cervical facet joint space for the spine in neutral and torsion. *Spine (Phila Pa 1976),* 39**,** 664-72.

JIANG, L., YUAN, F., YIN, X. & DONG, J. 2014. Responses and adaptations of intervertebral disc cells to microenvironmental stress: a possible central role of autophagy in the adaptive mechanism. *Connect Tissue Res,* 55**,** 311-21.

JOHNSON, E. F., CHETTY, K., MOORE, I. M., STEWART, A. & JONES, W. 1982. The distribution and arrangement of elastic fibres in the intervertebral disc of the adult human. *J Anat,* 135**,** 301-9.

JOHNSON, W. E., CATERSON, B., EISENSTEIN, S. M., HYNDS, D. L., SNOW, D. M. & ROBERTS, S. 2002. Human intervertebral disc aggrecan inhibits nerve growth in vitro. *Arthritis Rheum,* 46**,** 2658-64.

JOHNSON, W. E., CATERSON, B., EISENSTEIN, S. M. & ROBERTS, S. 2005. Human intervertebral disc aggrecan inhibits endothelial cell adhesion and cell migration in vitro. *Spine (Phila Pa 1976),* 30**,** 1139-47.

JOHNSTONE, B. & BAYLISS, M. T. 1995. The large proteoglycans of the human intervertebral disc. Changes in their biosynthesis and structure with age, topography, and pathology. *Spine (Phila Pa 1976),* 20**,** 674-84.

KANG, R., LI, H., RINGGAARD, S., RICKERS, K., SUN, H., CHEN, M., XIE, L. & BUNGER, C. 2014. Interference in the endplate nutritional pathway causes intervertebral disc degeneration in an immature porcine model. *Int Orthop,* 38**,** 1011-7.

KIANI, C., CHEN, L., WU, Y. J., YEE, A. J. & YANG, B. B. 2002. Structure and function of aggrecan. *Cell Res,* 12**,** 19-32.

KIM, Y. E., GOEL, V. K., WEINSTEIN, J. N. & LIM, T. H. 1991. Effect of disc degeneration at one level on the adjacent level in axial mode. *Spine (Phila Pa 1976),* 16**,** 331-5.

KIRKALDY-WILLIS, W. H. & FARFAN, H. F. 1982. Instability of the lumbar spine. *Clin Orthop Relat Res***,** 110-23.

KIRKALDY-WILLIS, W. H., WEDGE, J. H., YONG-HING, K. & REILLY, J. 1978. Pathology and pathogenesis of lumbar spondylosis and stenosis. *Spine (Phila Pa 1976),* 3**,** 319-28.

KIRSCH, T. & VON DER MARK, K. 1991. Ca2+ binding properties of type X collagen. *FEBS Lett,* 294**,** 149-52.

KITAMURA, K., HASEGAWA, H. & KANAI, H. 2012. Accurate Estimation of Carotid Luminal Surface Roughness Using Ultrasonic Radio-Frequency Echo. *Japanese Journal of Applied Physics,* 51**,** 07GF08.

KLARA, P. M. & RAY, C. D. 2002. Artificial nucleus replacement: clinical experience. *Spine (Phila Pa 1976),* 27**,** 1374-7.

KOELLER, W., MUEHLHAUS, S., MEIER, W. & HARTMANN, F. 1986. Biomechanical properties of human intervertebral discs subjected to axial dynamic compression—Influence of age and degeneration. *Journal of Biomechanics,* 19**,** 807-816.

KORECKI, C. L., KUO, C. K., TUAN, R. S. & IATRIDIS, J. C. 2009. Intervertebral disc cell response to dynamic compression is age and frequency dependent. *J Orthop Res,* 27**,** 800-6.

KORECKI, C. L., MACLEAN, J. J. & IATRIDIS, J. C. 2008. Dynamic compression effects on intervertebral disc mechanics and biology. *Spine (Phila Pa 1976),* 33**,** 1403-9.

LAMA, P., ZEHRA, U., BALKOVEC, C., CLAIREAUX, H. A., FLOWER, L., HARDING, I. J., DOLAN, P. & ADAMS, M. A. 2014. Significance of cartilage endplate within herniated disc tissue. *Eur Spine J,* 23**,** 1869-77.

LANDHAM, P. R., BAKER-RAND, H. L., GILBERT, S. J., POLLINTINE, P., ANNESLEY-WILLIAMS, D. J., ADAMS, M. A. & DOLAN, P. 2015a. Is kyphoplasty better than

vertebroplasty at restoring form and function after severe vertebral wedge fractures? *Spine J,* 15**,** 721-32.

LANDHAM, P. R., GILBERT, S. J., BAKER-RAND, H. L., POLLINTINE, P., ROBSON BROWN, K. A., ADAMS, M. A. & DOLAN, P. 2015b. Pathogenesis of Vertebral Anterior Wedge Deformity: A 2-Stage Process? *Spine (Phila Pa 1976),* 40**,** 902-8.

LANSADE, C., LAPORTE, S., THOREUX, P., ROUSSEAU, M. A., SKALLI, W. & LAVASTE, F. 2009. Three-dimensional analysis of the cervical spine kinematics: effect of age and gender in healthy subjects. *Spine (Phila Pa 1976),* 34**,** 2900-6.

LAO, L., DAUBS, M. D., SCOTT, T. P., LORD, E. L., COHEN, J. R., YIN, R., ZHONG, G. & WANG, J. C. 2015a. Effect of disc degeneration on lumbar segmental mobility analyzed by kinetic magnetic resonance imaging. *Spine (Phila Pa 1976),* 40**,** 316-22.

LAO, L., DAUBS, M. D., TAKAHASHI, S., LORD, E. L., COHEN, J. R., ZHONG, G. & WANG, J. C. 2015b. Kinetic magnetic resonance imaging analysis of lumbar segmental motion at levels adjacent to disc herniation. *Eur Spine J*.

LATHAM, J. M., PEARCY, M. J., COSTI, J. J., MOORE, R., FRASER, R. D. & VERNON-ROBERTS, B. 1994. Mechanical consequences of annular tears and subsequent intervertebral disc degeneration. *Clin Biomech (Bristol, Avon),* 9**,** 211-9.

LEE, S. H., DAFFNER, S. D. & WANG, J. C. 2014. Does lumbar disk degeneration increase segmental mobility in vivo? Segmental motion analysis of the whole lumbar spine using kinetic MRI. *J Spinal Disord Tech,* 27**,** 111-6.

LEE, S. H., DAFFNER, S. D., WANG, J. C., DAVIS, B. C., ALANAY, A. & KIM, J. S. 2015. The change of whole lumbar segmental motion according to the mobility of degenerated disc in the lower lumbar spine: a kinetic MRI study. *Eur Spine J,* 24**,** 1893-900.

LIU, J. T., LI, C. S., CHANG, C. S. & LIAO, W. J. 2015. Long-term follow-up study of osteoporotic vertebral compression fracture treated using balloon kyphoplasty and vertebroplasty. *J Neurosurg Spine,* 23**,** 94-8.

LOTZ, J. C. & CHIN, J. R. 2000. Intervertebral Disc Cell Death Is Dependent on the Magnitude and Duration of Spinal Loading. *Spine,* 25**,** 1477-1483.

LOTZ, J. C., COLLIOU, O. K., CHIN, J. R., DUNCAN, N. A. & LIEBENBERG, E. 1998. Compression-induced degeneration of the intervertebral disc: an in vivo mouse model and finite-element study. *Spine (Phila Pa 1976),* 23**,** 2493-506.

LUO, J., ADAMS, M. A. & DOLAN, P. 2010. Vertebroplasty and Kyphoplasty Can Restore Normal Spine Mechanics following Osteoporotic Vertebral Fracture. *J Osteoporos,* 2010**,** 729257.

LUO, J., DAINES, L., CHARALAMBOUS, A., ADAMS, M. A., ANNESLEY-WILLIAMS, D. J. & DOLAN, P. 2009. Vertebroplasty: only small cement volumes are required to normalize stress distributions on the vertebral bodies. *Spine (Phila Pa 1976),* 34**,** 2865-73.

LUO, J., POLLINTINE, P., ANNESLEY-WILLIAMS, D. J., DOLAN, P. & ADAMS, M. A. 2015. Vertebroplasty reduces progressive creep' deformity of fractured vertebrae. *J Biomech*.

LUO, J., SKRZYPIEC, D. M., POLLINTINE, P., ADAMS, M. A., ANNESLEY-WILLIAMS, D. J. & DOLAN, P. 2007. Mechanical efficacy of vertebroplasty: influence of cement type, BMD, fracture severity, and disc degeneration. *Bone,* 40**,** 1110-9.

LYSACK, J. T., DICKEY, J. P., DUMAS, G. A. & YEN, D. 2000. A continuous pure moment loading apparatus for biomechanical testing of multi-segment spine specimens. *J Biomech,* 33**,** 765-70.

MALAKOUTIAN, M., VOLKHEIMER, D., STREET, J., DVORAK, M. F., WILKE, H. J. & OXLAND, T. R. 2015. Do in vivo kinematic studies provide insight into adjacent segment degeneration? A qualitative systematic literature review. *Eur Spine J,* 24**,** 1865-81.

MARCHAND, F. & AHMED, A. M. 1990. Investigation of the laminate structure of lumbar disc anulus fibrosus. *Spine (Phila Pa 1976),* 15**,** 402-10.

MARSHALL, L. W. & MCGILL, S. M. 2010. The role of axial torque in disc herniation. *Clin Biomech (Bristol, Avon),* 25**,** 6-9.

MCGILL, S. 2007. *Low back disorders: Evidence-based prevention and rehabilitation,* Champaign, IL, Human Kinetics.

MEAKIN, J. R., REDPATH, T. W. & HUKINS, D. W. 2001. The effect of partial removal of the nucleus pulposus from the intervertebral disc on the response of the human annulus fibrosus to compression. *Clin Biomech (Bristol, Avon),* 16**,** 121-8.

MELROSE, J. & ROUGHLEY, P. 2014. Proteoglycans of the Intervertebral Disc. *In:* SHAPIRO, I. M. & RISBUD, M. V. (eds.) *The Intervertebral Disc.* Wien, Austria: Springer.

MERCER, S. & BOGDUK, N. 1999. The ligaments and annulus fibrosus of human adult cervical intervertebral discs. *Spine (Phila Pa 1976),* 24**,** 619-26; discussion 627-8.

MERCERON, C., MANGIAVINI, L., ROBLING, A., WILSON, T. L., GIACCIA, A. J., SHAPIRO, I. M., SCHIPANI, E. & RISBUD, M. V. 2014. Loss of HIF-1alpha in the notochord results in cell death and complete disappearance of the nucleus pulposus. *PLoS One,* 9**,** e110768.

MORGAN, W. E. 2013. *The Lumbar MRI in Clinical Practice*, Health Path Education.

MUGGLETON, J. M. & ALLEN, R. 1997. Automatic location of vertebrae in digitized videofluoroscopic images of the lumbar spine. *Med Eng Phys,* 19**,** 77-89.

MURAKAMI, H., YOON, T. S., ATTALLAH-WASIF, E. S., KRAIWATTANAPONG, C., KIKKAWA, I. & HUTTON, W. C. 2010. Quantitative differences in intervertebral disc-matrix composition with age-related degeneration. *Med Biol Eng Comput,* 48**,** 469-74.

NACHEMSON, A. L. 1981. Disc pressure measurements. *Spine (Phila Pa 1976),* 6**,** 93-7.

NATARAJAN, R. N., ANDERSSON, G. B., PATWARDHAN, A. G. & VERMA, S. 2002. Effect of annular incision type on the change in biomechanical properties in a herniated lumbar intervertebral disc. *J Biomech Eng,* 124**,** 229-36.

NEAME, P. J. & BARRY, F. P. 1993. The link proteins. *Experientia,* 49**,** 393-402.

NERLICH, A. G., BOOS, N., WIEST, I. & AEBI, M. 1998. Immunolocalization of major interstitial collagen types in human lumbar intervertebral discs of various ages. *Virchows Arch,* 432**,** 67-76.

NERLICH, A. G., SCHLEICHER, E. D. & BOOS, N. 1997. 1997 Volvo Award winner in basic science studies. Immunohistologic markers for age-related changes of human lumbar intervertebral discs. *Spine (Phila Pa 1976),* 22**,** 2781-95.

NOSIKOVA, Y. S., SANTERRE, J. P., GRYNPAS, M., GIBSON, G. & KANDEL, R. A. 2012. Characterization of the annulus fibrosus-vertebral body interface: identification of new structural features. *J Anat,* 221**,** 577-89.

NOWITZKE, A., WESTAWAY, M. & BOGDUK, N. 1994. Cervical zygapophyseal joints: geometrical parameters and relationship to cervical kinematics. *Clin Biomech (Bristol, Avon),* 9**,** 342-8.

OEGEMA, T. R., JR., BRADFORD, D. S. & COOPER, K. M. 1979. Aggregated proteoglycan synthesis in organ cultures of human nucleus pulposus. *J Biol Chem,* 254**,** 10579-81.

PALLAN, A., KINGSNORTH, A. & BOWLEY, D. 2011. *Fundamentals of Surgical Practice*, Cambridge University Press.

PANJABI, M., BROWN, M., LINDAHL, S., IRSTAM, L. & HERMENS, M. 1988. Intrinsic disc pressure as a measure of integrity of the lumbar spine. *Spine (Phila Pa 1976),* 13**,** 913-7.

PANJABI, M. M., DURANCEAU, J. S., OXLAND, T. R. & BOWEN, C. E. 1989. Multidirectional instabilities of traumatic cervical spine injuries in a porcine model. *Spine (Phila Pa 1976),* 14**,** 1111-5.

PARK, C. K., RYU, K. S., LEE, K. Y. & LEE, H. J. 2012. Clinical outcome of lumbar total disc replacement using ProDisc-L in degenerative disc disease: minimum 5-year follow-up results at a single institute. *Spine (Phila Pa 1976),* 37**,** 672-7.

PARK, W. M., KIM, K. & KIM, Y. H. 2013. Effects of degenerated intervertebral discs on intersegmental rotations, intradiscal pressures, and facet joint forces of the whole lumbar spine. *Comput Biol Med,* 43**,** 1234-40.

PARKINSON, R. J. & CALLAGHAN, J. P. 2007. Can periods of static loading be used to enhance the resistance of the spine to cumulative compression? *J Biomech,* 40**,** 2944-52.

PARKINSON, R. J. & CALLAGHAN, J. P. 2009. The role of dynamic flexion in spine injury is altered by increasing dynamic load magnitude. *Clin Biomech (Bristol, Avon),* 24**,** 148-54.

PARKINSON, R. J., DURKIN, J. L. & CALLAGHAN, J. P. 2005. Estimating the compressive strength of the porcine cervical spine: an examination of the utility of DXA. *Spine (Phila Pa 1976),* 30**,** E492-8.

PATWARDHAN, A. G., HAVEY, R. M., GHANAYEM, A. J., DIENER, H., MEADE, K. P., DUNLAP, B. & HODGES, S. D. 2000. Load-Carrying Capacity of the Human Cervical Spine in Compression Is Increased Under a Follower Load. *Spine,* 25**,** 1548-1554.

PEACOCK, A. 1952. Observations on the postnatal structure of the intervertebral disc in man. *J Anat,* 86**,** 162-79.

PEZOWICZ, C. A., ROBERTSON, P. A. & BROOM, N. D. 2006. The structural basis of interlamellar cohesion in the intervertebral disc wall. *J Anat,* 208**,** 317-30.

PFIRRMANN, C. W., METZDORF, A., ZANETTI, M., HODLER, J. & BOOS, N. 2001. Magnetic resonance classification of lumbar intervertebral disc degeneration. *Spine (Phila Pa 1976),* 26**,** 1873-8.

POKHARNA, H. K. & PHILLIPS, F. M. 1998. Collagen crosslinks in human lumbar intervertebral disc aging. *Spine (Phila Pa 1976),* 23**,** 1645-8.

POLLINTINE, P., DOLAN, P., TOBIAS, J. H. & ADAMS, M. A. 2004a. Intervertebral disc degeneration can lead to "stress-shielding" of the anterior vertebral body: a cause of osteoporotic vertebral fracture? *Spine (Phila Pa 1976),* 29**,** 774-82.

POLLINTINE, P., PRZYBYLA, A. S., DOLAN, P. & ADAMS, M. A. 2004b. Neural arch load-bearing in old and degenerated spines. *J Biomech,* 37**,** 197-204.

PRZYBYLA, A., POLLINTINE, P., BEDZINSKI, R. & ADAMS, M. A. 2006. Outer annulus tears have less effect than endplate fracture on stress distributions inside intervertebral discs: relevance to disc degeneration. *Clin Biomech (Bristol, Avon),* 21**,** 1013-9.

RAJASEKARAN, S., BAJAJ, N., TUBAKI, V., KANNA, R. M. & SHETTY, A. P. 2013. ISSLS Prize winner: The anatomy of failure in lumbar disc herniation: an in vivo, multimodal, prospective study of 181 subjects. *Spine (Phila Pa 1976),* 38**,** 1491-500.

RAY, C. D. 2002. The PDN prosthetic disc-nucleus device. *Eur Spine J,* 11 Suppl 2**,** S137-42.

REPANTI, M., KOROVESSIS, P. G., STAMATAKIS, M. V., SPASTRIS, P. & KOSTI, P. 1998. Evolution of disc degeneration in lumbar spine: a comparative histological study between herniated and postmortem retrieved disc specimens. *J Spinal Disord,* 11**,** 41-5.

REUBER, M., SCHULTZ, A., DENIS, F. & SPENCER, D. 1982. Bulging of lumbar intervertebral disks. *J Biomech Eng,* 104**,** 187-92.

RICHARDSON, S. M., PURMESSUR, D., BAIRD, P., PROBYN, B., FREEMONT, A. J. & HOYLAND, J. A. 2012. Degenerate human nucleus pulposus cells promote neurite outgrowth in neural cells. *PLoS One,* 7**,** e47735.

RIESENBURGER, R. I., SAFAIN, M. G., OGBUJI, R., HAYES, J. & HWANG, S. W. 2015. A novel classification system of lumbar disc degeneration. *J Clin Neurosci,* 22**,** 346-51.

RISBUD, M. V. & SHAPIRO, I. M. 2014. Role of cytokines in intervertebral disc degeneration: pain and disc content. *Nat Rev Rheumatol,* 10**,** 44-56.

ROBERTS, S., AYAD, S. & MENAGE, P. J. 1991a. Immunolocalisation of type VI collagen in the intervertebral disc. *Ann Rheum Dis,* 50**,** 787-91.

ROBERTS, S., MENAGE, J., DUANCE, V., WOTTON, S. & AYAD, S. 1991b. 1991 Volvo Award in basic sciences. Collagen types around the cells of the intervertebral disc and cartilage end plate: an immunolocalization study. *Spine (Phila Pa 1976),* 16**,** 1030-8.

ROBERTS, S., MENAGE, J. & URBAN, J. P. 1989. Biochemical and structural properties of the cartilage end-plate and its relation to the intervertebral disc. *Spine (Phila Pa 1976),* 14**,** 166-74.

ROBERTS, S., URBAN, J. P., EVANS, H. & EISENSTEIN, S. M. 1996. Transport properties of the human cartilage endplate in relation to its composition and calcification. *Spine (Phila Pa 1976),* 21**,** 415-20.

RODRIGUEZ, A. G., RODRIGUEZ-SOTO, A. E., BURGHARDT, A. J., BERVEN, S., MAJUMDAR, S. & LOTZ, J. C. 2012. Morphology of the human vertebral endplate. *J Orthop Res,* 30**,** 280-7.

RODRIGUEZ, A. G., SLICHTER, C. K., ACOSTA, F. L., RODRIGUEZ-SOTO, A. E., BURGHARDT, A. J., MAJUMDAR, S. & LOTZ, J. C. 2011. Human disc nucleus properties and vertebral endplate permeability. *Spine (Phila Pa 1976),* 36**,** 512-20.

ROUGHLEY, P. J. 2004. Biology of intervertebral disc aging and degeneration: involvement of the extracellular matrix. *Spine (Phila Pa 1976),* 29**,** 2691-9.

RUBERTE, L. M., NATARAJAN, R. N. & ANDERSSON, G. B. 2009. Influence of single-level lumbar degenerative disc disease on the behavior of the adjacent segments--a finite element model study. *J Biomech,* 42**,** 341-8.

RUDERT, M. & TILLMANN, B. 1993. Lymph and blood supply of the human intervertebral disc. Cadaver study of correlations to discitis. *Acta Orthop Scand,* 64**,** 37-40.

SCANNELL, J. P. & MCGILL, S. M. 2009. Disc prolapse: evidence of reversal with repeated extension. *Spine (Phila Pa 1976),* 34**,** 344-50.

SCHOLLMEIER, G., LAHR-EIGEN, R. & LEWANDROWSKI, K. U. 2000. Observations on fiber-forming collagens in the anulus fibrosus. *Spine (Phila Pa 1976),* 25**,** 2736-41.

SHAPIRO, I. M. & RISBUD, M. V. 2014. Introduction to the Structure, Function, and Comparative Anatomy of the Vertebrae and the Intervertebral Disc. *In:* SHAPIRO, I. M. R., M. V. (ed.) *The Intervertebral Disc.* Wien, Austria: Springer.

SHARMA, A., LANCASTER, S., BAGADE, S. & HILDEBOLT, C. 2014. Early pattern of degenerative changes in individual components of intervertebral discs in stressed and nonstressed segments of lumbar spine: an in vivo magnetic resonance imaging study. *Spine (Phila Pa 1976),* 39**,** 1084-90.

SHIM, C. S., LEE, S. H., SHIN, H. D., KANG, H. S., CHOI, W. C., JUNG, B., CHOI, G., AHN, Y., LEE, S. & LEE, H. Y. 2007. CHARITE versus ProDisc: a comparative study of a minimum 3-year follow-up. *Spine (Phila Pa 1976),* 32**,** 1012-8.

SHINE, K. M., SIMSON, J. A. & SPECTOR, M. 2009. Lubricin distribution in the human intervertebral disc. *J Bone Joint Surg Am,* 91**,** 2205-12.

SILVA-CORREIA, J., MIRANDA-GONCALVES, V., SALGADO, A. J., SOUSA, N., OLIVEIRA, J. M., REIS, R. M. & REIS, R. L. 2012. Angiogenic potential of gellan-gum-based hydrogels for application in nucleus pulposus regeneration: in vivo study. *Tissue Eng Part A,* 18**,** 1203-12.

SILVA-CORREIA, J., OLIVEIRA, J. M., CARIDADE, S. G., OLIVEIRA, J. T., SOUSA, R. A., MANO, J. F. & REIS, R. L. 2011. Gellan gum-based hydrogels for intervertebral disc tissue-engineering applications. *J Tissue Eng Regen Med,* 5**,** e97-107.

SINGH, K., MASUDA, K., THONAR, E. J., AN, H. S. & CS-SZABO, G. 2009. Age-related changes in the extracellular matrix of nucleus pulposus and anulus fibrosus of human intervertebral disc. *Spine (Phila Pa 1976),* 34**,** 10-6.

SMITH, L. J. & FAZZALARI, N. L. 2009. The elastic fibre network of the human lumbar anulus fibrosus: architecture, mechanical function and potential role in the progression of intervertebral disc degeneration. *Eur Spine J,* 18**,** 439-48.

SMITH, S. M., WHITELOCK, J. M., IOZZO, R. V., LITTLE, C. B. & MELROSE, J. 2009. Topographical variation in the distributions of versican, aggrecan and perlecan in the foetal human spine reflects their diverse functional roles in spinal development. *Histochem Cell Biol,* 132**,** 491-503.

STEFANAKIS, M., AL-ABBASI, M., HARDING, I., POLLINTINE, P., DOLAN, P., TARLTON, J. & ADAMS, M. A. 2012. Annulus fissures are mechanically and chemically conducive to the ingrowth of nerves and blood vessels. *Spine (Phila Pa 1976),* 37**,** 1883-91.

STEFANAKIS, M., LUO, J., POLLINTINE, P., DOLAN, P. & ADAMS, M. A. 2014. ISSLS Prize winner: Mechanical influences in progressive intervertebral disc degeneration. *Spine (Phila Pa 1976),* 39**,** 1365-72.

STOKES, I. A. & IATRIDIS, J. C. 2004. Mechanical conditions that accelerate intervertebral disc degeneration: overload versus immobilization. *Spine (Phila Pa 1976),* 29**,** 2724-32.

SZTROLOVICS, R., ALINI, M., MORT, J. S. & ROUGHLEY, P. J. 1999. Age-related changes in fibromodulin and lumican in human intervertebral discs. *Spine (Phila Pa 1976),* 24**,** 1765-71.

SZTROLOVICS, R., ALINI, M., ROUGHLEY, P. J. & MORT, J. S. 1997. Aggrecan degradation in human intervertebral disc and articular cartilage. *Biochem J,* 326 (Pt 1)**,** 235-41.

SZTROLOVICS, R., GROVER, J., CS-SZABO, G., SHI, S. L., ZHANG, Y., MORT, J. S. & ROUGHLEY, P. J. 2002. The characterization of versican and its message in human articular cartilage and intervertebral disc. *J Orthop Res,* 20**,** 257-66.

TAMPIER, C., DRAKE, J. D., CALLAGHAN, J. P. & MCGILL, S. M. 2007. Progressive disc herniation: an investigation of the mechanism using radiologic, histochemical, and microscopic dissection techniques on a porcine model. *Spine (Phila Pa 1976),* 32**,** 2869-74.

TANAKA, N., AN, H. S., LIM, T. H., FUJIWARA, A., JEON, C. H. & HAUGHTON, V. M. 2001. The relationship between disc degeneration and flexibility of the lumbar spine. *Spine J,* 1**,** 47-56.

TANG, S. & REBHOLZ, B. J. 2012. Does lumbar microdiscectomy affect adjacent segmental disc degeneration? A finite element study. *J Surg Res,* 28**,** 00815-3.

TCHAKO, A. & SADEGH, A. M. 2009. Stress changes in intervertebral discs of the cervical spine due to partial discectomies and fusion. *J Biomech Eng,* 131**,** 051013.

THOMPSON, J. P., PEARCE, R. H., SCHECHTER, M. T., ADAMS, M. E., TSANG, I. K. & BISHOP, P. B. 1990. Preliminary evaluation of a scheme for grading the gross morphology of the human intervertebral disc. *Spine (Phila Pa 1976),* 15**,** 411-5.

THOMPSON, R. E., PEARCY, M. J. & BARKER, T. M. 2004. The mechanical effects of intervertebral disc lesions. *Clin Biomech (Bristol, Avon),* 19**,** 448-55.

TROUT, J. J., BUCKWALTER, J. A. & MOORE, K. C. 1982. Ultrastructure of the human intervertebral disc: II. Cells of the nucleus pulposus. *Anat Rec,* 204**,** 307-14.

TZERMIADIANOS, M. N., RENNER, S. M., PHILLIPS, F. M., HADJIPAVLOU, A. G., ZINDRICK, M. R., HAVEY, R. M., VORONOV, M. & PATWARDHAN, A. G. 2008. Altered disc pressure profile after an osteoporotic vertebral fracture is a risk factor for adjacent vertebral body fracture. *Eur Spine J,* 17**,** 1522-30.

URBAN, J. P., HOLM, S., MAROUDAS, A. & NACHEMSON, A. 1977. Nutrition of the intervertebral disk. An in vivo study of solute transport. *Clin Orthop Relat Res***,** 101-14.

URBAN, J. P. & MAROUDAS, A. 1981. Swelling of the intervertebral disc in vitro. *Connect Tissue Res,* 9**,** 1-10.

URBAN, J. P., MAROUDAS, A., BAYLISS, M. T. & DILLON, J. 1979. Swelling pressures of proteoglycans at the concentrations found in cartilaginous tissues. *Biorheology,* 16**,** 447-64.

URBAN, J. P. & MCMULLIN, J. F. 1988. Swelling pressure of the lumbar intervertebral discs: influence of age, spinal level, composition, and degeneration. *Spine (Phila Pa 1976),* 13**,** 179-87.

URBAN, J. P., SMITH, S. & FAIRBANK, J. C. 2004. Nutrition of the intervertebral disc. *Spine (Phila Pa 1976),* 29**,** 2700-9.

URBAN, J. P. G., ROBERTS, S. & RALPHS, J. R. 2000. The Nucleus of the Intervertebral Disc from Development to Degeneration1. *American Zoologist,* 40**,** 53-61.

VAN DEN BROEK, P. R., HUYGHE, J. M., WILSON, W. & ITO, K. 2012. Design of next generation total disk replacements. *J Biomech,* 45**,** 134-40.

VAN DER REST, M. & MAYNE, R. 1988. Type IX collagen proteoglycan from cartilage is covalently cross-linked to type II collagen. *J Biol Chem,* 263**,** 1615-8.

VAN MAMEREN, H. 1988. Motion patterns in the cervical spine (Ph. D. Thesis). *Maastricht, The Netherlands: University of Limburg,* 150.

VAN MAMEREN, H., DRUKKER, J., SANCHES, H. & BEURSGENS, J. 1990. Cervical spine motion in the sagittal plane (I) range of motion of actually performed movements, an X-ray cinematographic study. *Eur J Morphol,* 28**,** 47-68.

VELDHUIS, J. H., BRODLAND, G. W., WIEBE, C. J. & BOOTSMA, G. J. 2005. Multiview robotic microscope reveals the in-plane kinematics of amphibian neurulation. *Ann Biomed Eng,* 33**,** 821-8.

VELDUIS, J. H. & BRODLAND, G. W. 1999. A deformable block-matching algorithm for tracking epithelial cells. *Image and Vision Computing,* 17**,** 905-911.

VERNENGO, J., FUSSELL, G. W., SMITH, N. G. & LOWMAN, A. M. 2008. Evaluation of novel injectable hydrogels for nucleus pulposus replacement. *J Biomed Mater Res B Appl Biomater,* 84**,** 64-9.

VIDEMAN, T., BATTIE, M. C., GILL, K., MANNINEN, H., GIBBONS, L. E. & FISHER, L. D. 1995. Magnetic resonance imaging findings and their relationships in the thoracic and lumbar spine. Insights into the etiopathogenesis of spinal degeneration. *Spine (Phila Pa 1976),* 20**,** 928-35.

WADE, K. R., ROBERTSON, P. A. & BROOM, N. D. 2011. A fresh look at the nucleus-endplate region: new evidence for significant structural integration. *Eur Spine J,* 20**,** 1225-32.

WADE, K. R., ROBERTSON, P. A. & BROOM, N. D. 2012. On the extent and nature of nucleus-annulus integration. *Spine (Phila Pa 1976),* 37**,** 1826-33.

WALLACE, W. A. & JOHNSON, F. 1981. Detection and correction of geometrical distortion in x-ray fluoroscopic images. *J Biomech,* 14**,** 123-5.

WALMSLEY, R. 1953. The development and growth of the intervertebral disc. *Edinb Med J,* 60**,** 341-64.

WALSH, A. J. & LOTZ, J. C. 2004. Biological response of the intervertebral disc to dynamic loading. *J Biomech,* 37**,** 329-37.

WALTER, B. A., KORECKI, C. L., PURMESSUR, D., ROUGHLEY, P. J., MICHALEK, A. J. & IATRIDIS, J. C. 2011. Complex loading affects intervertebral disc mechanics and biology. *Osteoarthritis Cartilage,* 19**,** 1011-8.

WANG, J., MARKOVA, D., ANDERSON, D. G., ZHENG, Z., SHAPIRO, I. M. & RISBUD, M. V. 2011. TNF-alpha and IL-1beta promote a disintegrin-like and metalloprotease with thrombospondin type I motif-5-mediated aggrecan degradation through syndecan-4 in intervertebral disc. *J Biol Chem,* 286**,** 39738-49.

WATANABE, H., CHEUNG, S. C., ITANO, N., KIMATA, K. & YAMADA, Y. 1997. Identification of hyaluronan-binding domains of aggrecan. *J Biol Chem,* 272**,** 28057-65.

WIEBE, C. & BRODLAND, G. W. 2005. Tensile properties of embryonic epithelia measured using a novel instrument. *J Biomech,* 38**,** 2087-94.

WILKE, H. J., NEEF, P., CAIMI, M., HOOGLAND, T. & CLAES, L. E. 1999. New in vivo measurements of pressures in the intervertebral disc in daily life. *Spine (Phila Pa 1976),* 24**,** 755-62.

WILLBURGER, R. E., EHIOSUN, U. K., KUHNEN, C., KRÄMER, J. & SCHMID, G. 2004. Clinical Symptoms in Lumbar Disc Herniations and Their Correlation to the Histological Composition of the Extruded Disc Material. *Spine,* 29**,** 1655-1661.

WONG, A., DUNK, N. M. & CALLAGHAN, J. P. 2009. A systematic approach to feature tracking of lumbar spine vertebrae from fluoroscopic images using complex-valued wavelets. *Comput Methods Biomech Biomed Engin,* 12**,** 607-16.

WONG, J. J., COTE, P., QUESNELE, J. J., STERN, P. J. & MIOR, S. A. 2014. The course and prognostic factors of symptomatic cervical disc herniation with radiculopathy: a systematic review of the literature. *Spine J,* 14**,** 1781-9.

WONG, K. W., LUK, K. D., LEONG, J. C., WONG, S. F. & WONG, K. K. 2006. Continuous dynamic spinal motion analysis. *Spine (Phila Pa 1976),* 31**,** 414-9.

XU, H. G., YU, Y. F., ZHENG, Q., ZHANG, W., WANG, C. D., ZHAO, X. Y., TONG, W. X., WANG, H., LIU, P. & ZHANG, X. L. 2014. Autophagy protects end plate chondrocytes from intermittent cyclic mechanical tension induced calcification. *Bone,* 66**,** 232-9.

YATES, J. P., GIANGREGORIO, L. & MCGILL, S. M. 2010. The influence of intervertebral disc shape on the pathway of posterior/posterolateral partial herniation. *Spine (Phila Pa 1976),* 35**,** 734-9.

YIN, R., LORD, E. L., COHEN, J. R., BUSER, Z., LAO, L., ZHONG, G. & WANG, J. C. 2015. Distribution of Schmorl nodes in the lumbar spine and their relationship with lumbar disk degeneration and range of motion. *Spine (Phila Pa 1976),* 40**,** E49-53.

YINGLING, V. R., CALLAGHAN, J. P. & MCGILL, S. M. 1997. Dynamic loading affects the mechanical properties and failure site of porcine spines. *Clin Biomech (Bristol, Avon),* 12**,** 301-305.

YINGLING, V. R., CALLAGHAN, J. P. & MCGILL, S. M. 1999. The porcine cervical spine as a model of the human lumbar spine: an anatomical, geometric, and functional comparison. *J Spinal Disord,* 12**,** 415-23.

YINGLING, V. R. & MCGILL, S. M. 1999. Anterior shear of spinal motion segments. Kinematics, kinetics, and resultant injuries observed in a porcine model. *Spine (Phila Pa 1976),* 24**,** 1882-9.

YU, J., TIRLAPUR, U., FAIRBANK, J., HANDFORD, P., ROBERTS, S., WINLOVE, C. P., CUI, Z. & URBAN, J. 2007. Microfibrils, elastin fibres and collagen fibres in the human intervertebral disc and bovine tail disc. *J Anat,* 210**,** 460-71.

ZHAO, F., POLLINTINE, P., HOLE, B. D., DOLAN, P. & ADAMS, M. A. 2005. Discogenic origins of spinal instability. *Spine (Phila Pa 1976),* 30**,** 2621-30.

ZHAO, F. D., POLLINTINE, P., HOLE, B. D., ADAMS, M. A. & DOLAN, P. 2009. Vertebral fractures usually affect the cranial endplate because it is thinner and supported by less-dense trabecular bone. *Bone,* 44**,** 372-9.

ZHAO, H., NI, C. F., HUANG, J., ZHAO, S. M., GU, W. W., JIANG, H., CHEN, L. & TAN, T. S. 2014. Effects of bone cement on intervertebral disc degeneration. *Exp Ther Med,* 7**,** 963-969.

ZHENG, Y., NIXON, M. S. & ALLEN, R. 2004. Automated segmentation of lumbar vertebrae in digital videofluoroscopic images. *IEEE Trans Med Imaging,* 23**,** 45-52.

Appendix A

Development of a novel tracking algorithm for measuring spine segmental motion under fluoroscopic imaging

9.1 Background

Measurement of vertebral body motion for the purpose of obtaining spine segmental angles is a difficult endeavor in that the spine is not easily accessible via conventional instrumentation. Gross displacements of the spine can be obtained through various strategies using skin surface techniques, but offer no information with respect to movements at a single vertebral level. X-ray techniques offer a method to examine individual vertebrae, but expose an individual to a high amount of ionizing radiation and only offer insight into static postures, neglecting any movement. Fluoroscopic imaging offers real-time monitoring of vertebral motion and the potential to identify aberrant movement. Biomechanically, the ability to monitor and quantify spine motion during active dynamic tasks represents a powerful tool with respect to understanding individual movement strategies. This can offer insight into why some individuals become injured while others do not, and how pathology changes the way people move. Quantifying vertebral motion with high precision represents an attractive means to establish dysfunction when a particular pathology presents with aberrant movement.

There are a number of manual (Cholewicki et al., 1991, Breen et al., 1989) and semi-automated (Bifulco et al., 2001, Wong et al., 2009, Wong et al., 2006, Breen et al., 2012, Zheng et al., 2004) methods to tracking the spine under fluoroscopy. Tracking methods which utilize rigid templates are excellent at identifying the shape of the vertebral body and tracking it through time. Any inherent noise in a rigid template however, will affect all of the tracked points

and result in a larger magnitude of error compared to random noise from the movement of free points that can be removed using digital filtering techniques. Feature-point tracking (Wong et al., 2009) has also been employed with the benefit of using independently moving points, and currently represents one of the most accurate ways to track a spine under fluoroscopy. Finally, manual methods (Cholewicki et al., 1991, Breen et al., 1989) have been used but are not practical for processing large sets of data.

Initial tracking of the fluoroscopic images presents the most difficult hurdle in extracting angular displacement data of segmental sagittal plane movement of the spine. Building upon previously developed techniques has the potential to further improve the fidelity of spine segment motion tracking.

9.2 Significance

Developing a novel technique for quantifying spine motion under fluoroscopic imaging will help to add further advancement to an area that has been largely under-researched. Continually striving to identify new methods of tracking vertebral motion will only serve to add impetus in bringing more research interest to this area. The development of this technique will allow segmental spine motion to be quantified in order to gain meaningful insight into how disc height loss affects spine kinematics *in-vivo*. A major challenge lay in the need to quantify individual segmental motion.

9.3 Methods

9.3.1 Tracking Algorithm

The tracking algorithm used for the purposes of tracking vertebral bodies under fluoroscopic imaging was based on an established image registration technique (Velduis and

Brodland, 1999). The underlying principles of the technique use a traditional normalized cross-correlation with the added feature of being able to account for deformation of an image template. In its simplest terms, a block of pixels is selected manually; a normalized cross-correlation function will then take a second image, and starting at the location in the previous region, begin to compare blocks of pixels within a pre-defined search region. Each iteration creates a correlation value, the region with the highest correlation is selected as the best match, and the location of the original block of pixels will be applied to this region. The following set of figures are based off of the original figures from (Velduis and Brodland, 1999) and are used to explain the functionality of the normalized cross-correlation function.

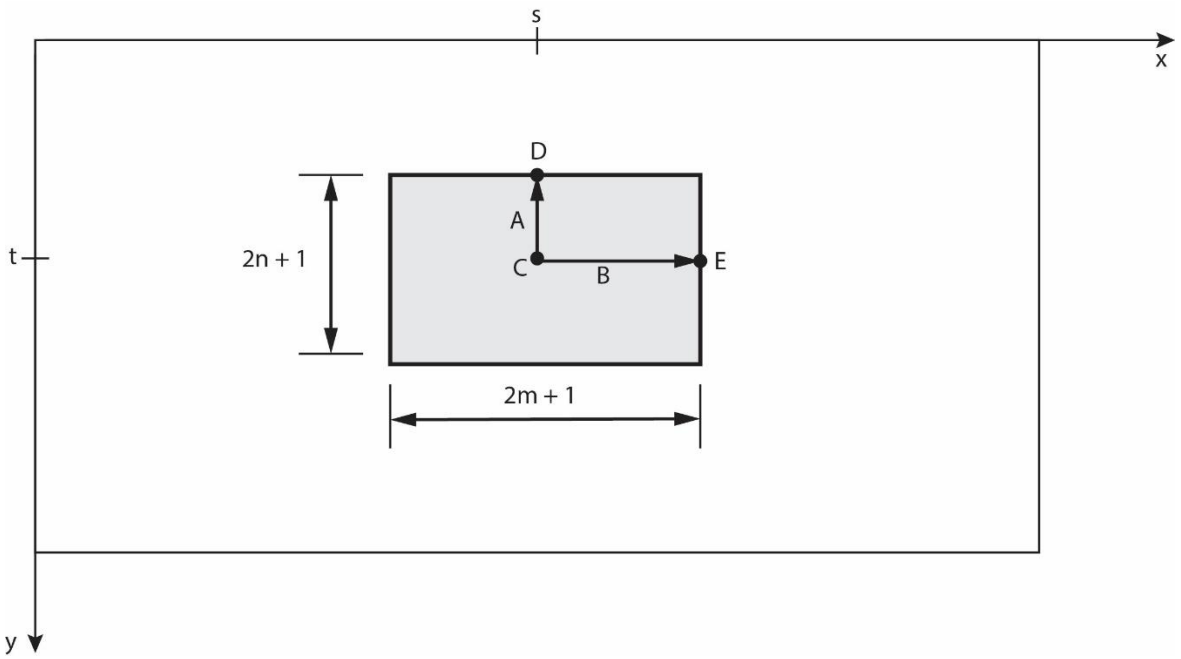

Figure 9.1 Source template. A 2m+1 by 2n+1 block of pixels within an image.

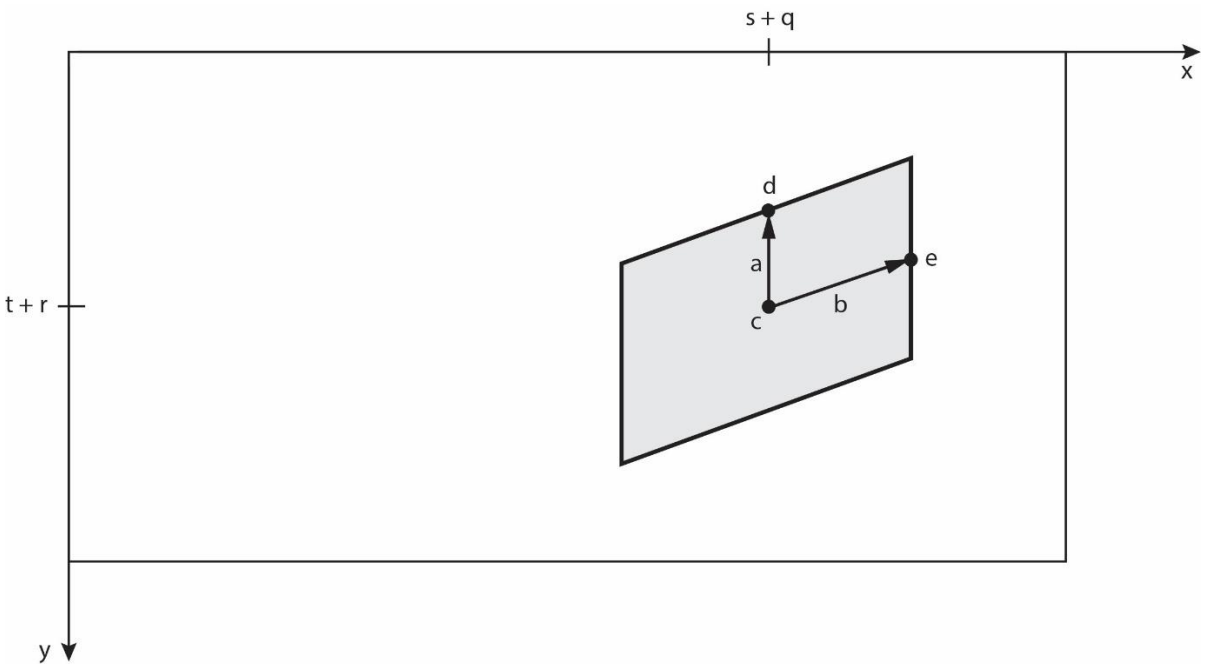

Figure 9.2 Deformed target in subsequent image.

Figure 9.1 shows a block of pixels defined by an arbitrary length and width; this block can be defined with the vectors **A** and **B.** These vectors have the ability to undergo any type of rotation, translation, skewing, widening, or narrowing. A tensor **F** can be applied to **A** and **B** that describes this:

$$FA = a$$

$$FB = b$$

This can also be written as follows:

$$\begin{bmatrix} F_{11} & F_{12} \\ F_{21} & F_{22} \end{bmatrix} = \begin{bmatrix} a_1 & b_1 \\ a_2 & b_2 \end{bmatrix} \begin{bmatrix} A_1 & B_1 \\ A_2 & B_2 \end{bmatrix}^{-1}$$

This deformation tensor can be used to map any pixel (i, j) in a reference image to a new location:

$$\begin{bmatrix} F_{11} & F_{12} \\ F_{21} & F_{22} \end{bmatrix} \begin{pmatrix} i \\ j \end{pmatrix} = \begin{bmatrix} F_{11}i & F_{12}j \\ F_{21}i & F_{22}j \end{bmatrix}$$

Thus, a cross-correlation function can be created that starts at location (s, t), is deformed by **F**, and is translated by (q, r) in another image. By entering in values for q, r, and F, a region can be scanned and defined to identify the location in the new image with the best match based on the entered parameters.

$$C(q,r,f) = \frac{\sum_{i=-m}^{m}\sum_{j=-n}^{n} S(s+i,t+j)T(s+q+F_{11}i+F_{12}j, t+r+F_{21}i+F_{22}j)}{\sqrt{\sum_{i=-m}^{m}\sum_{j=-n}^{n} S^2(s+i,t+j)\sum_{i=-m}^{m}\sum_{j=-n}^{n} T^2(s+q+F_{11}i+F_{12}j, t+r+F_{21}i+F_{22}j)}}$$

Where: $\mathrm{S}(\mathrm{a}, \mathrm{b})$ is the intensity of the pixel at coordinates (a, b) in the source image.

$\mathrm{T}(\mathrm{c}, \mathrm{d})$ is the intensity of the pixel at coordinates (c, d) in the target image.

9.3.2 Tracking Parameters

Development and adaptation of the algorithm to track vertebral body motion required a series of adjustments based on the underlying principles outlined in Section 9.3.1. Fluoroscopy produces an image with a lower radiation dose per frame (compared to traditional static x-ray) enhanced by an image intensifier. Due to this, there is a low signal to noise ratio in the frames that are taken. In addition, soft tissue artifact can distort bony elements and the contraction and relaxation of muscles coupled with soft tissues changing position during movement can alter the visual characteristics of the structures that are being tracked. All of these factors create a unique challenge for image registration techniques in accurately tracking vertebral body motion under fluoroscopy.

The overall tracking scheme relied on performing iterative “passes” of an image set. A first pass established a rough location of each vertebral body, while subsequent passes further refined the position of individual coordinates established previously.

The first tracking pass focused on obtaining a rough position of each vertebral body that was inside of the fluoroscope field of view. An operator manually selected four points for each vertebra placed at points with distinct features for the first image in a sequence. Following this, pixel templates were created around the vertebral bodies and all points were tracked as a group within a specified search region for each of the remaining images using the normalized cross-correlation function described in Section 9.3.1 (Figure 9.3). For this step, in addition to regular translation of the template within the search region, the cross-correlation function also iteratively compared rotations of the template up to a specified degree to find the best match.

Following the first tracking pass, the results could be visually inspected to ensure that the templates matched the general motion of the vertebral bodies. A second pass was then performed that allowed the individual points to be tracked without influence of the other points. This refined the location of the individual points and was able to achieve a level of accuracy that the bulk tracking of all four coordinates together could not achieve (Figure 9.4). At the same time, a smaller search region, and the general location of each coordinate already established, prevented the individual coordinates from being “lost” due to localized noise and changes in the image relative to the template. This refinement tracking was repeated three times in total; including the initial rough tracking, a total a four passes was performed on an image set to obtain a finalized set of coordinate data (Figure 9.5).

All image tracking was performed on a computer with a 1.9GHz dual core processor (Intel Core i5-4300U). Total tracking time for all passes together was 0.486s per coordinate tracked. For a typical patient image sequence consisting of 6 vertebral bodies tracked (24 coordinates) this amounted to a total tracking time of 11.7s/frame.

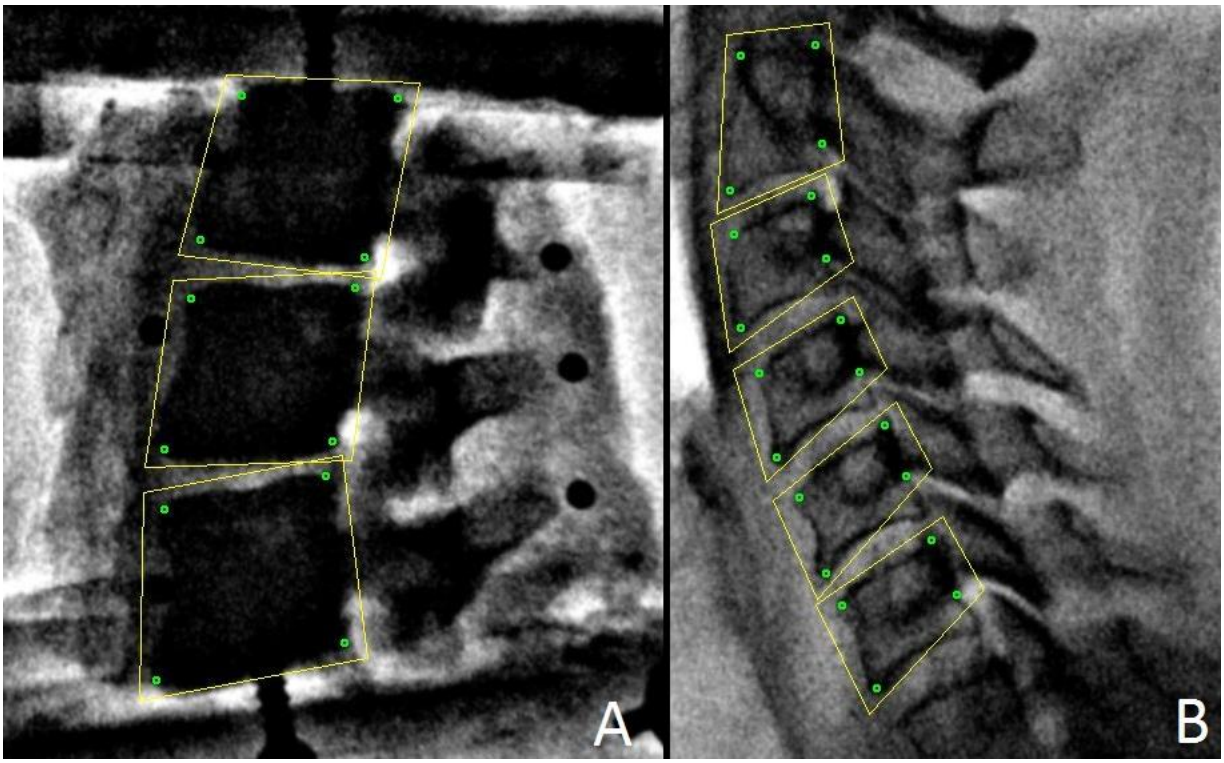

Figure 9.3 A. Pixel templates created around porcine vertebral bodies. B. Pixel templates on patient images

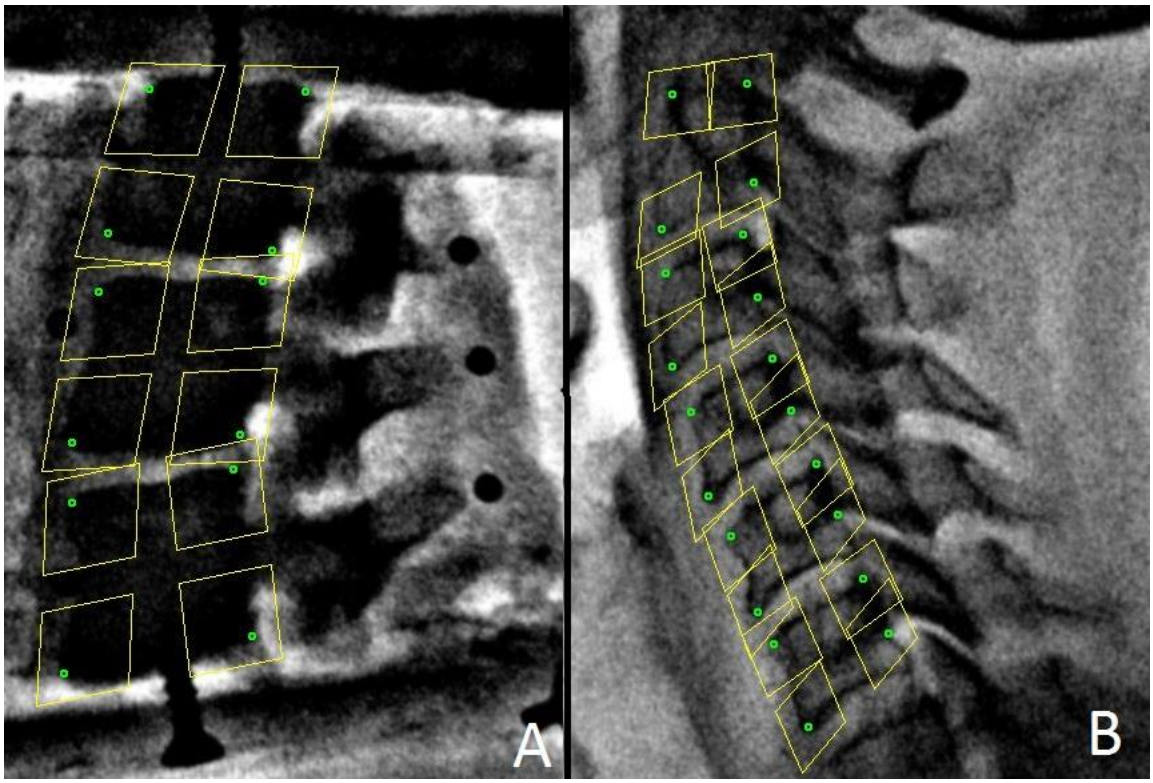

Figure 9.4 Pixel templates for single points after the initial rough tracking pass.

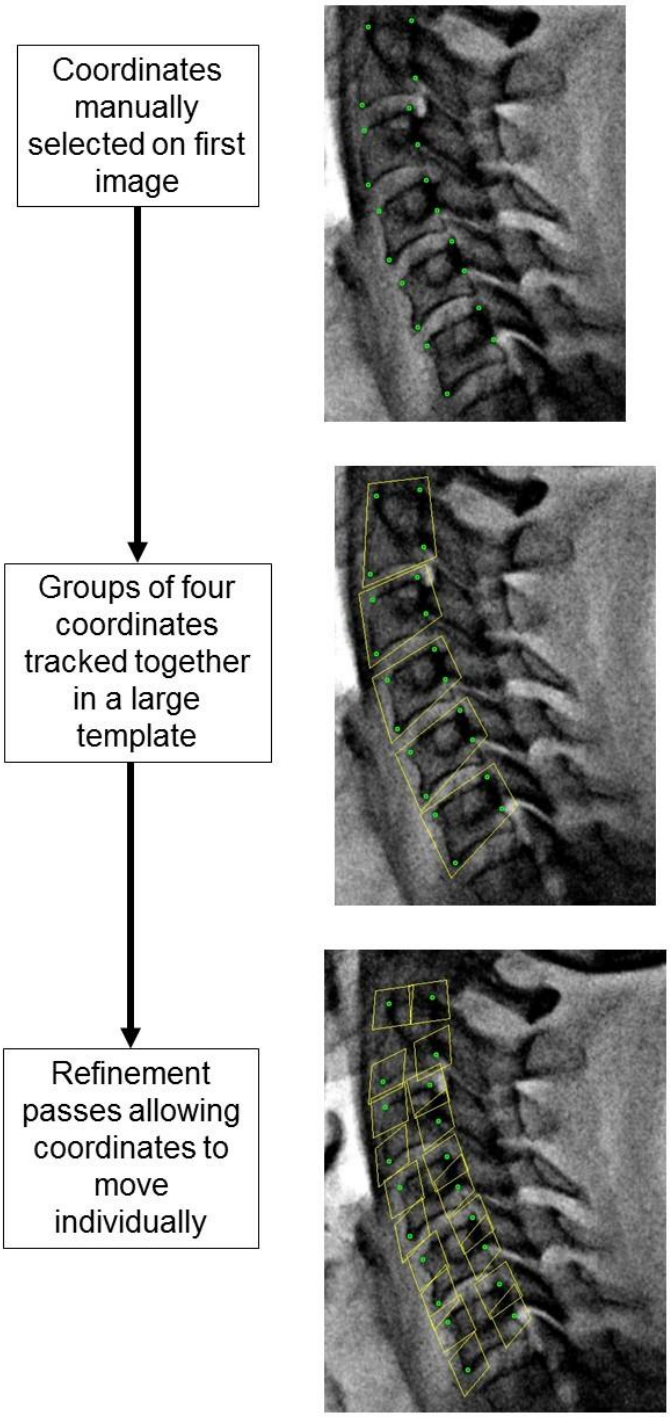

Figure 9.5 Flow chart of the procedure for tracking vertebral body motion.

9.3.3 Image Processing

In order to enhance the efficacy of the tracking software in identifying the specific location of the template vertebral bodies, images were processed to reduce the pincushion distortion inherent in fluoroscopic image sequences (Wallace and Johnson, 1981), and emphasize the edges on the vertebral bodies.

Rather than performing a correction on the final coordinates to account for the pincushion distortion present in the images (Cholewicki et al., 1991), a correction was applied to the images themselves. The following formula was applied to each image resulting in a re-mapping of the pixels:

$$s = r\left(1 + k(r^2)\right)$$

Where: s is the modified coordinate

r is the radial distance from the center of the image

k is a radial distortion coefficient

In order to find the optimal radial distortion coefficient, a wire grid consisting of equally spaced 12.7mm squares was placed in the field of view of the fluoroscope under the same focal parameters that were used to image patients. From this sequence of images, radial distortion coefficients could be applied heuristically until all squares on the grid appeared to be approximately the same size (Figure 9.6). This radial distortion coefficient was then used on all of the images to correct the inherent pincushion distortion prior to tracking.

Following pincushion distortion correction, the images were enhanced using a smart sharpen filter (amount: 500%, radius: 20 pixels) in Adobe Photoshop (Adobe, San Jose, CA, USA) followed by a Gaussian Blur (radius: 1 pixel) which added some smoothing to the images (Figure 9.7). Performing both image processing steps (distortion removal and edge

enhancement) helped produce an image that had much more clearly defined edges and enhanced the precision of the tracking software.

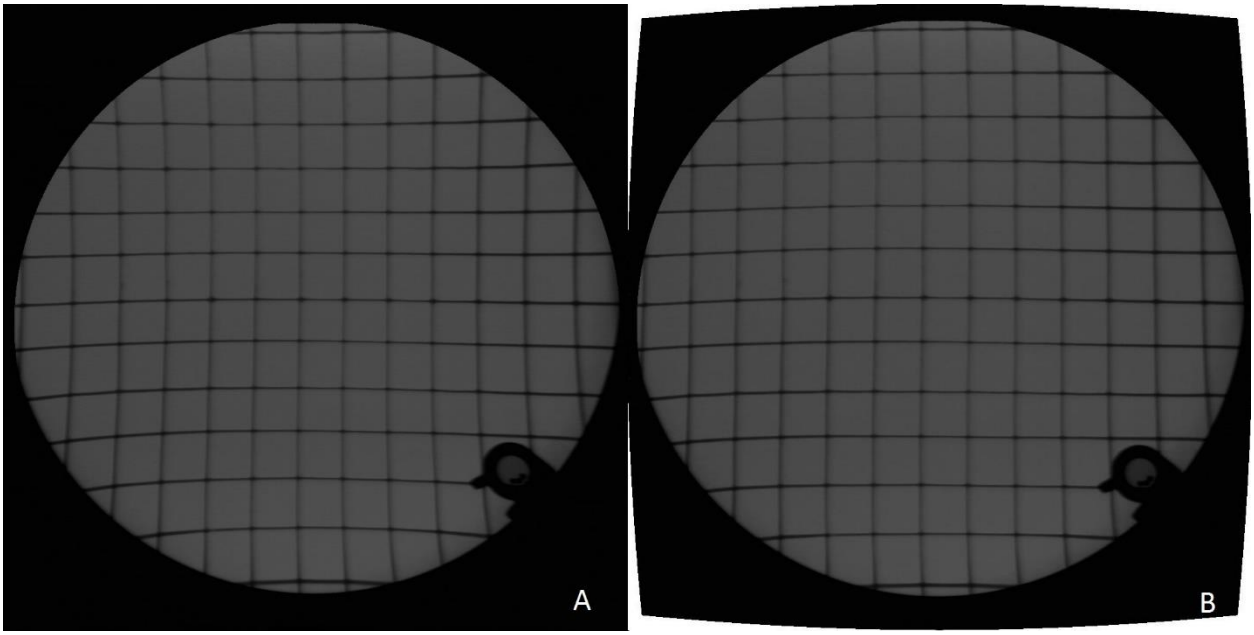

Figure 9.6 A. Uncorrected frame with a wire grid consisting of equally sized squares. B. Corrected frame where all squares in the frame were brought to approximately equal size.

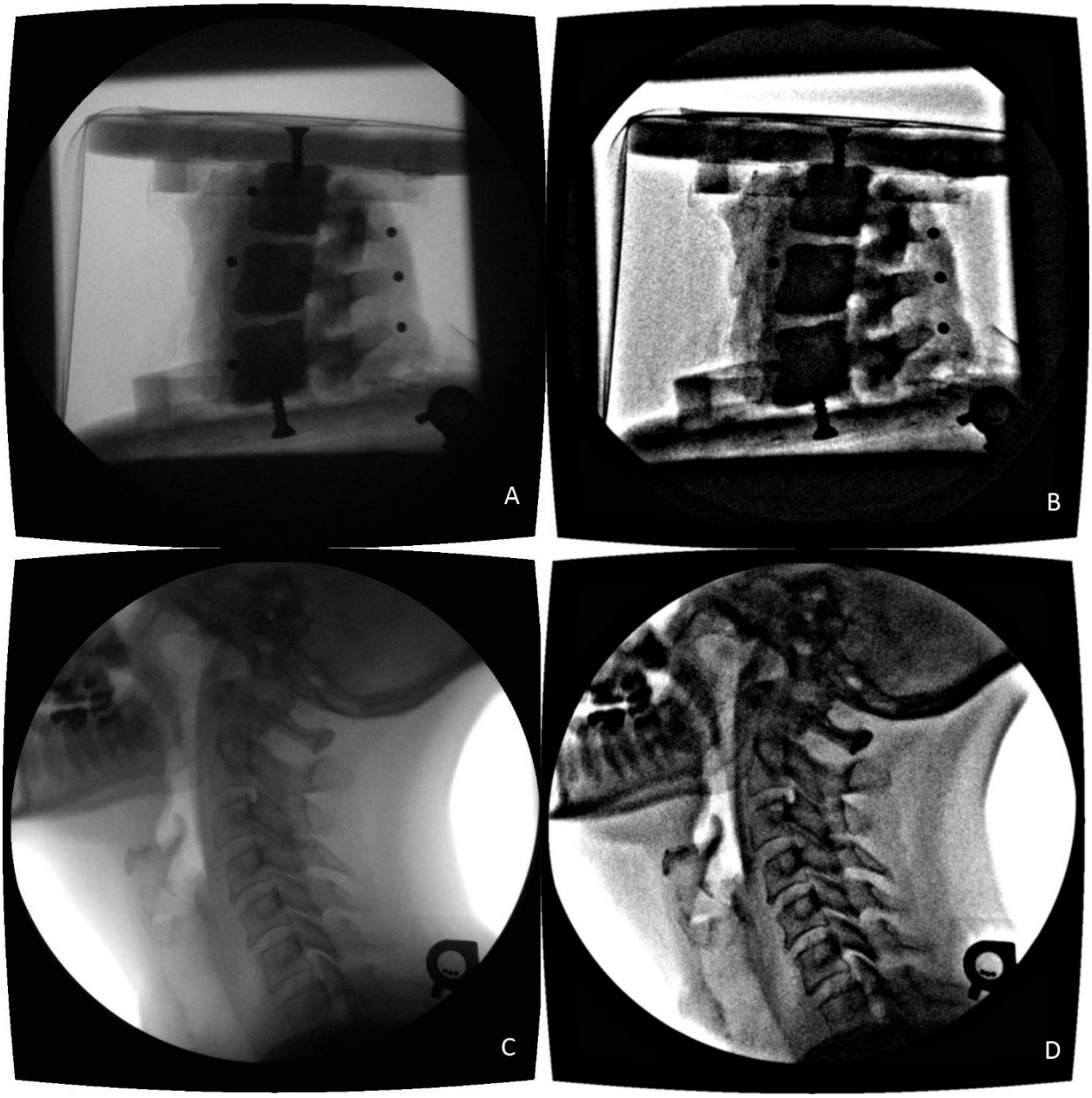

Figure 9.7 A. Porcine specimen prior to edge enhancement. B. Porcine spine after edge enhancement. C. Patient spine before edge enhancement. D. Patient spine after edge enhancement.

9.3.4 Experimental Setup

The accuracy of the tracking algorithm was tested via a rotating arm with a porcine spine specimen consisting of three vertebral bodies and two intervening discs mounted to the top (Figure 9.8). A potentiometer (Bourns, model: 6637, Riverside, CA, USA) was mounted to the

rotation point of the arm and was considered to be the a priori gold-standard. On each vertebra, lead markers were rigidly mounted to the anterior portion of the vertebral body and the posterior aspect of the spinous process using cyanoacrylate adhesive. Given the high contrast that they created when under fluoroscopic imaging, the tracking technique could capture these points and track them with high accuracy. These served as a further method to obtain angular displacements of the specimen.

All tissue was left on the spine specimen in an effort to mimic the soft tissue artifact produced when recording motions *in-vivo*. This created a highly challenging phantom to track since the tissue produced a gradient of intensity around the vertebrae rather than a distinct edge which would have been easier for the algorithm to handle (Figure 9.9).

The entire apparatus was placed in such a way that the spine specimen was located in the fluoroscope field of view. The specimen was rotated on the arm throughout the field to simulate flexion-extension motions. A foot pedal synchronized the recording between the fluoroscope and the potentiometer. Three trials of full flexion-extension (one edge of the field of view to the other) were taken (Figure 9.10). Fluoroscopic image sequences were taken with a Digital Motion X-Ray that provided continuous x-ray at 70-90 kVp at 2-3.5 mA at a 40-inch flange focal distance. A 9-inch image intensifier (Precise Optics, Bay Shore, NY, USA) transferred the signal to a digital CCD camera outputting a 150dpi stream to a DICOM recorder (NAI Tech Products, Auburn, CA, USA).

Each vertebra for each trial was tracked ten times using the tracking algorithm. For each case, an operator manually selected points for the first frame, while the tracking algorithm tracked those points for the remaining images. Points were chosen on each of the four corners of the vertebral bodies, a distinct feature with high contrast that could be identified and distinguished by the tracking algorithm (Figure 9.11). With 30 total points of tracking for three trials, this produced 90 sets of tracking results.

For each trial, the lead markers were tracked individually to create a secondary set of gold standard angular displacement data. Specific information on the methods and calculations used to extract angles from the tracked vertebrae, lead markers, and potentiometer is located in Appendix B. Further, computations of relative joint shear between vertebral bodies are located in Appendix B.

Angular displacements from the tracked vertebrae were compared to the synchronized potentiometer data as well as the data obtained from tracking the lead markers. For each of the 10 trials, the RMS error in degrees was calculated for each vertebra compared to the gold standard measurement. This yielded 10 RMS values for each vertebra, for each of the three trials (90 values total). The average RMS value was taken for each vertebra, for each trial to yield nine RMS values that could be compared to the gold-standard measurements. Finally, average RMS error for each vertebra over the three trials was taken to yield three error values.

Further, the RMS error in degrees was calculated between vertebrae. For each trial, the RMS error was calculated between vertebra 1 and vertebra 2, vertebra 1 and vertebra 3, and vertebra 2 and vertebra 3. This served to determine the relative error between tracked vertebrae, an important measure for the purposes of calculating relative (joint) angles. RMS error was computed and averaged in the same manner as the gold-standard data.

Relative joint shear was calculated for the two intervertebral joints as a function of one vertebral body over another. For each trial, two time-series sequences of shear calculations were generated. Since the vertebral bodies did not move relative to one another, the theoretical shear was 0mm. Thus, RMS error between the calculated shear values for each joint in each trial was computed against a theoretical time-series of 0mm of shear displacement.

9.3.5 Patient Data Testing

Despite not having ground-truth measurements for actual patient data, tracking of real patient image sequences was performed to assess the repeatability of the algorithm. Three

patient image sequences were selected and tracked using the algorithm. An operator created ten separate tracking runs for each image sequence. From this, the coordinates for each tracked image sequence were averaged together and acted as the standard for the ten trials to be compared against. Angular displacement of the vertebral bodies and relative shear for vertebral bodies was computed for all ten trials for each image sequence. The RMS error between each tracking instance and the average of all of the tracking instances was calculated. This gave insight with respect to how dependable and consistent the angular and shear measures could be.

9.3.6 Secondary Gold-Standard Measurements

After careful analysis of the potentiometer data as the reference gold standard, it was determined that the output angular displacement was not entirely accurate to ground-truth. Using the lead markers, two separate individuals made hand measurements of the maximum flexion and maximum extension postures compared to the neutral posture for the three porcine spine image sequences. The findings of these measurements did not correspond to the maximum output angle of the potentiometer; from this, more investigation was warranted. All six lead markers were tracked using the same normalized cross-correlation function (Figure 9.12), but under the same method used previously (Velduis and Brodland, 1999, Wiebe and Brodland, 2005, Eilaghi et al., 2009, Bootsma and Brodland, 2005, Kitamura et al., 2012), and not the algorithm developed for tracking vertebral bodies. From this tracking, all six markers could be incorporated into the least-squares algorithm described in Appendix B. This yielded a highly accurate calculation of angular displacement using six vectors based on the positions of six markers. Further, since the deformation tensor is decomposed into a rotation and stretch tensor, the efficacy of correcting for the pincushion distortion could be assessed. If there was significant pincushion distortion still left in the corrected images, the marker coordinates would deform from their true positions as the specimen moved through the field of view. There would

be evidence of this in the calculated stretch tensor. Conversely, no pincushion distortion in the corrected image (and perfectly tracked coordinates) would yield the identity matrix (or in reality, values very close to the identity matrix).

Analysis of the potentiometer data yielded values that deviated from the tracked vertebrae (Figure 9.13). From the time-history graph, there appeared to be a gain error in the potentiometer itself. For collection, the circuit used a precision potentiometer (Model: 6637, Bourns, Riverside, CA, USA) to divide a regulated voltage from an LM7805 chip. A voltage supply with a fixed gain was used to condition the signal and before being sent to a 16-bit analog to digital signal converter (Model: AI-1608AY-USB, Contec, Osaka, Japan). The digital signal was offset to make its zero correspond with the reference geometry of the specimen, and so the discrepancy between the potentiometer measurement and the digital tracking appears to be due primarily to gain error.

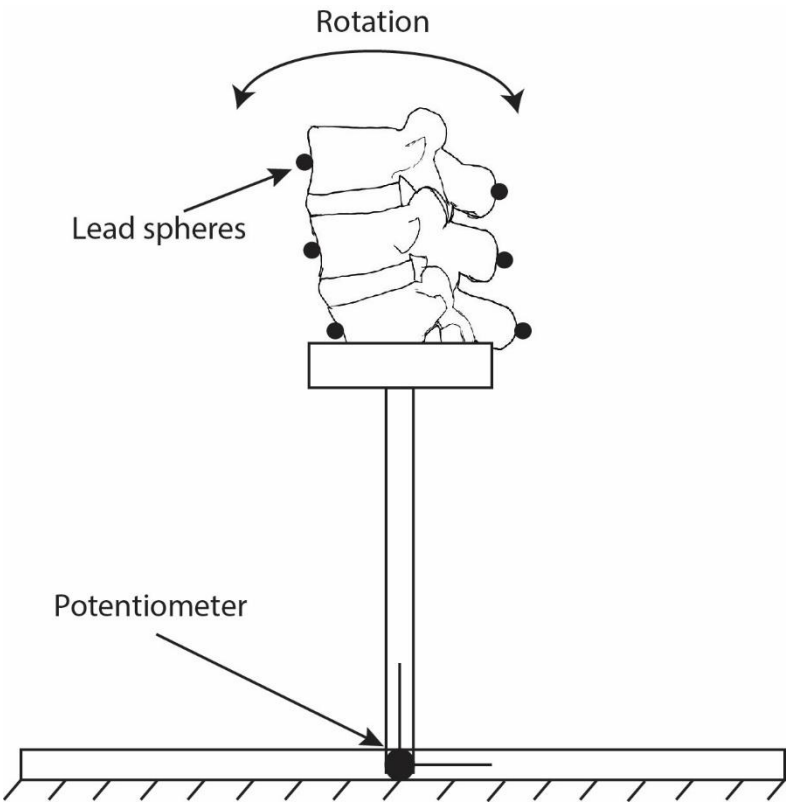

Figure 9.8 Testing apparatus used to evaluate the tracking algorithm.

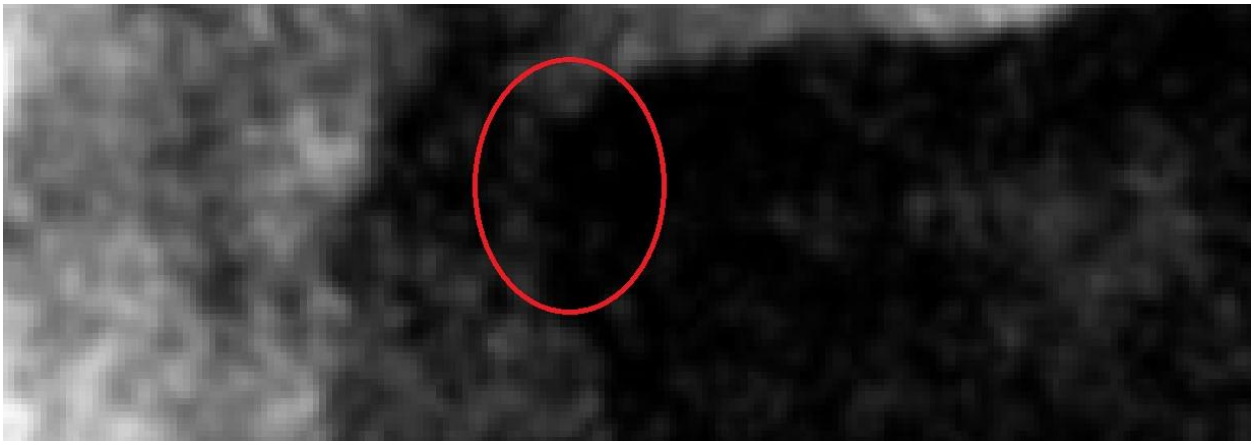

Figure 9.9 There was not always a clear edge between the surrounding tissue and the vertebral body, creating a challenging image sequence for the algorithm to track.

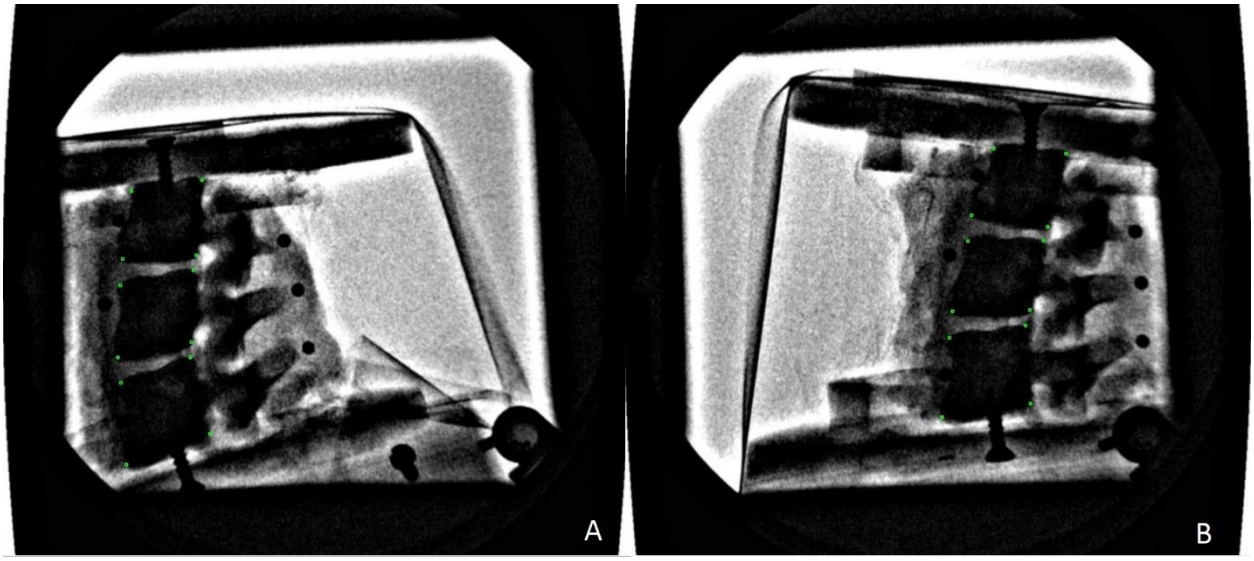

Figure 9.10 The test specimen was rotated throughout the field of view to simulate flexion (A) to extension (B).

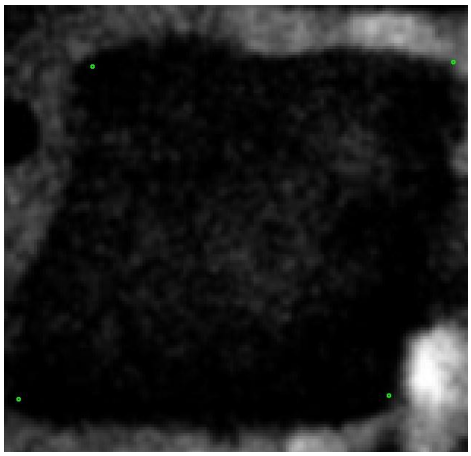

Figure 9.11 Coordinates were chosen at each of the four corners of the vertebral bodies. These regions offered the highest contrast and most likely sites to track successfully.

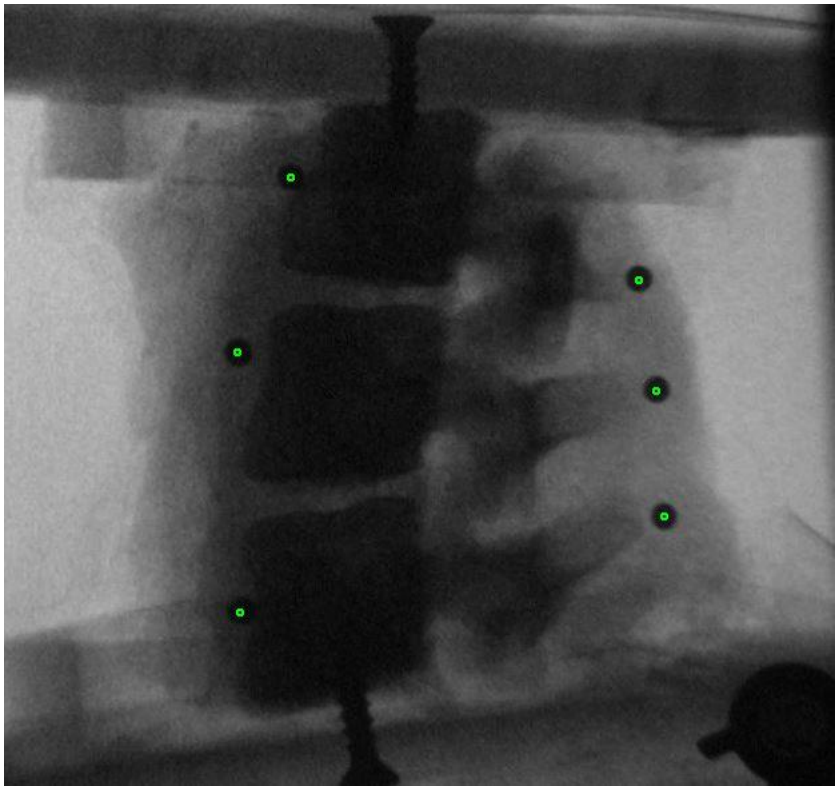

Figure 9.12 Tracking the lead markers placed on the specimen. These markers could be tracked using the normalized cross-correlation function without the tracking points losing the markers.

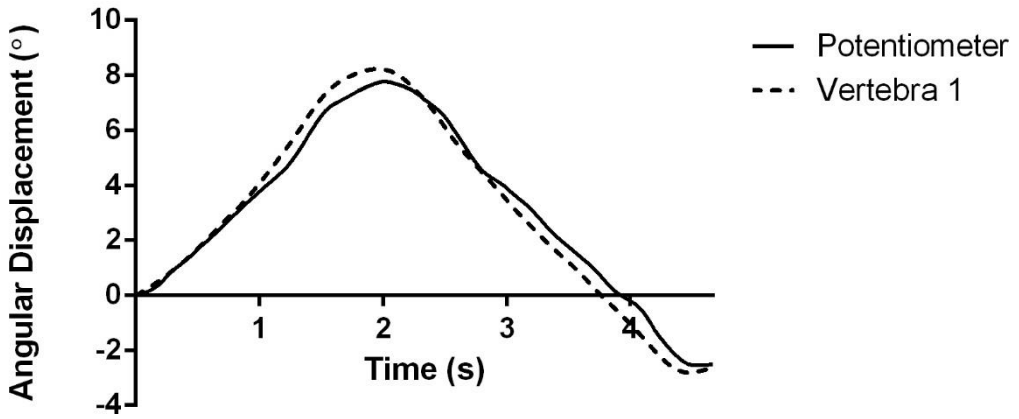

Figure 9.13 Sample time-series data of the potentiometer compared to tracking results. There appeared to be a gain error in the potentiometer, and the marker data was used instead.

9.4 Results

Time history sequences for each tracked vertebra relative to the gold standard data for all trials is presented in Figure 9.14, Figure 9.15, and Figure 9.16. Average RMS error across the three trials was 0.230° ± 0.038°, 0.400° ± 0.005°, and 0.225° ± 0.080° for the superior, middle, and inferior vertebral bodies respectively (Table 9.1). RMS error between the angular displacements calculated for each vertebral body was also very low over the three trials, with values of 0.376° ± 0.069°, 0.291° ± 0.101°, and 0.355° ± 0.113° for vertebral body 1 versus. 2, vertebral body 1 versus 3, and vertebral body 2 versus 3 respectively (Table 9.2).

Relative joint shear error was very low, with average error levels over a trial of 0.030mm ± 0.003mm and 0.055mm ± 0.025mm for joint 1 and joint 2 respectively (Table 9.3).

Analysis of the patient tracking trials revealed RMS error lower than the highest error in the porcine spine tracking results. Average RMS for the 10 trials compared to the mean of the trials for each patient image sequence is presented in Table 9.4. Further, the shear RMS values were found to be lower than the error in the porcine spine tracking results Table 9.5. Sample time-histories for angular displacement and shear measurements for the patient data is

presented in Figure 9.17 and Figure 9.18 respectively. A complete series of images for the patient image sequence results is located in Appendix G.

Table 9.1. RMS Error in Degrees between the Tracked Vertebral Body Data and the Gold-Standard Measurements

	Vertebra 1 vs. Gold-Standard (RMS°)	Vertebra 2 vs. Gold-Standard (RMS°)	Vertebra 3 vs. Gold-Standard (RMS°)
Trial 1 Average (SD)	0.204 (0.081)	0.400 (0.089)	0.295 (0.047)
Trial 2 Average (SD)	0.213 (0.050)	0.395 (0.050)	0.139 (0.037)
Trial 3 Average (SD)	0.273 (0.092)	0.405 (0.075)	0.242 (0.086)
Average (SD)	**0.230 (0.038)**	**0.400 (0.005)**	**0.225 (0.080)**

Table 9.2. RMS Error in Degrees between the Tracked Vertebrae (Relative Error).

	Vertebra 1 vs. Vertebra 2 (RMS°)	Vertebra 1 vs. Vertebra 3 (RMS°)	Vertebra 2 vs. Vertebra 3 (RMS°)
Trial 1 Average (SD)	0.346 (0.095)	0.271 (0.095)	0.255 (0.092)
Trial 2 Average (SD)	0.328 (0.073)	0.202 (0.065)	0.333 (0.075)
Trial 3 Average (SD)	0.455 (0.154)	0.401 (0.108)	0.478 (0.113)
Average (SD)	**0.376 (0.069)**	**0.291 (0.101)**	**0.355 (0.113)**

Table 9.3. Relative Joint Shear RMS Error Values in mm

	Vertebra 1 Shear Relative to Vertebra 2 (RMS mm)	Vertebra 2 Shear Relative to Vertebra 3 (RMS mm)
Trial 1 Average (SD)	0.030 (0.019)	0.035 (0.016)
Trial 2 Average (SD)	0.032 (0.016)	0.083 (0.033)
Trial 3 Average (SD)	0.026 (0.023)	0.047 (0.024)
Average (SD)	**0.030 (0.003)**	**0.055 (0.025)**

Table 9.4. Average RMS Error in Angular Displacement between Ten Iterations of Tracked Patient Image Sequences and the Average Coordinate Positions of the Ten Trials.

	Vertebra 1 (RMS°)	Vertebra 2 (RMS°)	Vertebra 3 (RMS°)	Vertebra 4 (RMS°)	Vertebra 5 (RMS°)
Patient 1 (SD)	0.284 (0.169)	0.169 (0.080)	0.228 (0.091)	0.203 (0.131)	0.203 (0.093)
Patient 2 (SD)	0.285 (0.144)	0.338 (0.167)	0.395 (0.151)	0.385 (0.236)	0.351 (0.203)
Patient 3 (SD)	0.153 (0.086)	0.251 (0.099)	0.209 (0.101)	0.118 (0.055)	0.243 (0.123)

Table 9.5. Average RMS Error in Shear between Ten Iterations of Tracked Patient Image Sequences and the Average Coordinate Positions of the Ten Trials.

	Joint 1 Shear (RMS, mm)	Joint 2 Shear (RMS, mm)	Joint 3 Shear (RMS, mm)	Joint 4 Shear (RMS, mm)
Patient 1 (SD)	0.040 (0.028)	0.032 (0.021)	0.050 (0.024)	0.040 (0.021)
Patient 2 (SD)	0.047 (0.021)	0.052 (0.027)	0.043 (0.022)	0.038 (0.026)
Patient 3 (SD)	0.047 (0.022)	0.029 (0.020)	0.025 (0.014)	0.031 (0.011)

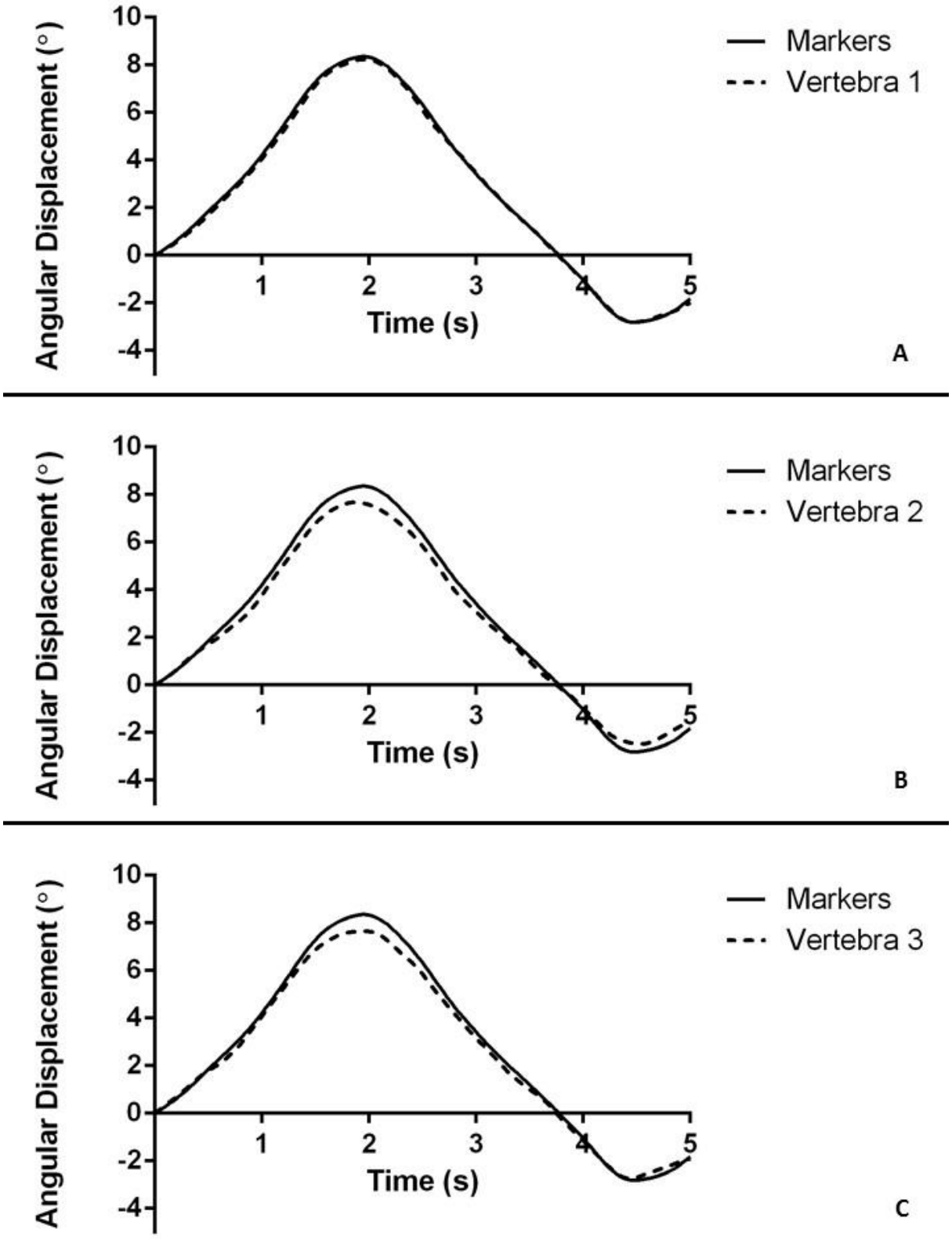

Figure 9.14 Time-history data of tracked vertebral bodies and gold-standard angular data for trial 1.

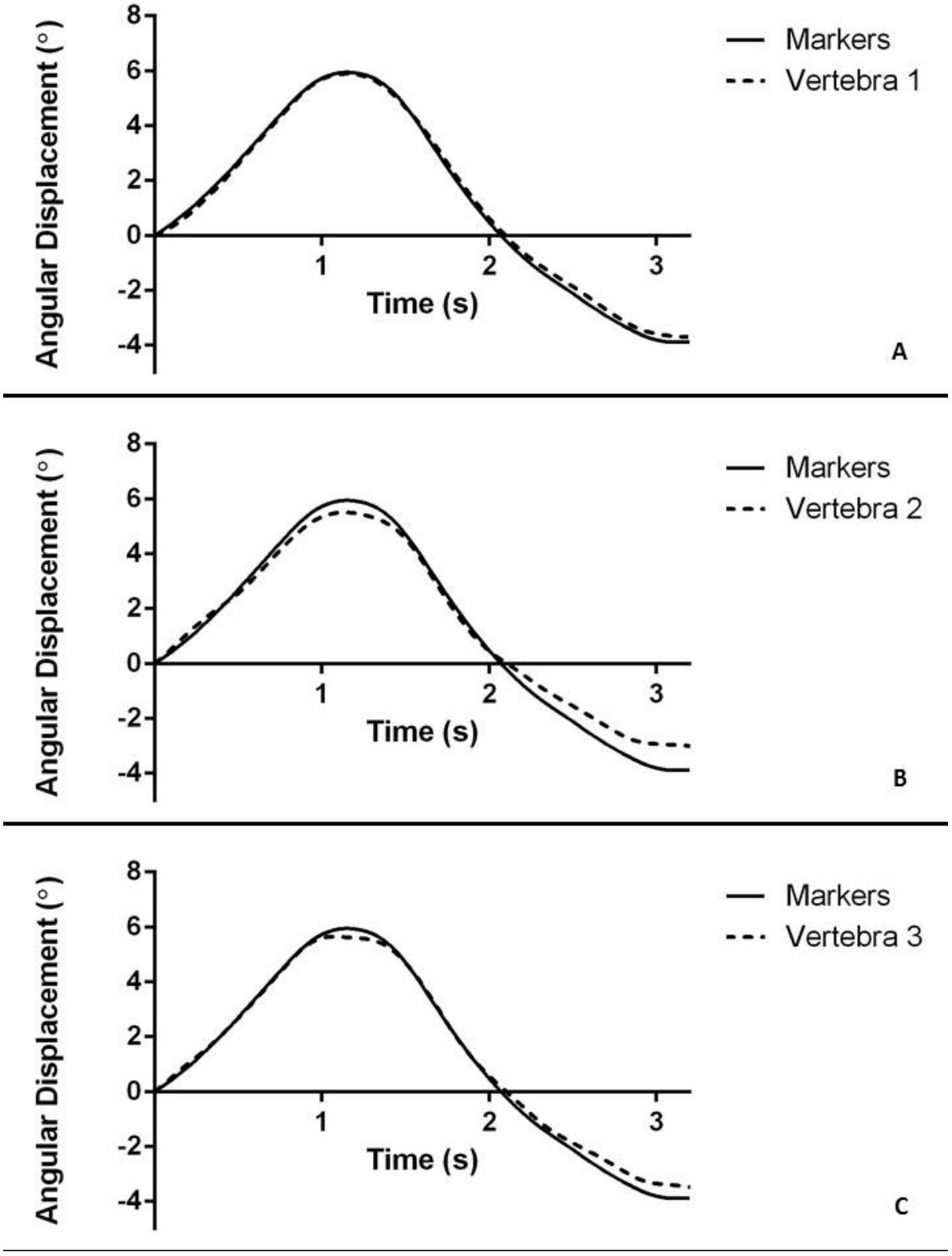

Figure 9.15 Time-history data of tracked vertebral bodies and gold-standard angular data for trial 2.

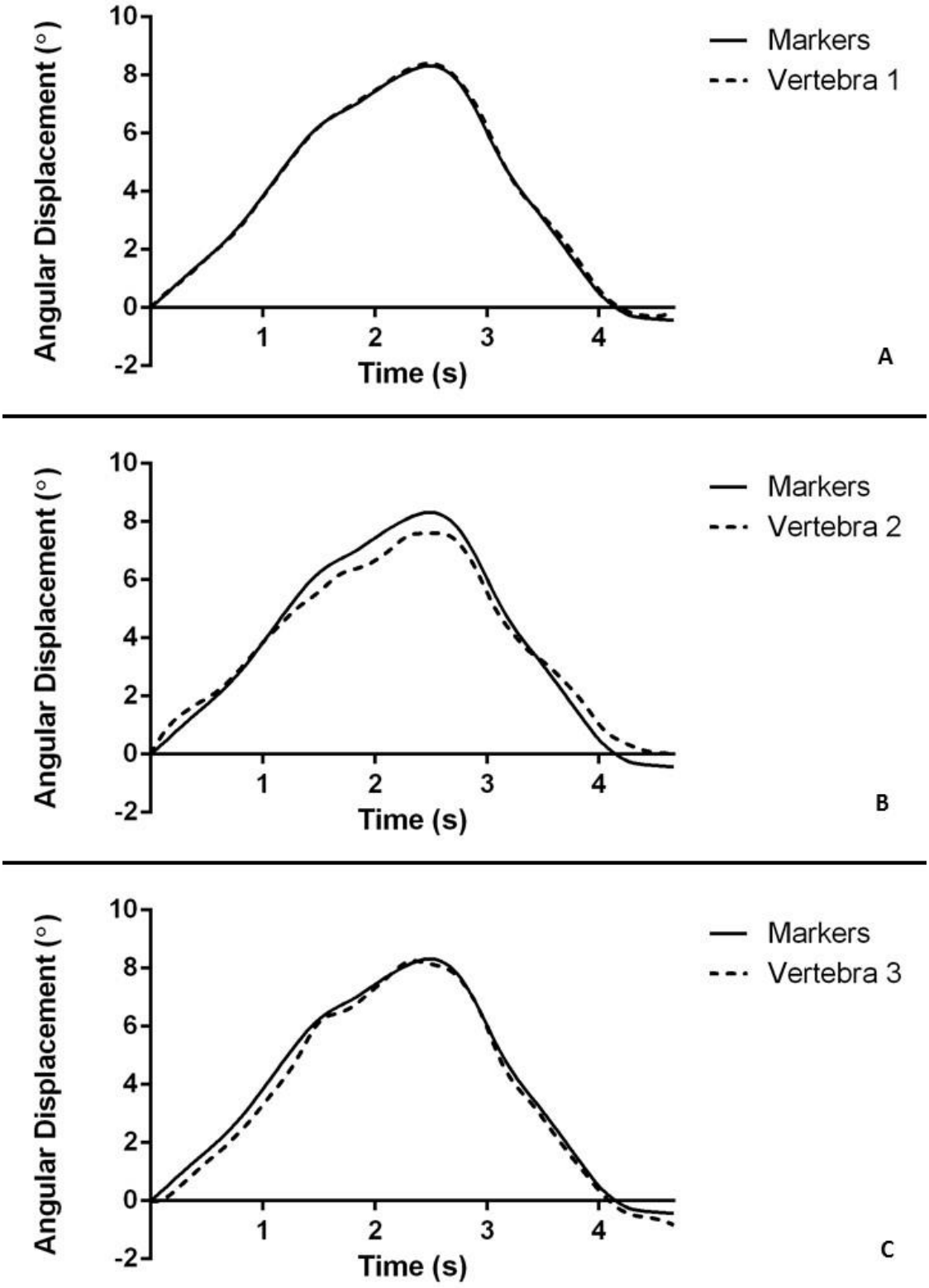

Figure 9.16 Time-history data of tracked vertebral bodies and gold-standard angular data for trial 3.

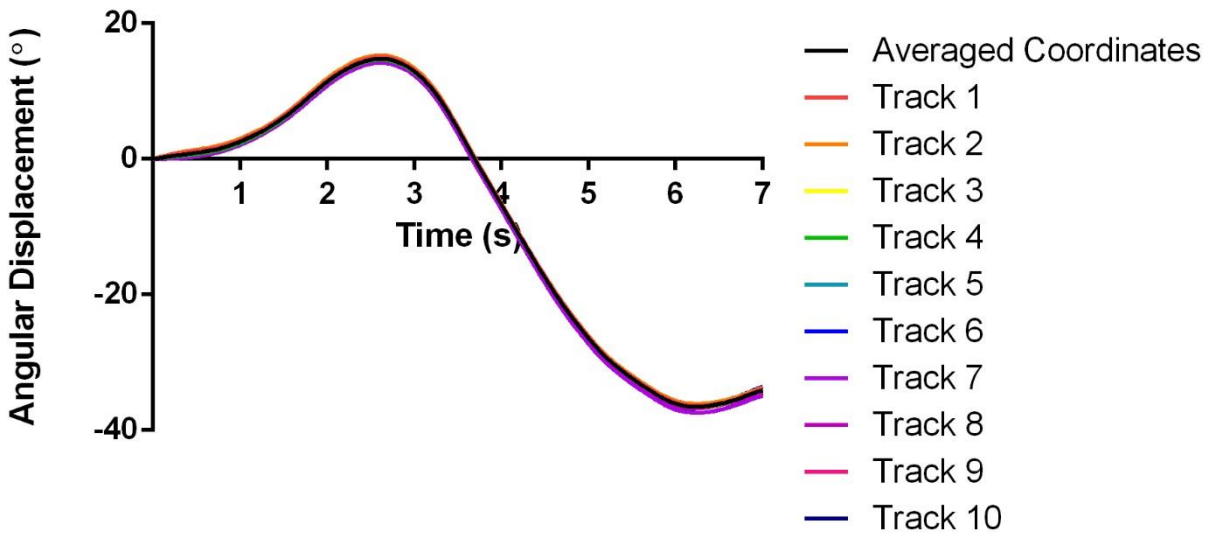

Figure 9.17 Sample time-history data of angular displacement for a tracked vertebral body from a patient image sequence. Ten tracking sequences were performed and then each was compared to the average of all the trials.

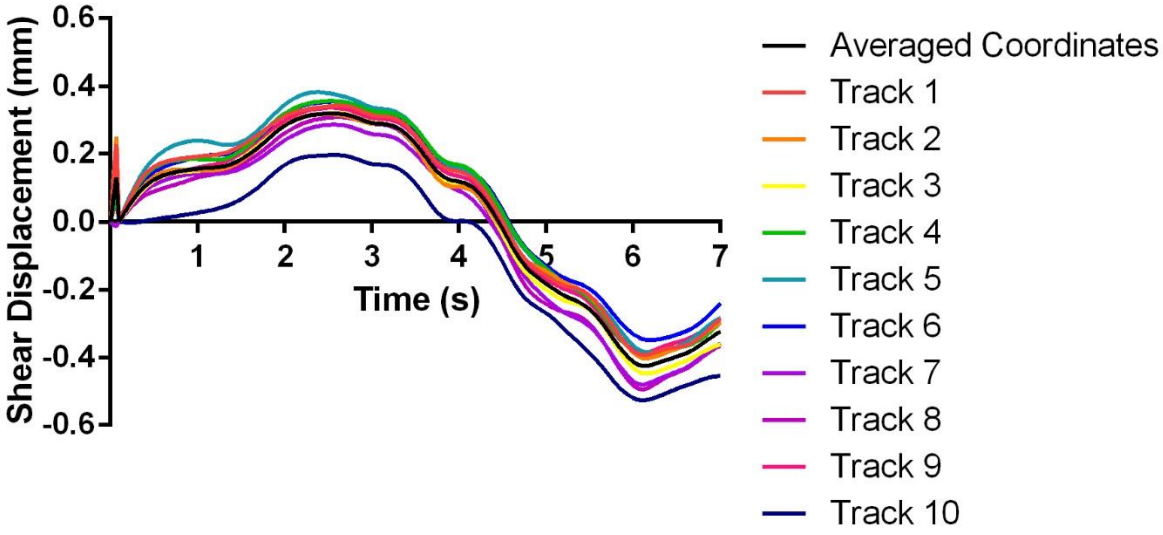

Figure 9.18 Sample time-history data of shear displacement for two adjacent vertebral bodies from a patient image sequence. Ten tracking sequences were performed and then each was compared to the average of all the trials.

9.5 Discussion

The novel tracking algorithm tested in this investigation was able to track the porcine spine specimen with an accuracy that was deemed appropriate for use in measuring sagittal plane spine motions. Vertebral body rotations were observed to rotate nearly 60° through a flexion/extension sequence (Figure 9.17), even tracking errors up to 1° would represent approximately 2% error for this amount of displacement. The highest error over the course of a trial measured was 0.4°, and in all of the other trials, the error levels were below this. Calculations of relative shear displacement were also highly accurate with average errors of 0.03mm and 0.055mm. Further, the patient data that was tested highlights the ability of the tracking algorithm to reliably track vertebral bodies through sagittal plane motions.

The novel algorithm presented here is highly accurate at tracking vertebral body motion under fluoroscopy. Indirect comparisons can be made between other tracking algorithms, however, different validation methods have been used. Bifulco and colleagues (Bifulco et al., 2001), who used a similar cross-correlation method calculated errors as high as 0.8 degrees in their static validation model. Wong and colleagues (Wong et al., 2006) used a robotic arm moving at a constant pace and measured the error in tracking angular speed of a cadaveric vertebra, which was 0.32° ± 0.24° per second. Ahmadi and colleagues (Ahmadi et al., 2009) used a calibrated board and computed the RMS error in degrees of 30 randomly selected frames which was 0.41°. Muggleton and Allen (Muggleton and Allen, 1997), again using a cross-correlation approach found errors in a static model of up to 0.6°. Wong and colleagues (Wong et al., 2009) evaluated their method against the RMS error in the distance the algorithm was off from feature points made by hand measurements and found errors below 0.4mm.

The apparatus and specimen used for this investigation was chosen for the challenge that it would provide the novel algorithm presented in tracking vertebral body motion. The use of a porcine spine with all tissue left intact created a close comparison to its intended use. The

gold-standard measure was highly precise and utilized a form of the current algorithm already validated in previous work (Velduis and Brodland, 1999) and widely used for tracking points (Wiebe and Brodland, 2005, Bootsma and Brodland, 2005, Eilaghi et al., 2009, Kitamura et al., 2012). The use of the lead markers created a high contrast that could be tracked with ease and far higher precision than any hand measurements. Static measurements under fluoroscopy are inherently easier to track as there is no movement through a distorted image field and no potential for tissue structures to alter the template being tracked. Further, use of a validation specimen with no tissue present or one that is crafted out of a material that will produce a high contrast such as metal is insufficient in its accuracy to what will be tracked *in-vivo*. These are also easier to track as they produce a highly distinct edge (similar to the lead markers tracked by the present algorithm with high precision). Hand measurements for the purpose of validation are inherently inaccurate and their use as a gold-standard eliminates the underlying reason to develop an automated registration technique.

The use of an animal model moving throughout the field of view in this investigation is highly robust and a sufficient "challenge" for the tracking algorithm to be considered adequate to track human spine motion under fluoroscopy. Human spines create a much more distinct edge on the vertebral body compared to the porcine spine used in this investigation; a more easily tracked feature. The presence of tissue on the porcine spine also mimicked an *in-vivo* scenario more closely, and masked the edge on some portions of the vertebral bodies. Despite these challenges, the algorithm was able to track the vertebrae with error that represents a very small (< 1%) proportion of observed angular displacement.

Use of this algorithm for measuring human vertebral motion will help to add further confidence and accuracy in measurements. Coupling this algorithm with already existing ones could also help to add further confidence and redundancy in measurements. The ability to track vertebral motion will help to further spine research, as the quantification and characterization of human spine motion will serve as a tool for identifying pain generators and clinical subgroups.

Future work and improvement involves the enhancement of the algorithm's recognition abilities and its use in additional planes of view such as the frontal plane. Removing the manual marker registration stage prior to tracking and allowing the algorithm to "recognize" a vertebral body and track that through time represents the next stage in the evolution of tracking spine segmental motion, further enhancing accuracy and broadening the scope of cases which are able to be accurately tracked.

Appendix B: Relative Angle Calculations for Multiple Segment Spine Specimens and Measurement System Sensitivity Testing

10.1 Relative Angle Calculation

The method for calculating relative angles was based on the method outlined by Veldhuis and colleagues (Veldhuis et al., 2005). The specific procedure used for the analysis of multiple segment spine specimens in this thesis is outlined in detail below.

The first step was to describe the position of the three rigid body marker clusters on the specimens with the non-moving (global) reference cluster fixed to the Instron. Centroids of each cluster (including the global cluster) were calculated by averaging the coordinates of each of the four markers on each cluster:

$$Centroid(x,y) = \frac{(marker1 + marker2 + marker3 + marker4)}{4}$$

Following the calculation of centroids, eight vectors were defined using the coordinates of the markers themselves, as well as the newly calculated centroid (Figure 10.1). Calculated vectors were then used to describe a deformation tensor '**F**' which could be used to describe the rotation and stretch between two sets of vectors. In the case of this work, the deformation tensor was used to describe each set of vectors from the three rigid bodies to the global marker cluster:

$$\begin{bmatrix} F_{11} & F_{12} \\ F_{21} & F_{22} \end{bmatrix} = \begin{bmatrix} \sum_{i=1}^{n} G_{ix} R_{ix} & \sum_{i=1}^{n} G_{ix} R_{iy} \\ \sum_{i=1}^{n} G_{iy} R_{ix} & \sum_{i=1}^{n} G_{iy} R_{iy} \end{bmatrix} \begin{bmatrix} \sum_{i=1}^{n} G_{ix} G_{ix} & \sum_{i=1}^{n} G_{ix} G_{iy} \\ \sum_{i=1}^{n} G_{iy} G_{ix} & \sum_{i=1}^{n} G_{iy} G_{iy} \end{bmatrix}^{-1}$$

Where: G_{ix} is the x-component vector of the global marker cluster.

R_{ix} is the x-component vector of one of the rigid body clusters on the specimen (a deformation tensor was calculated for each of the three rigid body clusters on the specimen).

The y-component vectors are defined the same as described above for the x-component vectors, but with the 'y' subscript.

After calculation of the deformation tensor, it is decomposed into the rotation and stretch tensors:

$$F = RU$$

Where: R is the rotation tensor.

U is the stretch tensor.

The rotation and stretch tensor are calculated as follows:

$$R = \frac{sign(F_{11} + F_{22})}{\sqrt{1 + \left(\frac{F_{11} + F_{22}}{F_{21} - F_{12}}\right)^2}} \begin{bmatrix} \frac{F_{11} + F_{22}}{F_{21} - F_{12}} & -1 \\ 1 & \frac{F_{11} + F_{22}}{F_{21} - F_{12}} \end{bmatrix}$$

$$U = \frac{sign(F_{11} + F_{22})}{\sqrt{1 + \left(\frac{F_{11} + F_{22}}{F_{21} - F_{12}}\right)^2}} \begin{bmatrix} F_{11} \frac{F_{11} + F_{22}}{F_{21} - F_{12}} + F_{21} & F_{12} \frac{F_{11} + F_{22}}{F_{21} - F_{12}} + F_{22} \\ F_{21} \frac{F_{11} + F_{22}}{F_{21} - F_{12}} - F_{11} & F_{22} \frac{F_{11} + F_{22}}{F_{21} - F_{12}} - F_{12} \end{bmatrix}$$

Where: $sign(F_{11} + F_{22})$ is the calculation of $F_{11} + F_{22}$. If this sum is positive, then $sign(F_{11} + F_{22}) = 1$. Whereas if the sum is negative, then $sign(F_{11} + F_{22}) = -1$.

These steps are used to calculate the reference orientation of each rigid body marker cluster relative to the global marker cluster. Following this calculation, the orientations of the rigid body marker clusters can be calculated for the trials that were taken during the experiment; this is performed identically to the procedure outlined above. The trial orientations can then be expressed relative to the reference orientation as follows:

$$R_{corrected} = [R_{Trial}]\left[R_{Reference}\right]^{-1}$$

Where: $R_{corrected}$ is the rotation tensor relative to the reference orientation.

R_{Trial} is the rotation tensor computed for a rigid body cluster relative to the global marker cluster.

$R_{Reference}$ is the rotation tensor computed for the calibration trial for a rigid body cluster relative to the global marker cluster.

With the corrected rotation tensor calculated, the vertebral joint angles are calculated next. These angles are defined as the relative orientation of one rigid body marker cluster relative to another. If the three rigid bodies on the specimen from superior to inferior are labelled 1 to 3 then:

$$R_{UpperJoint} = [R_2][R_1]^{-1}$$

$$R_{LowerJoint} = [R_3][R_2]^{-1}$$

Where: $R_{UpperJoint}$ is the rotation tensor of the upper vertebral joint (C3/C4).

$R_{LowerJoint}$ is the rotation tensor of the lower vertebral joint (C4/C5).

R_i is the corrected rotation tensor of rigid bodies 1-3.

With the rotation tensors of both vertebral joints calculated, angles can be extracted from the tensors based on a 2-dimensional rotation matrix where:

$$R = \begin{bmatrix} \cos\theta & -\sin\theta \\ \sin\theta & \cos\theta \end{bmatrix}$$

For the purposes of the discussed experiment, the vertebral joint angle (α) was extracted as follows:

$$\alpha = -\sin^{-1}(R_{12})$$

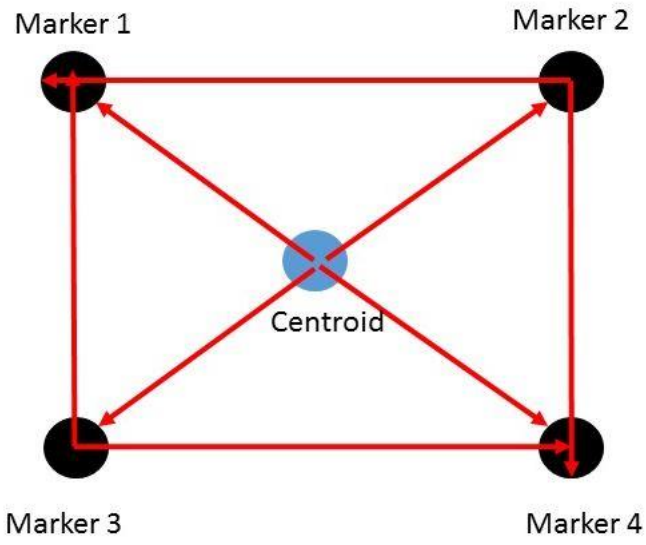

Figure 10.1 Schematic of vectors created using digitized marker locations. A centroid was calculated based on the points of all four markers, from here, eight vectors (denoted in red arrows) were created.

10.2 Assessment of Video Measurement System Accuracy

10.2.1 Experimental Setup

In order to assess the accuracy of using the outlined video measurement and marker digitization paradigm, the entire system was tested without a specimen under both static and dynamic conditions. Under these conditions, the motor arm of the Instron was assumed to

travel to the same target angles each time, so any deviation between trials of calculated angles via the video measurement system was presumed to be inherent error in this system.

Two sets of three trials were collected where the motor arm of the Instron was brought to target flexion and extension angles. The angular magnitude between both tracking sets was changed. Rigid bodies that were used for mounting on specimens were mounted on the superior and inferior steel mounting cups (same configuration as the specimen) while the central rigid body was mounted to a block of rubber (Figure 10.2). The superior rigid body moved with the motor arm while the remaining two rigid bodies remained stationary. Markers were digitized using commercial software (Maxtraq: Innovision Systems, Columbiaville, MI, USA) and angles computed using the procedure outlined in section 9.1.

A further three trials were collected with the same rigid body configuration, but in a purely static configuration. These trials were also digitized and angles computed using the procedure outlined in section 9.1.

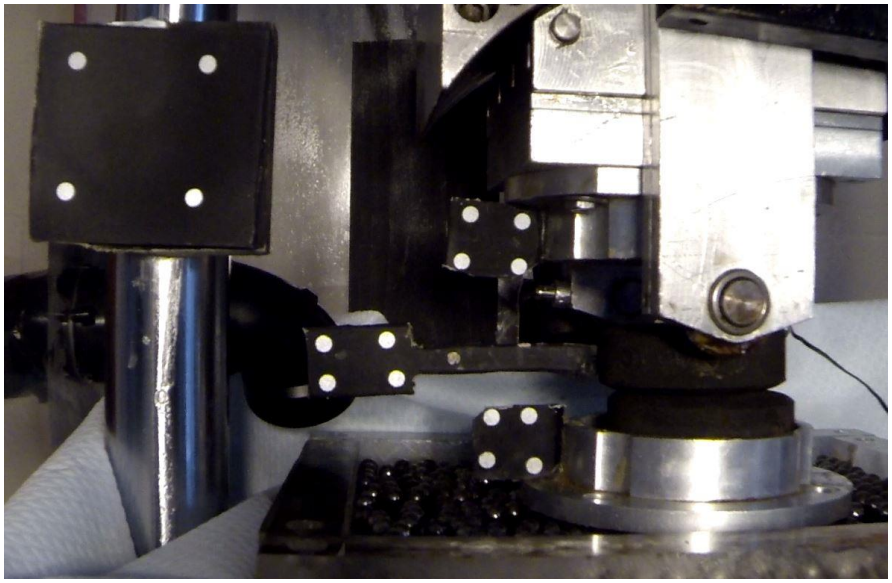

Figure 10.2 Rigid body placements for video measurement system evaluation. The lower two rigid bodies remained stationary while the uppermost rigid body was rotated by the Instron motor arm.

10.2.2 Results of Accuracy Tests

The maximum error was calculated as the discrepancy in the total angular magnitude between trials that were taken to identical flexion/extension angles. From this calculation the maximum error was found to be 0.35°. For the static trial and for the second series of flexion/extension trials, the maximum error calculated was lower (0.10° and 0.18° respectively).

Table 10.1. Maximum error calculated using video measurement system

	Flexion/Extension 1 (°)	**Flexion/Extension 2 (°)**	**Flexion/Extension 3 (°)**
Trial 1	21.02	26.52	0.08
Trial 2	21.20	26.17	0.10
Trial 3	21.08	26.49	0.07
Maximum error	**0.18**	**0.35**	**0.10**

Appendix C: Relative Angle Calculations for Coordinates and Instrumentation in Appendix A

Relative angles for the tracked vertebral bodies were calculated in a similar manner as in Appendix B. The equations used were identical to Appendix B, but the overall procedure had some slight differences which are outlined here. Further, the methods used to calculate the angles for the potentiometer and tracked lead markers are outlined in detail.

11.1 Tracked Vertebral Bodies

A rotation matrix and stretch tensor were calculated for each vertebra in each trial as outlined in Appendix B. In this case, the reference frame was defined simply as the first frame of coordinates for each vertebral body rather than being normalized to an arbitrary set of coordinates since relative angles between vertebral bodies were not calculated.

11.2 Potentiometer

Potentiometer data was synchronized with the video frames via a foot pedal that triggered collection of both systems. The potentiometer was collected and sampled at 300Hz. A linear calibration was performed to convert the raw voltage output into degrees. A static trial in a “flexed” position was taken at a known angle followed by a second static trial in an “extended” position. Another static trial at a neutral (zero) position was also taken. These values were used to generate a slope and y-intercept to create a linear equation in the form $y=mx+b$.

11.3 Tracked Lead Sphere Markers

Each vertebra had two lead markers rigidly fixed to the anterior portion of the vertebral body and the posterior aspect of the spinous process. The first frame in the image sequence was defined as the reference frame. For each frame, a midpoint was calculated from an average of all six marker positions and then six vectors were defined from the position of the midpoint to each lead marker on the spine specimen (Figure 11.1). The relative angle of the porcine specimen was then calculated using the least-squares calculation described in Appendix B creating a highly accurate angular displacement output. Using this method, the efficacy of the image distortion correction technique could also be tested. Since the decomposition of the deformation tensor yielded both a rotation and a stretch tensor, if there was still distortion present in the image, the stretch tensor would deviate from the identity matrix. In all frames, each cell of the stretch tensor was within 0.1 of the identity matrix.

11.4 Relative Joint Shear Calculations

Relative joint shear was calculated as the projection of two vectors on a shear axis oriented between the inferior aspect of the superior vertebral body and the superior aspect of the inferior vertebral body (mid-disc range). This followed the same method as Frobin and colleagues (Frobin et al., 1996).

Midpoints were calculated using the coordinates at the anterior and posterior aspects of the two vertebral bodies. Using the two midpoints, a vector was calculated that was defined as the shear axis, bisecting the two vertebral bodies. From here, center points were calculated for each of the vertebral bodies and the intervertebral disc space. Vectors were defined between the center points in the disc spaces and vertebral bodies Figure 11.2.

The projection of the vectors onto the shear axis was then calculated using the following formula (Figure 11.3):

$$a_1 = \overrightarrow{A} \cdot \hat{b}$$

Where: $\vec{A}$ is the vector between the disc space center point and the vertebral body center point.

$\hat{b}$ is the unit vector of the shear axis.

a_1 is the scalar projection of $\vec{A}$ onto $\hat{b}$.

From this, the vector $\vec{a}_1$ can be calculated by multiplying it by its scalar projection. The vector perpendicular to the shear axis can then be found by:

$$\vec{a}_2 = \overrightarrow{A} - \vec{a}_1$$

Following this, the distance between the two perpendicular vectors (one from the vertebra above, one from below) is calculated via:

$$Distance = \sqrt{(x_1 - x_2)^2 + (y_1 - y_2)^2}$$

The relative joint shear throughout the trial will then be the distance for each frame subtracted from the initial distance in the first frame.

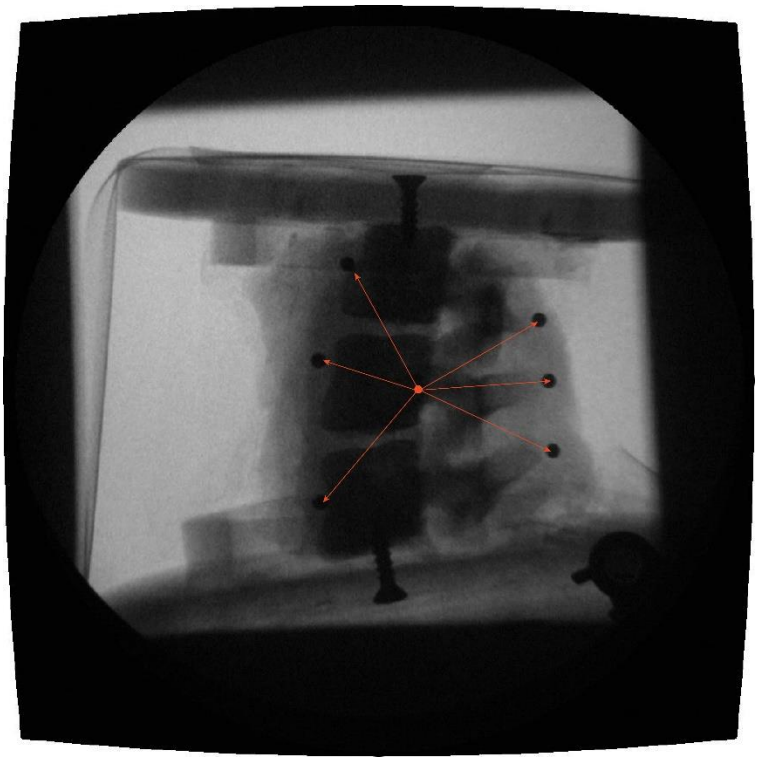

Figure 11.1 Six vectors were defined to act as inputs into the least-squares calculation for angular displacement

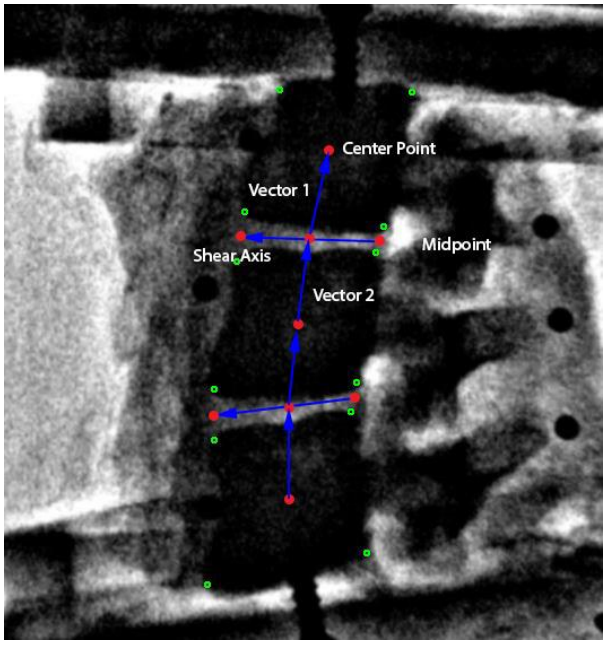

Figure 11.2 Setup of vectors and coordinates for the purposes of calculating relative joint shear. Shear was calculated by taking the difference between the projections of vector 1 and 2 onto a shear axis.

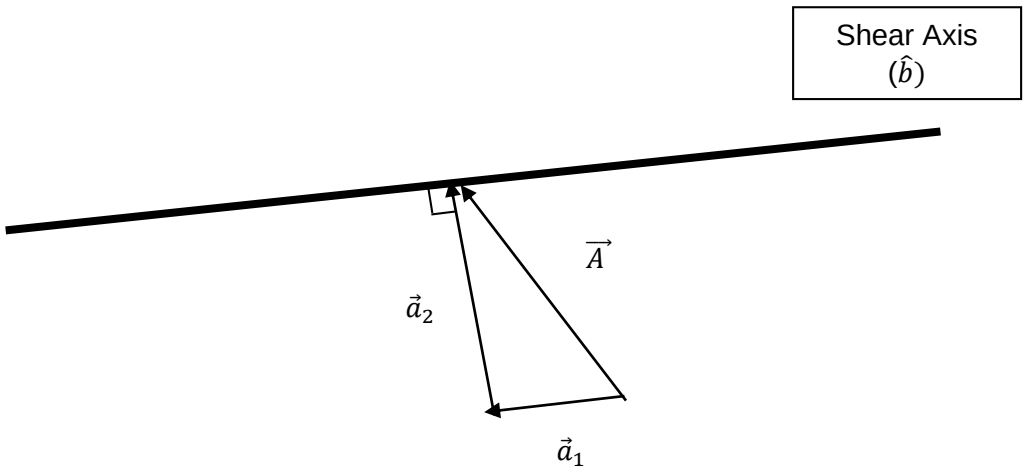

Figure 11.3 Setup of vectors for the purposes of calculating relative joint shear.

Appendix D: Patient Consent Form for Fluoroscopy Data Processing, Additional Patient Information, and Calculation of Disc Height Index

The following page contains a copy of the consent form signed by patients at the Markham Chiropractic Centre. This form allows for the use of patient data for research purposes. Additionally, a table is included below that provides more detailed background information for each patient. Detailed information on the calculation of disc height index is also included.

12.1 Additional Patient Information

Table 12.1. Summary of patient cases for Study 3.

Case	Age (Gender)	Complaint	Event Causing Complaint	Additional Information
DH1	50 (F)	Neck pain, headaches, seizure	Motor-vehicle accident (head on) causing loss of consciousness	History of low back pain
DH2	57 (F)	Left shoulder pain, headaches	Slip and fall	No history
DH3	68 (F)	Neck pain, headaches	Motor-vehicle accident (rear-ended)	No history
MH1	51 (F)	Neck pain	Hit by 10lb object, left sided head injury causing concussion	No history
MH2	58 (M)	Neck pain, headaches	Motor-vehicle accident (rear-ended)	No history
MH3	58 (F)	Neck pain, headaches	Motor-vehicle accident (left-front impact) causing loss of consciousness	No history

MH4	54 (F)	Neck pain, headaches	Motor-vehicle accident (rear-ended) causing loss of consciousness	Previous history of plane crash with facial surgery
MH5	29 (F)	Neck pain, rib fracture, headaches	Motor-vehicle accident (head-on)	No history
MH6	39 (M)	Fracture of C0, C1, C4, Loss of consciousness	Motor-vehicle accident (rollover) causing loss of consciousness	No history
MH7	45 (M)	Neck pain, headaches, shoulder pain	Motor-vehicle accident (rear-ended)	No history
MH8	35 (F)	Neck pain, headaches	Motor-vehicle accident (rear-ended)	No history
NH1	53 (M)	Neck pain, headaches	Train crash causing loss of consciousness	No history
NH2	41 (F)	Neck pain, headaches	Motor-vehicle accident (rear-ended)	No history
NH3	42 (M)	Neck pain, headaches	Motor-vehicle accident (rollover) causing loss of consciousness	No history
NH4	39 (M)	Neck pain, headaches	Motor-vehicle accident (rear-ended)	No history
NH5	40 (F)	Neck pain, headaches	Motor-vehicle accident (right-front impact)	No history
NH6	42 (M)	Neck pain, low-back pain, headaches	Motor-vehicle accident (rear-ended)	No history
NH7	25 (M)	Neck pain, headaches	Assault with head strikes	No history
NH8	57 (F)	Neck pain, headaches	Motor-vehicle accident (head-on) causing loss of consciousness	No history
NH9	45 (F)	Headaches	Motor-vehicle accident (head-on) causing loss of consciousness	No history

12.2 Calculation of Disc Height Index

Disc height index was calculated using the method of Frobin and colleagues (2002). The anterior and posterior margins of each vertebra were digitized for a single frame where the patient was in a neutral posture. From this, the distance between anterior points on adjacent vertebrae was used to calculate anterior disc height using the following formula:

$$distance = \sqrt{(x_2 - x_1)^2 + (y_2 - y_1)^2}$$

The same formula was used to calculate the posterior disc height. From this, the average of the anterior and posterior disc heights was calculated to generate a single value of height for each disc. Vertebra height was calculated in the same manner as disc height (anterior and posterior portions) using the distance formula above. From the anterior and posterior vertebra heights, a single average value was calculated for each vertebra. Another average was calculated for the purposes of disc height index calculation. For a given disc, the average vertebra height between its superior and inferior disc was calculated. From here, disc height index was calculated by dividing the disc height by the average height of its superior and inferior vertebrae.

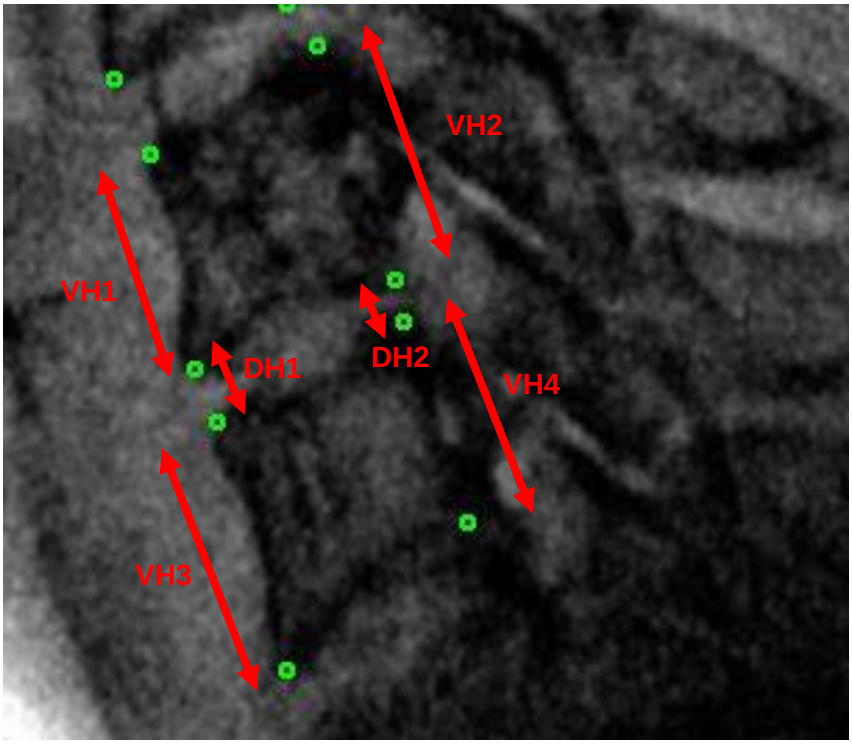

Figure 12.1 Relevant measures for disc height index calculation. Vertebral body heights (VH) were averaged to create a single value and then disc heights (DH) values were averaged to calculate a single value. Disc height was divided by vertebral body height to yield disc height index.

.D.I.O.

Diagnostic Services
369 Main Street North, Markham, ON L3P 1Z3
TEL: (905) 294-6000 FAX: (905) 294-6009

Radiographic Analysis Requisition Form

Patient Name: (Last name) _____ (First name) _____

Birth Date: m ___ d ___ y ___ **Phone:** (___) ___ (___) ___

Address: _____ **City:** _____ **Postal Code:** _____

Marital Status: S M D W **Sex:** M F **Are you employed?** Y N **Have you returned to work?** Y N

***Date of Loss:** m ___ d ___ y ___ **Policy No:** _____ **Claim No:** _____ *

This section must be completed, signed by the patient and witnessed:

❑ Please invoice me directly for your report. ❑ Please invoice my insurer directly for your report

I understand that the motor vehicle accident insurance claim noted above is based upon a contractual agreement between the insurance carrier and myself. I understand that A.D.I.O. Diagnostic Services will prepare any necessary reports and forms to assist me in making collection from the insurance company. However, I clearly understand and agree that all services are rendered on my behalf and are charged to me directly and that I am personally responsible for payment for services rendered by A.D.I.O. Diagnostic Services. I will verify that all accounts in favour of A.D.I.O. Diagnostic Services have been paid prior to giving final release of this claim, or I shall honour this account from direct proceeds of settlement and herein give my legal representative(s) good and sufficient direction to settle A.D.I.O. Diagnostic Services unpaid accounts out of proceeds of settlement of the above noted claim. I give A.D.I.O. Diagnostic Services my consent to have access to my personal information and distribute any part of it as they may deem to be necessary from time to time in support of my claim or my best interests. Furthermore, I hereby authorize A.D.I.O. Diagnostic Services to utilize the data from this assessment in studies which will result in publication in peer reviewed literature with the provision that my identity will be protected and will not appear in any article submitted for peer review.

Patient Signature: _____ **Date:** m ___ d ___ y ___ **Witness:** _____

Adjuster: _____ **Company:** _____ **Phone:**(___) ___-____

Address: _____ **City:** _____ **Postal Code:** _____ **Fax :**(___) ___-____

Doctor: _____ **DC** ❑ **MD** ❑ **Other** ❑ **Phone:**(___) ___-____

Address: _____ **City:** _____ **Prov:** ____ **Postal Code:** ____

Other Doctor/Rehab: _____ **DC** ❑ **MD** ❑ **Other** ❑ **Phone:**(___) ___-____

Address: _____ **City:** _____ **Prov:** ____ **Postal Code:** _____

Direction and Certificate

Please provide: ❑ **Digital Radiographic Analysis** ❑ **Verbal Report of Findings ASAP**

I hereby certify that this service is a reasonable and necessary expense for this patient's rehabilitation.

Signature: _____ **Date:** _____

Figure 12.2 Patient consent form for fluoroscopic imaging

Appendix E: Research Experiences at the University of Bristol

13.1 Research

During the course of my PhD training, I was afforded the opportunity to spend six months working with Dr. Michael Adams and Dr. Patricia Dolan at the University of Bristol. During this time, I was able to work with cadaveric spine specimens on a research project that involved identifying the weak point of the intervertebral disc in tension. Two papers were published as a result of this work: (Lama et al., 2014, Balkovec et al., 2015). To summarize the findings, when the intervertebral disc is placed in tension, the failure point is nearly always at the interface between the hyaline cartilage and subchondral bone (Figure 13.1). Cartilage fragments were also found in nearly half of the samples taken from herniated disc material. Removing hyaline cartilage from bone has implications with respect to the internal pressurization of the intervertebral disc as well as modic change and infection, this is also a likely mechanism for cartilage fragments ending up in herniated disc material in some cases of disc herniation. Cartilage fragments in herniated disc material have implications with respect to the spontaneous resorption of disc herniations. As these fragments do not swell or readily lose proteoglycans, they may persist for much longer compared to nucleus pulposus, resulting in a prolonging of symptoms.

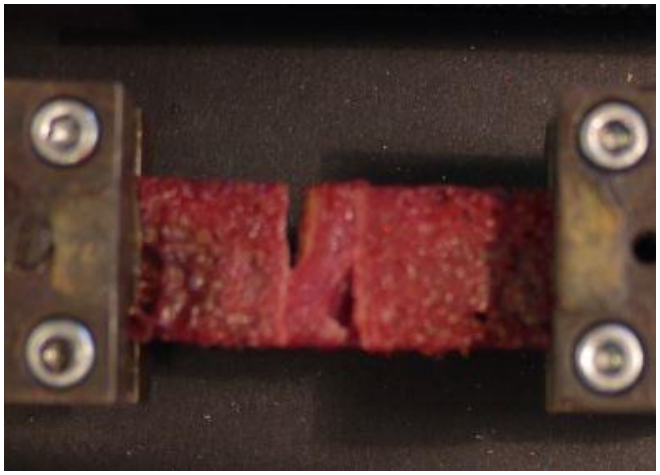

Figure 13.1 Typical failure location of the disc in tension. Hyaline cartilage is peeled off of the subchondral bone.

13.2 Observations and Comparisons between Cadaveric and Porcine Spines

Firsthand work using cadaveric spines allows for some interesting comparisons to be drawn between elderly cadaveric lumbar spines and juvenile porcine cervical spines. There are several notable differences between the two, but overall, both appear relatively similar. Porcine cervical spines have large anterior processes that articulate with processes on adjacent vertebral bodies and serve as attachment points for muscle (Figure 13.2). Human lumbar spines are also larger in size overall compared to porcine cervical spines; while there are individual differences, generally, porcine cervical spines are approximately two-thirds the size of human lumbar spines. Trabecular bone structure within the vertebral bodies of both porcine and human spines vary markedly from each other. Young porcine cervical spines are densely packed with trabecular bone to the point where it is almost difficult to see spacing between individual trabeculae with the naked eye (Figure 13.3). Elderly cadaver spines on the other hand, have significantly lower density trabecular bone structure (Figure 13.4).

Figure 13.2 Vertebral body structure of porcine cervical spine. Porcine cervical spines have large anterior processes, contrary to human lumbar spines.

Figure 13.3 Dense trabecular bone structure on a porcine cervical spine.

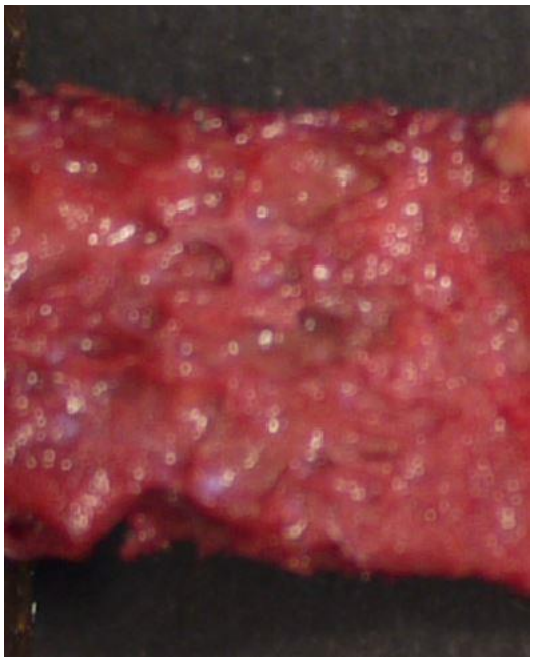

Figure 13.4 Elderly cadaver trabecular bone structure. The trabeculae are less densely packed compared to porcine cervical spines.

Examining the discs of porcine and cadaver spines reveals large differences. Adolescent porcine cervical spines contain a pristine annulus with no visible fissures or defects, it is white in appearance and clearly separate from the central nucleus pulposus. The nucleus pulposus itself is gelatinous and highly hydrated, it is in optimal condition to distribute load evenly between neighboring vertebral bodies. Elderly cadaver discs are less hydrated and more fibrotic compared to porcine cervical spines. They have an annulus that is usually yellow or brown in appearance, and forms less of a distinct border with the nucleus pulposus; this is a result of the aging process. Differences between juvenile porcine and elderly cadaver discs are outlined in (Figure 13.5).

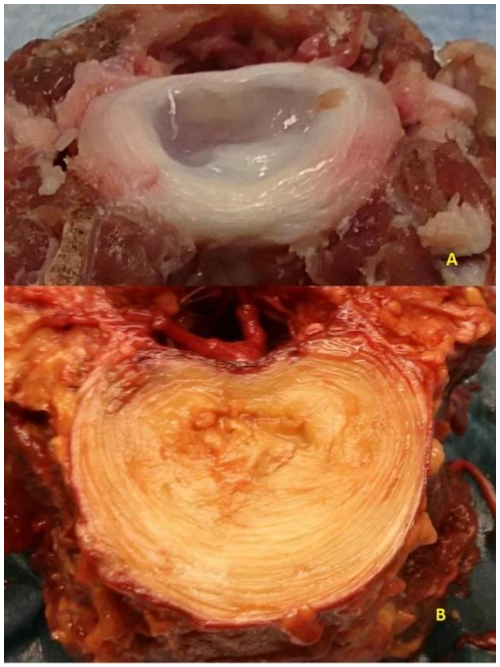

Figure 13.5 A. Porcine cervical disc highlighting the hydrated, gelatinous nucleus and clear distinction between nucleus and annulus. B. Elderly cadaver disc outlining the much more fibrotic nucleus and less clear distinction between nuclear and annular regions.

Differences between porcine cervical spines and elderly cadaveric lumbar spines are important factors to consider when deciding which is most appropriate for use in a given study. Use of cadaver spines provides the validity of a human model as opposed to approximating the anatomical and biological structures with an animal model. It is important to consider however, that a cadaver spine is an approximation as well, and the properties of an elderly spine may not match those of someone who is younger or even middle-aged. Porcine cervical spines can be thought of as the other end of the spectrum, and more closely resemble the spine of an adolescent human with respect to the mechanical properties of the intervertebral disc.

An advantage of porcine cervical spines over cadaveric lumbar spines is the greater level of control due to specimen homogeneity. Factors such as age, weight, diet, and genetics can all be accounted for with porcine spines, whereas cadaver spines are much more heterogeneous. Porcine spines are also much easier to obtain in larger quantities; cadaver spines are simply not as readily available. The porcine spine is thus a good model to use in lieu

of a readily available source of homogeneous cadaveric spines. Porcine spines are an excellent model for basic science research in the mechanical properties of the spine. Their homogeneity ensures high levels of control that eliminate confounding factors when attempting to determine the effect or mechanism of an intervention. Cadaver spines provide researchers with the ability to continue on where an animal model leaves off and begins to add further validity of a human model for a research study.

The advantages, disadvantages, and differences of porcine and cadaver spines in research must be clearly thought out by the researcher prior to determining the best option for a particular study. When used together, both porcine and cadaver spines present the ability to gain more insightful conclusions regarding the functioning and properties of the spine. Performing research with human spines at the University of Bristol has provided the insight necessary to know when using a porcine model is a good approximation of how a human spine will function and when it would be best to revisit the research study with a cadaver specimen. It has also facilitated in developing the expertise to dissect and properly mount these specimens for mechanical testing. Comfort and knowledge of both human and animal models for tissue testing will help to facilitate future projects and ultimately lead to higher quality research and collaborations.

Appendix F: Use of the Servohydraulic Testing Apparatus with Multi-Segmented Spine Specimens

Use of the Instron servohydraulic testing apparatus with multiple segment specimens results in changes to the loading applied to each segment specifically. The following discussion attempts to explain and account for the forces and moments occurring at each of the segments during testing. First, the observed motions are presented in images of an actual test specimen and an accompanying schematic diagram. Following this, the free body diagrams for the schematics are presented. After the diagrams have been described, a sensitivity analysis is performed that attempts to provide estimated moment values for each of the segments in each of the postures as well as upper and lower bounds of applied moments to the specimens.

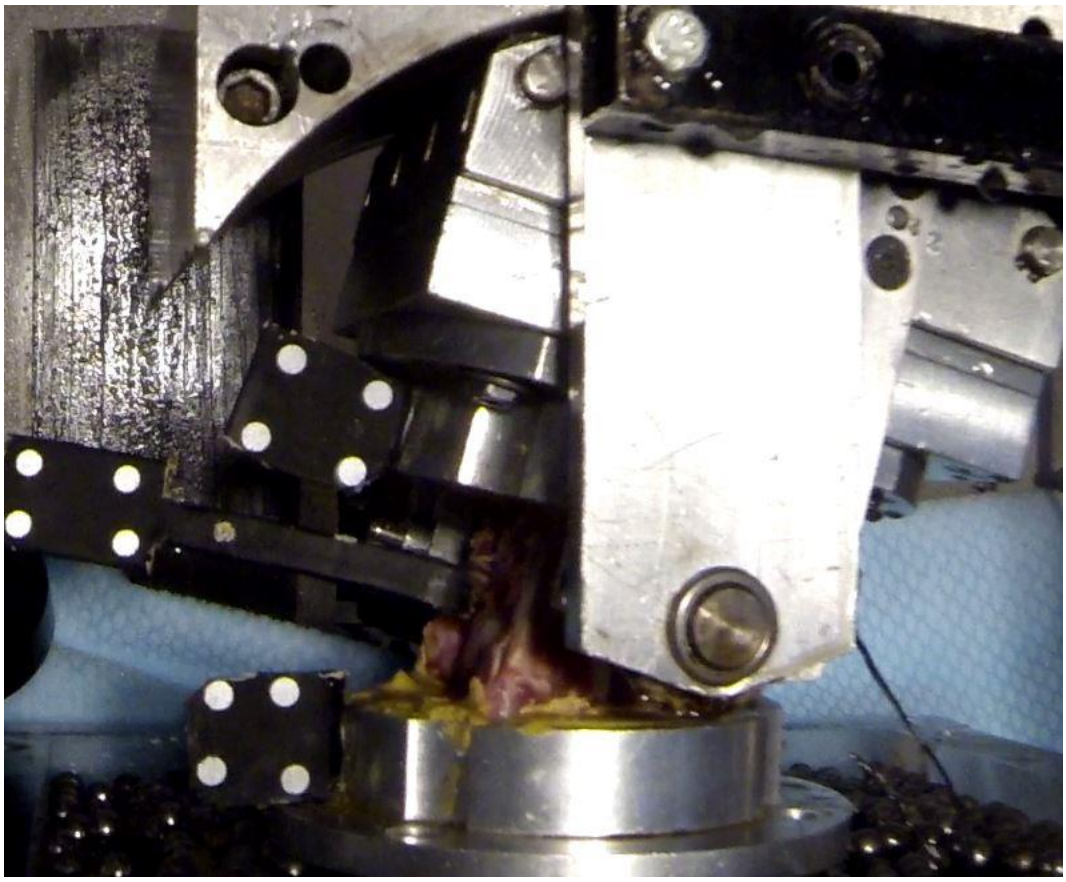

Figure 14.1 Starting neutral configuration of the multi-segmented specimen. The lordotic posture was reflective of the same posture *in-vivo*.

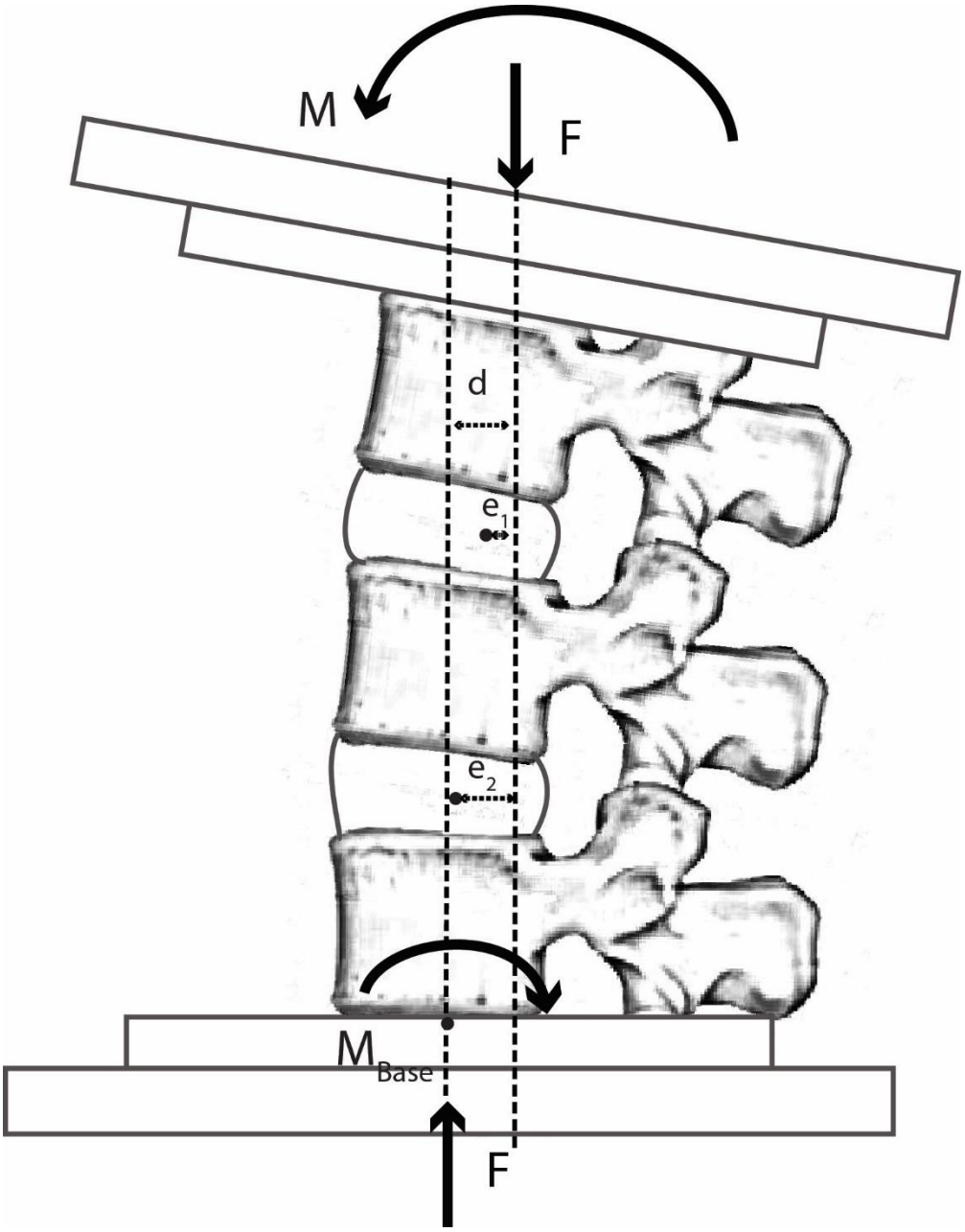

Figure 14.2 Schematic of the starting neutral posture for the multi-segmented specimen. Due to the force application at the center of the superior mounting cup, bending moments were applied at the upper and lower segment. The moment at the base is a function of the moment applied by the motor arm and the bending moment created by the applied compressive force. The initial stiffness of the specimen required a high rate of torque application from the motor to overcome the bending moment being applied, following this, the rate of torque application decreased. Motion was observed to occur only about the upper segment initially.

Terms for Figure 14.2 are defined as follows:

'M' is the moment applied by the motor arm.

'F' is the vertically applied force of the hydraulic ram.

'M_{Base}' is the moment applied at the base.

'd' is the horizontal distance between the vertically applied force from the hydraulic ram at the top of the specimen and the center of the lower mounting cup.

'e_1' is the distance from the vertically applied force from the hydraulic ram and the center of rotation of the upper disc (also assumed to be the fulcrum of the segment).

'e_2' is the distance from the vertically applied force from the hydraulic ram and the center of rotation of the lower disc (also assumed to be the fulcrum of the segment).

Centers of rotation of each joint (also assumed to be the fulcrum of each segment) are defined by the circular black dots.

The neutral posture as determined using the point where there was zero moment applied to the specimen put the specimens in a lordotic position (Figure 14.1). The vertically applied force from the hydraulic ram was assumed to be applied at the center of the superior mounting cup. The opposing force from the lower specimen mounting cup was assumed to be applied at the center of the inferior mounting cup. Under the 1000N compressive load, and the lordotic posture adopted by the specimen, it was assumed that the center of rotation for the superior segment was positioned closer to the applied force compared to the lower segment. Under this, the bending moment generated about the lower segment will be greater than the bending moment generated about the upper segment since $e_2 > e_1$ (Figure 14.2). Thus, rotation will occur about the upper segment initially (and was observed to be the case). The point where rotation stopped about the upper segment and commenced about the lower

segment is the point where the superior mounting cup was perpendicular to the applied force from the ram.

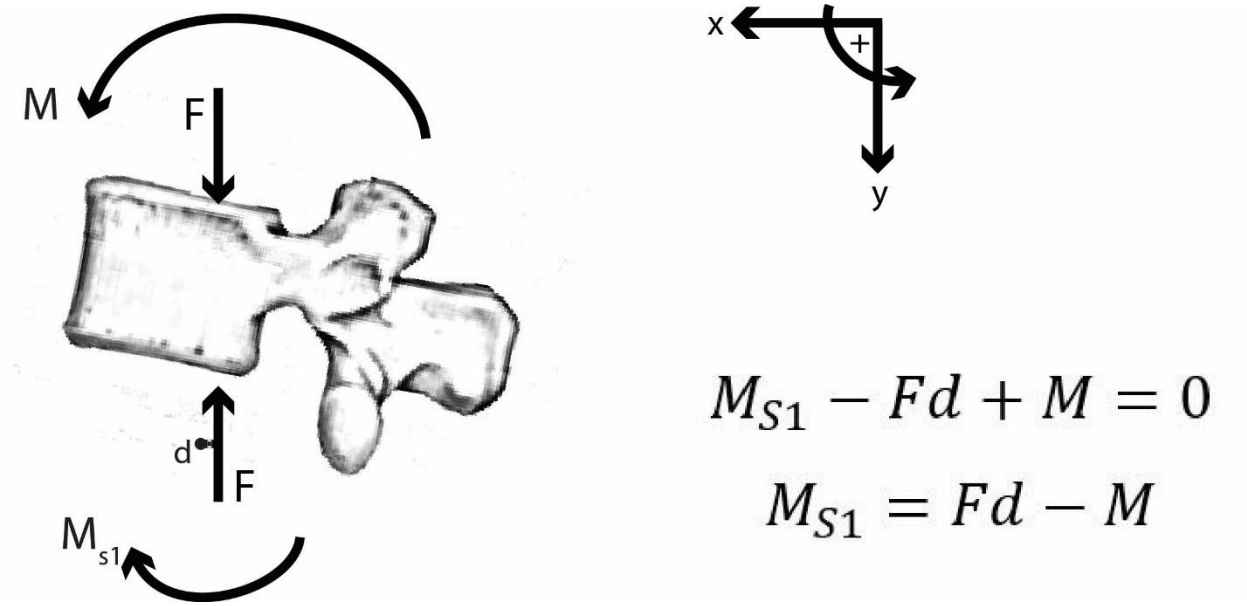

Figure 14.3 Free-body diagram of the superior vertebral body in the starting neutral configuration. A small bending moment is applied to this vertebra along with the moment from the motor arm and resisted by a support-moment (M_{S1}).

Terms for Figure 14.3 are defined as follows:

'M' is the moment applied by the motor arm.

'F' is the vertically applied force of the hydraulic ram.

'M_{S1}' is the support moment from the resistance to rotation of the passive tissues.

'd' is the horizontal distance between the vertically applied force from the hydraulic ram and the fulcrum about which the vertebra rotates.

The center of rotation of the vertebra (also assumed to be the fulcrum) is defined by the circular black dot.

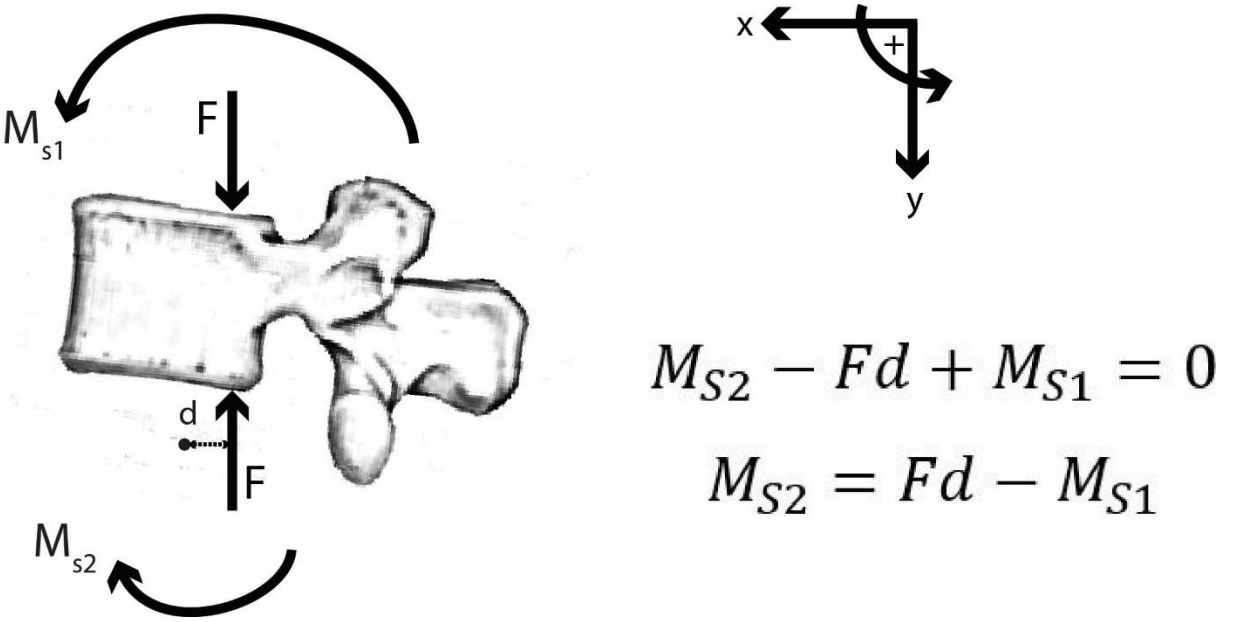

Figure 14.4 Free-body diagram of the middle vertebral body in the starting neutral configuration. The bending moment applied to this vertebra is assumed to be larger than the one applied to the vertebra above given the observed motion of the whole specimen.

Terms for Figure 14.4 are defined as follows:

'M_{S1}' is the moment applied by the superior vertebra.

'F' is the vertically applied force from the superior vertebra.

'M_{S2}' is the support moment from the resistance to rotation of the passive tissues.

'd' is the horizontal distance between the vertically applied force from the hydraulic ram and the fulcrum about which the vertebra rotates.

The center of rotation of the vertebra (also assumed to be the fulcrum) is defined by the circular black dot.

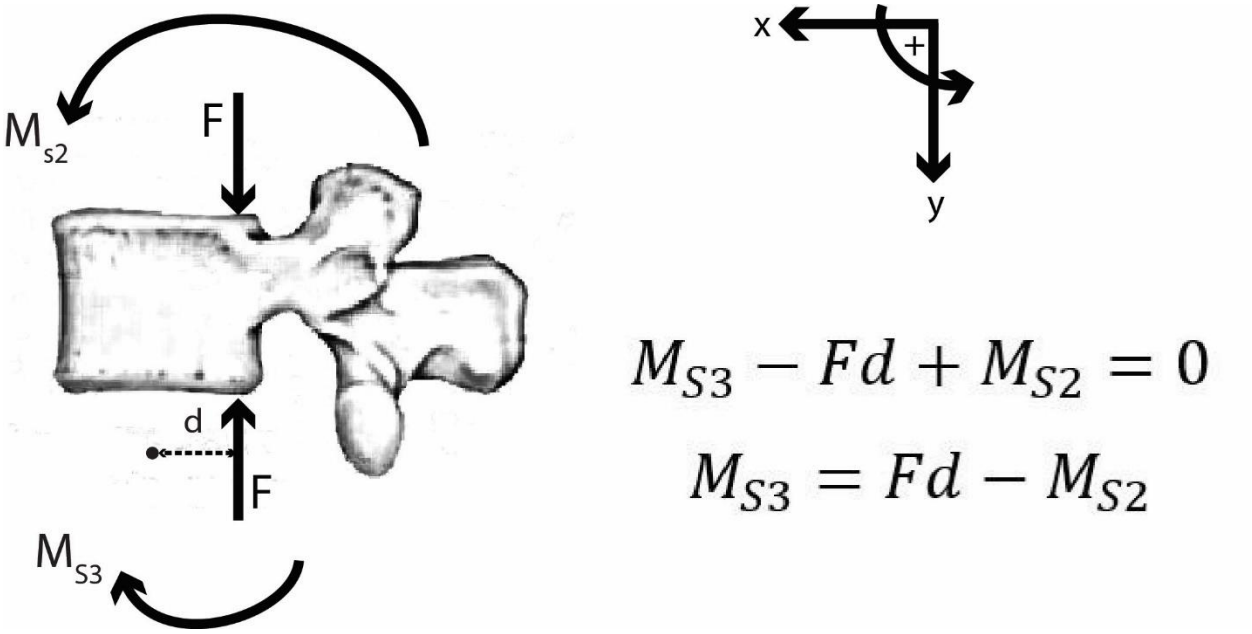

Figure 14.5 Free-body diagram of the lower vertebral body in the starting neutral configuration. The bending moment applied to this vertebra is the largest and is resisted by the bearing tray.

Terms for Figure 14.5 are defined as follows:

'M_{S2}' is the moment applied by the superior vertebra.

'F' is the vertically applied force from the superior vertebra.

'M_{S3}' is the support moment from the resistance to rotation of the passive tissues.

'd' is the horizontal distance between the vertically applied force from the hydraulic ram and the fulcrum about which the vertebra rotates.

The center of rotation of the vertebra (also assumed to be the fulcrum) is defined by the circular black dot.

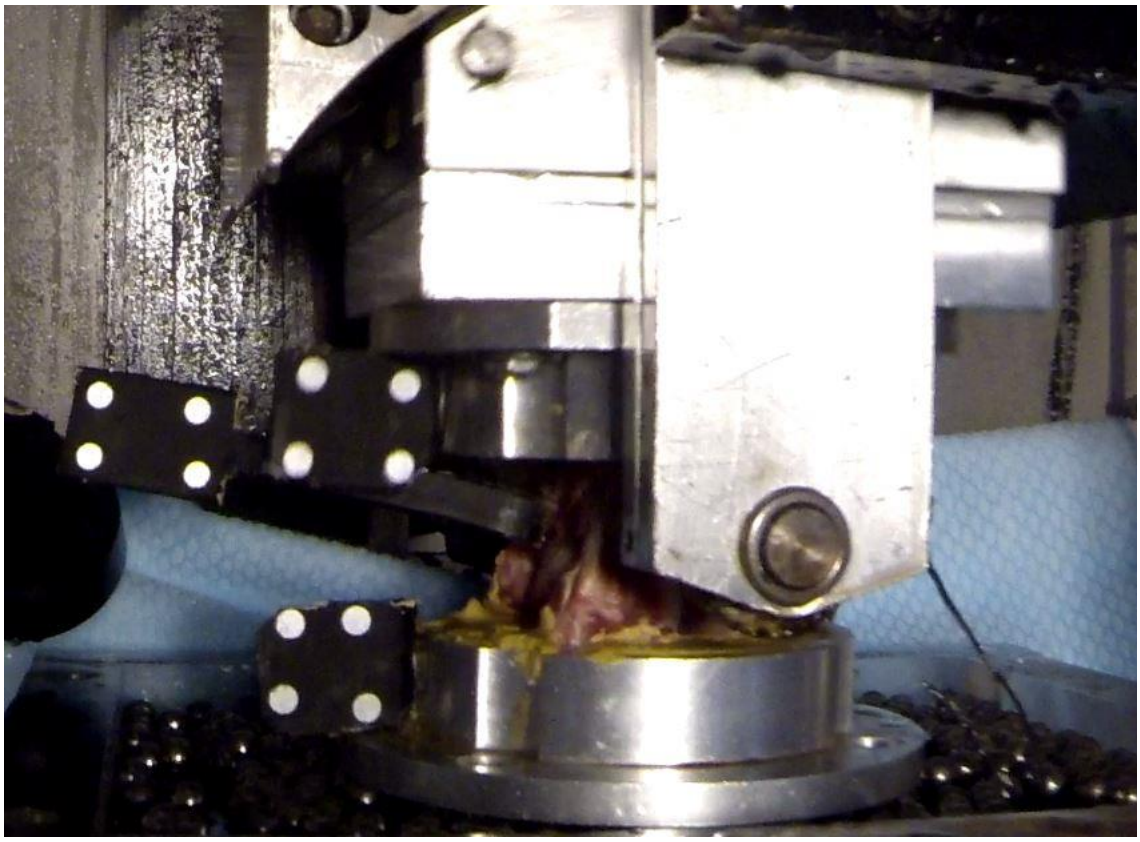

Figure 14.6 Changing point between rotation of the upper segment and lower segment. At this point, where the applied compressive force is perpendicular to the specimen mounting cups, rotation stopped about the upper segment and commenced about the lower segment. Up until this point, no translation had occurred at the base.

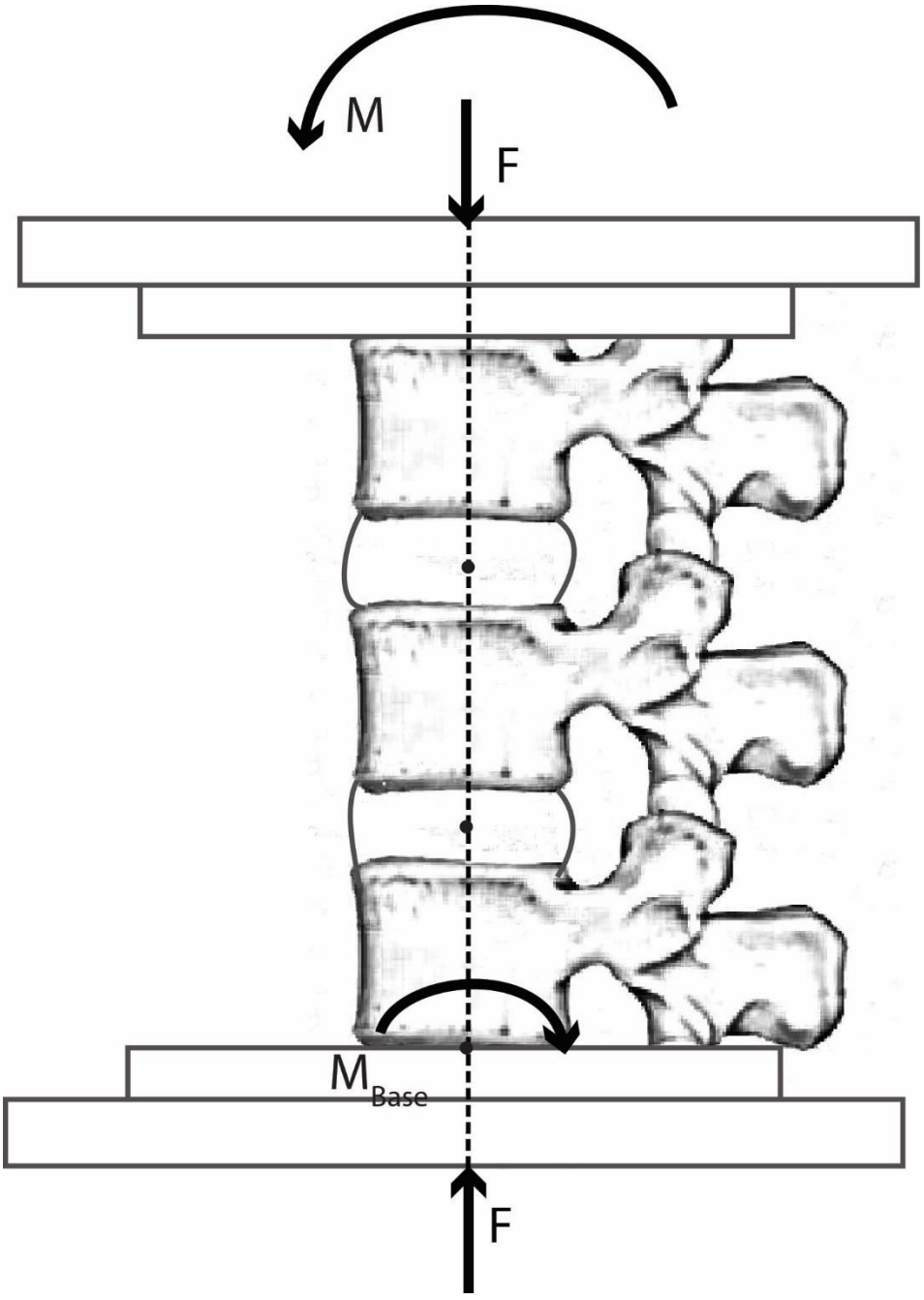

Figure 14.7 Schematic of the changing point for rotation at the upper and lower segments. At this point, the transmissible vector of the applied force is assumed to go through the centers of rotation between the upper and lower discs. From this configuration, no bending moments are applied to the segments. Given that the upper segment has been rotating up until this point while the lower segment has not, stiffness would be greater at this segment compared to the lower segment, thus, rotation commences about the lower segment.

Terms for Figure 14.7 are defined as follows:

'M' is the moment applied by the motor arm.

'F' is the vertically applied force of the hydraulic ram.

'M_{Base}' is the moment applied at the base.

Centers of rotation of each joint (also assumed to be the fulcrum of each segment) are defined by the circular black dots.

Rotation occurred about the upper segment without any translation at the base. In the configuration depicted in Figure 14.6 and Figure 14.7, the centers of rotation of both the upper and lower segments were assumed to be aligned and both mounting cups were perpendicular to the applied force from the hydraulic ram. In this configuration, no bending moments were assumed to be applied at either level. From this position onwards, rotation occurred about the lower segment.

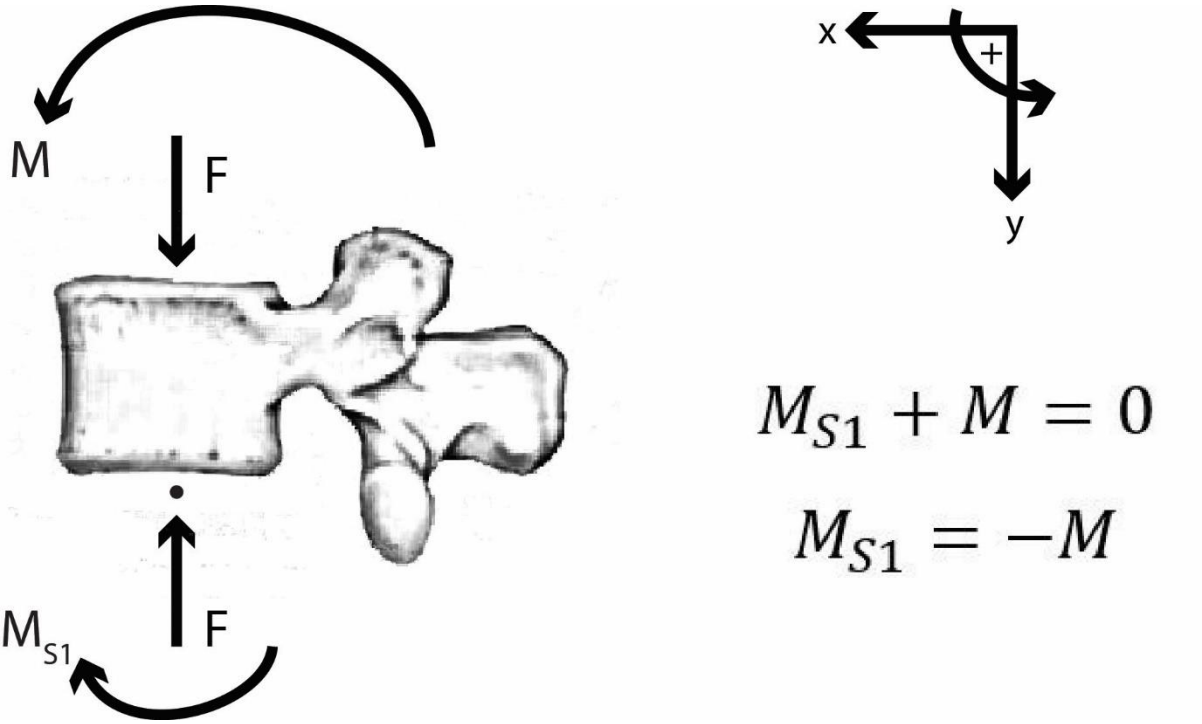

Figure 14.8 Free-body diagram of the superior vertebral body in the changing point for segmental rotation. The support-moment is a result of the moment applied by the motor arm as no bending moment is applied by the hydraulic ram in this configuration.

Terms for Figure 14.8 are defined as follows:

'M' is the moment applied by the motor arm.

'F' is the vertically applied force of the hydraulic ram.

'M_{S1}' is the support moment from the resistance to rotation of the passive tissues.

The center of rotation of the vertebra (also assumed to be the fulcrum) is defined by the circular black dot.

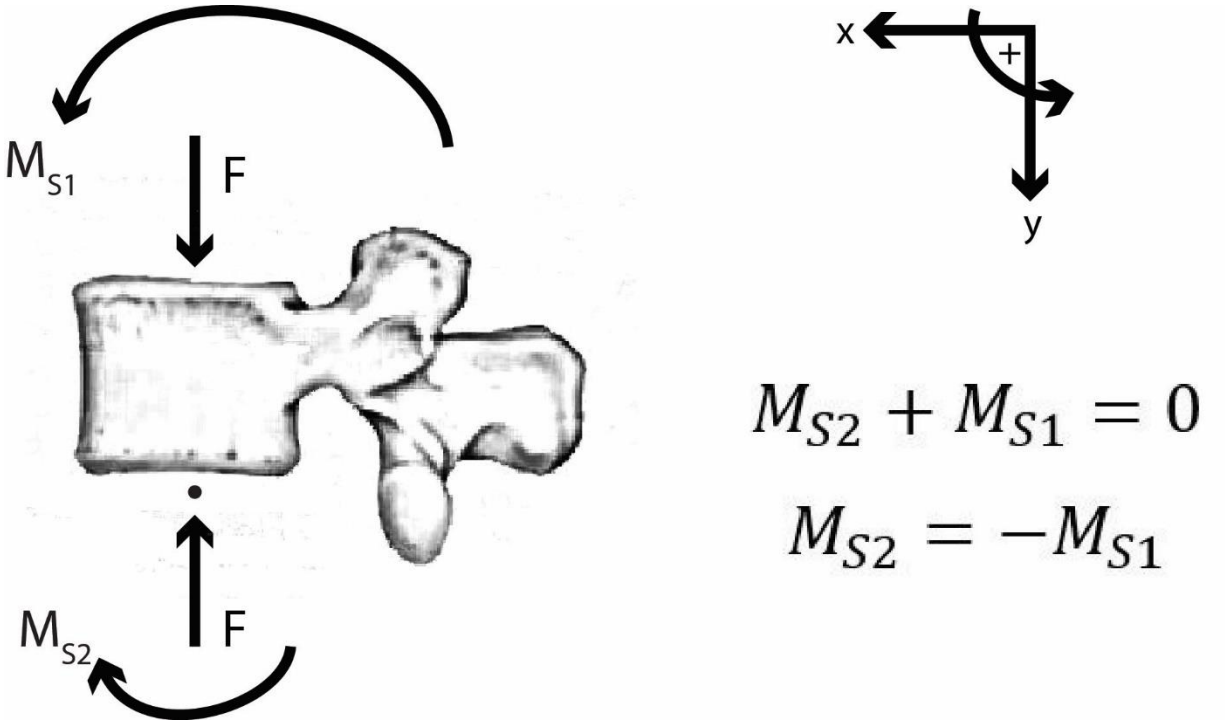

Figure 14.9 Free-body diagram of the middle vertebral body in the changing point for segmental rotation. There is no applied bending moment.

Terms for Figure 14.9 are defined as follows:

'M_{S1}' is the moment applied by the superior vertebra.

'F' is the vertically applied force from the superior vertebra.

'M_{S2}' is the support moment from the resistance to rotation of the passive tissues.

The center of rotation of the vertebra (also assumed to be the fulcrum) is defined by the circular black dot.

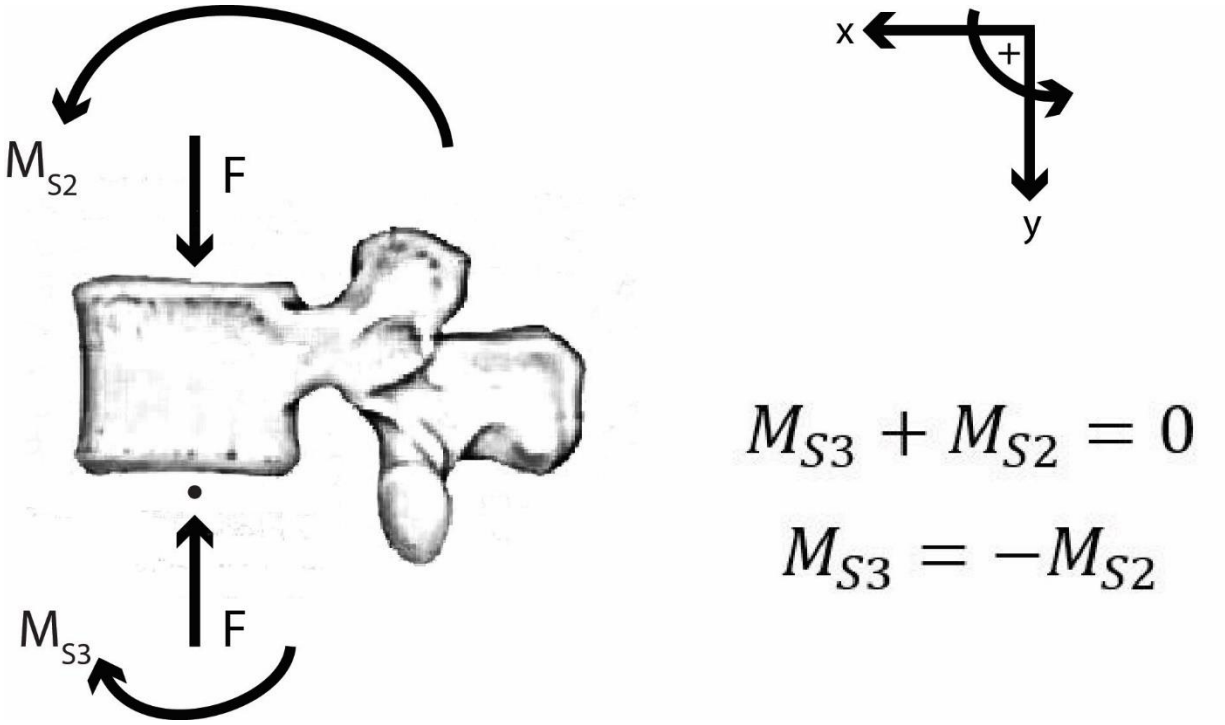

Figure 14.10 Free-body diagram of the lower vertebral body in the changing point for segmental rotation. There is no applied bending moment.

Terms for Figure 14.10 are defined as follows:

'M_{S2}' is the moment applied by the superior vertebra.

'F' is the vertically applied force from the superior vertebra.

'M_{S3}' is the support moment from the resistance to rotation of the passive tissues.

The center of rotation of the vertebra (also assumed to be the fulcrum) is defined by the circular black dot.

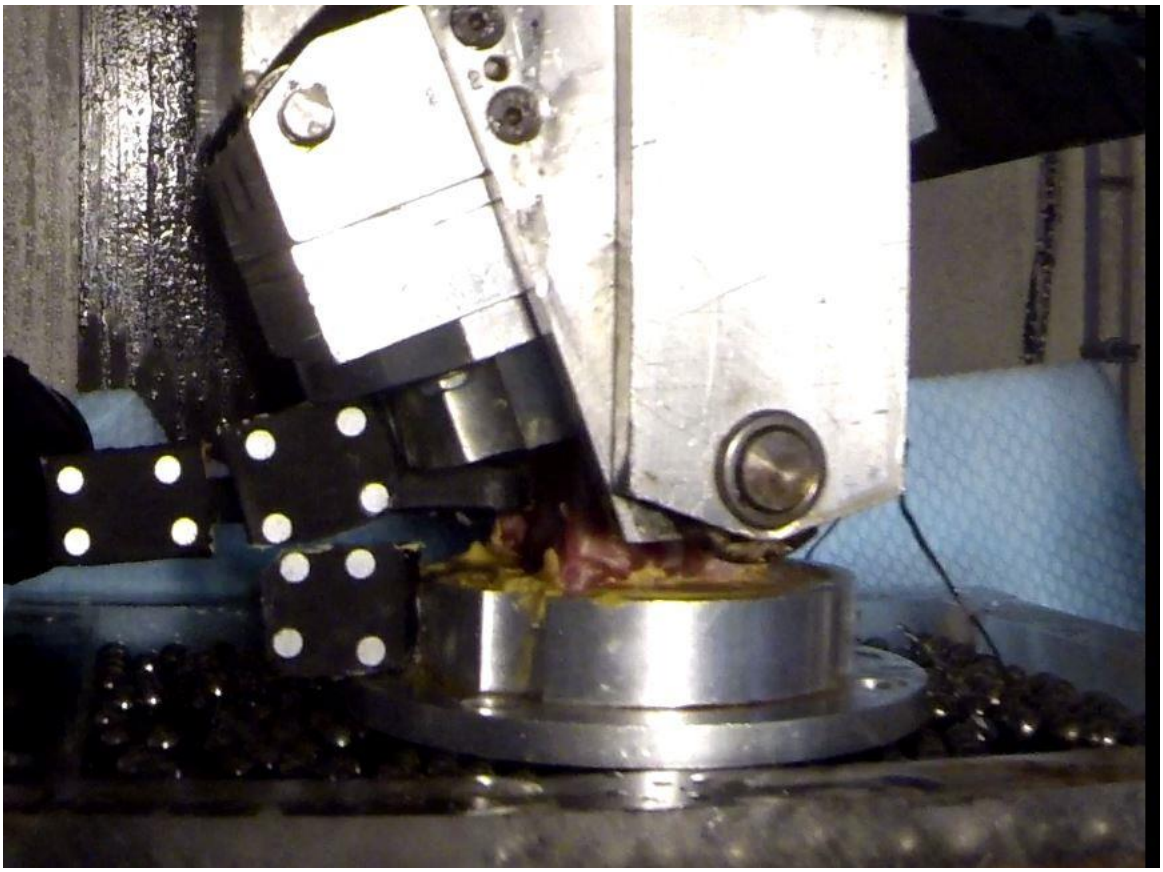

Figure 14.11 Fully flexed position of the specimen. Between the previous configuration (applied force perpendicular to mounting cups) and this position, translation of the specimen had occurred, resulting in the application of bending moments to each of the segments from the applied compressive force.

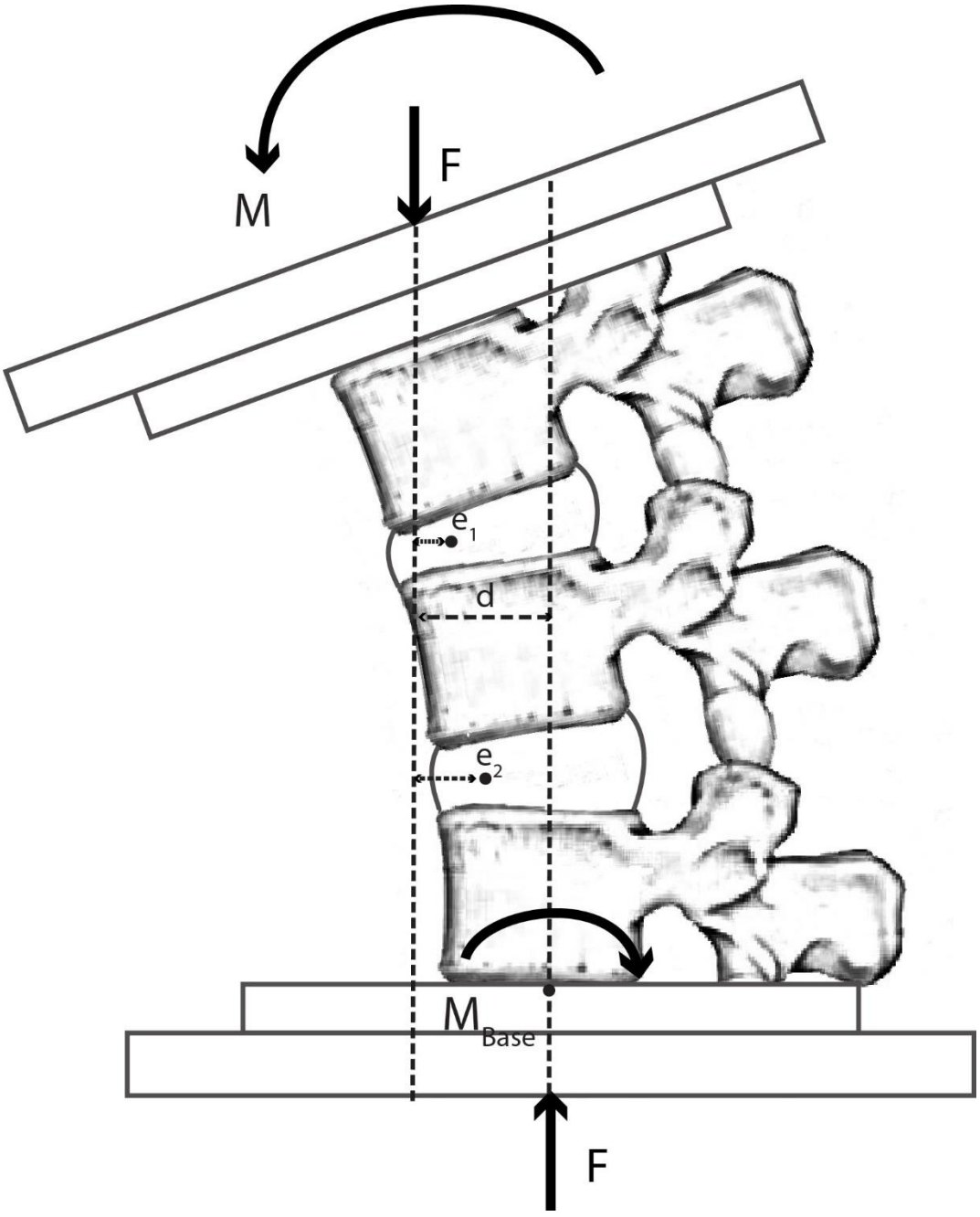

Figure 14.12 Schematic of the fully flexed position of the specimen. Bending moments were applied to each of the segments with the greater bending moment being applied at the lower segment. The cumulative moment applied at any given point varied, with the lower-bound being the moment applied by the motor arm at the superior segment and the upper-bound being moment at the base of the specimen. Thus, the applied moment increased further down the specimen towards the bearing tray.

Terms for Figure 14.12 are defined as follows:

'M' is the moment applied by the motor arm.

'F' is the vertically applied force of the hydraulic ram.

'M_{Base}' is the moment applied at the base.

'd' is the horizontal distance between the vertically applied force from the hydraulic ram at the top of the specimen and the center of the lower mounting cup.

'e_1' is the distance from the vertically applied force from the hydraulic ram and the center of rotation of the upper disc (also assumed to be the fulcrum of the segment).

'e_2' is the distance from the vertically applied force from the hydraulic ram and the center of rotation of the lower disc (also assumed to be the fulcrum of the segment).

Centers of rotation of each joint (also assumed to be the fulcrum of each segment) are defined by the circular black dots.

At the point of full-flexion, the specimen had translated a total distance (d) which resulted in bending moments being applied at the upper and lower segments. From the position described in Figure 14.6 and Figure 14.7, rotation occurred about the lower segment since the bending moment applied to the lower segment was greater given that $e_2 > e_1$.

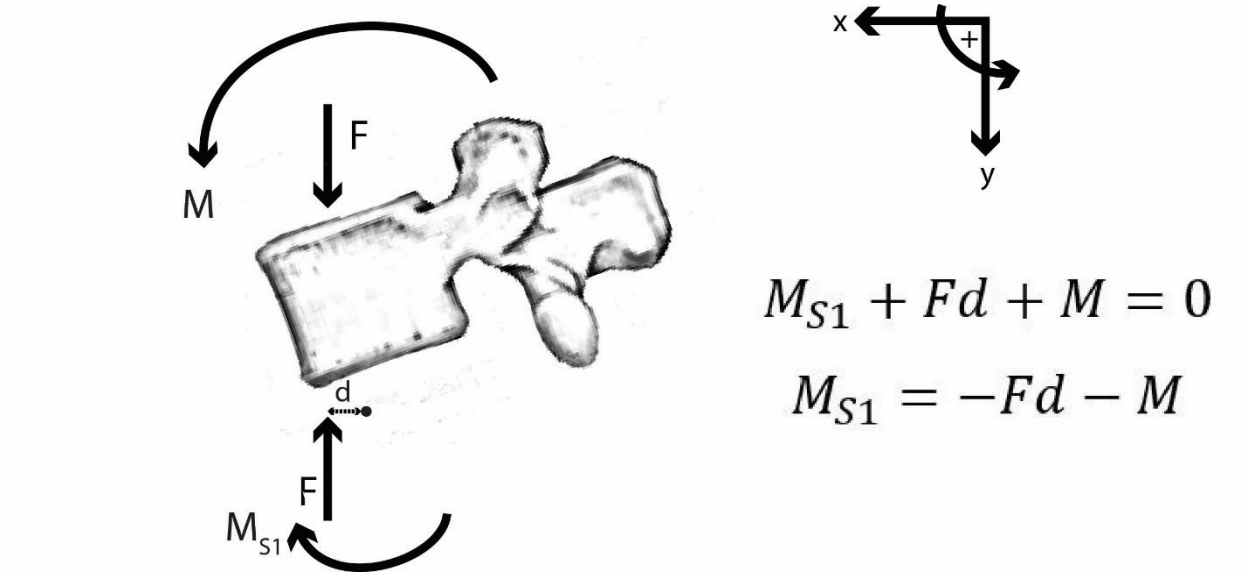

Figure 14.13Free-body diagram of the superior vertebral body in the fully-flexed configuration. A small bending moment is applied to this vertebra along with the moment from the motor arm and resisted by a support-moment (M_{S1}).

Terms for Figure 14.13 are defined as follows:

'M' is the moment applied by the motor arm.

'F' is the vertically applied force of the hydraulic ram.

'M_{S1}' is the support moment from the resistance to rotation of the passive tissues.

'd' is the horizontal distance between the vertically applied force from the hydraulic ram and the fulcrum about which the vertebra rotates.

The center of rotation of the vertebra (also assumed to be the fulcrum) is defined by the circular black dot.

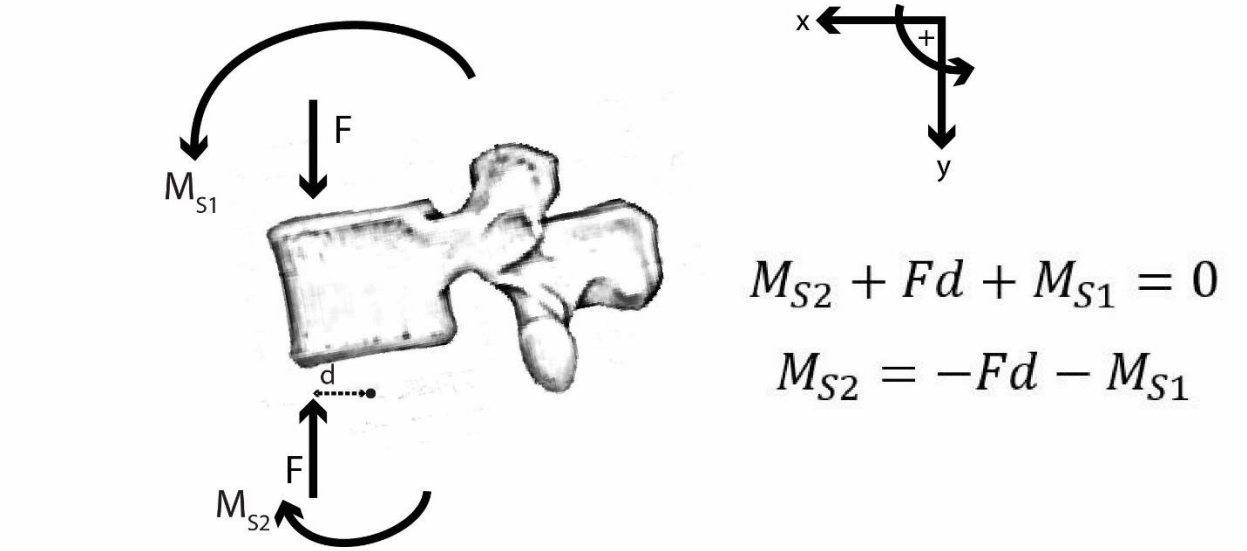

Figure 14.14Free-body diagram of the middle vertebral body in the fully-flexed configuration. The bending moment applied to this vertebra is larger than the bending moment applied to the vertebra above.

Terms for Figure 14.14 are defined as follows:

'M_{S1}' is the moment applied by the superior vertebra.

'F' is the vertically applied force from the superior vertebra.

'M_{S2}' is the support moment from the resistance to rotation of the passive tissues.

'd' is the horizontal distance between the vertically applied force from the hydraulic ram and the fulcrum about which the vertebra rotates.

The center of rotation of the vertebra (also assumed to be the fulcrum) is defined by the circular black dot.

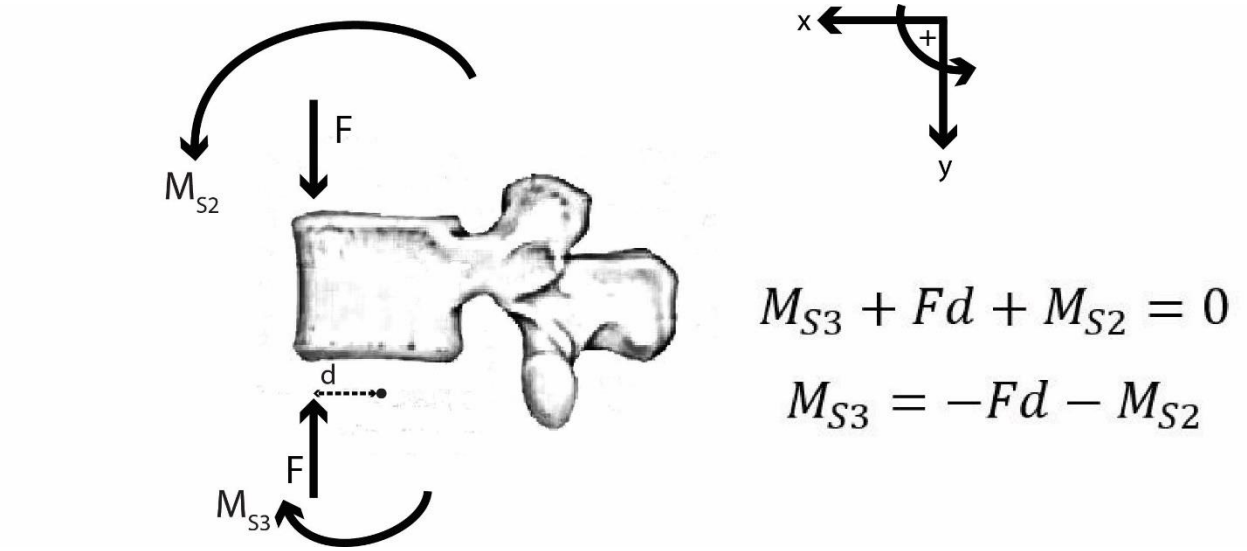

Figure 14.15 Free-body diagram of the lower vertebral body in the fully-flexed configuration. The bending moment applied to this vertebra is the largest and is resisted by the bearing tray.

Terms for Figure 14.15 are defined as follows:

'M_{S2}' is the moment applied by the superior vertebra.

'F' is the vertically applied force from the superior vertebra.

'M_{S3}' is the support moment from the resistance to rotation of the passive tissues.

'd' is the horizontal distance between the vertically applied force from the hydraulic ram and the fulcrum about which the vertebra rotates.

The center of rotation of the vertebra (also assumed to be the fulcrum) is defined by the circular black dot.

The total moment applied at each segment will be somewhere between the moment applied by the motor arm at the top of the segment and the moment at the base of the lower mounting cup. For Figure 14.2, the moment at the base can be described with the following equation:

$$M_{Base} - Fd + M = 0$$

$$M_{Base} = Fd - M$$

To get a sense of the moment at the base during full flexion, values have been substituted into the above equation:

$$M_{Base} = (1000N)(0.0035m) - (-1.5Nm)$$

$$M_{Base} = 5Nm$$

Thus, the applied moments at each of the segments during full-flexion are assumed to be between the lower-bound of -1.5Nm and the upper-bound of -5Nm. The moment at any arbitrary point (M_{Point}) on the specimen can be described with the above equation as well and used to estimate moments at each of the vertebral joints as follows:

$$M_{Point} = Fe - M$$

Estimated values for 'e' for the upper segment and lower segment are 1mm and 3mm, respectively. Thus, the estimated support moments at the upper and lower segments are calculated by:

$$M_{UpperSegment} = (1000N)(0.001m) - (-1.5Nm)$$

$$M_{UpperSegment} = 2.5Nm$$

$$M_{LowerSegment} = (1000N)(0.003m) - (-1.5Nm)$$

$$M_{LowerSegment} = 4.5Nm$$

Therefore, the estimated support moments at the upper and lower segments in the starting configuration are 2.5Nm and 4.5Nm respectively.

For Figure 14.7, the moment at the base can be described with the following equation:

$$M_{Base} + M = 0$$

$$M_{Base} = -M$$

To get a sense of the moment at the base during full flexion, values have been substituted into the above equation:

$$M_{Base} = -9Nm$$

Thus, the applied moments at each of the segments during full-flexion are assumed to be equal, at approximately 9Nm. This configuration is unique, in that the moment at each of the segments is assumed to be equivalent to the moment applied by the motor arm, as there is assumed to be no applied bending moment.

For Figure 14.12, the moment at the base can be described using the following equation:

$$M_{Base} + Fd + M = 0$$

$$M_{Base} = -Fd - M$$

To get a sense of the moment at the base during full flexion, values have been substituted into the above equation:

$$M_{Base} = -(1000N)(0.0075m) - 15Nm$$

$$M_{Base} = -22.5Nm$$

Thus, the applied moments at each of the segments during full-flexion are assumed to be between the lower-bound of 15Nm and the upper-bound of 22.5Nm. As in Figure 14.2, the moment at any arbitrary point (M_{Point}) on the specimen can be described with the above equation as well and used to estimate moments at each of the vertebral joints as follows:

$$M_{Point} = -Fe - M$$

Estimated values for ‘e’ for the upper segment and lower segment are 2mm and 5mm, respectively. Thus, the estimated support moments at the upper and lower segments are calculated by:

$$M_{UpperSegment} = -(1000N)(0.002m) - (15Nm)$$

$$M_{UpperSegment} = -17Nm$$

$$M_{LowerSegment} = -(1000N)(0.005m) - (15Nm)$$

$$M_{LowerSegment} = -20Nm$$

Therefore, the estimated support moments at the upper and lower segments in the starting configuration are -17Nm and -20Nm respectively.

While the different moments at each level is a limitation of the test setup, this is not necessarily contrary to what occurs *in-vivo*. Unequal moments at each segment would occur as an individual flexes forward and there is a gravitational loading of the torso. The translating base is representative of the free-floating body *in-vivo* and this horizontal movement in the test apparatus is what creates a moment arm for the applied compressive force. The applied compressive force is representative of the gravitational loading that would occur from body parts above the spine-segment together with muscle and passive-tissue tensions required to hold the quasi-static body posture. This vector follows the principle of transmissibility such that it moves anterior to the lower segments when flexed creating a larger flexion bending moment.

A further complicating factor neglected by the above diagrams is that the intervertebral discs positioned between the rigid vertebral bodies are deformable. It is plausible that there is an applied moment initially to the upper vertebra but no applied moment to the next lower vertebra until rotation occurs. The bending disc then applies the moment onto the next vertebra. If buckling had occurred at lower segments, and especially the floating middle vertebra, there would be rotation at that level prior to rotation at the superior segment. This was not found to be the case during the experimental protocol as motion was observed to be

stepwise, where rotation occurred first about the upper segment, and then about the lower segment.

In Study 1, the observed kinematics were a function of the applied forces and moment to each of the segments as well as the changing stiffness of discs being bent, compressed, and injured. When stiffness increases at a local level, more rotation will occur about a more compliant level. In the case of Study 1, loss of disc height increased the local stiffness of the injured disc, and so more motion occurred about the level that had not been injured (and was more compliant). Position control was used in Study 1, under this, a higher moment is applied to achieve the same position. Were torque control used, the overall moment applied would be the same, but less motion would have occurred. Thus, the results from Study 1 are only applicable when going to the same target angle.

The observed results from Study 1 are applicable only during certain loading paradigms. Given the use of position control, an equivalent *in-vivo* scenario would occur when an individual flexes their spine to the same target angle. A further limitation is the infinite stiffness created at the interface between the bearing tray and the bottom cup (no rotation can occur about this point). There are many more segmental levels *in-vivo* in addition to joints outside the spine where compensation can occur during a position controlled movement. It is uncertain if the movement behaviour that occurred in Study 1 would be identical to that seen *in-vivo.*

Appendix G: Patient Image Sequence Vertebral Body Tracking for Appendix A

This section contains all time history images for the patient image sequence tracking from Appendix A. In this study, three patient image sequences were selected. Each of these sequences was tracked ten times using the vertebral body tracking algorithm. The average of all ten sets of coordinates was taken and the angular displacement and shear outputs for each trial was compared with the average. Each patient image sequence tracked 5 vertebral bodies, yielding 5 sets of angular displacement data and 4 sets of relative joint shear data for each image sequence. In many of the shear displacement time-histories there is what appears to be non-physiologic rapid shearing within the first several frames. This was due to some of the templates rapidly moving as they initially began to track vertebral body motion. Following this initial movement, the algorithm easily steadied its tracking of the respective templates and the non-physiologic representation of segment movement was removed. As a result of this, the first several frames of shear displacement are not considered part of the physiologic analysis but are presented here for completeness.

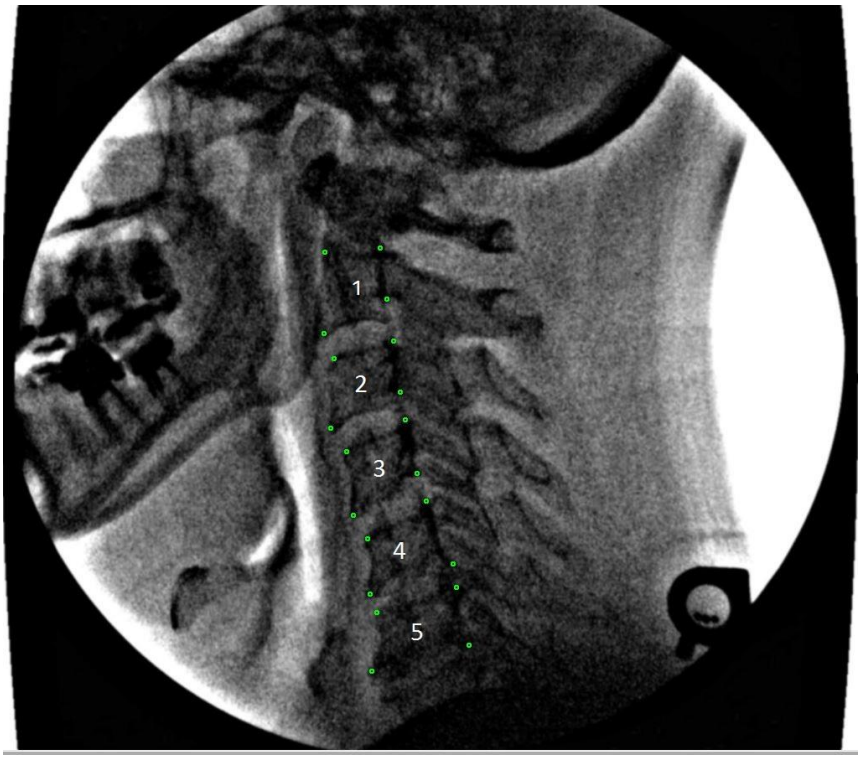

Figure 15.1 Vertebral body naming system for the first image sequence.

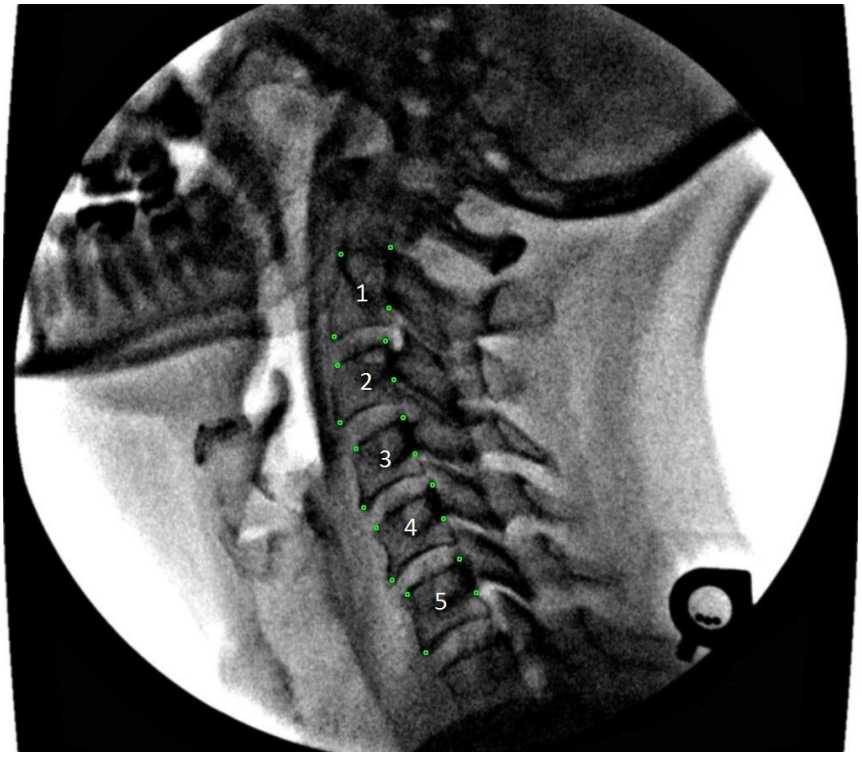

Figure 15.2 Vertebral body naming system for the second image sequence.

Figure 15.3 Vertebral body naming system for the third image sequence.

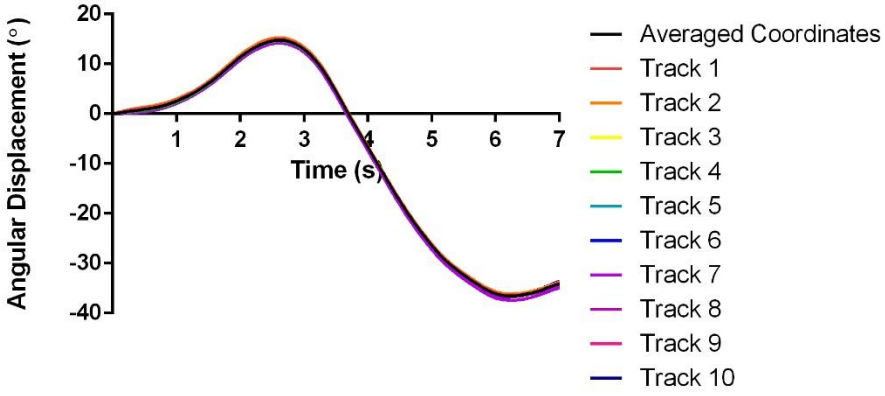

Figure 15.4 Image sequence 1 vertebral body 1.

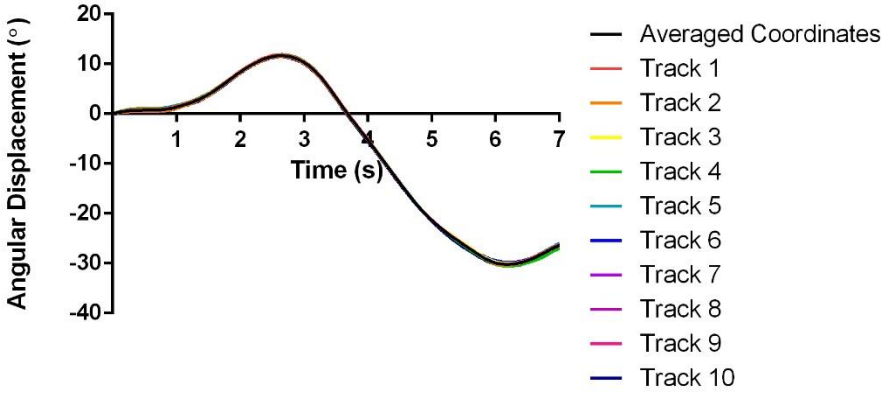

Figure 15.5 Image sequence 1 vertebral body 2.

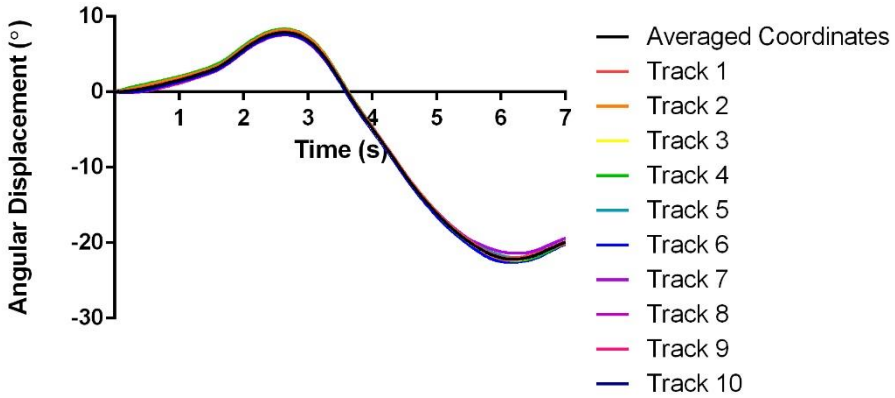

Figure 15.6 Image sequence 1 vertebral body 3.

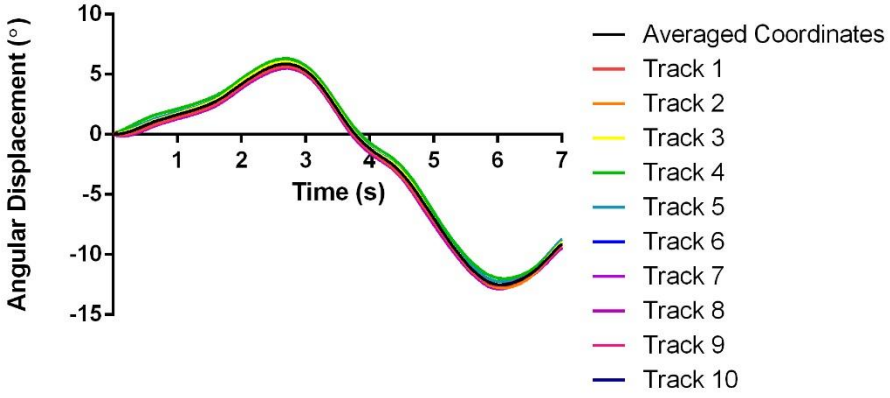

Figure 15.7 Image sequence 1 vertebral body 4.

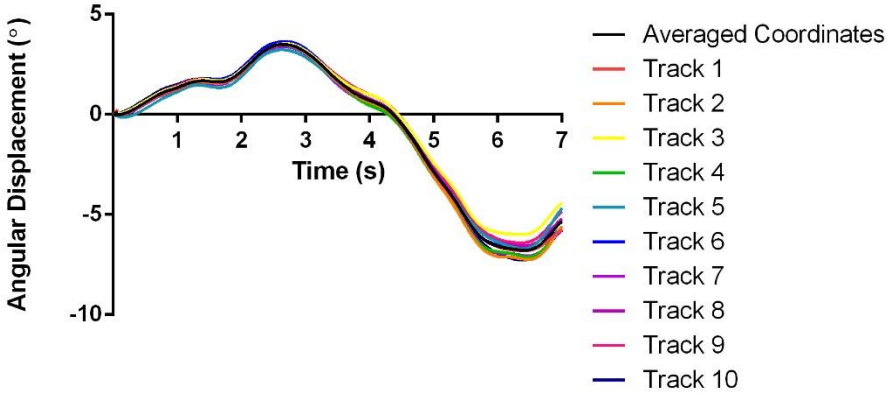

Figure 15.8 Image sequence 1 vertebral body 5.

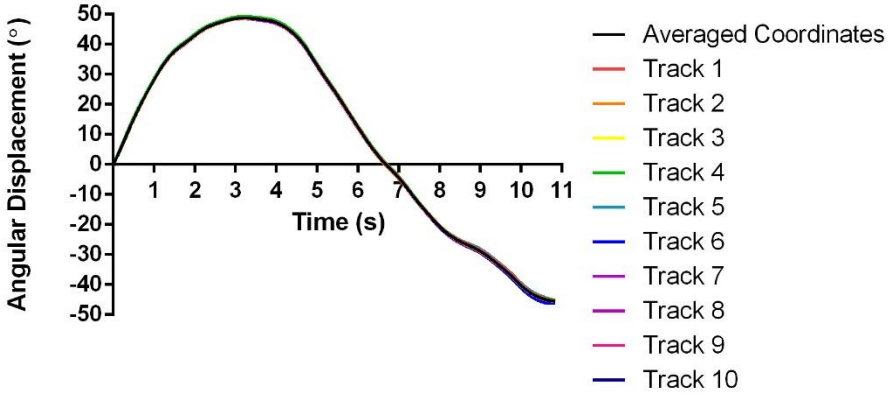

Figure 15.9 Image sequence 2 vertebral body 1.

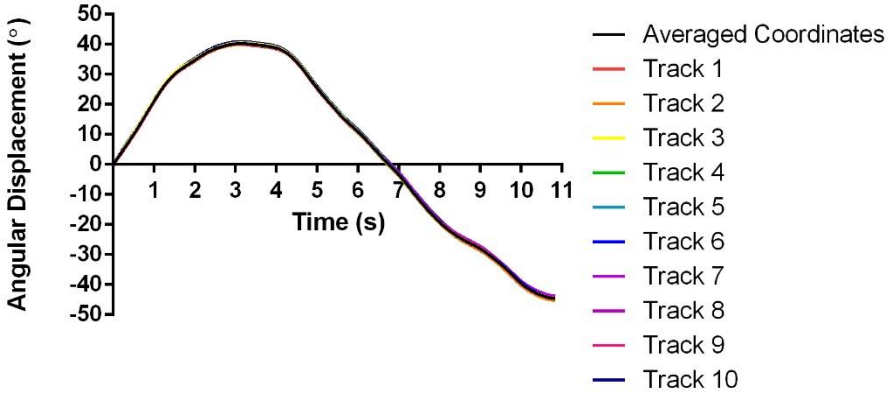

Figure 15.10 Image sequence 2 vertebral body 2.

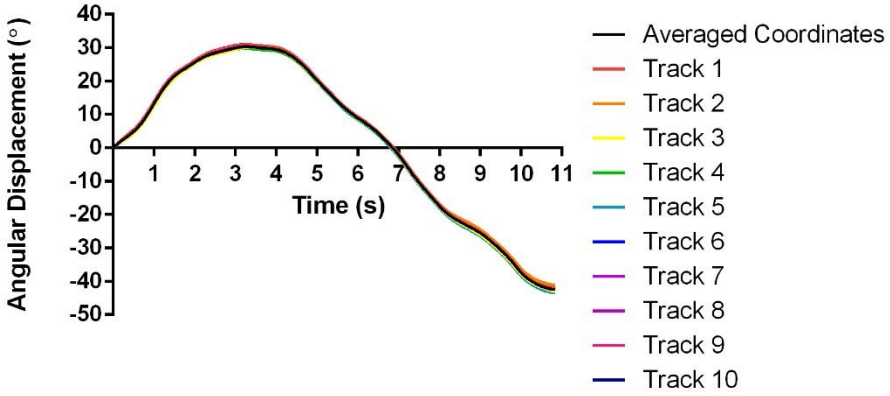

Figure 15.11 Image sequence 2 vertebral body 3.

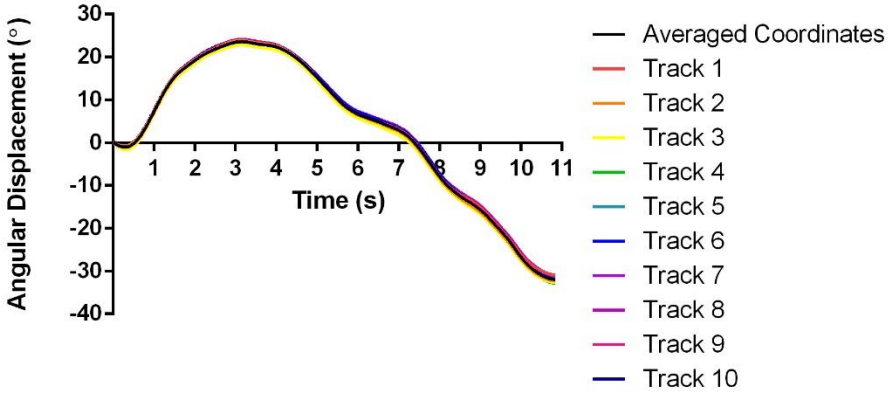

Figure 15.12 Image sequence 2 vertebral body 4.

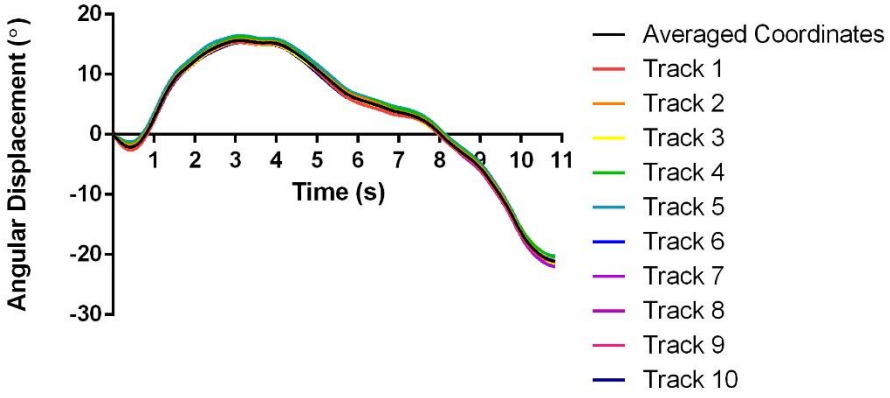

Figure 15.13 Image sequence 2 vertebral body 5.

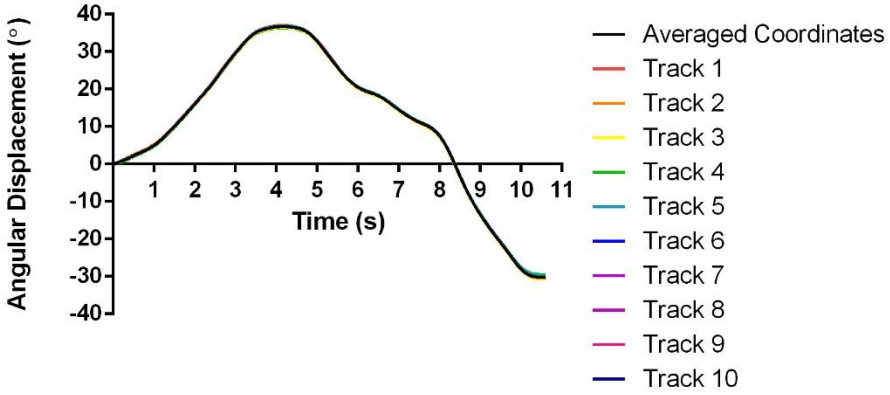

Figure 15.14 Image sequence 3 vertebral body 1.

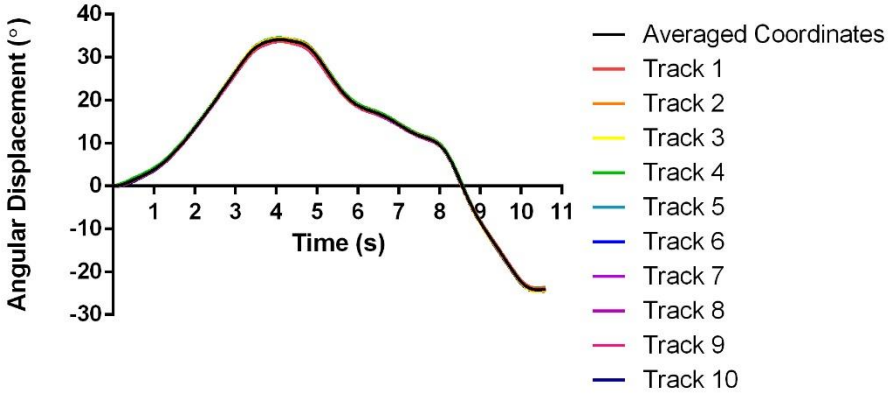

Figure 15.15 Image sequence 3 vertebral body 2.

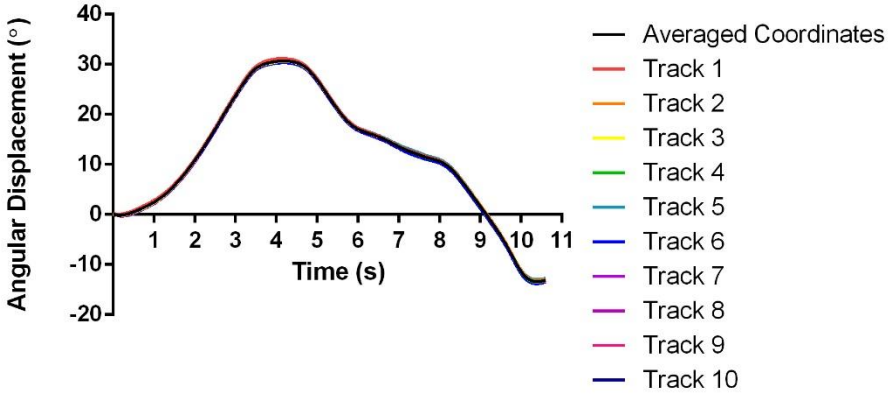

Figure 15.16 Image sequence 3 vertebral body 3.

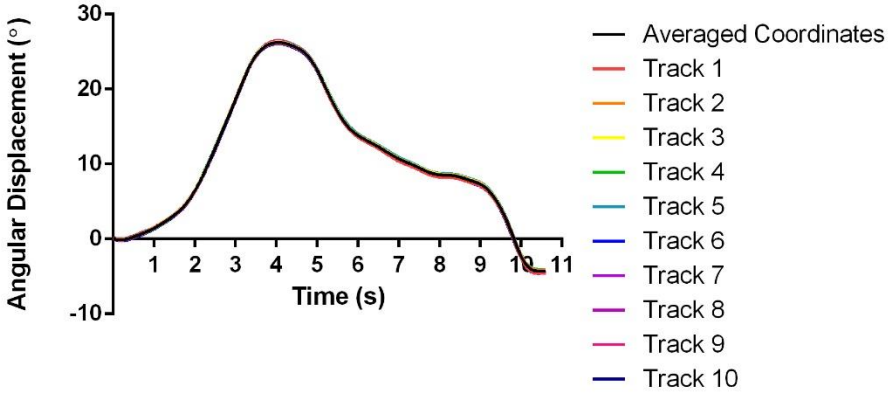

Figure 15.17 Image sequence 3 vertebral body 4.

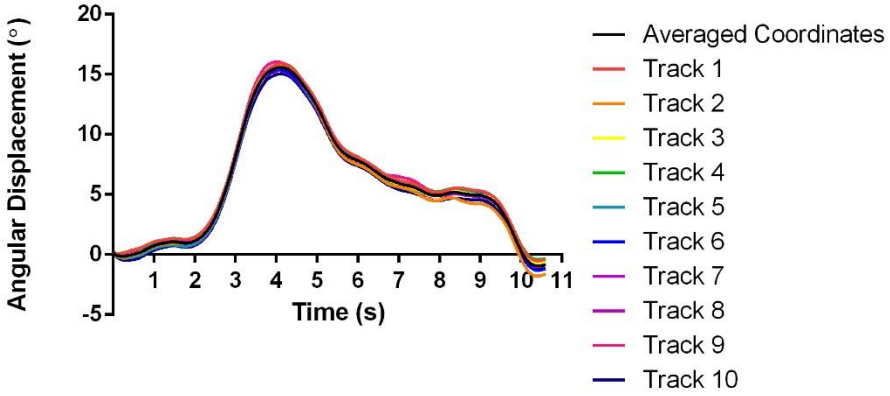

Figure 15.18 Image sequence 3 vertebral body 5.

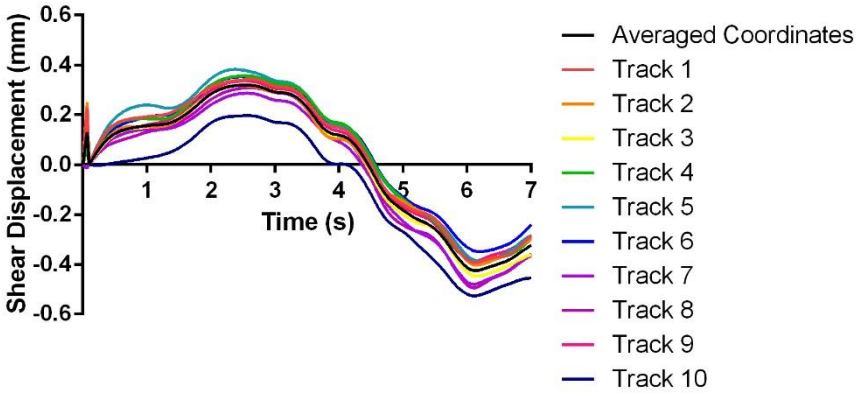

Figure 15.19 Image sequence 1 relative joint shear 1.

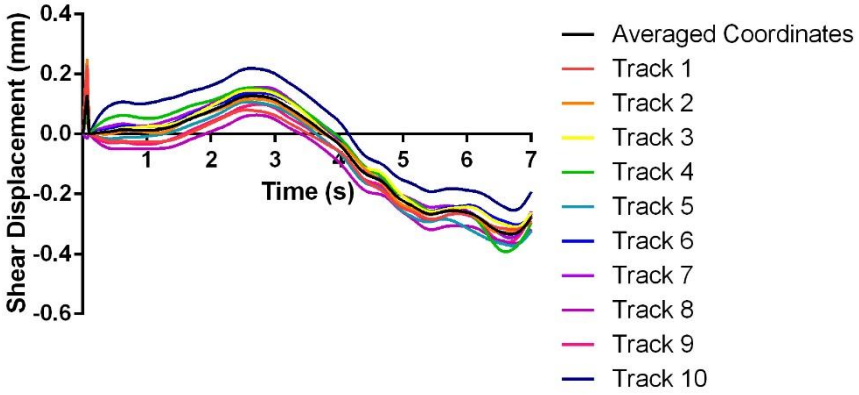

Figure 15.20 Image sequence 1 relative joint shear 2.

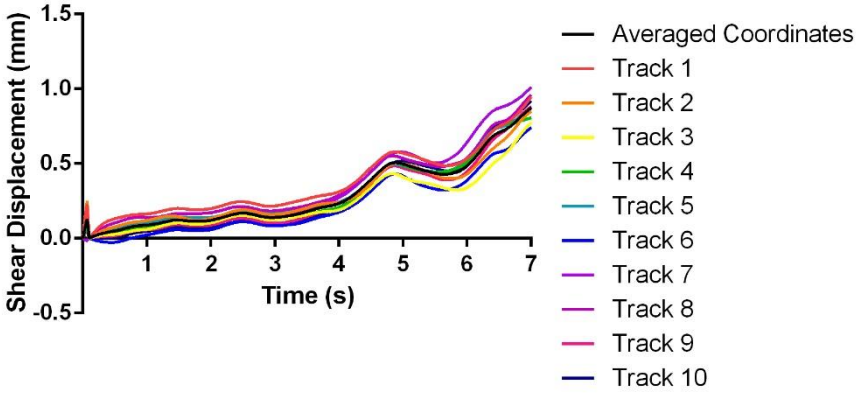

Figure 15.21 Image sequence 1 relative joint shear 3.

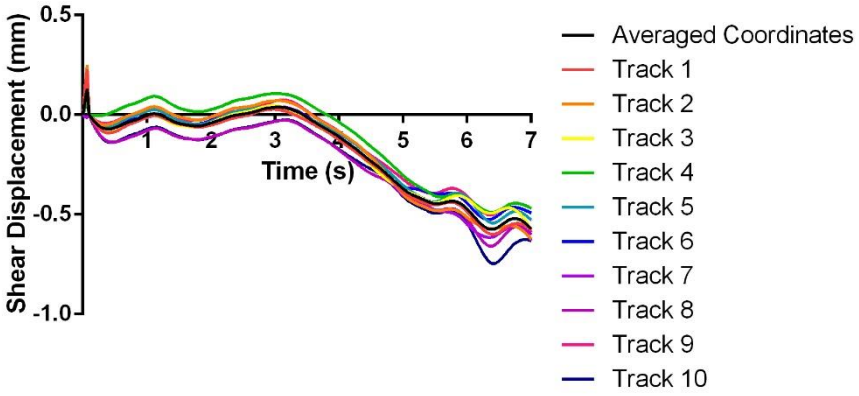

Figure 15.22 Image sequence 1 relative joint shear 4.

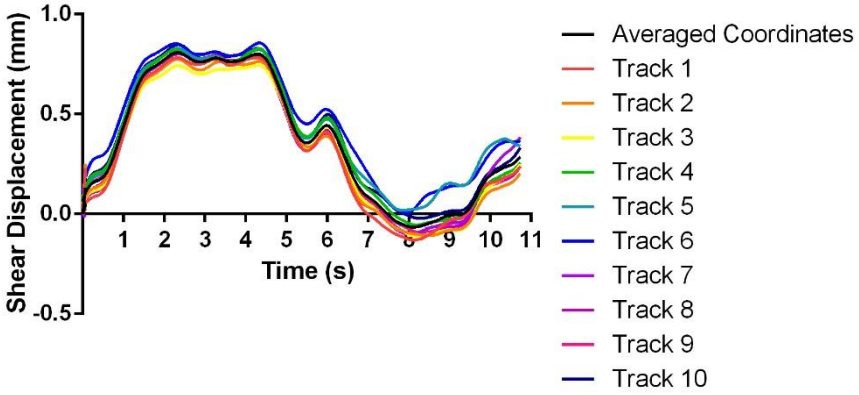

Figure 15.23 Image sequence 2 relative joint shear 1.

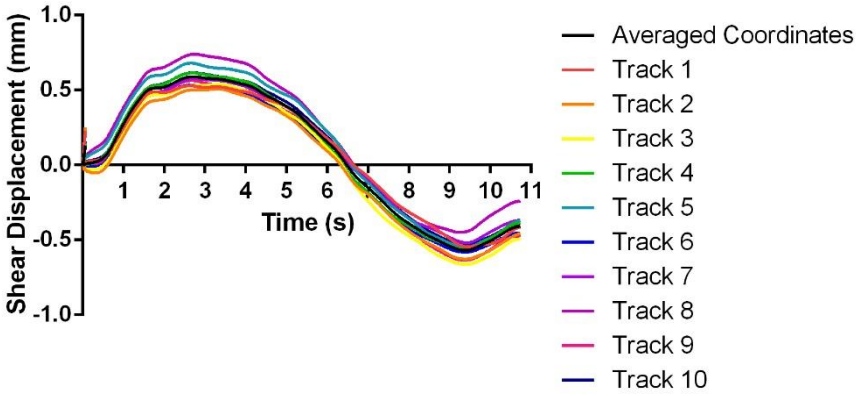

Figure 15.24 Image sequence 2 relative joint shear 2.

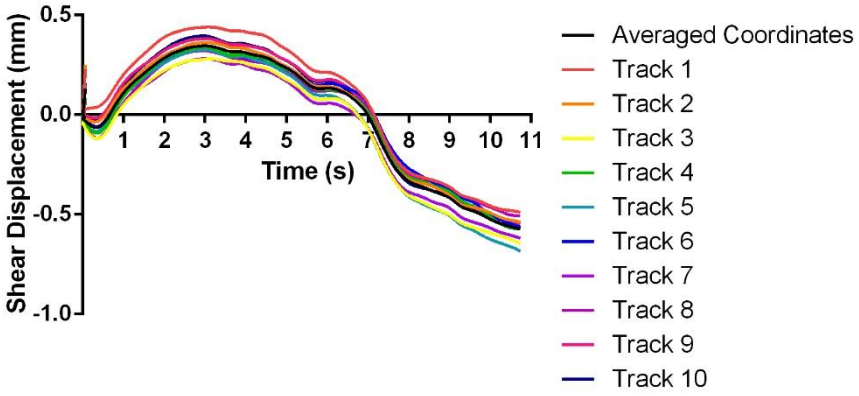

Figure 15.25 Image sequence 2 relative joint shear 3.

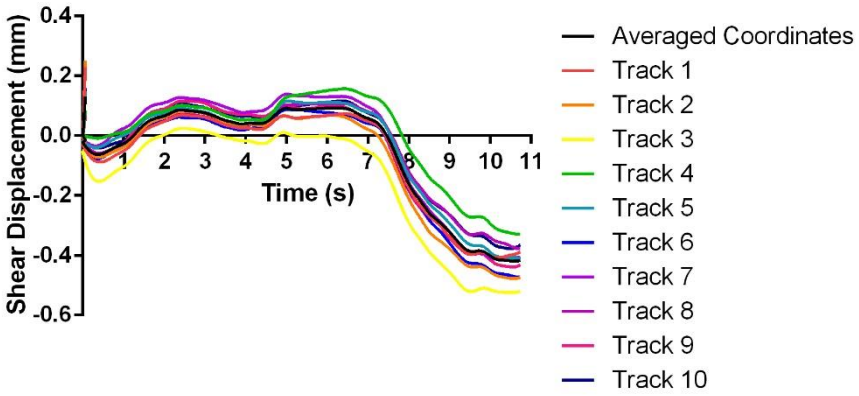

Figure 15.26 Image sequence 2 relative joint shear 4.

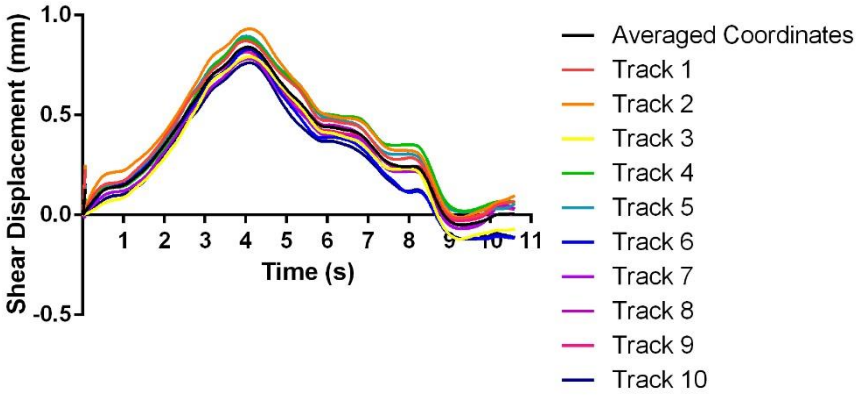

Figure 15.27 Image sequence 3 relative joint shear 1.

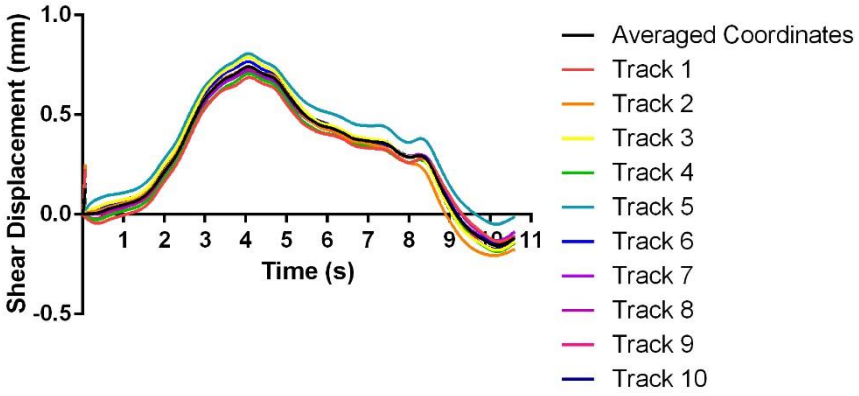

Figure 15.28 Image sequence 3 relative joint shear 2.

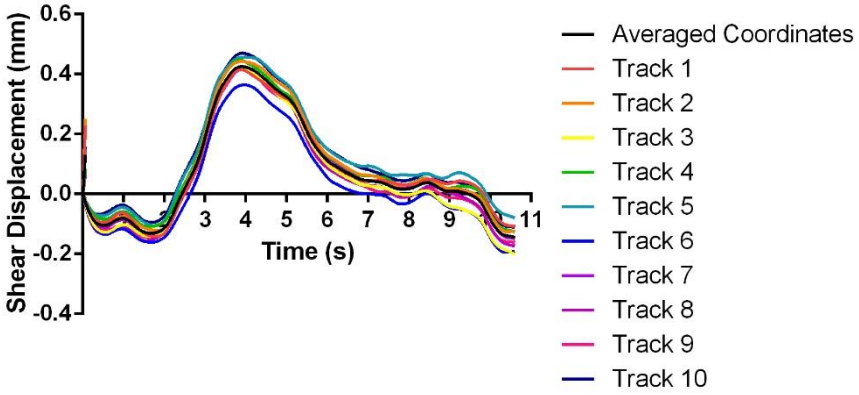

Figure 15.29 Image sequence 3 relative joint shear 3.

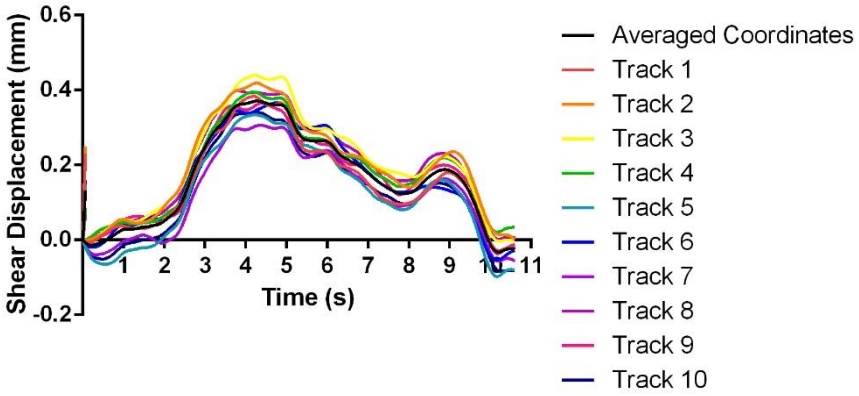

Figure 15.30 Image sequence 3 relative joint shear 4.

Appendix H: Radiographs and Time-History Sequences of All Cases from Study 3.

In this appendix all neutral posture radiographs and sagittal plane time-history graphs of relative joint motion are presented. The disc height loss cases are presented first, followed by the mild height loss cases, and finally the non-height loss cases. Radiographs are presented in their processed format, that is, with the pincushion distortion corrected along with sharpen and blur filters applied.

16.1 Disc Height Loss Cases

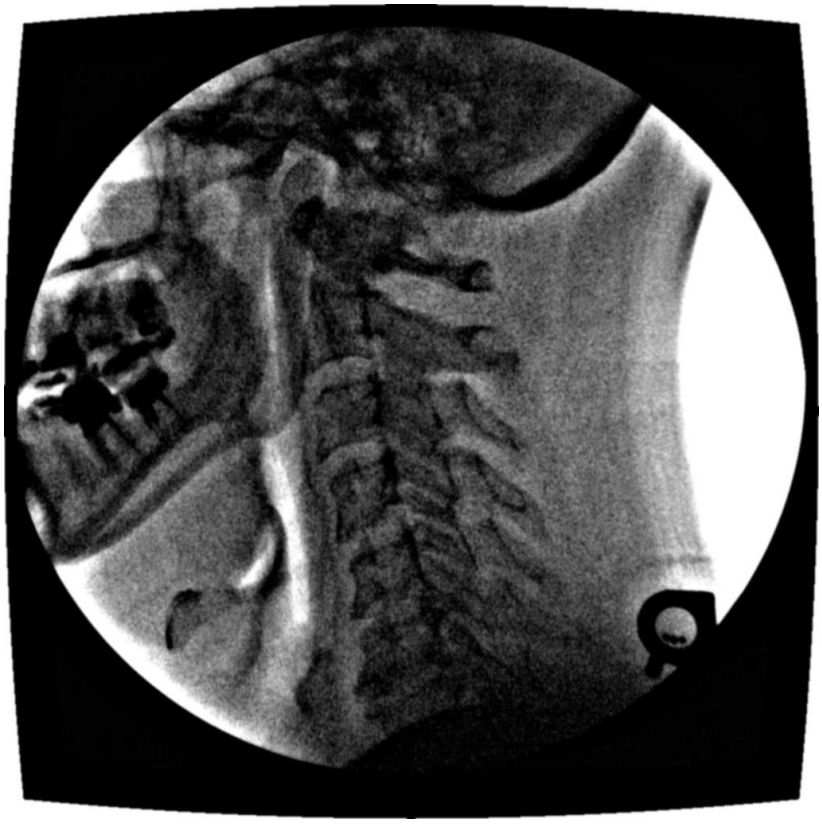

Figure 16.1 Disc height loss Case 1 (DH1).

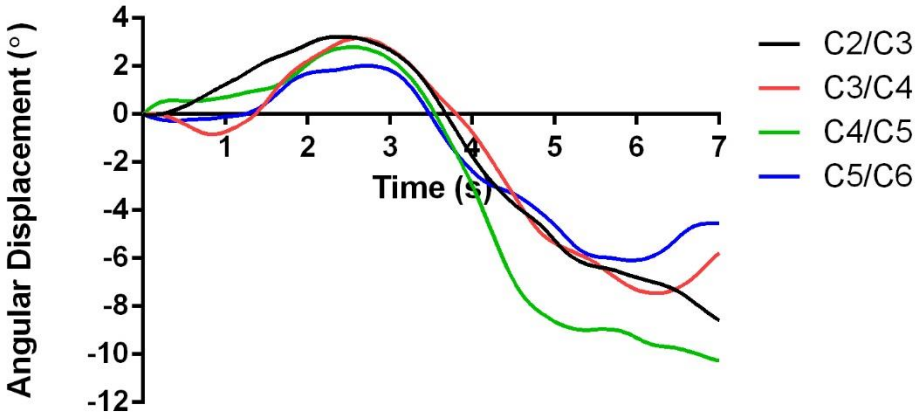

Figure 16.2 Time-history graph of relative angular displacement for disc height loss Case 1.

Figure 16.3 Disc height loss Case 2 (DH2).

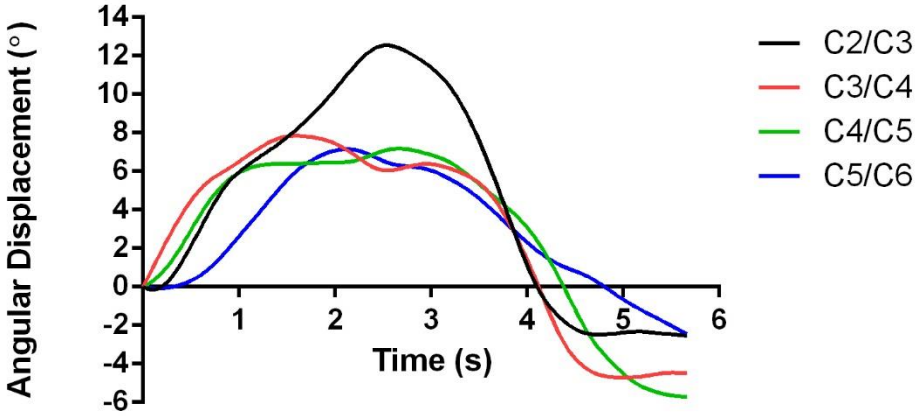

Figure 16.4 Time-history graph of relative angular displacement for disc height loss Case 2.

Figure 16.5 Disc height loss Case 3 (DH3).

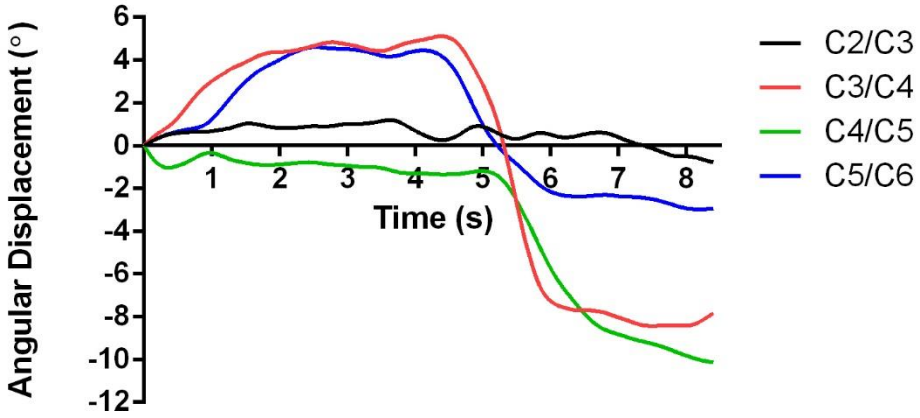

Figure 16.6 Time-history graph of relative angular displacement for disc height loss Case 3.

16.2 Mild Disc Height Loss Cases

Figure 16.7 Mild disc height loss Case 1 (MH1).

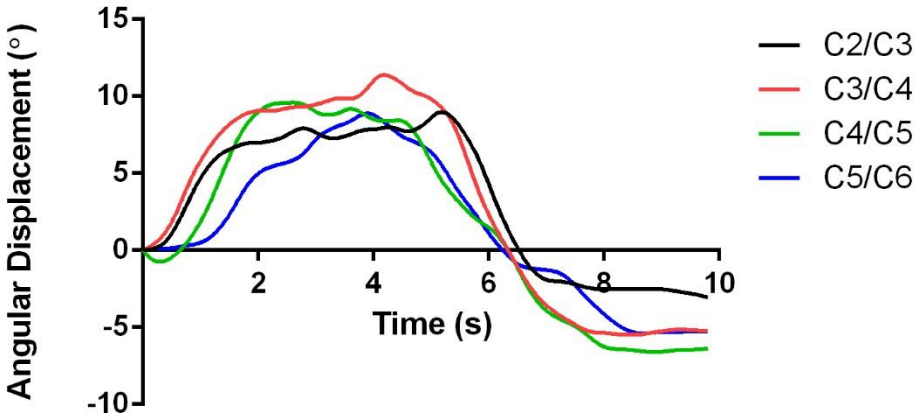

Figure 16.8 Time-history graph of relative angular displacement for mild disc height loss Case 1.

Figure 16.9 Mild disc height loss Case 2 (MH2).

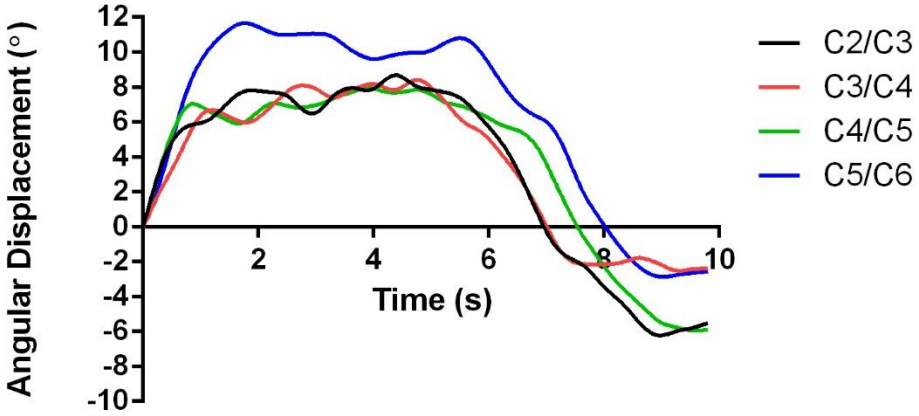

Figure 16.10 Time-history graph of relative angular displacement for mild disc height loss Case 2.

Figure 16.11 Mild disc height loss Case 3 (MH3).

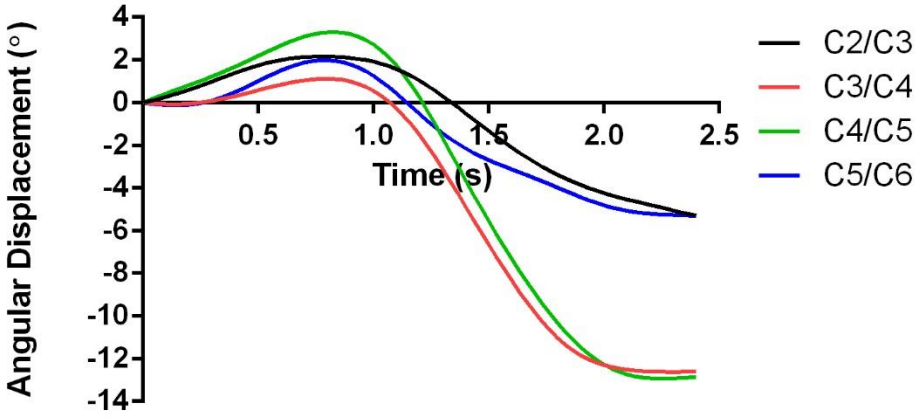

Figure 16.12 Time history graph of relative angular displacement for mild disc height loss Case 3.

Figure 16.13 Mild disc height loss Case 4 (MH4).

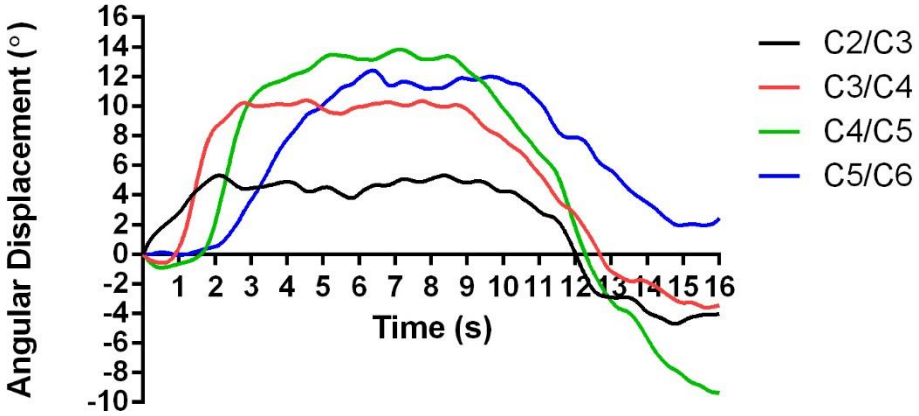

Figure 16.14 Time history graph of relative angular displacement for mild disc height loss Case 4.

Figure 16.15 Mild disc height loss Case 5 (MH5).

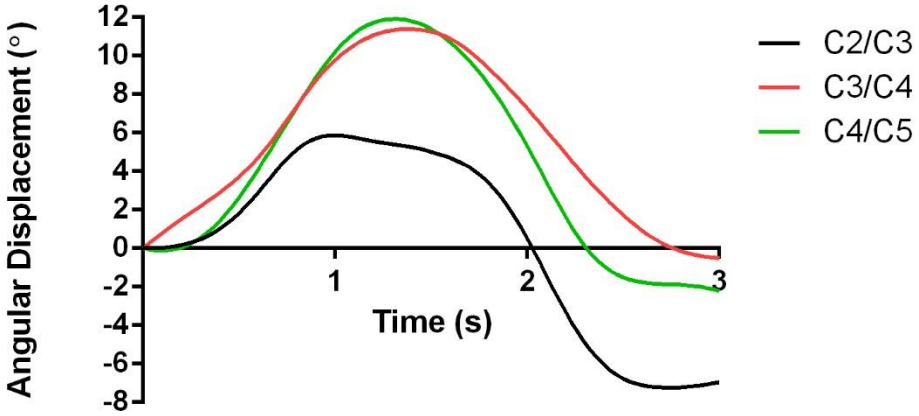

Figure 16.16 Time history graph of relative angular displacement for mild disc height loss Case 5.

Figure 16.17 Mild disc height loss Case 6 (MH6).

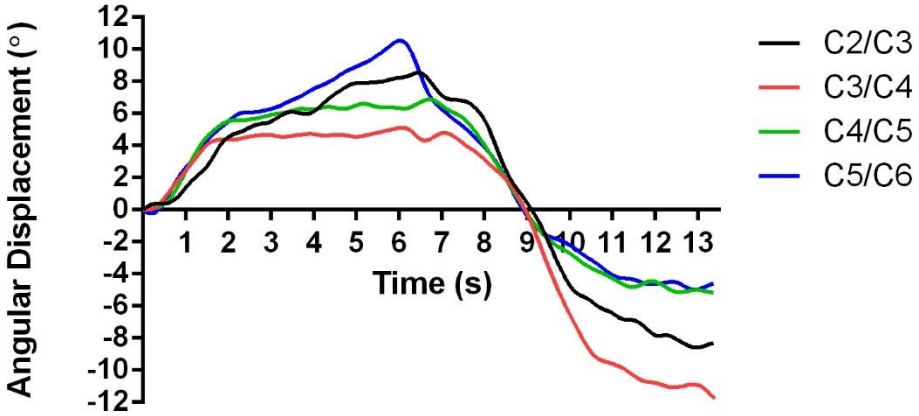

Figure 16.18 Time history graph of relative angular displacement for mild disc height loss Case 6.

Figure 16.19 Mild disc height loss Case 7 (MH7).

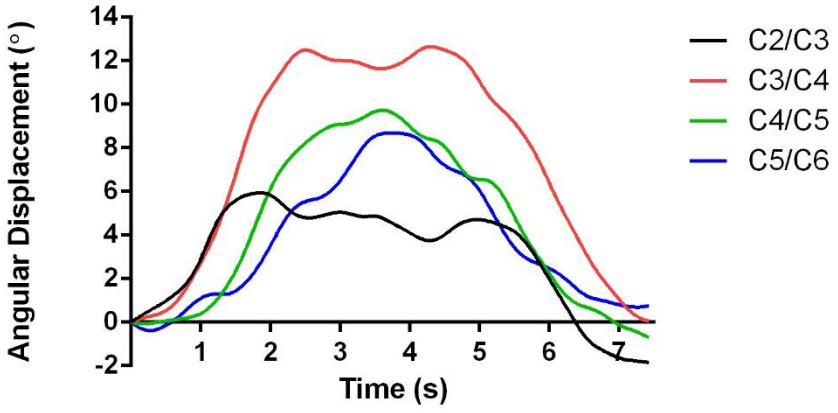

Figure 16.20 Time history graph of relative angular displacement for mild disc height loss Case 7.

Figure 16.21 Mild disc height loss Case 8 (MH8).

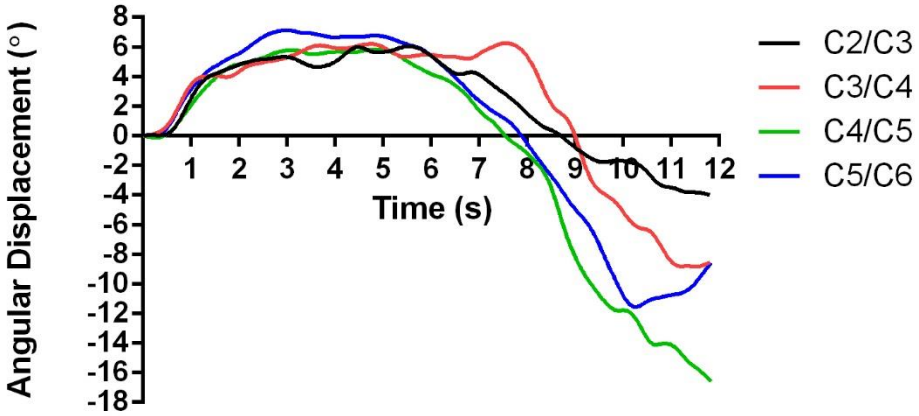

Figure 16.22 Time history graph of relative angular displacement for mild disc height loss Case 8.

16.3 Non-Disc Height Loss Cases

Figure 16.23 Non-disc height loss Case 1 (NH1).

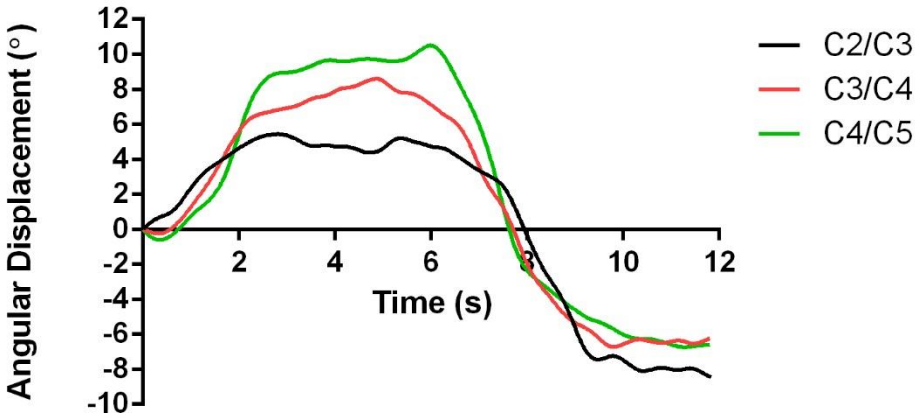

Figure 16.24 Time history graph of relative angular displacement for non-disc height loss Case 1.

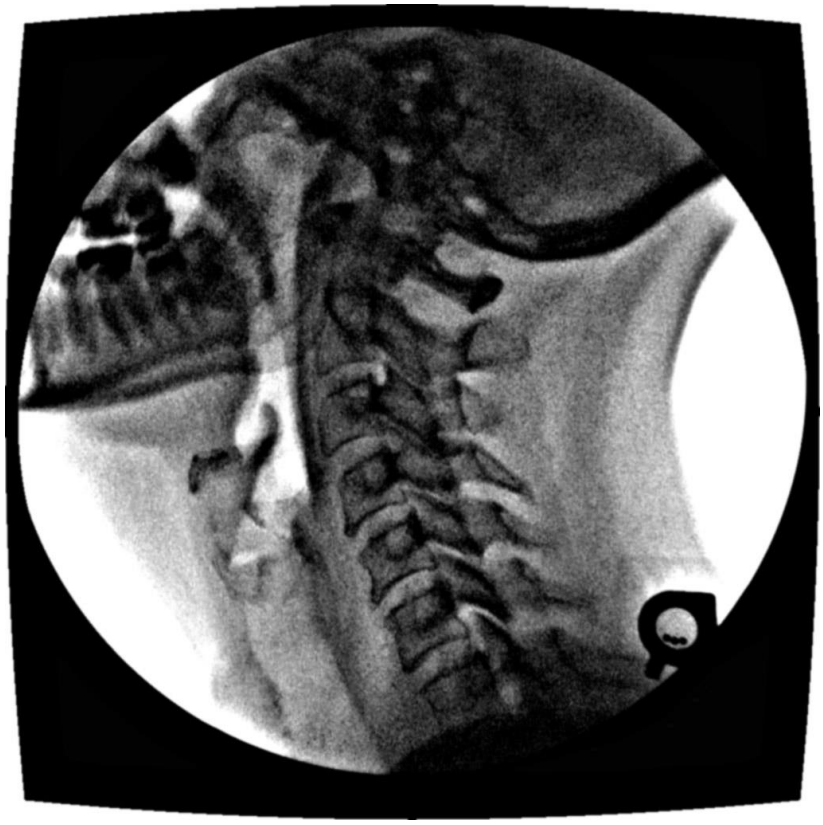

Figure 16.25 Non-disc height loss Case 2 (NH2).

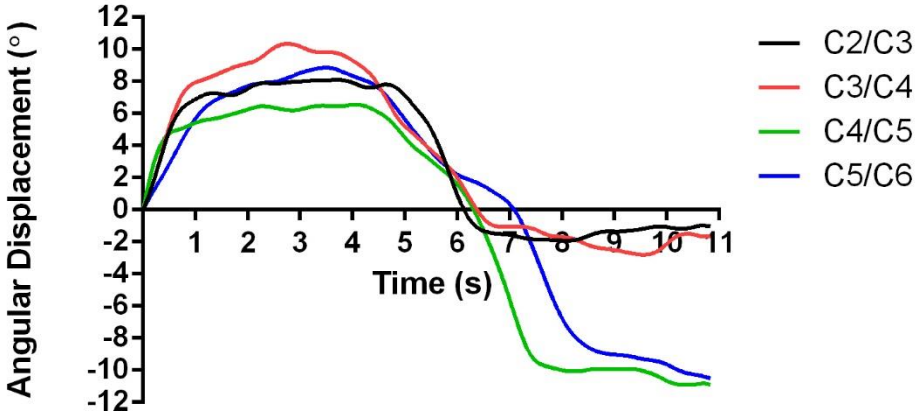

Figure 16.26 Time history graph of relative angular displacement for non-disc height loss Case 2.

Figure 16.27 Non-disc height loss Case 3 (NH3).

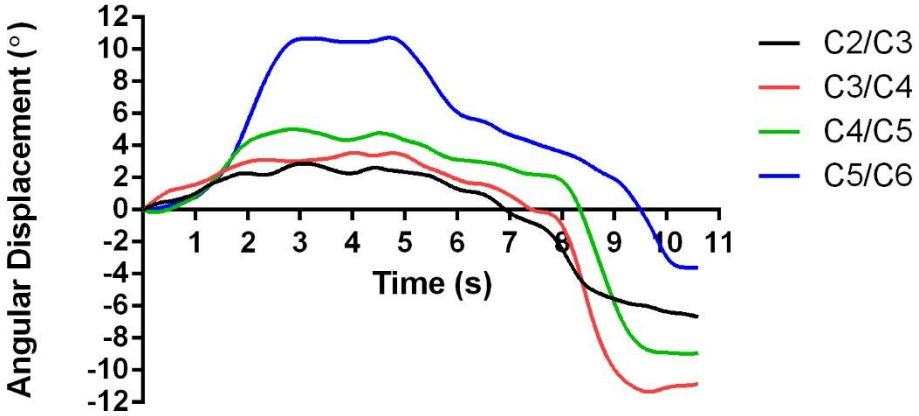

Figure 16.28 Time history graph of relative angular displacement for non-disc height loss Case 3.

Figure 16.29 Non-disc height loss Case 4 (NH4).

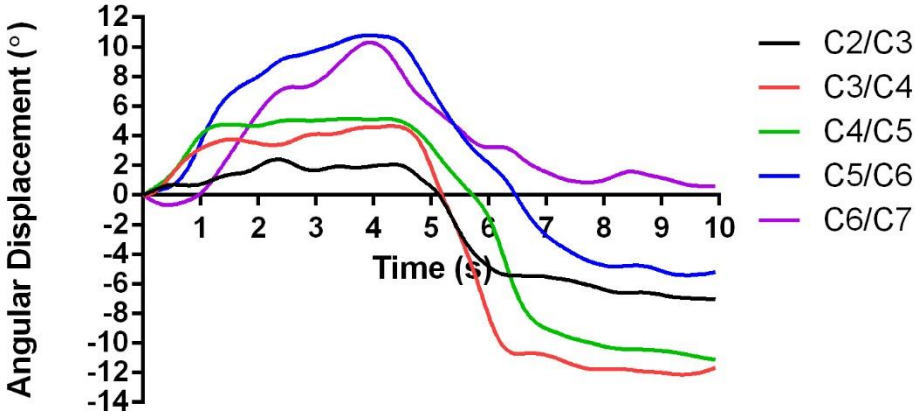

Figure 16.30 Time history graph of relative angular displacement for non-disc height loss Case 4.

Figure 16.31 Non-disc height loss Case 5 (NH5).

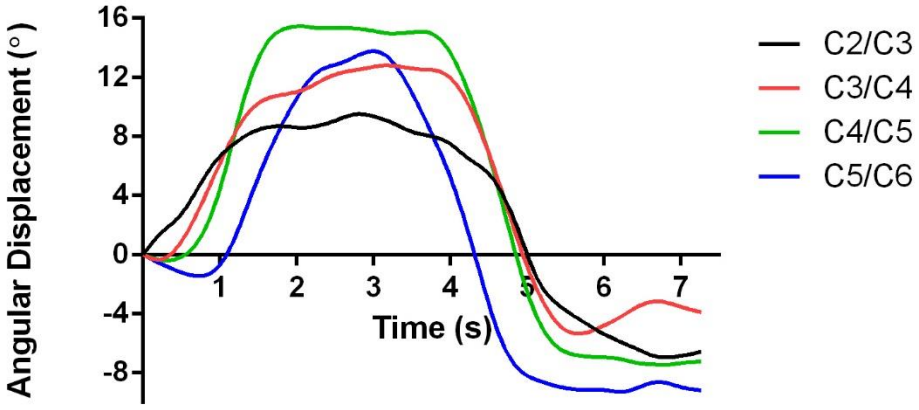

Figure 16.32 Time history graph of relative angular displacement for non-disc height loss Case 5.

Figure 16.33 Non-disc height loss Case 6 (NH6).

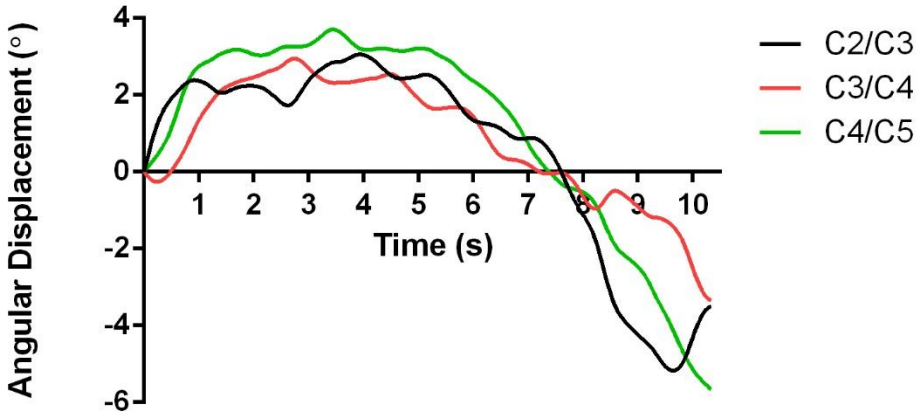

Figure 16.34 Time history graph of relative angular displacement for non-disc height loss Case 6.

Figure 16.35 Non-disc height loss Case 7 (NH7).

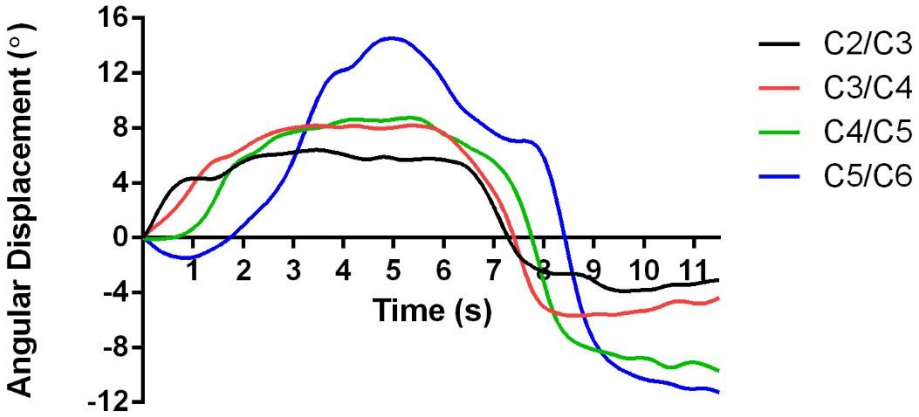

Figure 16.36 Time history graph of relative angular displacement for non-disc height loss Case 7.

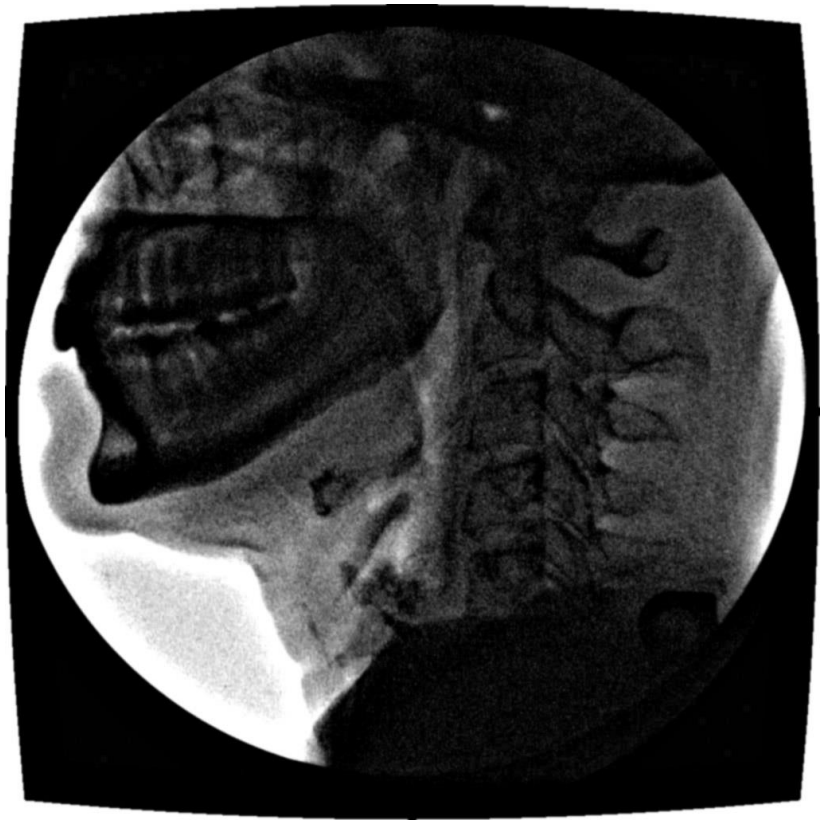

Figure 16.37 Non-disc height loss Case 8 (NH8).

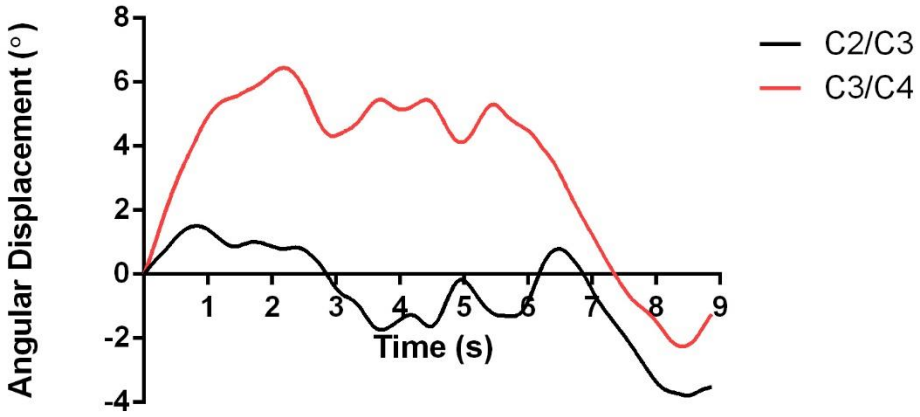

Figure 16.38 Time history graph of relative angular displacement for non-disc height loss Case 8.

Figure 16.39 Non-disc height loss Case 9 (NH9).

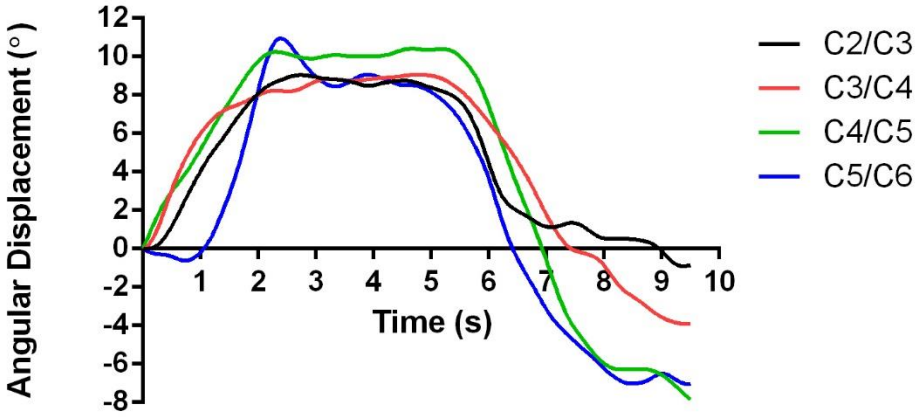

Figure 16.40 Time history graph of relative angular displacement for non-disc height loss Case 9.